Optimization of Coating for Austenitic Stainless Steel Pipeline in Buried, Above-ground and Splashed Condition

Thesis submitted by

Surajit Ghosal

Doctor of Philosophy (Engineering)

Department of Metallurgical & Material Engineering,

Faculty of Engineering & Technology

Jadavpur University

Kolkata, India

2024

Jadavpur University
Kolkata 700032, India

INDEX No. 89/17/E

1. Title of the thesis:

Optimization of Coating for Austenitic Stainless Steel Pipeline in Buried, Above-ground and Splashed Condition

2. Name, designation, and institution of the supervisors:

- Dr. Rajib Dey, Prof. Metallurgical & Material Engineering, Jadavpur University, Kolkata 700032, West Bengal, India
- Dr. Buddhadeb Duari, Corrosion Specialist, A/172, Lake Garden, Kolkata - 700045, West Bengal, India.

3. List of Publications

Thesis Related Papers published in International Journals:

a) Surajit Ghosal, Rajib Dey, Buddhadeb Duari, **"Comparison of Coatings Adhesion Performances for Buried SS316L Pipelines"**, *Oriental Journal of Chemistry, Vol. 39 (2023), No. (2), pages 246-254.*

b) S. Ghosal, R. Dey, B. Duari, **"Evaluation of Coatings Suitability for Buried SS316L Pipelines"**, *Progress in Color, Colorants and Coatings, Vol.16 (2023), Issue 4, pages 361-375.*

4. List of Patents:

Nil

5. List of Presentations (National/International):

Nil

Statement-of-Originality

I. Surajit Ghosal, registered on 31-01-2017 do hereby declare that this thesis entitled - **Optimization of Coating for Austenitic Stainless Steel Pipeline in Buried, Above-ground and Splashed Condition** contains literature-survey and original research-work done by the undersigned as part of doctoral-studies.

All information in this thesis have been obtained & presented in accordance with existing academic-rules & ethical-conduct. I declare that as required by these rules & conduct, I have fully cited & referred all materials & results that are not original to this work.

I also declare that I have checked this thesis as per the policy on anti-plagiarism, Jadavpur University 2019 & the level of similarity as checked by iThenticate software is 8 %.

Signature of the candidate -   Surajit Ghosal
                                24/01/2024
Date -

Certified by the supervisors -

(Signature, date, seal)

1. Rajib Dey 24/1/24

Professor
Metallurgical & Material Engg. Dept.
Jadavpur University
Kolkata - 700032

2. Buddhadeb Das 24/01/24

Certificate from Supervisors

This is to certify that the thesis entitled - **Optimization of Coating for Austenitic Stainless Steel Pipeline in Buried, Above-ground and Splashed Condition** submitted by Shri. **Surajit Ghosal** got his name registered on 31-01-2017 for the award of Ph.D. (Engineering) degree of Jadavpur University is absolutely based on his own work under the supervision of Dr. Rajib Dey and Dr. Buddhadeb Duari and that neither his thesis nor any part of the thesis has been submitted for any degree, diploma, academic or award before.

1. _Rajib Dey 21/·/24_
   Signature of supervisor, date, seal

   Professor
   Metallurgical & Material Engg. Dept.
   Jadavpur University
   Kolkata - 700032

2. _Buddhadeb Da 24/01/24_
   Signature of supervisor, date, seal

   NACE CORROSION SPECIALIST
   CERT NO. 14687

Dedication

This thesis is dedicated to my late parents, my in-laws, my family, my sister and
her family, my late aunt and her family, my late maternal uncle and his family,
my friends, who believed in me, encouraged me, and supported me
every step of the way.

Acknowledgement

Date: 24.01.2024

Surajit Ghosal

Table of Contents

List of Figures

xvii

List of Tables

Optimization of Coating for Austenitic Stainless Steel Pipeline in Buried, Above-ground and Splashed Condition+

Surajit Ghosal

ABSTRACT

The petrochemical products are transported via austenitic stainless steel pipelines to keep the product purity. Pipelines are installed mostly buried and are marginally above-ground and splashed conditions. Austenitic stainless steel resists dry corrosion due to the formation of a chromium oxide passive film in atmospheric exposure. But an uncoated austenitic stainless steel pipeline buried in soil is doubtful because soil resistivity may be low enough due to the presence of water with chloride salts and deficient in oxygen. Passive film may then get attacked locally by such corrosive soil resulting in numerous pitting on pipe surface. As localized pitting corrosion penetrates rapidly, there is every likelihood that it will perforate pipeline within a short time without significant weight loss of metal. It is, therefore, important and necessary to protect external surfaces of austenitic stainless steel pipelines from soil corrosion. Application of protective coatings to external surfaces of austenitic stainless steel pipelines is found to be appropriate in the first place for primary protection of buried pipelines to dispatch products economically and safely to distant places.

Available literature and research papers have shown pitting corrosion of austenitic stainless steel structures in marine environment and corrosion under insulation (CUI). Metallic coatings or polymeric coatings have been studied by the researchers to protect austenitic stainless steel structures in these environments. But suitable coatings for austenitic stainless steel structures buried in soil are found to be lacking. There is an opportunity to study this issue thoroughly.

To address this issue, SS316L pipes of 4-inch in diameters have been selected in the present study. Solution-annealed SS316 with low carbon (i.e., SS316L grade) contains molybdenum (Mo) and has superior corrosion resistance against aquatic soils than other usual austenitic stainless steel grades. Six external polymeric coatings commonly used for buried or submerged carbon steel pipelines in the petroleum, petrochemical and natural gas industries have been chosen for SS316L pipelines. The polymeric coatings are 3-Layer Poly-Ethylene (3LPE), 3-Ply/2-Ply Cold-Applied Tape (3p-2p CAT), Polyurethane (PU), Visco Elastic (VE) Polyolefin, Liquid Epoxy (LE), Heat Shrink Sleeve (HSS).

In the beginning of the research work, the characterization of SS316L pipes have been performed by chemical and mechanical tests, microstructural examination, cyclic potentiodynamic polarization in 3.5% NaCl solution, pitting corrosion in 6% $FeCl_3$ solution. After preparing the external surfaces of SS316L pipes by fused Al_2O_3 fine particles, each type of coating has been applied separately to each SS316L pipe. The samples extracted from the coated SS316L pipes have been subjected to relevant tests for SS316L pipeline in buried and splashed conditions. As no coating is needed for SS316L pipeline in above-ground condition under atmospheric exposure, still one coating has been selected for mechanical testing.

For SS316L pipeline in buried condition, the samples have been subjected to relevant tests such as thickness measurement, holiday detection, Shore-D hardness measurement, impact resistance, indentation resistance in thermostatically controlled chamber under a load of 2.5 kg for 24 hours, water absorption in distilled water for 28 days, cathodic disbondment in 3% NaCl solution for 28 days, peel strength at 23^0C & $50\text{-}60^0C$, pull-off adhesion strength at 23^0C & $50\text{-}60^0C$, hot tap water immersion in a heated vessel at $50\text{-}60^0C$ for 100 days, specific electrical insulation resistance in 0.1 mol/litre of NaCl solution for 100 days applying a DC voltage of 100V, electrochemical impedance spectroscopy in 3.5% NaCl solution for 14 days with an applied AC voltage of 100 mV_{rms} in the frequency range from 100 kHz to 10 mHz.

For SS316L pipeline in above-ground condition, LE coating has been applied to SS316L plate samples. The samples have been subjected to the Taber abrasion resistance test under abrading C-17 wheels for a load of 1000g on each wheel for 1000 cycles of abrasion.

For SS316L pipeline in splashed condition, the virgin coatings and the coatings exposed to salt spray environments in 5% NaCl solution at 35^0C in the pH range from 6.5 to 7.2 for 3000 hours have been subjected to Fourier Transform Infrared Spectroscopy covering the spectral range from 4000 to 500 cm^{-1} wave number and Shore-D hardness measurement.

The experimental data have been analysed for SS316L pipeline in all conditions. The best coating among six coatings and the overall rankings of the coatings are evaluated by a simplified arithmetic mean system. The best coating and the rankings of the first three coatings obtained by a simplified arithmetic mean system have been validated by a mathematical modeling.

Chapter - 1

Introduction

Chapter - 1: Introduction

1. Introduction

An oil refinery refines petroleum into liquefied-petroleum gas (LPG), gasoline/petrol, aviation fuel, gas oil/diesel, and naphtha etc. The petrochemical plants, on the other hand, use the refinery streams such as ethane, propane, and refining gas as the feedstock and make petrochemical products like plastic, solvents, rubber, synthetic fibres. When refinery and petrochemical plant are working separately, each operation is not flexible. But if they are integrated, their operations are flexible to process and distribute products. The best profitable business nowadays is to integrate petrochemical complexes with adjacent refineries to maximize the use of feedstock as shown in Figure 1.1 [1] and to improve the refining margins. The integrated refinery and petrochemical plants produce Olefin (Ethylene, Propylene), Aromatics (BTX - Benzene, Toluene and Xylene), Oxo-Alcohols, Acrylic Acid, and Acrylate etc. For transporting these petrochemical products to distant places including remote regions, pipelines are the safest, most efficient, reliable and economical. Pipelines are installed marginally in above-ground and splashed conditions, and mostly in buried condition to prevent physical damage and spillage to avoid ecological disaster.
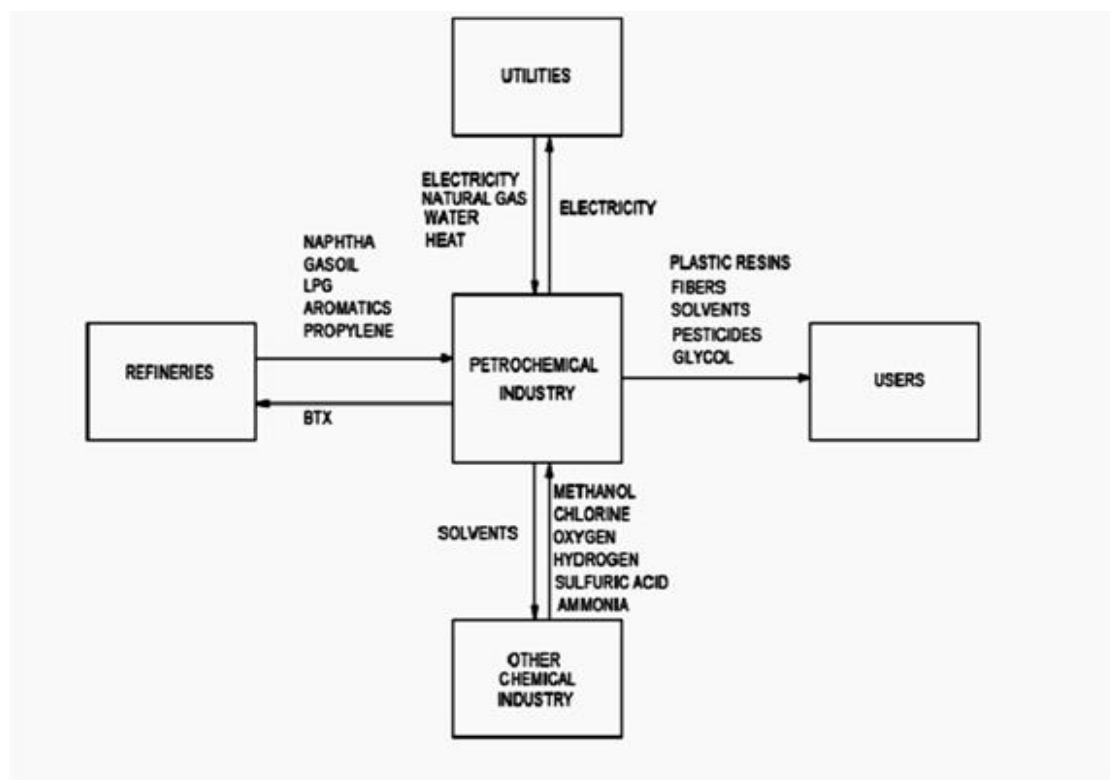
Figure 1.1: Integrated Refinery and Petrochemical Plants

Austenitic stainless steel is usually selected for pipeline material for transporting these petrochemical products as austenitic stainless steel grades have excellent corrosion resistance to maintain the purities of the products. Moreover, good formability and weldability combined with ease of fabrication are particularly advantageous to austenitic stainless steel pipeline. But, buried austenitic stainless steel pipelines can suffer localized corrosion in aquatic soil in the presence of chloride ions.

Over the years external corrosion is considered the major reason behind most buried pipeline material failure. Corrosion is a natural phenomenon that occurs between material and atmosphere i.e., moisture, oxygen, sulphur dioxide, carbon dioxide, ionic species, chemicals and pollutants. Three elements - an anode, a cathode, and an electrolyte and their connection are essential to conduct electricity between anode and cathode for corrosion to occur. In corrosion process, an oxidation reaction occurs at the anodic site by losing valance electrons and positive metal ions form and dissolve into the electrolyte. To maintain neutrality, electrons lost in oxidation reaction are consumed by the reduction reaction. The dissolved ions under soil moisture move to anodic and cathodic sites according to their charges. The corrosion of buried pipeline is influenced by many factors such as moisture content in soil, pH, soluble ions content and salt concentration, soil temperature, dissimilar soil type, differential aeration, ground water table, soil resistivity, oxidation-reduction potential, and the presence of microbes in the soil. For that reason, corrosion protection is a requisite for safe operation of a buried pipeline.

1.1 Stainless Steels

Stainless steels are corrosion resistant alloys of iron when minimum of 10.5% chromium (Cr) by weight or more are added to iron. Other important elements found in stainless steels are manganese, nickel, molybdenum, nitrogen. Stainless steel in the atmospheric exposure forms a film that gives corrosion protection. Stainless steels have a strong affinity for oxygen. With a little of oxygen, they maintain passivity. This film is self-healing and has the advantage compared to a paint layer. Chemical or mechanical damage to the passive film to an extent can heal or re-passivate in oxidizing environment.

Five major families of stainless steels based on chemical compositions, metallurgical structures and mechanical properties are as follows [2] :

1) Ferritic
2) Austenitic
3) Martensitic
4) Duplex (Ferritic-Austenitic)
5) Precipitation-Hardening.

1.2 Austenitic Stainless Steels

Austenitic stainless steels are austenite (face-centered cubic) crystalline structure, which are achieved by adding austenite stabilizing elements such as carbon, nickel, manganese and nitrogen. The alloying elements each have a specific effect on the properties of the austenitic stainless steels. The most widely used austenitic stainless steel grades are 18-8 type steels: 16-18% chromium (Cr) and 8-11% nickel (Ni). Corrosion resistances of these grades are increased by alloying molybdenum (Mo) of the order of 2-3%. These grades are non-magnetic. By heat treatment, these grades cannot be made hardenable. They possess very good ductility and toughness with low yield strength. Due to these properties, they can be welded and fabricated easily. Austenitic grades are most common among other stainless steels.

Brief overviews of some elements and their effects on chemical composition are given below:

1.2.1 Chromium (Cr)

Chromium gives ferrite microstructure in stainless steels. Cr being an important element forms a passive layer of Cr-oxide (Cr_2O_3) after reacting with oxygen in the atmosphere. A little amount of oxygen is sufficient to form this passive film in stainless steels. The passive film gives protection against corrosion. The corrosion resistance property of stainless steel is directly proportional to Cr content. When Cr content increases, the corrosion resistance property increases. Higher Cr content also gives benefit of higher oxidation resistance.

1.2.2 Nickel (Ni)

The addition of nickel gives austenite microstructure in stainless steels. Ductility and toughness are increased by the increasing amount of Ni. Higher Ni content increases resistance against acidic corrosion and it is a great advantage. Ni is an effective element in promoting re-passivation in reducing environments.

1.2.3 Molybdenum (Mo)

The addition of molybdenum to Cr helps effectively to stabilize the passive film. Mo substantially increases resistance to localized pitting and crevice corrosion in chloride bearing environment. It increases the mechanical strength and gives ferrite microstructure in stainless steels.

1.2.4 Nitrogen (N)

Nitrogen gives austenite microstructure in stainless steels. N increases mechanical strength. The addition of N to Cr, Mo increases pitting resistance index of stainless steels, resulting in resistance to localized pitting corrosion in chloride bearing environment.

1.2.5 Carbon (C)

Carbon reacts with Cr and forms chromium carbides when stainless steels are exposed to heat like welding. Chromium carbides precipitate on grain boundaries and there is depletion of chromium in the immediate vicinity. This phenomenon is commonly known as sensitization. In chloride bearing environment, it suffers inter-granular corrosion. It is greatly prevented by the use of lower carbon, which is less than 0.03%.

1.3 Susceptibility to Localized Corrosion of Austenitic Stainless Steels

The reason for widespread use of austenitic stainless steels is their corrosion resistance, but in some environments, austenitic stainless steels may experience corrosion. Austenitic stainless steels form protective films on their surfaces when Cr reacts with oxygen in atmosphere. The film is Cr_2O_3 and very thin, about 1-3 nanometres (nm) [3]. This passive film acts as a barrier

to occurring corrosion from corrosive atmosphere. Due to the addition of a minimum of 10.5% Cr by weight to steel, corrosion rate is decreased. 11-13% Cr is needed to obtain an adhered passive film and 18% Cr is needed for austenitic stainless steels [4]. Low C, Mo, Ni, N also provide resistance to corrosion in an aggressive environments.

The passive film in austenitic stainless steels is porous and heterogeneous in composition and contains defects & non-metallic inclusions. Due to this, the passive film is vulnerable to attack by halides. Once the pitting corrosion starts, it continues due to strong acidic salts in the pit bottom making the reaction autocatalytic in nature [5].

1.3.1 Pitting Corrosion

Pitting corrosion is a form of extremely localized attack and normally occurs on free surfaces. Pits in most cases are relatively small and are isolated or close together. Pitting is one of the most destructive forms of corrosion. A tiny perforation due to pitting occurs without any weight loss of the structure. Corrosion products cover pits on the structure. In this situation, pits cannot be detected. Pit type corrosion occurs as the small active area is being attacked where the large & passivated area remains unaffected. An active-passive cell is set up with a difference in potential of 500-600 mV [6] in these relative areas. This active-passive cell accelerates the corrosion causing the pits to penetrate deeper. Pits usually grow in the direction of gravity, downward from horizontal surfaces. Once pit is initiated and attains a stable form, a stable pit penetrates metal structure at an ever-increasing rate. Due to a very high pitting corrosion rate, the failure of the structure occurs suddenly and unexpectedly within a few days and without any significant metal loss of the structural components. The mechanism of pitting corrosion of austenitic stainless steels in presence of chloride ions is shown in Figure 1.2 a), b) [7].
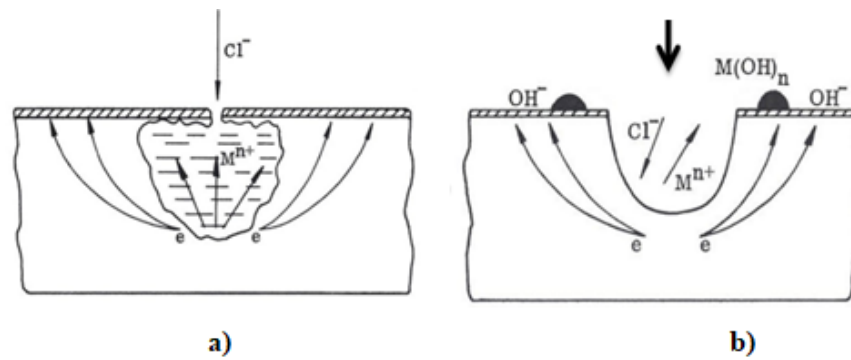
Figure 1.2: Mechanism of Pitting Corrosion - a) Adsorption of Cl⁻ ions on Metal Surface, b) Electrochemical Reaction and Metal Dissolution

1.3.2 Crevice-Corrosion

Another form of localized corrosion is crevice-corrosion. Corrosive electrolyte remains in the shielded areas to form crevices. It clearly defines attacked area and usually, larger area is corroded compared to the area corroded in pitting corrosion. Crevice corrosion occurs when liquid solution shelters and stagnant in the enclosed area. Electrochemical reaction occurs in the crevice resulting in increasing Cl⁻ions concentration and decreasing the local pH. The mechanism of crevice corrosion of austenitic stainless steels in presence of chloride ions is shown in Figure 1.3 [8]. Such situation is giving rise to the formation of a concentration cell where the supplies of oxygen are limited. In this situation, stainless steels are unable to maintain the passive protective films.
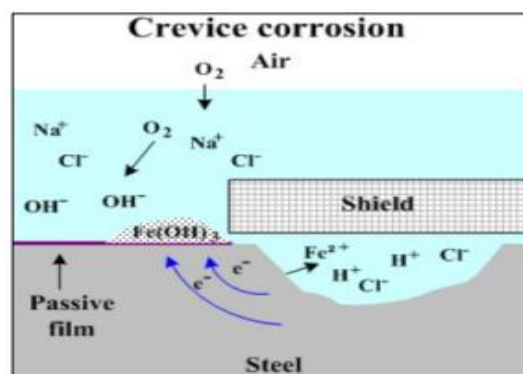
Figure 1.3: Mechanism of Crevice Corrosion

1.4 Austenitic Stainless Steel Pipeline in Buried Condition

The performance of austenitic stainless steel buried in wet soil depends on the nature of the buried environment because soil corrosion is complex. The corrosivity of soils also depends on chemical compositions of soils and water content. Clay, silt or loam soils retain high moisture, whereas sand and gravel soils allow good/excellent drainage. In principle, austenitic stainless steel provides excellent service in buried condition if the soil is dry, well drained and has a high resistivity [9]. Soil resistivity is an operative parameter for characterization of soil corrosiveness as it is directly dependent of salt content and presence of water in soil. Pitting corrosion of austenitic stainless steels in soils depends on chloride contents, soil temperature and soil aeration. Soil corrosivity is influenced by various factors such as pH, moisture, halide ions, different oxygen content, micro-biological species, soil-resistivity etc. Though bare or uncoated austenitic stainless steel pipelines in buried conditions are in use on a limited scale, there are doubts about corrosion resistance of stainless steel in wet soil [10]. Pitting corrosion remains unpredictable and undetectable until leaks because the localized attack is covered by the porous corrosion products [11]. A schematic of pitting corrosion of buried austenitic stainless steel pipeline is shown Figure 1.4.
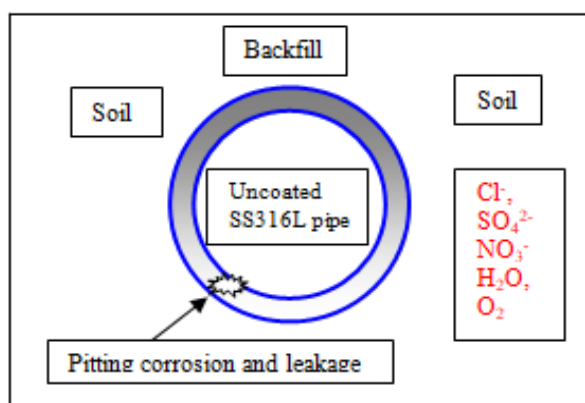
Figure 1.4: Pitting Corrosion of Buried Austenitic Stainless Steel Pipeline

Austenitic stainless steels are usually avoided in moist and aquatic soil applications because of their susceptibilities to localized pitting corrosion. As austenitic stainless steel pipelines are more expensive than carbon steel pipelines usually used for transportation of petroleum products in the oil and gas industry, the failure of austenitic stainless steel pipelines due to external wet

corrosive soil is not permitted. External cathodic protection is imperative to be applied to these pipelines in buried or submerged condition. The external surfaces of austenitic stainless steel pipelines are coated [12] to prevent aquatic soil corrosion and to reduce the current needed for cathodic protection system.

1.4.1 Corrosion Protection for Austenitic Stainless Steel Pipeline in Buried Condition

The method used to mitigate the effects of external corrosion of pipeline is the application of protective coating in combination with cathodic protection system as longevity and reliability are essential for austenitic stainless steel pipeline in the petroleum, petrochemical and natural gas industries. The reason behind this is to isolate pipeline metal in contact with the surrounding earth and to stop corrosion to occur on metal surface. The protective coating provides primary protection of buried pipeline. Hence, less power is needed for cathodic protection systems. The protective coating should show some important aspects of corrosion protection such as free from holidays, good adhesion on metal substrate, resistance to cathodic disbonding from metal substrate, effective barrier, and resistance to water permeability through coating, ionic resistance, high electrical insulation resistance, alkali-resistant, severe and extreme temperature resistant. The cathodic protection system causes the cathodic metal surface to become strong alkaline, which is the primary cause of cathodic disbonding. In this condition, water and salts enter and penetrate the coating by three processes - osmosis, electroosmosis and electrophoresis [13]. In osmosis process, an osmotic pressure exists between the soil and the pipe surface and water transportation occurs through the organic coatings, which are semi-permeable membranes. Electroosmosis is related to electrical current flow and in this process, water flows from one side to the other when a potential difference is maintained between the soil and the pipe. Applied voltage and flow rate are directly proportional. Charges carried by water determine flow direction. Water is transported faster when PSP (Pipe-to-Soil Potential) is high enough. On the other hand, water is transported slow when coating thickness is high. In electrophoresis process, due to a difference in potential, the electrodes of opposite charges attract electrically charged ions. Electrophoresis process occurs under the influence of PSP when coating has holidays. A combination of the three processes i.e., water absorption & transportation, moisture vapour transmission through the coating occurs. This has resulted in loss of adhesion of the protective coating to the metal substrate. Therefore, it is essential to conduct relevant tests to the coating to ascertain the requisite characteristics that provide adequate corrosion protection for buried austenitic stainless steel pipeline.

1.4.2 Advantages of Coatings over other Corrosion Protection Methods

There are many methods to minimize corrosion of buried pipelines, but specifically corrosion protection (or prevention) and control methods [14] are broadly classified as below:

1.4.2.1 Active Corrosion Protection (corrosion-resistant alloys or corrosion inhibitors),

1.4.2.2 Passive Corrosion Protection (barrier coatings),

1.4.2.3 Temporary Corrosion Protection (cathodic protection with sacrificial anodes),

1.4.2.4 Permanent Corrosion Protection (cathodic protection with permanent anodes).

1.4.2.1 Active Corrosion Protection

The aim of the active corrosion protection is either to resist corrosion using corrosion-resistant alloys or to control corrosion reaction to a minimum level by the addition of corrosion inhibitors to the corrosive and aggressive environment. In the present study, the pipeline material i.e., austenitic stainless steel is a corrosion-resistant alloy that needs protection from the localized corrosion in aquatic soil. The addition of corrosion inhibitor to control corrosion in wet soil appears to be unfeasible because buried pipeline can pass through different soils and pipeline is subjected to dissimilar soil corrosion. Moreover, the presence of microorganisms and their activities induce microbiological corrosion, which are coupled with some types of electrochemical corrosion. Corrosion by aerobic or anaerobic microorganisms occurs in the presence or absence of oxygen respectively. It is difficult to prevent and control corrosion by the addition of corrosion inhibitors due to number of microorganisms, variety of species, and many unrecognized microorganisms involved in electrochemical corrosion processes [15].

1.4.2.2 Passive Corrosion Protection

In the passive corrosion protection, protective coating is applied that isolates the external surface from the aggressive media, such as water, ions, salts, acids, oxygen. A coating would stop corrosion if the coating material remains with time as a perfect film, remains with time without any holiday, behaves as a perfect insulator. If there are holidays or defects in the coating during service, corrosion can occur within a very short period of time.

1.4.2.3 Temporary Corrosion Protection

The temporary corrosion protection is provided by applying sacrificial cathodic protection system for a short duration like during commissioning of a newly installed pipeline.

1.4.2.4 Permanent Corrosion Protection

This method provides corrosion protection to a pipeline for its designed life using protective coating in conjunction with Impressed Current Cathodic Protection (ICCP) system.

Among all corrosion protection methods described above, the permanent corrosion protection method (i.e. anti-corrosion protective coating combined with ICCP system) is installed as an essential attribute for longevity and reliability of a pipeline. Barrier protective coating provides primary protection of buried or submerged pipeline from external corrosion and reduces power consumption in cathodic protection system. Therefore, economical and effective external protective coating is paramount for the lifetime of a pipeline to minimize the deteriorating effects of corrosion.

1.4.3 Polymeric Coatings for Austenitic Stainless Steel Pipeline in Buried Condition

The polymeric coatings give prime protection against external corrosion of the austenitic stainless steel pipelines. A coating film prevents the corrosive elements to ingress and reach to the metallic substrate beneath. The polymeric coatings being dielectric materials behave as insulators. A coating offers high electrical resistance by high dielectric strength of the coating material, and it restricts electrical conductivity in the corrosion circuits. A coating in conjunction with the cathodic protection system counteracts the corrosion current and inhibits the corrosion process.

The polymeric coatings for the pipelines should possess the following properties [16] that prove adequate performance and long-term durability:

- High specific electrical insulation resistance and dielectric strength
- An efficient barrier to moisture/water/corrosive species
- Good ductile material so that cracking can be resisted

- Adequate strength and adhesion properties so that soil stress can be mitigated
- Compatible with CP systems
- Resist physical damage during shipping, transportation and storage
- Pose no environmental threat or health hazards to public.

For several decades, buried or submerged carbon steel pipeline in oil and gas industry has been protected by applying external polymeric coatings because they are anti-corrosion materials and very economical. As a part of technological advancements, various polymeric coatings have been commercially developed over the few decades. Among various coatings commonly used for buried carbon steel pipelines, six coatings have been chosen for austenitic stainless steel pipelines. Six generic types of coatings are as follows:

1.4.1.1 3-Layer Poly-Ethylene (**3LPE**)

1.4.1.2 3-ply/2-ply Cold-Applied Tape (**3p/2p CAT**)

1.4.1.3 Polyurethane (**PU**)

1.4.1.4 Visco-Elastic (**VE**)

1.4.1.5 Liquid Epoxy (**LE**)

1.4.1.6 Heat-Shrink Sleeve (**HSS**).

The International Standards ISO 21809-1 [17], ISO 21809-3 [18] that address requirements for qualification, application and testing of external coatings for buried or submerged carbon steel pipelines in the petroleum, petrochemical and natural gas industries have been considered applicable to the external coatings for austenitic stainless steel pipeline in buried condition. Each type of coating has been applied separately on each austenitic stainless steel pipe external surface after surface preparation. The coated pipe samples are subjected to various tests to determine the performances of coatings in buried condition.

Brief descriptions of coatings, including application method and drying time, are given below:

1.4.3.1 3-Layer Poly-Ethylene (3LPE)

This coating system is plant-applied three-layer side extruded polyethylene and conforms to the requirements as per ISO 21809-1. This anti-corrosion system consists of 1st layer - FBE (200 μ), 2nd layer - co-polymer adhesive grafted compound (200-250 μ) and 3rd outer layer - UV stabilized HDPE (2400-2600 μ). After blasting and cleaning the pipe from contamination, the pipe is heated by induction heating at about 200°C. FBE powder is sprayed on this heated pipe surface. FBE easily melts and provides excellent adhesion to steel. The adhesive layer is applied by extrusion before the gel time of FBE coating. Extruded polyethylene layer is applied over the adhesive layer immediately. 3LPE coated pipe is then sent for water quenching and holiday detection test. -40°C to 80°C is the operating temperature range for this coating system.

1.4.3.2 3-ply/2-ply Cold-Applied Tape (3p/2p CAT)

The cold-applied multilayer coating system conforms to the requirements as per ISO 21809-3 and consists of a liquid adhesive primer (butyl rubber), a 3-ply layer, and a mechanical outer layer (MDPE with UV stabilizers). After blasting, the pipe surface is made clean & dry, and free from contamination. A liquid adhesive primer (80-100 μ) is applied uniformly on the pipe surface. 3ply anti-corrosion inner layer (tape thickness about 800 μ) is applied spirally (with no less than a 50% overlap) over the primer when it is dry to touch. The outer layer (tape thickness of about 500 μ) is also applied spirally (with no less than a 50% overlap) over the inner layer. Total thickness is about 2500 μ for 3-ply/2-ply CAT. Maximum 60°C is the operating temperature for this coating system.

1.4.3.3 Polyurethane (PU)

The aromatic PU is a reaction product between alcohol and isocyanate. PU coating is Solvent-free and conforms to the requirements as per ISO 21809-3. After thoroughly mixing the resin and activator (usually 3:1 ratio in volume), coating is applied by using heated plural component airless equipment to the blast- cleaned pipe surface to achieve a thickness of about 1000-1500 μ. - 20°C to 80°C is the operating temperature range for this coating system.

1.4.3.4 Visco-Elastic (VE)

Chemical composition of VE coating is Poly-Isobutene. VE is non-crystalline, non-cross-linked, non-reactive. VE is cold applied to the substrate. VE conforms to the requirements as per ISO 21809-3. The thickness of VE tape is about 2000-2500 μ. UV stabilized PVC (Poly-Vinyl Chloride) tape about 500 μ with adhesive is applied over VE tape. Maximum 60°C is the operating temperature for this coating system.

1.4.3.5 Liquid Epoxy (LE)

This coating system is Solvent-Free. This is high-build novolac epoxy. This coating system conforms to the requirements as per ISO 21809-3. After thoroughly mixing part A and part B (usually 3.5:1 ratio in volume), the coating is applied by using heated plural component airless equipment to the blast-cleaned pipe surface to achieve thickness of 800-1500 μ. - 20°C to 80°C is the operating temperature range for this coating system.

1.4.3.6 Heat-Shrink Sleeve (HSS)

This coating system is 3-layer system and conforms to the requirements as per ISO 21809-3. 1st layer - epoxy primer (200-220 μ), 2nd layer - adhesive (200-225μ), and 3rd layer - UV stabilized HDPE (cross-linked) (2000-2500 μ). The blast-cleaned pipe surface is heated at about 80°C and solvent-free two component liquid epoxy primer is applied to the pipe surface. Heat-Shrinkable Sleeve is wrapped around immediately over the wet epoxy. The sleeve is then heated with a propane torch until it shrinks and fits tightly around the joint. The joints between the pipes are welded in the field. The weld joints of the buried pipelines are protected by HSS. Maximum 80°C is the operating temperature for this coating system.

1.5 Austenitic Stainless Steel Pipeline in Above-ground Condition

For above ground portion of austenitic stainless steel pipeline, no coating system is used on their external surface due to the presence of protective passive layer of Cr_2O_3 in atmospheric exposure. Uncoated austenitic stainless steel is prevalent in above ground condition in the petroleum, petrochemical and natural gas industries. For above ground condition, one coating has been selected among six coatings and is subjected to mechanical testing in order to evaluate resistance to damage caused to coating by handling or during transportation and storage.

1.6 Austenitic Stainless Steel Pipeline in Splashed Condition

The pipeline traverses mostly in buried and marginally above-ground conditions, but it can pass sometimes through the areas that are very similar to splashed condition. A splashed condition is defined as the state originated by dropping continuously a small amount of water in the form of droplet on the surface of the structure. Six coatings are subjected to the FTIR analysis and Type D Shore Durometer hardness tests, before and after the salt spray tests, in order to find out the coatings properties [19].

1.7 Research Objectives

The originality of the problem is that bare or uncoated austenitic stainless steels are susceptible to localized pitting corrosion in chloride environment [20, 21] in buried and splashed condition. For above-ground conditions, austenitic stainless steels are susceptible to corrosion in marine environments and under thermal insulation. The objective and scope are evaluation of six coatings on stainless steel pipes in various conditions. Corrosion prevention is crucial in marine environments and under thermal insulation for above-ground conditions. An attempt has been made to evaluate six coatings performances on austenitic stainless steel pipes in different prevalent conditions along with the correlation of the performances with basic parameters.

1.8 References

[1] M.R. Jafari Nasr et al., "Integration of Petrochemical and Refinery Plants as an Approach to Compete in Hydrocarbon Market", ResearchGate Publication 268430340

[2] ASM International, ASM Handbook, "Corrosion: Materials", Volume 13B, (2005), p.55-58

[3] C-O-A Olsson, D-Landolt, "Passive-films on stainless-steels - chemistry, structure, and growth", Electrochimica-Acta, April (2003), p.1093

[4] Béla Leffler, "STAINLESS - Stainless Steels and Their Properties, Passivity", p.9

[5] Mars G Fontana, "Corrosion Engineering", third edition, p.63-67

[6] Herbert H. Uhlig, R. Winston Revie, "Corrosion and Corrosion Control", fourth Edition, p.352

[7] International Stainless Steel Forum (ISSF), Chapter 05, "Corrosion Resistance of Stainless Steels - Pitting and Crevice Corrosion"

[8] ASM International, ASM Handbook, Volume 13C, "Corrosion: Environments and Industries", (2006), p.525

[9] Australian Stainless Steel Development Association (ASSDA), "Guidelines for Use of Stainless Steel underground"

[10] L-Sjögren, G-Camitz et al., "Corrosion-resistance of stainless-steel pipes in soil", European-Commission, Technical Steel-Research, Final-Report (2008), p.15-64

[11] D. A. Jones, "Principles and Prevention of Corrosion", Chapter 7, Macmillan Publishing Company, New York, p.198

[12] ASM International, ASM Hand-book, Volume 13, "Corrosion", fourth printing, (1992), p.3172

[13] Dennis-Neal, "Pipeline-Coating-Failure – Not-Always What-You-Think It Is", Corrosion (2000), Paper-No. 00755

[14] Pierre R. Roberge, ''Corrosion Engineering - Principles and Practice" 2008, p.249

[15] J-M-Sharpley, "Microbiological-Corrosion and its Control", Corrosion-Inhibitors, Edited by CC Nathan, Second-Edition (1974), NACE, p.228

[16] Ronald L. Bianchetti, "Peabody's Control of Pipeline Corrosion, Chapter-2 - Pipeline Coatings", Second Edition (2001), NACE International, p.7-10

[17] International Standard ISO: 21809-1 (2018), 2nd Edition, "Petroleum and Natural Gas Industries - External coatings for buried or submerged-pipelines used in pipeline transportation systems - Part 1: Polyolefin coatings (3-layer PE and 3-layer PP)"

[18] International Standard ISO: 21809-3 (2016), 2nd Edition, "Petroleum and Natural Gas Industries - External coatings for buried or submerged-pipelines used in pipeline transportation systems - Part 3: Field-Joint Coatings"

[19] Amy Forsgren, "Corrosion Control through Organic Coatings", Edition (2006), p.129

[20] Y. Ait Albrimi et al., "Electrochemical Behaviour of AISI-316 Austenitic-Stainless-Steel in Acidic-Media Containing Chloride-Ions". Int. J. Electrochem. Sci., 6 (2011), p. 4614 - 4627

[21] Jung-Gu Kim et al., "Effect of Sulphide and Chloride-Ions on Pitting-Corrosion of Type 316 Austenitic-Stainless-Steel ………", MDPI, Materials (2024), 17, 178, p.1-14.

Chapter - 2

Literature Review

Chapter - 2: Literature Review

2. Introduction

Reviewing the literature is to comprehend existing research pertinent to the present study. It helps to learn about concepts, research methods and experimental techniques that are implemented in the study. The benefit of a literature review is gaining an understanding of the methodology and findings of the existing research. The advantage of a literature review is identifying and highlighting the gaps in the existing research that have not been researched yet. Then it is feasible to address and fill those gaps appropriately through a new research. This chapter provides scientific information that present current knowledge to the chosen topic for research.

2.1 Stainless Steels

Stainless steels are resistant to atmospheric corrosion when minimum 10.5% Cr (chromium) by weight is added to their chemical compositions. Stainless steels are made stable corrosion resistant alloys by adding minimum 12% Cr by weight with less than 1.2% C (carbon)by weight[1, 2]. Corrosion resistance is further improved [3] by adding Ni (nickel) [4-7], Mo (molybdenum) [8-10], Nb (niobium) [11-15], Mn (manganese) [16], N (nitrogen) [17-22], Cu (copper) [23-27], Si (silicon) [28-32] and V (vanadium) [33-35], The stainless steel alloys are shown in Figure 2-1[36].
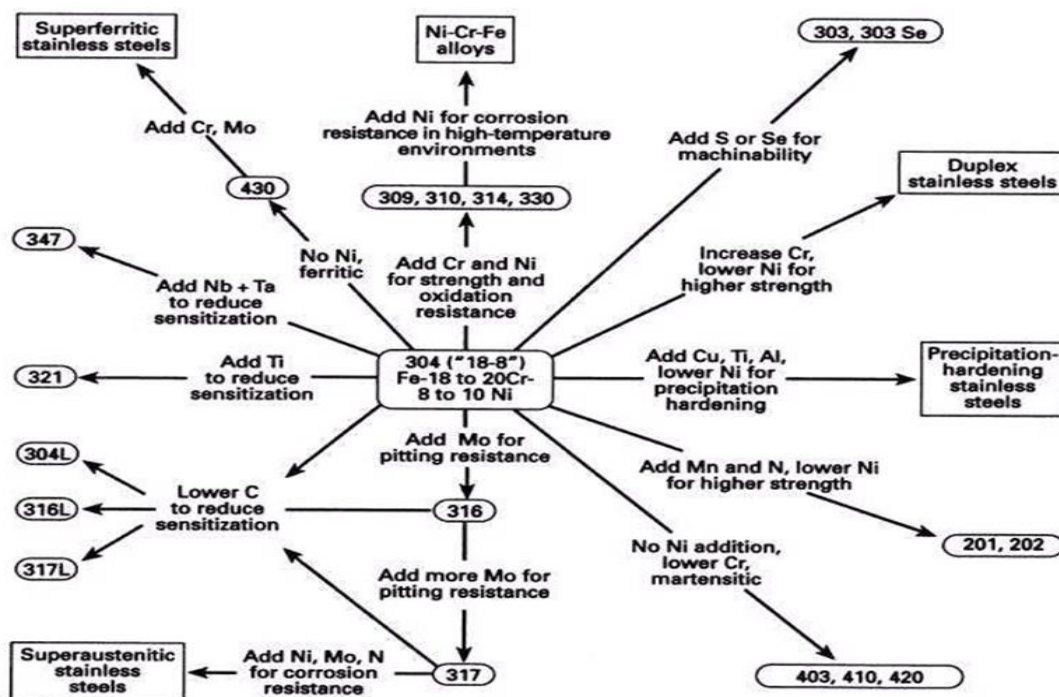
Figure 2.1: Stainless Steel Alloys

Five major families of stainless steels as defined by crystallographic structures are – ferritic, austenitic, martensitic, duplex (ferritic-austenitic), and precipitation-hardening.

Stainless-steels have shown high corrosion resistance in air, water, acid and alkali solutions due to the formation of thin chromium oxide (Cr_2O_3) passive films to few nanometres (nm) on the steel surfaces [37]. When all Cr in chromium stainless steel is in the solid solution and the steel has a single phase structure, the corrosion resistance is very pronounced. But the corrosion resistance is lowered in the presence of the higher carbon content due to the formation of chromium carbide associated with the depletion of Cr from the solid solution[38, 39].

2.1.1 Formation of a Passive Film

The addition of Cr has a thermodynamic effect on corrosion resistance because it increases the stability and protectiveness of the oxide film on steel surface. From the anodic polarization curves for iron-chromium alloys as shown in Figure 2.2 [40], it has been observed that Cr decreases i_{crit} (critical current for passivation), E_{pass} (passivation potential), and i_{pass} (passive current). It can also be seen from this figure that when the steel contains more than 12% Cr (curve 3), a complete passivation is achievable. By the addition of Ni up to 8%, i_{crit}, E_{pass}, and i_{pass} can be decreased further. Based on this reason, 18% Cr-8% Ni steels are extensively used in the industry due to the superior corrosion resistance and ease of fabrication.
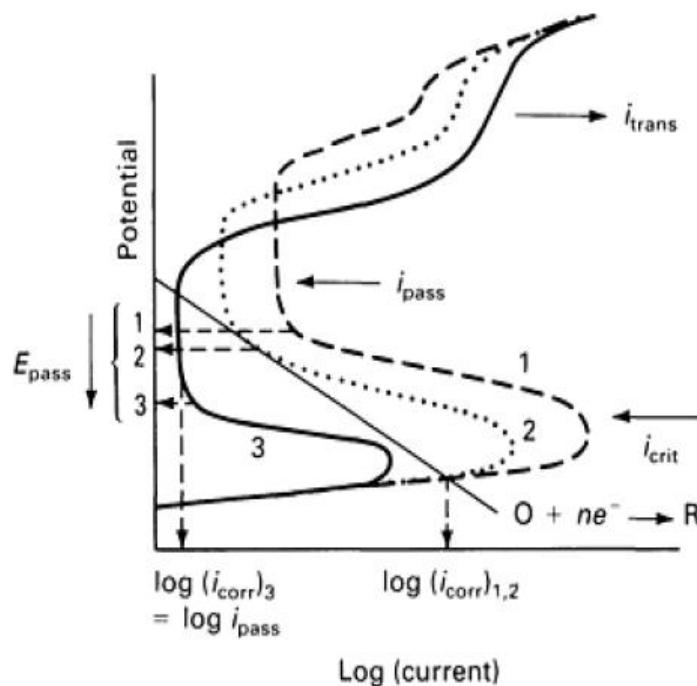
Figure 2.2: Schematic Anodic Polarization Diagrams for Iron-Chromium Alloys
1) 3% Cr, 2) 10%Cr, 3) 14% Cr

2.1.2 Electrochemical Basis for Passivity

The electrochemical basis for passivity of metal and alloys can be explained by studying the active-passive transition in the anodic polarization curve for iron-chromium alloys, as shown in Figure 2.3 [41].
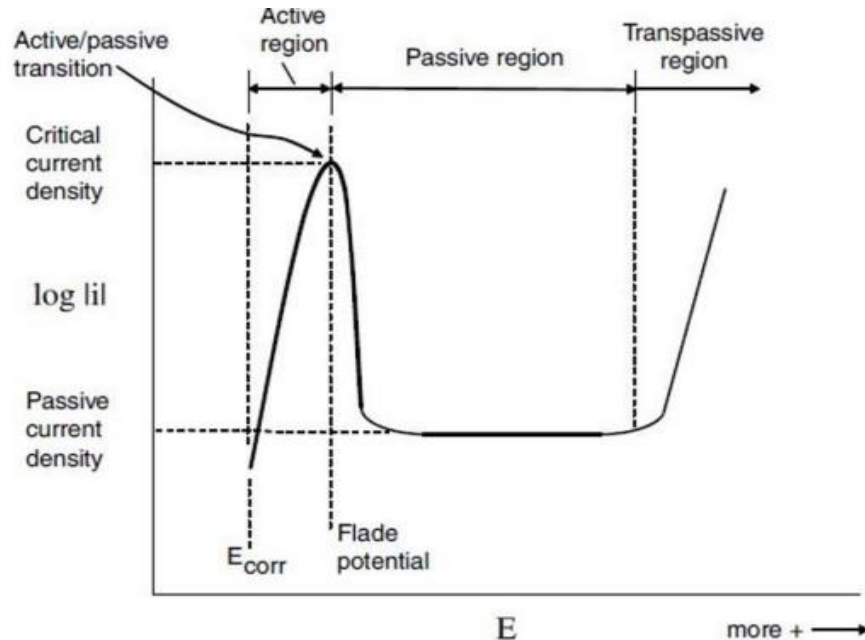
Figure 2.3: Active-Passive Transition for Iron-Chromium Alloys

Beginning with E_{corr} (open-circuit corrosion potential), metal passes through active corrosion region in the anodic direction. In this region, the anodic current density increases and reaches to a maximum value (known as critical current density). But after a certain anodic potential, the anodic current density decreases. Metal undergoes the transition to passive region from active region in the anodic polarization curve. This phenomenon occurs in the active/passive transition region because a protective passive film is formed on the metal surface. When the anodic potential increases further, the anodic current density remains constant (known as passive current density). With further increase in the anodic potential, the anodic current density starts to increase. This happens as metal enters in the transpassive region where due to the dissolution of metallic ion and the evolution of oxygen, the breakdown of passive film on the metal surface occurs.

2.1.3 Austenitic Stainless-Steels

Austenitic stainless-steels contain Cr 18-25 wt% and Ni 8-20 wt% with low-carbon and other elements. The metallurgical structure is austenite, and the crystalline structure is FCC (Face-Centred Cubic). By the additions of the austenite stabilizing elements (Ni, Mn, and N), the

austenite structure is achieved [42-46]. The most common austenitic stainless steels are covered under "300" series and they are 304, 316, 321 (titanium stabilized), 347 (niobium/columbium stabilized) for welding and corrosion resistance [47]. Austenitic stainless steels are not hardenable by heat treatment and are non-magnetic. Compared to ferritic and martensitic stainless steels, austenitic stainless steels provide superior corrosion resistance [48]. By varying C or Mo content, austenitic stainless steels can be suited for various service environments [49-51]. Austenitic stainless steels contain more grades/types than other groups of stainless steels. Austenitic stainless steels are the most common grades among stainless steels for their maximum usages due to their mechanical properties, and ease of fabrication. Typical applications of austenitic stainless steels include consumer items like washing machine, dishwashers, cutlery, kitchen equipment and sinks and industrial equipment like food and beverage, pulp and paper, textile, pharmaceutical, pipeline for transportation, tank and storage vessels, energy production, chemical, oil and gas industry, mining, cryogenic applications [52, 53].

2.1.4 Passivity of Austenitic Stainless Steel

A metal remains in a passive state when it corrodes at a very low rate, but it is active in the EMF (Electromotive Force) series. According to the adsorption theory, passivity of austenitic stainless steels occurs by direct chemisorption of oxygen from the air or from aqueous solutions as Cr has pronounced affinity for oxygen. The surface oxide changes from iron oxide (FeO) to ferric oxide (Fe_3O_4), ferric oxide (Fe_3O_4) to ferrous oxide (Fe_2O_3), and then finally a stable Cr_2O_3 film as the amount of chromium increases [54]. The passive film shifts the measured potential in the noble direction and the steel surface remains in the passive region due to a wide passive potential range of Cr. The passive film lowers the corrosion rate by several orders of magnitude [55, 56] because the thin film of few nanometres is adherent and continuous on the metal surface and acts as a barrier between corrosive environment and the substrate [57-59]. Due to the presence of this oxide films, it is very difficult to wet the surface.

Two basic mechanisms have been reported in the literature to prevail passivity. The first is a diffusion barrier stoichiometric oxide. The second is the formation of a thin surface film of chemisorbed oxygen. This film prevents metal ion hydration [60]. The transition metals (Cr, Ni, Co, Fe, Mo and W) in the periodic table and their alloys show passivity. The electrochemical stability of passivity depends on the passive film electronic property. For thick passive film, the electronic breakdown occurs. But for thin film, the ionic breakdown occurs in the presence of aggressive anions. Depending on the concentration of aggressive anions, either pitting corrosion

continues, or re-passivation occurs [61]. The passive films show low electronic and ionic conductivity at low and medium field strengths, which are less than 1MV/cm. Therefore, the passive films are mostly of barrier types and their reactivities are negligible [62].

The chemical composition as well as the thickness of an electrochemically formed passive film depends on various parameters like potential for passivation, time, temperature and composition of the electrolyte [63-66]. The anodic polarization of Fe-Cr alloy in an acidic solution causes Fe dissolution in the passive region and the passive film is enriched by Cr content [67, 68]. In an alkaline solution, the solubility of Cr is higher than Fe and hence, the passive film is enriched by Fe content [69, 70]. Enrichment or depletion of the different components of a metallic alloy i.e., the compositional changes of passive films occur due to different transport rates and preferential dissolution [71].

XPS (X-Ray Photoelectron Spectroscopy) measurement from a passive film formed on austenitic stainless steel in acidic solution has shown a three-layer model as depicted in Figure 2.4 [72]. Hydroxide is found over an oxide layer. Middle layer is Ni-enriched layer. Metal/film interface and oxide layer are found to be enriched in Ni and Cr respectively.
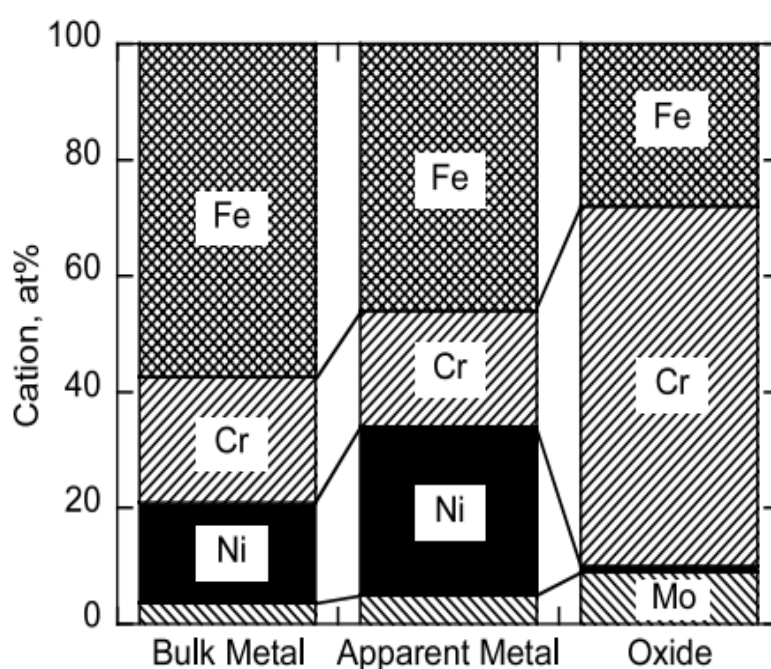
Figure 2.4: XPS Results from a Passive Film formed on Austenitic Stainless Steel

In acidic solution, a thin passive film of few nanometres is formed on the metal surface [73-77]. But it has been found a thick passive film on the metal surface in alkaline solution [78, 79]. It has been reported by another model that a passive film formed on Fe-Cr-Mo alloys consists

of Cr^{III} oxide in the inner layer and Fe^{III} hydroxide, Cr^{III} hydroxide, Mo^{IV-VI} oxide in the outer layer of the passive film. This is shown in Figure 2.5 [80-84].
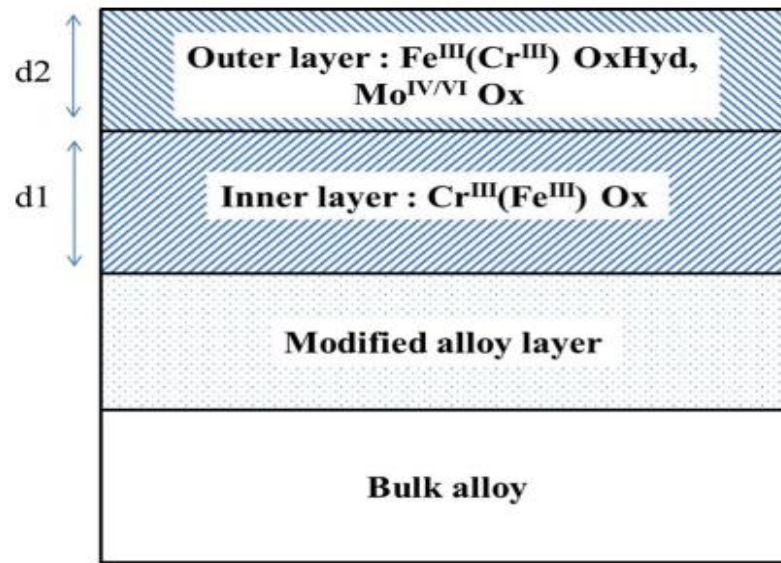
Figure 2.5: Hydroxide and Oxide in a Passive Film formed on Fe-Cr-Mo Alloys

Nickel (Ni) has no significant influence on the passive film [85] because Ni is less reactive with oxygen than Cr and Fe. The passive (oxide) film formed on austenitic stainless steel (Fe-Cr-Ni alloy) has been found similar composition to that of the film formed on stainless steel (Fe-Cr alloy) [86, 87]. A very little or almost no nickel oxide has been observed in the passive film. Ni plays an important role to improve ductility and toughness in austenitic stainless steels than corrosion. Mo has a beneficial effect to prevent anodic dissolution and to increase resistance to localized pitting corrosion in austenitic stainless steels [88, 89]. Mn being an austenite stabilizing element is an important alloying element, but it is harmful because it decreases resistance to localized pitting corrosion in austenitic stainless steels. The reason of the decreased corrosion resistance is due to the formation of non-metallic inclusions viz. MnS (Manganese Sulphides) and MnO (Manganese Oxide). The localized pitting corrosion initiates at these non-metallic inclusions sites [90-94].

2.1.5 Breakdown of Passive Film and Pitting Corrosion of Austenitic Stainless Steels

There is a certain safe range of oxidizing conditions. These conditions are electrochemically measured as oxidizing potentials. The potential range is narrowed in the presence of aggressive anions such as chlorides. Chloride ions(Cl^-) can attack the stainless steel surface when a critical corrosion potential or breakdown potential is reached.

In chloride bearing environment, there is a competitive adsorption on the passive film surface between Cl^- ions and O_2 because the film is usually not free from compositional heterogeneity, surface discontinuities or scratches, and non-metallic inclusions (sulphide inclusions). Cl^- ions migrate through oxygen vacancies into the passive film due to their strong permeability. Cl^- ions attack the passive film locally at an electrode potential which is less noble than the potential for O_2 evolution reaction. The passive film is then not stable over the entire passive region. Cr_2O_3 is dissolved to form CrO_4^{2-} ions. Aggressive Cl^- ions destroy the passive film by dissolving Cr [95]. The dissolution of Cr by Cl^- ions is shown by the Equation (2-1). Cl^- ions then penetrate and reach into metal substrate (Fe) beneath the passive film. The localized corrosion in a very small area of metal surface occurs with the rise of the current density due to rapid dissolution of metal. The attack manifests itself as numerous corrosion pits in a tiny area [96-100]. The passive film breakdown occurs only in isolated and localized locations. Reduction of dissolved O_2 to hydroxyl ions (OH^-) occurs to the adjacent unaffected metal surface. The dissolution of metal in the pit and the generation of hydroxyl ions at the outside of the pit are anodic (oxidation) and cathodic (reduction) reactions for an electrochemical corrosion and are shown by the Equation (2-2) and Equation (2-3) respectively. A combination of separate anodic reaction and cathodic reaction is the theoretical basis of the mixed potential theory published in 1938 by C.Wagner and W.Traud [101, 102]. The mixed potential theory postulates that the rates of anodic reactions are equal to the rates of reduction reactions on a corroding surface to maintain electrical neutrality. Very small anodes of active metal surrounded by large cathode areas of passive metal result in active-passive-cells with a potential difference of about 500 mV between such areas [103] to cause continuous dissolution of metal in the pit.

$$Cr^o + 3Cl^- \rightarrow CrCl_3 + 3e^- \ \ldots\ldots\ldots \ (2\text{-}1)$$
$$M - ne^- \rightarrow M^{+n} \ \ldots\ldots\ldots\ldots\ldots \ (2\text{-}2)$$
$$O_2 + 2H_2O + 4e^- \rightarrow 4OH^- \ \ldots\ldots\ldots \ (2\text{-}3)$$
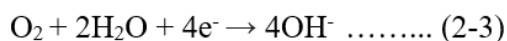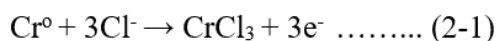
Where,

M = Metal

ne^- = Number of electrons participated in the reaction.

After initiation of pitting, the migration rates of Cl^- ions increase due to the increased concentrations of metal ions (M^+) in the pits for maintaining neutrality. The metal chlorides (M^+Cl^-) are formed by a reaction between M^+ and Cl^- ions. The hydrolysis of M^+Cl^- yields strong

hydrochloric acid in the pit as shown by the Equation (2-4). A high degree of acidity produces a very low pH value at the pit bottom to cause continuous dissolution of metal. A schematic diagram of pitting with its factor and a schematic diagram on the mechanism of pitting corrosion in austenitic stainless steel (SS316L) are shown in Figure 2.6 [104] and Figure 2.7 respectively.

$$M^+Cl^- + H_2O \rightarrow MOH + H^+Cl^- \text{............... (2-4)}$$
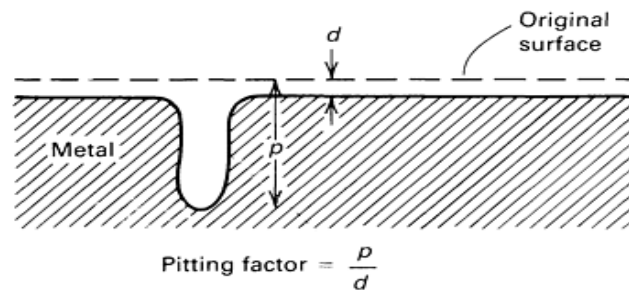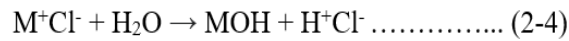
Figure 2.6: Schematic Diagram of Pitting with Pitting Factor
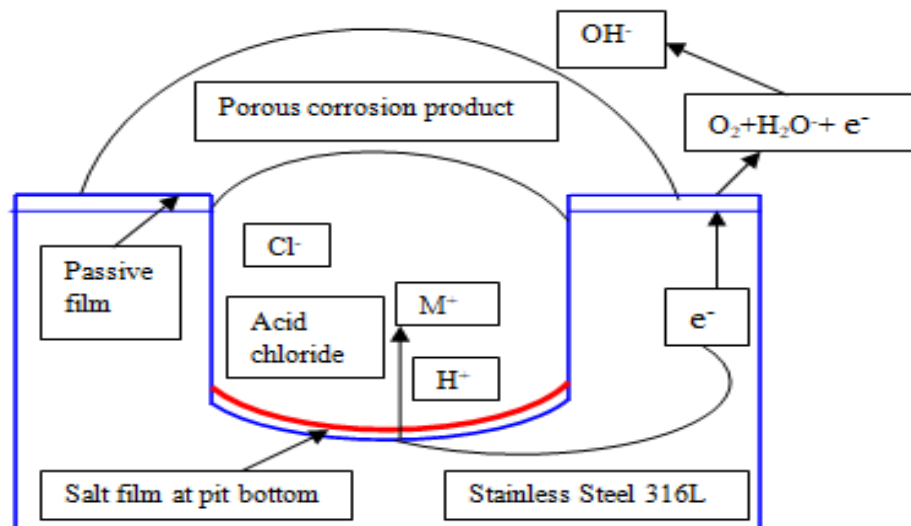
Figure 2.7: Schematic Diagram on the Mechanism of Pitting Corrosion

Once the corrosion pit is formed, there is an O_2 concentration cell in the pit and its adjacent unaffected metal surface. Metal in the pit is exposed to low O_2 concentration and is less positive potential (anodic). The unaffected metal surface is exposed to high O_2 concentration and is more positive potential (cathodic). This can be explained at neutral pH at 25ºC using the Nernst equation for the Equation (2-3):

$$E_L = E^o + (0.059/4) \log \{P(O_2)_L / [OH^-]^4\} \text{.................. (2-5)}$$

$$E_H = E^o + (0.059/4) \log \{P(O_2)_H / [OH^-]^4\} \text{................. (2-6)}$$

25

Where,

E_L = half-cell potentials of electrodes for low O_2 concentration,

E_H = half-cell potentials of electrodes for high O_2 concentrations,

E^o = Standard O_2 potential versus Standard Hydrogen Electrode (SHE),

$P(O_2)_L$ = Oxygen pressures for low O_2 concentrations in the solutions,

$P(O_2)_H$ = Oxygen pressures for high O_2 concentrations in the solutions.

From the Equation (2-5) and Equation (2-6), it can be observed that E_L is less than E_H because $P(O_2)_L$ is less than $P(O_2)_H$. In this situation, the concentrated hydrochloric acid (HCl) at the pit-bottom with O_2 deficiency prevent repassivation process producing the reaction autocatalytic in nature, as shown in Figure 2.8 [105-108]. It renders a difficult situation for repassivation of a growing pit. The repassivation is prevented by the presence of sulphide inclusions too. The high rates of metal dissolution in the pits lead to propagate the pits.
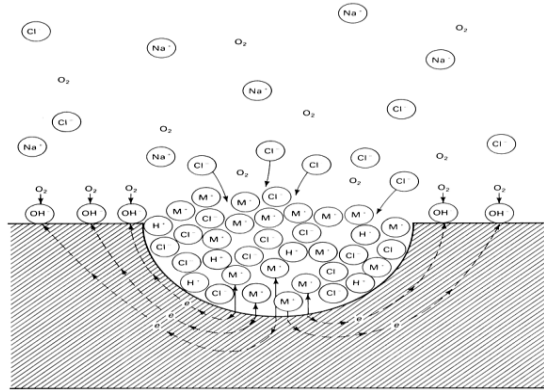
Figure 2.8: Autocatalytic Processes occurring in a Pit

Localized pitting corrosion is insidious because it penetrates to the thickness of austenitic stainless steel rapidly and perforates it within a few days without significant weight loss to the structure [109]. Pitting corrosion remains unpredictable and undetectable until leaks because the localized attack is covered by the porous corrosion products [110]. Passivity breakdown and pitting corrosion of austenitic stainless steels in the presence of Cl⁻ ions are major causes of failures of the structural components [111].

Localized pitting corrosion of austenitic stainless steels (SS316L) in chloride bearing environment can be explained well based on the critical pitting potential (E_{pit}) versus current density semi-logarithmic plot and is shown in Figure 2.9 a). This plot is obtained by the cyclic potentiodynamic polarization test of SS316L in 3.5% sodium chloride (NaCl) solution at 25°C [112-116]. Using the Tafel extrapolation method [117-122], open-circuit potential, and

corresponding current-density are found out. It can be observed from the plot that the current density increases steeply, which indicates the onset of stable pits formation from the transient metastable pitting [123-127]. In the transpassive region, a sharp increase in current density is noticed. It signifies growth of stable pits and
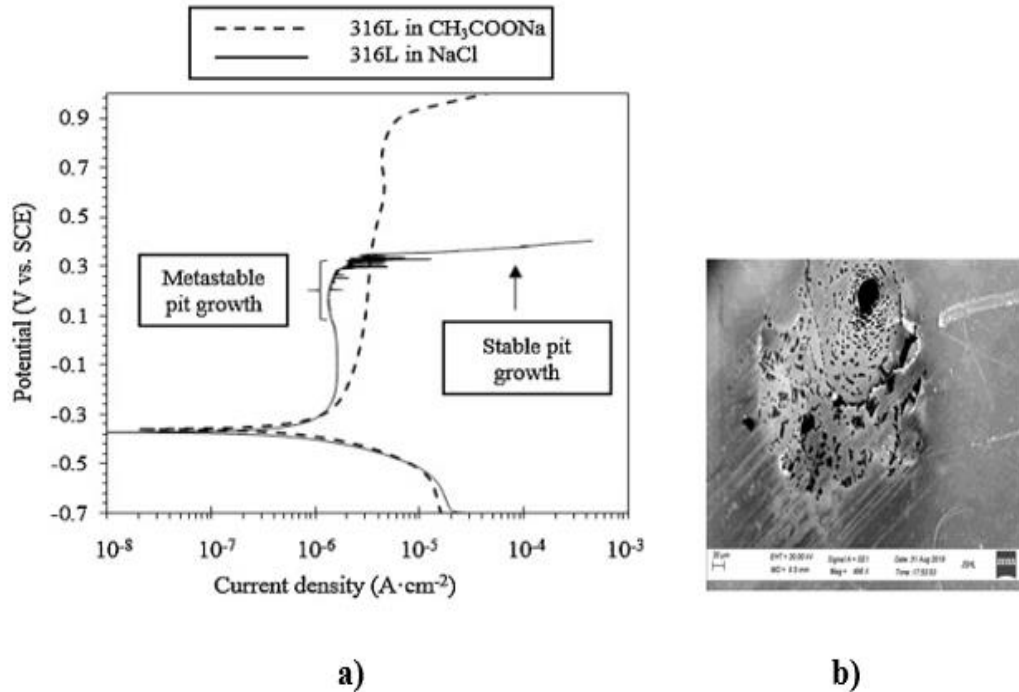
Figure 2.9: a) Cyclic Potentiodynamic Polarization Plot of SS316L, b) SEM Photograph on Pitting Corrosion of SS316L Surfaces

destruction of protective Cr_2O_3 passive film on austenitic stainless steel surface in chloride bearing environment. SEM (Scanning-Electron Microscopy) examination and Figure 2.9 b) have revealed numerous pits on the surface of SS316L material.

2.1.6 Critical Pitting Potential (CPP, E_{pit})

The CPP is the lowest potential at which stable pits are formed. Therefore, below the CPP, stable pits are not favoured, and stable pitting is expected not to occur. There is a chance of pitting due to the following situation:

- Amount of chlorides is high
- Temperature level is high
- pH is low
- No flow condition or flow velocity is low enough
- Low Mo content in stainless steel.

There is an established relationship between E_{pit} and logarithmic Cl⁻ ions concentration for austenitic stainless steels and is shown by the Equation (2-7) [128]. This equation shows that when the concentration of Cl⁻ ions increases, the positive potential of E_{pit} decreases to cause pitting corrosion quickly.

$$E_{pit} = - 0.067\log [Cl^-] - 1.01 \ldots\ldots\ldots (2\text{-}7)$$

Where,

E_{pit} = CPP in volt vs. SCE,

$[Cl^-]$ = Chloride ion concentration in molarity.

Above the critical pitting temperatures of austenitic stainless steels, the pitting potentials decrease slowly and linearly with increasing temperature. The average gradient of this reduction for austenitic stainless steels, types 304, 316, 904L, is -3.3 mV per °C. Such phenomenon occurs at higher temperatures because the passive film becomes thicker, but more porous and thus less protective [129].

2.1.7 Critical Pitting Temperature (CPT)

The CPT is the lowest temperature at which pitting corrosion occurs on the austenitic stainless steel surface [130]. Pitting tendency increases with increasing temperature. As the CPT increases, the CPP decreases. The CPT is usually measured in an aggressive Cl⁻ solution (NaCl or $FeCl_3$ solution). The CPT in combination with the PRE (Pitting Resistance Equivalent) is used to evaluate the susceptibility of austenitic stainless steel to pitting corrosion. The PRE value is computed based on the chemical composition of austenitic stainless steel, mainly Cr, Mo, and N. There are several equations to calculate the PRE values, but the following Equation (2-8) is commonly used in the industry to rank the susceptibility of stainless steels:

$$PRE = \%Cr + 3.3 \text{ x } \%Mo + 16 \text{ x } \%N \ldots\ldots\ldots (2\text{-}8)$$
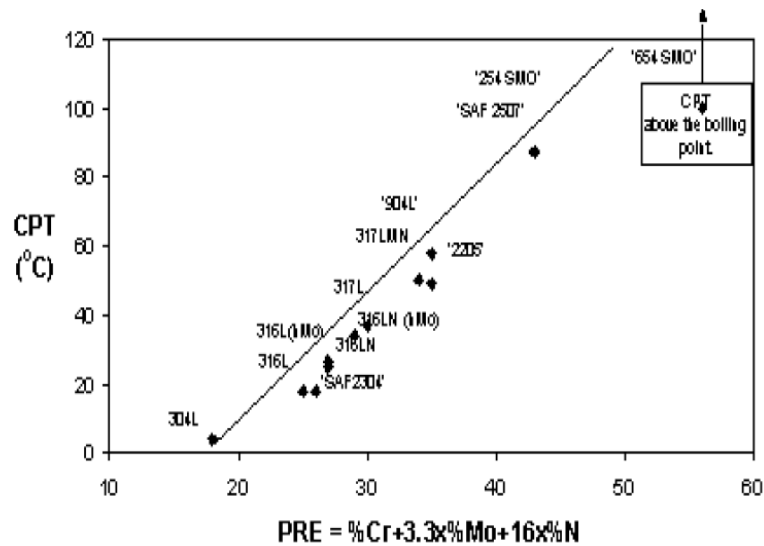
Figure 2.10: Relation between CPT and PRE Values of Austenitic Stainless Steels

The relation between the CPT and the PRE for austenitic stainless steels is shown in Figure 2.10 [131]. Higher PRE values indicate that higher temperatures are needed to initiate pitting attack on austenitic stainless steels surfaces.

2.2 Corrosion of Metals buried in Soils

Underground (buried condition) corrosion of metals occurs in aqueous environments. The aqueous environment is moist soil. The reactions in moist soil are electrochemical reactions. After these reactions, metals return to their native states as oxides and salts. Noble metals like gold, platinum and copper are resistant to corrosion. These metals exist in metallic states in nature. But other metals like carbon steel and low-alloy steels are used for underground structures after protecting them from moist soil. Unless protected, they can suffer corrosion damage, which is an irreversible process.

Many studies have been conducted on soil corrosivity of metallic structures those are placed in direct contact with the soil environment. The buried pipelines traverse long distances and pass through soils with varied textures and depths. Moreover, the dissolved salts in soils also increase the corrosivity of the soil. From practical experiences, it has been observed that the durability of the buried steel structures depends on corrosion susceptibility of soils [132].

There has been serious engineering as well as economic problems when the metallic structures like pipeline steels, carbon steel tanks and some selected stainless steels are in direct contact with soils or buried in soils [133, 134]. The external corrosion of carbon steel pipelines

and carbon steel tanks in buried conditions has attributed to their failures and hence, an underground corrosion is of great importance for buried structure [135]. To avoid or control corrosion, the pipeline shall be inspected and maintained regularly. Sometimes, it may need replacement also according to the condition. Figure 2.11(a) and Figure 2.11(b) [136] have shown situations where a buried steel pipeline is in direct contact with the soil environment and the pipeline is protected by a protective coating respectively. Corrosion does not occur where a protective coating remains intact because pipeline is not in direct contact with the soil environment. But, the trapped water or the ingress of water due to the failure of a coating can cause corrosion.
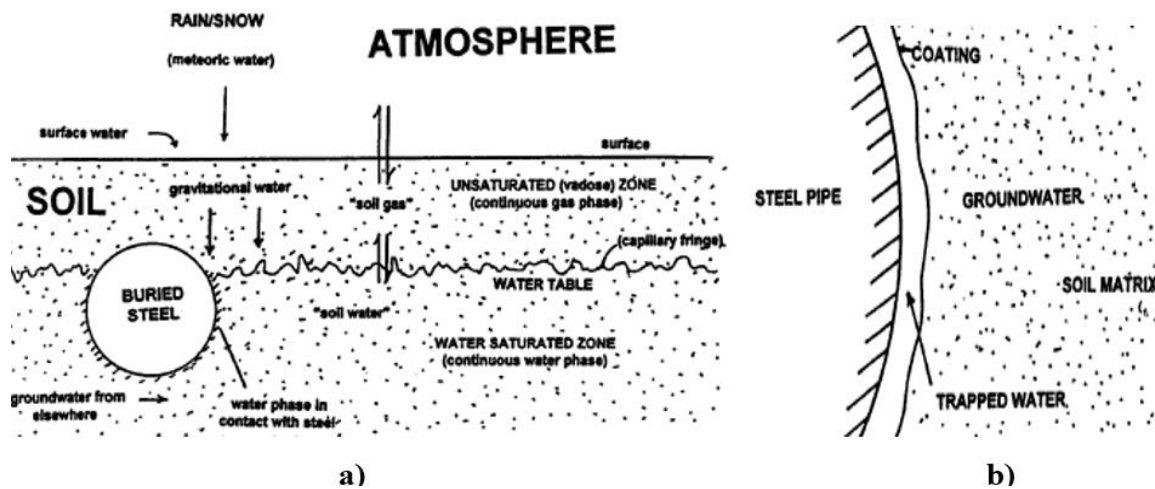
Figure 2.11: a) Buried Pipeline in contact with Soil Environment, b)Tapped Water or Ingress of Water causes Corrosion

Soils are complex materials. Soils are an admixture of disintegrated rock by physical action, precipitated materials from aqueous solution, and organic matter. Water and gas occupy the spaces between solid particles in soil and these spaces are about 50% volume of dry soil. Bulk water can flow through porous soil, but some water is bound to mineral surfaces. Water flows through soil depending on the size and distribution of the solid particles in the soil. In fine-grained soil, water is drawn by capillary action and stayed there. In such situation, soil remains saturated with water. Drainage is prevented and evaporation is retarded. A limited oxygen from atmosphere can reach to the pipeline buried in soil. On the other hand, good and excellent drainage is observed for coarse-grained soil. A fair amount of oxygen from atmosphere can reach to the buried pipeline.

The electrochemical corrosion occurs on metal surfaces in soil in the presence of the groundwater. The groundwater composition is influenced by the climate [137] and type of soil.

The groundwater in tropical climate is found to be very acidic, whereas the groundwater in desert region is found to be very corrosive due to high chlorides. Some clay soils buffer pH of the groundwater [138].

Most metals usually corrode by reacting with their environments. The three elements - an anode, a cathode, an electrolyte and their connections are responsible for occurring corrosion. Oxidation of metal 'M' occurs at anode. M^+ goes into the solution according to the following Equation (2-9)

$$M \rightarrow M^+ + e^- \ldots\ldots\ldots (2\text{-}9)$$
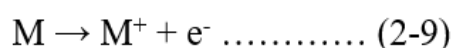
During corrosion of steel (which is mainly composed of iron), the anodic reaction occurs according to the following Equation (2-10)

$$Fe \rightarrow Fe^{2+} + 2e^- \ldots\ldots\ldots (2\text{-}10)$$

The electrons released by the oxidation reaction move through the metal circuit to the cathode, where reduction reactions occur. Corrosion rates of steel structures buried in soil are noticed higher than in the atmosphere, although these rates depend on the soil composition, pH, moisture and oxygen content, dissolved salts.

There are various factors that control corrosivity of a soil. Buried steel structures like tanks and pipelines suffer from soil corrosion due to the following factors:

- Soil with high water content,
- Soil pH less than 4.5,
- Soil resistivity less than 1000 ohm.cm,
- Soil with high level of salts like chlorides, sulphides, and other dissolved species,
- Soil with bacteria and microorganisms,
- Soil where there is presence of stray currents.

The anodic and cathodic polarization characteristics of a metal in a soil are also affected by these factors. Corrosion rates of underground structures are calculated using Stern-Geary linear polarization equation or by weight loss method.

2.2.1 Corrosion of Austenitic Stainless Steels buried in Soils

Uncoated or bare austenitic stainless steels have been provided excellent service in soils based on the nature of the buried condition. Austenitic stainless steels buried in soils have been performed well where the protective passive films remain in intact condition and where there is a good water drainage system, and soil has high resistivity. Although uncoated austenitic stainless steel pipelines have been reported to be in use in buried condition for different purposes on a limited scale[139], corrosion resistance of uncoated austenitic stainless steel pipelines in soil is doubtful and uncertain. Low resistivity soil with chlorides ions (Cl^-) and a deficient in oxygen is more vulnerable to attack stainless steel pipeline. Cl^- ions break down passive layer of austenitic stainless steel locally. Due to a breakdown of the passive film at localized or selective areas of the material surface, corrosion of austenitic stainless steel occurs. The localized attack leads to perforate austenitic stainless steel structures within a few days without significant loss in weight of the components.

2.2.2 Guidelines for Austenitic Stainless Steels buried in Soils

The general guidelines in the industry for austenitic stainless steels buried in soil [140, 141] are as follows:

- Uniform soil packing to avoid differential aeration effects,
- Well drained water from soil and good drainage system,
- Soil pH greater than 4.5,
- Resistivity of soil greater than 2000 ohm.cm,
- Backfilling stainless steel without organic materials to avoid microbial attack,
- To avoid carbon-containing ash in contact with stainless steel in soils to prevent. localized galvanic attack,
- Sand backfilling with good drainage system,
- At least a few ppb of oxygen to maintain passive film on stainless steels,
- To avoid chloride-bearing environment and high salinity in buried condition,
- Avoidance of stray current caused by local D.C (Direct Current) systems.

On a more practical level, it shall be ensured that unprotected austenitic stainless steel is suitable for the soil environment in buried condition, where no stagnant water is accumulated in contact with the buried pipe. The unprotected pipe otherwise can suffer localized corrosion. If such aggressive environments cannot be avoided or controlled, unprotected austenitic stainless

steels in buried conditions need to be coated with suitable polymeric coatings to prevent from soil corrosion.

2.2.3 Types of Soils

Natural soil is a mixture of sand, gravel, loam, silt and clay, where the particles sizes are varying. Some particles contain water and soluble salts, which make them highly corrosive. Some particles contain organic materials. The source of these organic materials is decaying plants or carbon-containing ash. These organic materials provide nutrients for Microbiologically Induced Corrosion (MIC) or galvanic corrosion. The presence of water and dissolved corrosive salts in soil and the access of oxygen from the atmosphere increase the rate of corrosion.

Soil corrosivity is determined by soil resistivity because corrosivity is associated with electrochemical reaction in soils. Corrosion reaction is slow when soil resistivity is high. Soil resistivity decreases with increasing moisture and the concentration of corrosive species. The classification of soil is made based on their types, particle sizes, moisture content etc. and is shown in Table 2.1 [142]. Soil resistivity provides a basis to estimate soil corrosivity. The corrosive nature of soil has been established based on the resistivity and is shown in Table 2.2 [143].

Table 2.1 and Table 2.2 are the simplified classifications of soils and soil corrosivity respectively. Sandy soils are least corrosive due to their high resistivity. Clay soils containing saline water are extremely corrosive because of their very low resistivity.

Table 2.1: Classifications of Soils
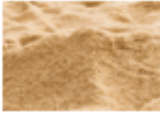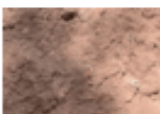
Type of Soil	Particle Size and Moisture	Chemical Composition (main constituents and contaminants)	Soil Resistivity (ohm.cm)
Sand	Fine : 0.02 / 0.06 mm Medium : 0.06 / 0.2 mm Coarse : 0.2 / 0.6mm Good drainage	SiO_2	10,000 - 500,000
Gravel	Fine : 2 / 6 mm Medium : 6 / 20 mm Coarse : 20 / 60 mm Excellent drainage	SiO_2	20,000 - 400,000
Loam	Plastic mixture, High moisture	SiO_2, Al_2O_3, ... Dissolved species: H^+, Cl^- SO_4^{2-}, HCO_3^-, ...	3,000 - 20,000
Silt	Very plastic mixture, High moisture	SiO_2, Al_2O_3, ... Dissolved species: H^+, Cl^- SO_4^{2-}, HCO_3^-, ...	1000 - 2000
Clay	Coarse clay, High moisture	SiO_2, Al_2O_3, ... Dissolved species: H^+, Cl^- SO_4^{2-}, HCO_3^-, ...	500 - 2000

Table 2.2: Soil Resistivity and Corrosivity Rating

Soil Resistivity (ohm.cm)	Corrosivity Rating
< 1000	Extremely corrosive
1000 - 3000	Highly corrosive
3000 - 5000	Corrosive
5,000 - 10,000	Moderately corrosive
10,000 - 20,000	Mildly corrosive
>20,000	Non-corrosive

Austenitic stainless steels have been subjected to localized corrosion in a wet soil containing chlorides where the soil conductivity is very high, or the soil resistivity is very low. In the absence of microbes in soil, the resistance of aquatic soil is taken into consideration the important parameter to occur or to prevent corrosion. Poorly-drained soils are recognized to be highly corrosive than well-drained ones.

2.2.3.1 Alkaline Soils

The pH of alkaline soil falls within the range 8-10. In dry and arid regions, soluble salts are transported to the upper soil layers through capillary action. Then these salts evaporate and make soil alkaline in nature. Reduction of water occurs under alkaline conditions, where the electrons released from the anodic sites are consumed by the following Equation(2-11):

$$O_2 + 2H_2O + 4e^- \rightarrow 4OH^- \quad \text{…………...} \quad (2\text{-}11)$$

The hydroxyl ions (OH^-) migrate through the soil moisture to the anode to react with positive metal (Fe) ions to produce solid corrosion products according to the Equation (2-12).

$$Fe^{2+} + 2OH^- \rightarrow Fe(OH^-)_2 \downarrow \quad \text{………….} \quad (2\text{-}12)$$
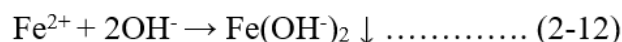
The final product is known as rust, as shown by the following Equation (2-13)

$$2Fe(OH^-)_2 + \tfrac{1}{2} O_2 + H_2O \rightarrow 2Fe(OH^-)_3 \quad \text{………} \quad (2\text{-}13)$$
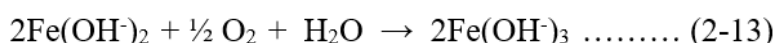
This product tends to deposit on iron surface. This product gives a barrier layer and ionic species cannot diffuse to iron.

2.2.3.2 Acidic Soils

Acidic soils are found to have pH below 6.0. The soil is made acidic when heavily leaching of mineral and salts occur. In the presence of oxygen, reduction of oxygen occurs under acidic conditions, and is shown by the Equation (2-14):

$$O_2 + 4H^+ + 4e^- \rightarrow 2H_2O \quad \text{…………...} \quad (2\text{-}14)$$
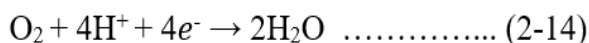
In the absence of oxygen, hydrogen reduction occurs according to the following Equation (2-15):

$$2H^+ + 2e^- \rightarrow H_2 \uparrow \ldots\ldots\ldots (2\text{-}15)$$
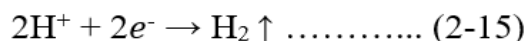
Under acidic soil conditions, no corrosion product is produced, and the steel substrate surface remains unprotected. Therefore, acidic soils pose a serious threat to construction materials including some stainless steel grades commonly used in the industry.
.

2.2.3.3 Effect of Soluble Salts in Soil on Corrosion

Soluble salts in soil are detrimental from corrosion point of view. An increase in soluble ions such as chlorides, sulphates, sulphides increase electrolytic conductivity and decrease soil resistivity resulting in an increasing corrosion rate of unprotected austenitic stainless steel. Some ions such as calcium and magnesium have the opposite effect. A deposit of insoluble calcium carbonate and magnesium carbonate on metal surface reduces corrosion rate [144-148].

2.2.3.4 Effect of Chloride Ions in Soil on Corrosion

Chlorides are found naturally in soils from geological seabed or from the brackish groundwater. Chlorides are ionized in aqueous solutions according to the following Equations (2-16), (2-17), (2-18), (2-19):

$$Fe + 2H^+ \rightarrow Fe^{2+} + H_2 \uparrow \ldots\ldots\ldots\ldots (2\text{-}16)$$

$$Fe^{2+} + O_2 + 4H^+ \rightarrow Fe^{3+} + 2H_2O \ldots\ldots\ldots(2\text{-}17)$$

$$Fe^{3+} + 3Cl^- \rightarrow FeCl_3 \ldots\ldots\ldots\ldots\ldots (2\text{-}18)$$

$$2FeCl_3 + 3H_2O \rightarrow Fe_2O_3 + 6HCl \ldots\ldots\ldots (2\text{-}19)$$
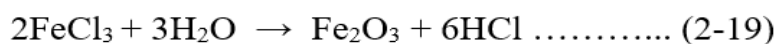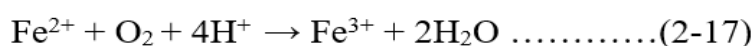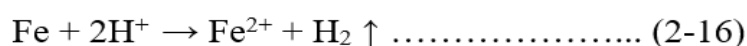
The concentration of Cl^- ions varies in the soil electrolyte based on the wet and dry conditions of the soil and makes soil corrosive or non-corrosive. They tend to decrease soil resistivity. Cl^- ions are harmful as they participate directly and cause pitting initiation of austenitic stainless steels in the localized region.

2.2.3.5 Effect of Sulphate Ion in Soil on Corrosion

The presence of sulphate in soil is found to be in different forms. These forms are water soluble (sodium sulphate), sparing soluble (calcium sulphate) and insoluble sulphate (potassium and ferric iron sulphate). Sulphate film is less protective than iron oxide film and hence, an active corrosion occurs from a buildup of sulphate film. Under immersion and cathodic protection conditions, sulphates are found to be very harmful when they are present alone or in combination with chlorides. In comparison with chlorides, sulphates alone are less aggressive. Soils that contain sulphates and are poorly aerated, anaerobic SRB (Sulphate Reducing Bacteria) are active. Soils become more corrosive than soils free from these bacteria. Due to this reason, the presence of sulphates poses a threat for austenitic stainless steels structures.

2.2.3.6 Microbiologically Induced Corrosion (MIC)

MIC refers to corrosion resulting from the activities of microorganisms. Anaerobic SRB plays a major role in soil corrosion. The products produced by the bacteria through their metabolism are very corrosive. It has been reported that under microbial consortia, i.e., the interaction of MRB (Metal Reducing Bacteria), APB (Acid Producing Bacteria), SRB (Sulphate Reducing Bacteria), MOB (Metal Oxidizing Bacteria) in complex manner, an aggressive MIC occurs [149, 150]. These bacteria convert sulphates to highly corrosive sulphides according to the following Equation (2-20):

$$SO_4^{2-} + 8H^+ + 8e^- \rightarrow S^- + 4H_2O \ldots\ldots\ldots\ldots\ldots (2-20)$$
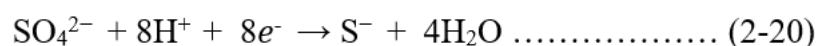
SRB reduces sulphate ions to sulphides ions. These sulphides ions react with metal surface to lead corrosion. The microorganisms usually operate under the following environmental conditions:

- Temperature = 25°C± 5°C
- pH = 6 - 8
- Resistivity of soil = 500 - 20,000 Ω.cm.

2.2.3.7 Oxygen Concentration Cell in Soil

Oxygen is needed for cathodic reaction to occur. But the oxygen levels at the cathodic sites remain different based on the types of soils. Clay soil contain low oxygen and is anodic, whereas loam soil contains high oxygen and is cathodic. A potential difference will remain between these areas and underground pipeline will experience corrosion in low oxygen area. This has been shown in Figure 2-12 [151].
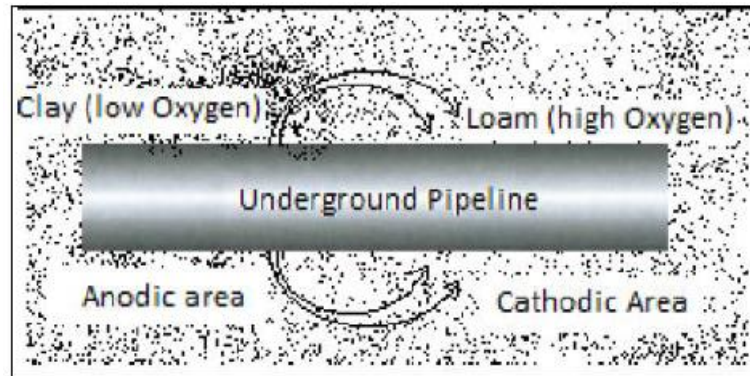
Figure 2.12: Differential Aeration Corrosion of Buried Pipeline

The area of lower oxygen concentration becomes the anode, whereas the area of higher oxygen concentration becomes the cathode. From the oxygen concentration of the soil moisture, the redox potential is determined. The higher oxygen content yields the higher redox potential. When redox potential is low, it provides an indication of low oxygen content that is a favourable condition to anaerobic bacteria (like SRB) to initiate their microbiological activities.

2.2.3.8 Stray Current Corrosion

Stray current is the undesired current. Stray current is found to be caused by the local direct current (DC) electric transportation systems. The typical systems are as follows:

- Railways, trams,
- Cathodic protection systems for pipelines buried in soils,
- DC power supply.
- DC welding equipment.

Corrosion caused by stray current is called stray current corrosion. Stray direct current (DC) [152] enters the metallic structure in one area from an outside source and flows onto the pipeline. When stray current leaves the pipeline at some other area and re-enter the earth, corrosion occurs at that area of the pipe. The circuit is completed by returning of the current to the original DC power source.

Stray current corrosion is identified as localized general loss rather than pitting. It is also very rapid. The stray current is suppressed with a proper electrical insulation of the pipe by applying polymeric coatings and/or cathodic protection (impressed current or sacrificial anode) system.

38

2.3 Corrosion Protection for Austenitic Stainless Steel Pipelines buried in Soils

It is imperative to select appropriate polymeric (organic) coatings and to apply on the external surfaces of austenitic stainless steel pipelines buried in soil for protection against underground corrosion. Protective coating in conjunction with CP system is used for pipeline longevity and reliability as well as safe transportation of the petrochemical products. In addition to the selection of the proper coatings, other variables such as underground environment, surface preparation of the substrate, application of coatings and their visual inspection are important.

2.3.1 Environment

The environment is an important factor because a surface coating is in direct contact with the electrolyte i.e., underground soil contaminated with water and dissolved salts. The environmental conditions can have a significant effect on the performance and durability of the coating.

2.3.2 Surface Preparation of Austenitic Stainless Steel Pipelines

The performance of the coating depends on appropriate surface preparation of a pipeline. Surface preparation lays the foundation that ensures proper adhesion and durability of a coating. Surface preparation plays an important role because it affects both surface tension and wetting as well as good bonding [153]. In most cases, coating failures are resulted from inadequate surface preparation. Sometimes, surface preparation can account about 50% of the total cost. The most effective surface preparation method for austenitic stainless steel pipelines is abrasive blasting. The external surfaces are prepared by fused alumina fine particles for a high level of adhesion [154, 155].

Fused alumina is a high purity of aluminium oxide and is an appropriate abrasive for austenitic stainless steel because this blasting medium is iron-free and reusable. Fused alumina is manufactured by the fusion of calcined alumina in electric arc furnaces. After electro-fusion, fused alumina is crushed and milled. Then the material is sieved to obtain the required grain sizes [156]. It results in transforming γ-aluminium oxide to α-aluminium oxide. Fused alumina is synthetic hard mineral. Hardness of fused alumina is 9 on the Mohs hardness scale. Due to high hardness, sharp-edged grains of fused alumina facilitate to achieve a very low roughness value (Roughness Average, Ra) of austenitic stainless steel surface finish and good polish. Such surface finish ensures proper adhesion and longevity of a coating on austenitic stainless steel surface.

2.3.3 Application of Coatings

Coatings are mostly shop-applied, but it can also be field-applied. The production rates of shop-applied coatings are high in comparison with field-applied coatings because shop application is performed at ease and controlled easily. Surfaces are made dry and free from contamination prior to coating.

2.3.4 Visual Inspection of Coated Surfaces

Visual inspections are carried out on all coated surfaces. Visual inspection of a coating applied on austenitic stainless steel pipe ensures that the coating is continuous, and the two parts of the coating overlap are maintained properly without any wrinkle. The coated surfaces are free from blisters, cracks, chips, pits, loosely adherent particles, lumps, coarse areas. The coating has a uniform appearance and no discoloration.

2.3.5 Polymeric Coatings for Pipeline External Corrosion Protection

The six generic polymeric coatings for austenitic stainless steel pipelines are:

- 3-Layer Poly-Ethylene (**3LPE**)
- 3-ply/2-ply Cold-Applied Tape (**3p/2p CAT**)
- Polyurethane (**PU**)
- Visco-Elastic (**VE**)
- Liquid Epoxy (**LE**)
- Heat-Shrink Sleeve (**HSS**).

The protective coating provides protection against corrosion primarily by two means - firstly, the coating film prevents ingress of corrosive species to the metal substrate by barrier resistance and secondly, the coating film restricts electrical conductivity by high electrical resistance as the coatings are electrically insulating materials with high dielectric strengths.

The protective coatings for buried pipelines should have the following properties:

- High electrical resistance in order to isolate pipeline external surface from the electrolyte,
- An effective moisture barrier to prevent corrosion,
- Good ductility to prevent cracking,
- Adequate strength and adhesion to mitigate soil stress and handling in the field,
- Compatible with cathodic protection to prevent shielding,
- Resistant to chemical and physical damage or degradation during storage and transportation,
- Do not pose a threat to environment or human health.

2.3.5.1 3-Layer Poly-Ethylene (3LPE)

3LPE consists of 3-layerscoating system and is applied in the plant only. First layer consists of FBE (Fusion Bonded Epoxy). Second layer is a copolymer adhesive, and third (top) layer is PE (Polyethylene). FBE is fusion bonded with the blasted steel surface. Copolymer adhesive has excellent chemical bonding between FBE and topcoat (i.e. PE). PE is used for protection against any physical damage of the pipes during transportation and storage. A schematic diagram of 3LPE coating manufacturing process and a typical 3LPE coated steel pipe are shown in Figure 2.13 and Figure 2.14 [157] respectively.
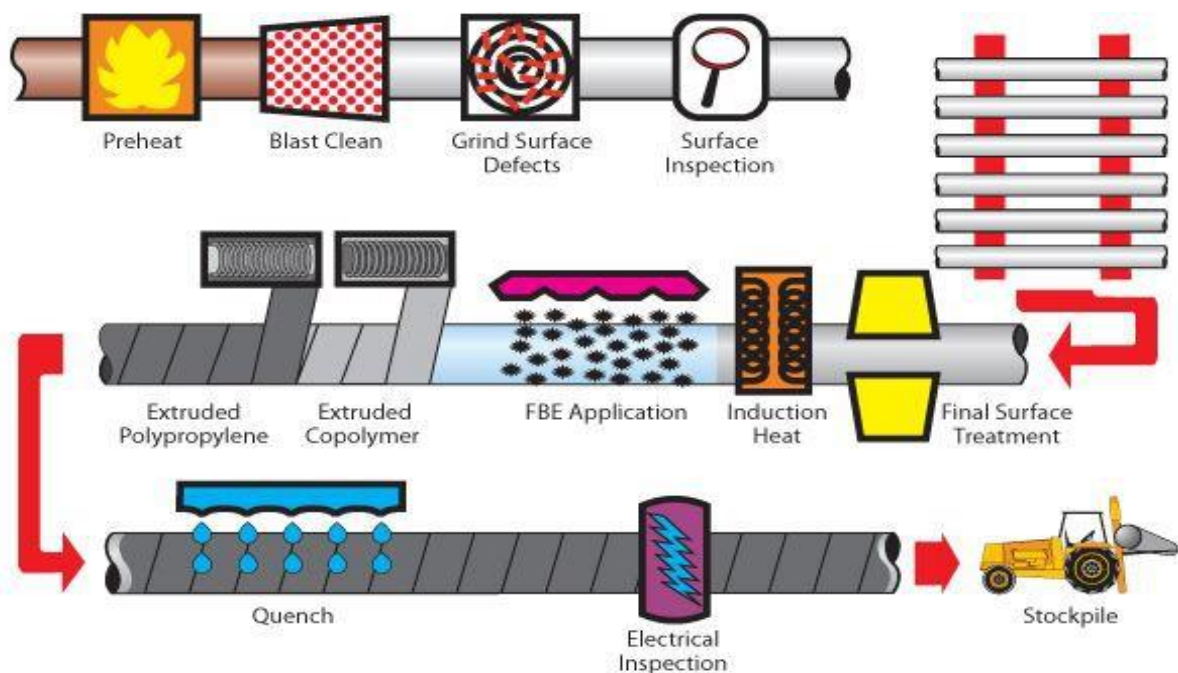
Figure 2.13:A Schematic Diagram of 3LPE Coating Manufacturing Process
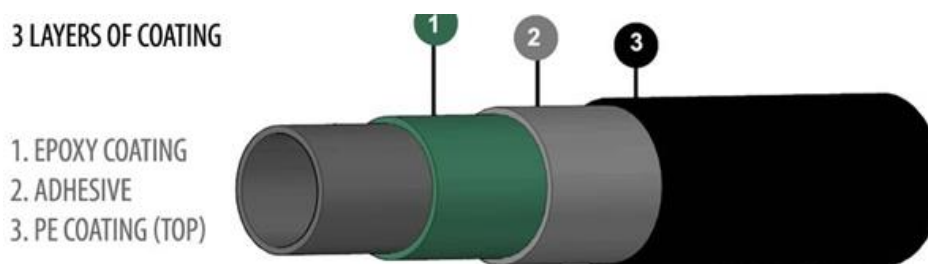
Figure 2.14:3LPE Coated Steel Pipe

The typical formulation for FBE coating consists of epoxy resin, curing agent, extenders and fillers, colour pigments, catalysts for regulating flow and stability. The resin and curing agent together is known as binder. In epoxy resin, one oxygen atom is connected to two carbon atoms i.e., it contains a three membered cyclic ring.

FBE resins are derivatives of bisphenol A and epichlorohydrin. The structure of unmodified bisphenol A type epoxy resin is shown in Figure 2.15, where n = number of polymerized sub-units = 0 - 25 [158].
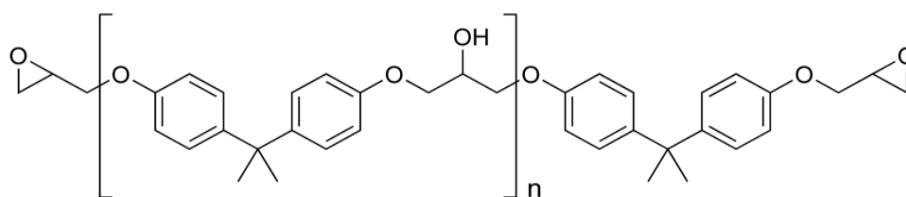
Figure 2.15: Bisphenol A - FBE Resin

In FBE coating, the epoxy resin is formulated to meet the specifications and protect steelas an anti-corrosion coating. Resins are available in various molecular lengths so that unique properties are achieved to the final coating. FBE is applied to the blasted and heated steel pipe as a primer coat. After coating application, the molten powder becomes a solid on the heated pipe surface within few seconds by chemical cross-linking of epoxy resin. The cross-linking reaction of epoxy resin is irreversible, and FBE coating is, therefore, a thermosetting coating.

The second layer is co-polymer hot melt adhesive. This adhesive is a maleic anhydride (MA) grafted PE (MA-g-PE) based thermoplastic polymer that contains anhydride functionality and is shown in Figure 2.16 [159].
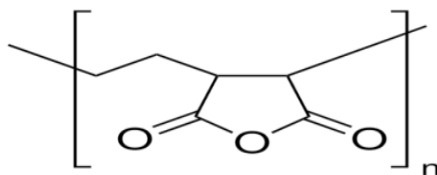
Figure 2.16: Maleic Anhydride (MA) Grafted PE

Grafting is a chemical reaction by polymerization, in which one or more polymer side chains are attached to the main chain of the base polymer via covalent bond. Grafting alters polymer charges, hydrophilic ability, and rheological properties of the base polymer. It enhances interfacial interaction between FBE (polar material) and PE topcoat (covalent and non-polar material). Other than grafting efficiency, finer particles sizes of adhesive and shorter coating interval time between adhesive and PE give the best adhesion performance of 3LPE coating systems [160].

The third layer (topcoat) is HDPE (High-Density Polyethylene), a linear version of polyethylene. HDPE is a thermoplastic polymer made from the polymerization of ethylene. Its generalized chemical formula is $(C_2H_4)_n$. The general chemical structure of HDPE is shown in Figure 2.17.HDPE possesses high strength-to-density ratio. It provides high molecular weight with a broad molecular weight distribution resulting in excellent melt strength for easy processing[161]. Due to this, it ensures heat deformation properties and high resistance to environmental stress cracking. It also enhances mechanical properties like impact, indentation, and abrasion resistance in the range of operating temperature from -45°C to +85°C.

Figure 2.17: Chemical Structure of HDPE

It provides complete protection against high water table, corrosive soil, severe weather those are likely to be encountered along the pipeline route. HDPE is used with UV stabilizers because UV radiation, moisture, heat are the major causes to degrade organic coatings exposed to sunlight. UV radiation breaks the bonds i.e., backbone of a polymeric coating [162]. HDPE with UV stabilizer provides tough, durable protection from UV radiation and thus increasing service life in outdoor environments such as storage and transportation.

2.3.5.2 3-ply/2-ply Cold-Applied Tape (3p/2p CAT)

The cold-applied multilayer coating system conforms to the requirements as per ISO 21809-3 and consists of a liquid adhesive primer (butyl rubber), a 3-ply layer, and a mechanical outer layer (MDPE with UV stabilizers). Maximum 60°C is the operating temperature for this coating system.

Butyl rubber is an elastomeric polymer and synthetic rubber. It is produced by copolymerizing isobutylene (98%) with a small amount of isoprene (2%). It is also known as Isobutylene-Isoprene Rubbers (IIR). The formula for IIR is shown in Figure 2.18 [163, 164, 165].
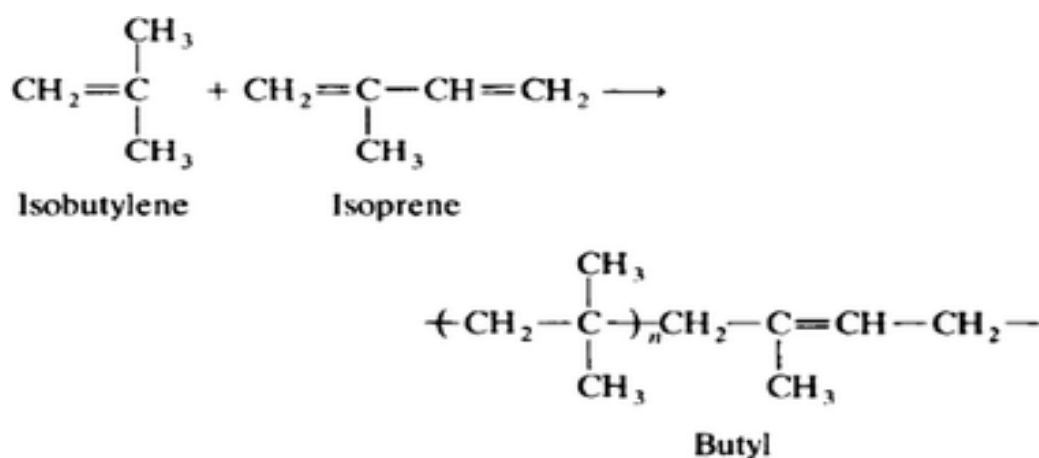
Figure 2.18: Chemical Structure of Butyl Rubber

Butyl rubber has relatively low strength and under loading condition, it tends to exhibit creep. It is widely used as sealant due to its low permeability to gases, vapours, and moisture. It is also able to flow and fill the small cavities of the steel surface. Without any heat, butyl rubber layers are self-amalgamated. Molecules of butyl rubber migrate into each other and form a homogeneous structure.

The word "ply" refers to the structure of one tape layer. Therefore, 3ply and 2ply refer 3 tape layers and 2 tape layers respectively. 3ply inner layer structure is butyl rubber adhesive layers on both sides of a PE carrier-film, whereas 2ply structure is butyl rubber adhesive layers on one side of a PE carrier-film. 3ply inner layer is an anti-corrosion layer that gives best corrosion protection. The cross-sectional view of 3ply (symmetrical structure) and 2ply (symmetrical structure) are shown in Figure 2.19 a) and b) respectively [166].
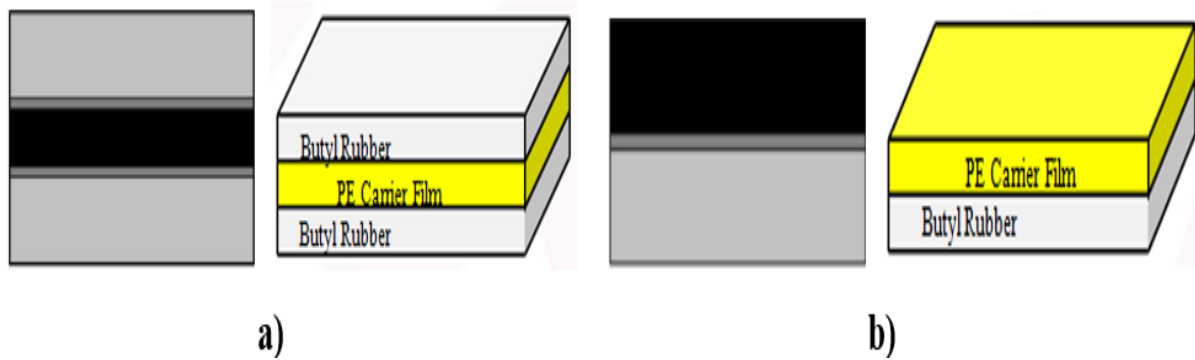
Figure 2.19: a) 3ply Symmetrical Structure, b) 2ply Symmetrical Structure

The cross-sectional view of 3ply asymmetrical structure is shown in Figure 2.20 [166].

Outer Adhesive Layer   PE-Layer   Co-Extruded Intermediate Layer   Inner Adhesive Layer
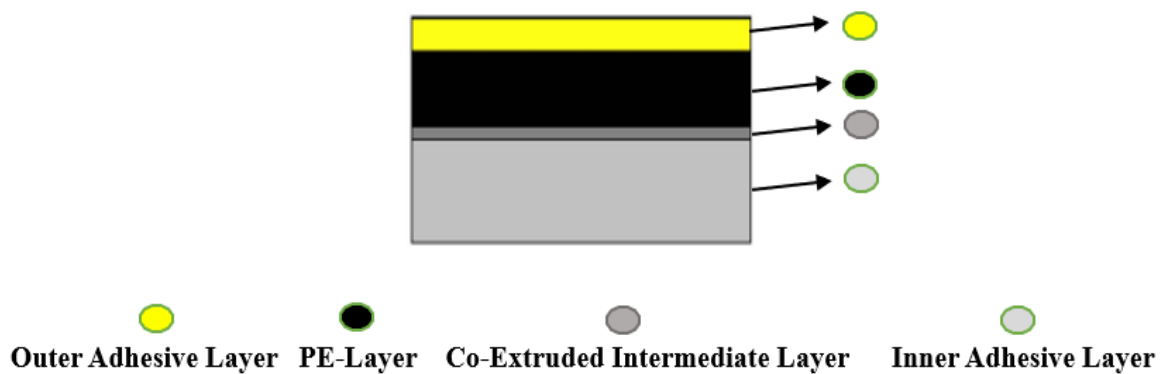
Figure 2.20: 3ply Asymmetrical Structure

Co-extruded intermediate layer is visible by microscopy and cannot be seen with the unaided (naked) eye. 3ply asymmetrical structure is preferred because better filling of surface irregularities and potential hollows are achieved by the inner adhesive layer.

If only 2ply is used for the inner wrap instead of 3-ply, an incompletely sealed interface remains in the tape overlap resulting in micro channels between the layers. After some years of operation, this interface will fail to prevent ingress of moisture and oxygen. Then there will be risk of spiral corrosion to occur on pipelines. Another important thing is that 2ply tape is used for mechanical protection of pipeline and it is not appropriate for corrosion protection. To avoid this situation, 3ply inner wrap is used because no interface with penetration paths remains within a wrapping in the tape overlap. In such arrangement, interface is completely sealed by butyl rubber and remains impermeable. The incompletely sealed tape overlap of 2ply tape wrapping and the completely sealed tape overlap of 3ply are shown in Figure 2.21 a), b) and Figure 2.22 respectively [166].
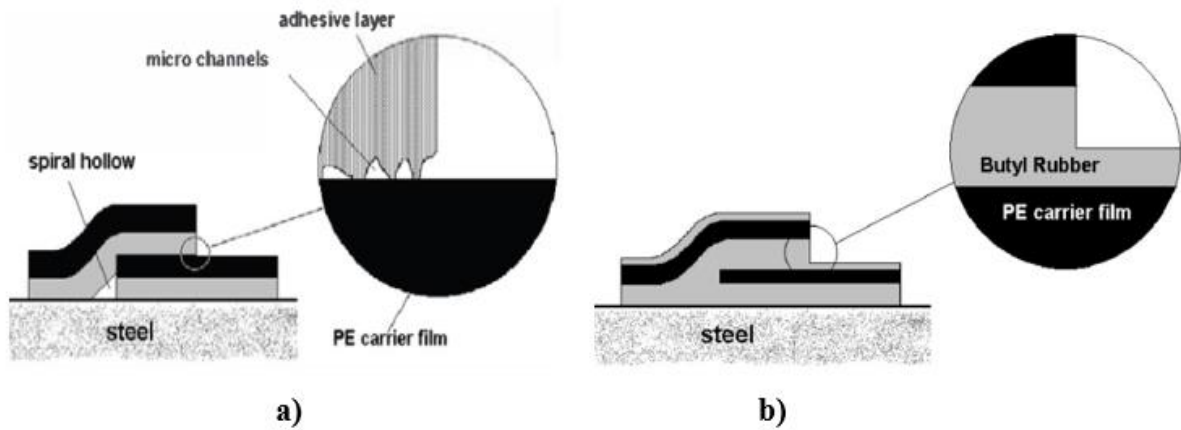
Figure 2.21: a) Incompletely sealed of 2-ply Tapes, b) Completely sealed of 3-ply Tapes
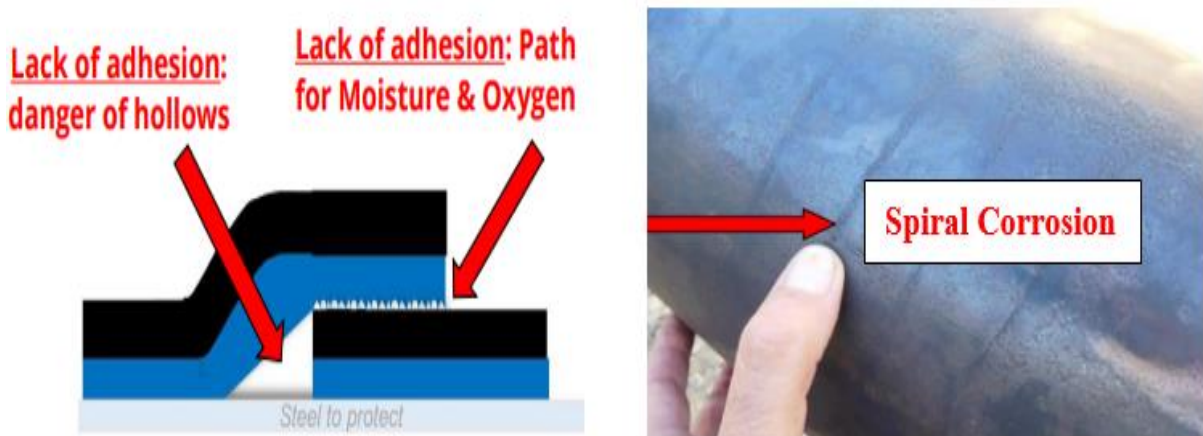
Figure 2.22: Incompletely sealed of 2-ply Tapes and Risk of Spiral Corrosion
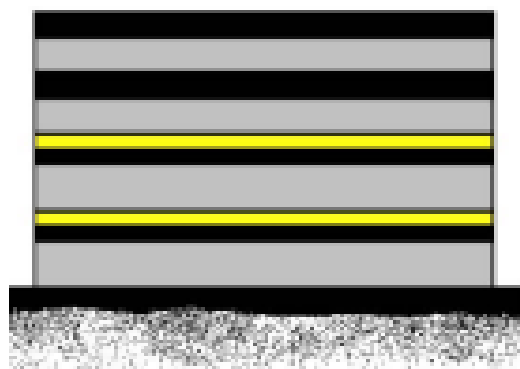
Figure 2.23: A Combination of 3ply/2ply Tapes

A combination of inner layer of 3ply and outer layer of 2 ply is found to be a perfect combination as it provides corrosion protection by sealing inner wrap completely as well as
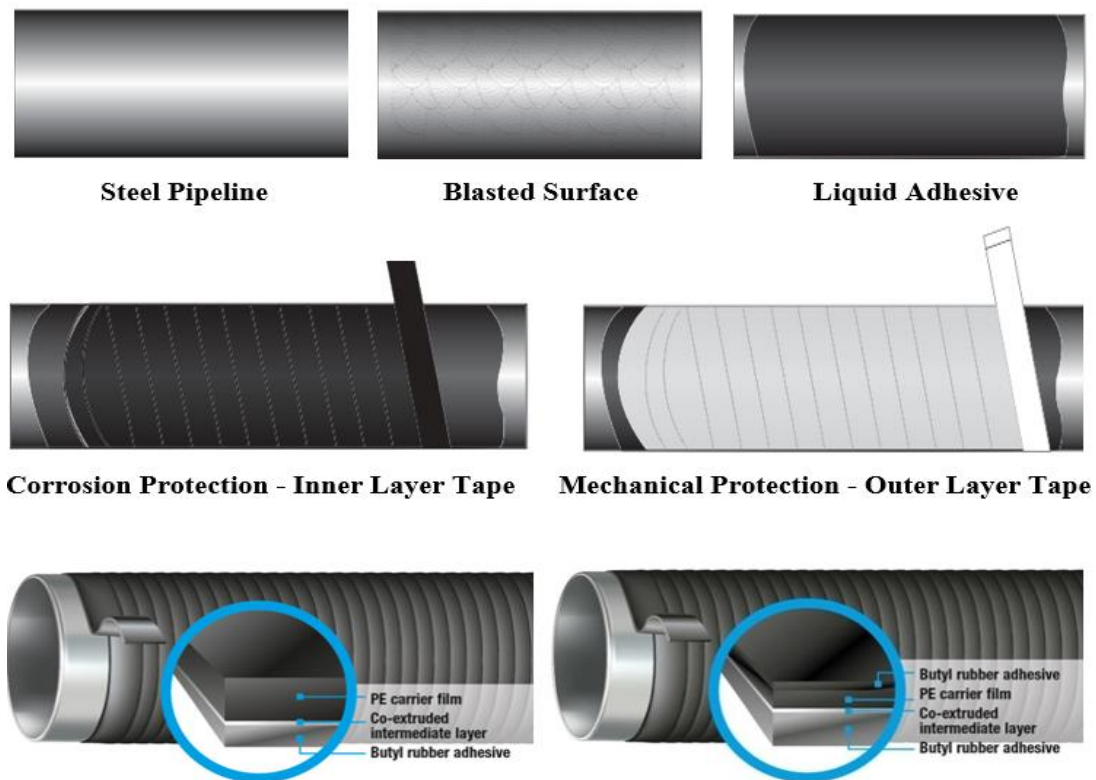
Figure 2.24: Application Procedure of 3ply/2ply Cold Applied Tape on Steel Pipeline

ensures mechanical protection like impact and indentation during handling and installation. Such combination is shown in Figure 2.23 [166]. The application procedure of 3ply/2ply is shown in Figure 2.24 [167].

2.3.5.3 Polyurethane (PU)

Polyurethane was first made through a basic reaction between an alcohol and an isocyanate by Dr. Otto Bayer and partners at IG Farben, Germany in 1937 [168]. The aromatic PU is a reaction product between alcohol and isocyanate. PU coating is Solvent-free and conforms to the requirements as per ISO 21809-3. After thoroughly mixing the resin and activator (usually 3:1 ratio in volume), coating is applied by using heated plural component airless equipment to the blast- cleaned pipe surface to achieve a thickness of about 1000-1500 µ. - 20°C to 80°C is the operating temperature range for this coating system.

Polyol and isocyanates are the main components to produce polyurethane. Polyurethane is formed by a reaction between polyol and isocyanate in the presence of chain extender and other additives. The reaction forms repeating urethane linkage and is shown in Figure 2.25 [169].To produce polyurethane, a minimum functionality of 2 is needed in both isocyanate and

polyol. The urethane groups, -NH-(C=O)-O-, link the molecular units for the synthesis of polyurethane.
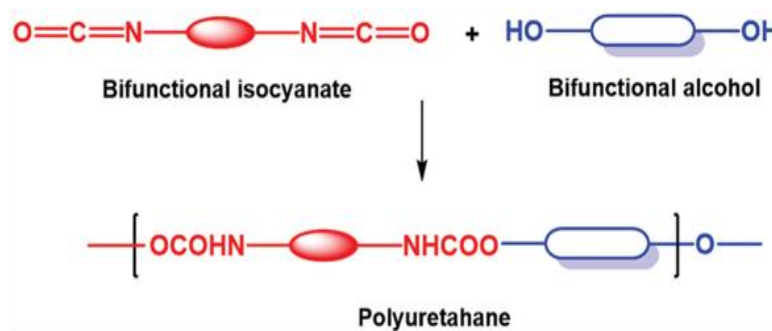
Figure 2.25: Synthesis of Polyurethane

Isocyanates are reactive groups with the structure (-N=C=O). For the synthesis of polyurethanes, these reactive groups react with hydroxyl. Aliphatic and aromatic isocyanates are usually used to make polyurethanes. To produce thermoset polyurethanes, aromatic MDI is the preferred isocyanates in industrial application due to its relatively low cost and high reactivity in comparison with other isocyanates. The chemical structure of MDI is shown in Figure 2.26 [169,170]
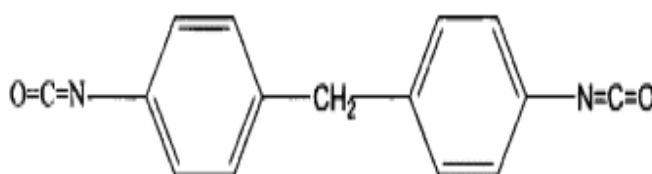
Figure 2.26: Chemical Structure of MDI

The high reactivity of MDI with polyol can be explained by its resonance structure as shown in Figure 2.27 [169]. Because of significant difference in electro-negativity, both nitrogen (N) and oxygen (O) become negatively charged, while carbon (C) becomes positively charged. In rigid polyurethane, urethane linkages interact with each other through active hydrogen i.e., R-OH bonding that is derived from polyol. As MDI is an aromatic group of isocyanate, R is an electron withdrawing group and therefore, the reactivity of MDI is high compared to aliphatic isocyanates.
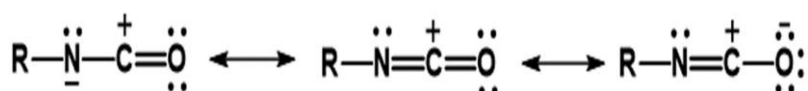
Figure 2.27: Resonance Structure of Isocyanate

The properties of polyurethane are affected by the molecular weight, functionality, and nature of polyols. Polyols are separated into two main groups-high molecular weight and low

molecular weight. For preparing flexible or elastic polyurethane, high molecular weight polyol with long alkyl segments is used. In flexible or elastic polyurethane, free rotation of linear chains with low functionality (2-3) and low degree of cross-linking is allowed. Elastic polyurethane contains open cell structure that permits free passage of air. The reaction between low molecular weight polyol and short aromatic segments of MDI produces rigid polyurethanes. In rigid polyurethane, it leads to high viscosity and highly branched chains with high functionality (about 3-8) and high degree of cross-linking [171]. In this case, there is a direct linkage between hydroxyl and urethane groups that increase interactions among the chains. In contrast to elastic polyurethane, rigid polyurethane contains about 90% closed cell structure that does not allow free passage of air. In preparing rigid polyurethane, both polyether and polyester polyol can be used. But the use of polyether is more common because polyether is versatile, lower cost, and high viscous material. Mobility is decreased by the aromatic cross-linking agent in rigid polyurethane. The elastomeric (aliphatic) polyurethane and rigid (aromatic) polyurethane are shown in Figure 2.28 a) and b) respectively [172]. The hard segment of aliphatic isocyanate is more flexible, more stable in ultra-violet rays, less susceptible to oxidation or degradation than that of aromatic isocyanate. Aliphatic isocyanates are rubbery materials. They have low tensile strength and high elongation in comparison with aromatic isocyanates [173].
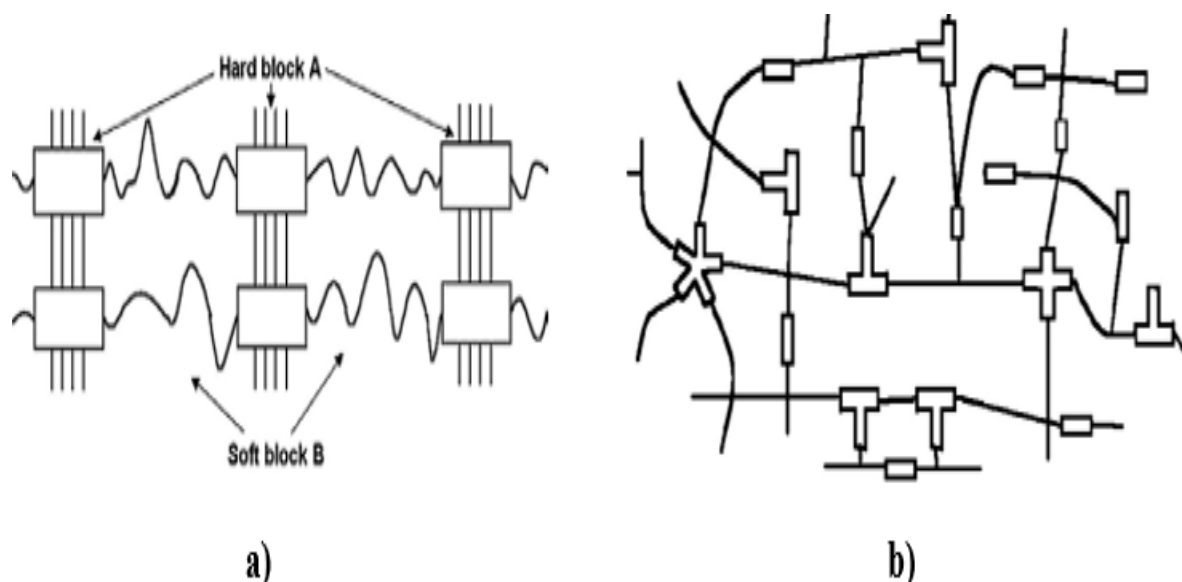
Figure 2.28:a) Elastomeric PU Coatings, b) Rigid PU Coatings

Based on the proportion of polyol and isocyanate, the properties of polyurethane make them suitable for specific applications. In general, polyol and isocyanate are flexible and rigid parts of polyurethane respectively. Isocyanate being an activator is responsible for curing of

polyurethane and is more reactive. Polyurethane is found to be softer and more hydrophilic when polyol proportion is more than isocyanate. On the other hand, polyurethane is found to be rigid and more hydrophobic when isocyanate proportion is more than polyol. Rigid polyurethanes are hydrophobic, whereas flexible (elastic) polyurethanes are hydrophilic. Therefore, a balance in the chemical structure (hydrophobicity and hydrophilicity) provides water-dispersible polyurethanes.

Rigid polyurethanes become brownish or yellowish when they are exposed to UV light for a long duration. Therefore, rigid polyurethane is used for indoor application or away from UV light. Aliphatic isocyanates, such as, hexamethylene diisocyanate (HMDI) and isophorone diisocyanate (IPDI) produce flexible polyurethane that are UV stabilized to retain their gloss.

Polyurethanes are used as coatings in the oil and gas, chemical industries with many applications such as aesthetics, gloss effect, anti-corrosion, hydrophobicity, antibacterial properties, scratch protection, UV resistance, and flame retardancy.

2.3.5.4 Visco-Elastic (VE)

The chemical composition of VE coating is Poly-Isobutene. VE is non-crystalline, non-cross-linked, non-reactive. VE is cold applied to the substrate. VE conforms to the requirements as per ISO 21809-3. The thickness of VE tape is about 2000-2500 μ. UV stabilized PVC (Poly-Vinyl Chloride) tape about 500 μ with adhesive is applied over VE tape. Maximum 60°C is the operating temperature for this coating system.

The purpose of the inner wrap i.e., poly-isobutene compound is to prevent corrosion of the steel substrate surface, and to prevent voids, and to repair small coating defects with self-healing properties [174]. The inner wrap is applied on the substrate without tension, but the outer wrap i.e., PVC tape is applied over the inner wrap with tension to accelerate the bond, support self-healing. It also provides circumferential compression and improves mechanical protection for the coating system that is requisite for transportation and operation. The cross-sectional view of visco-elastic polyolefin with outer polymeric tape is shown in Figure 2.29.
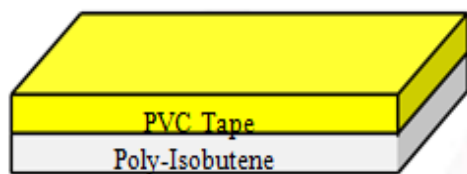
Figure 2.29: Visco-Elastic Polyolefin with outer Polymeric Tape

In visco-elastic coating system, poly-isobutene (poly-isobutylene) is a viscoelastic synthetic organic polymer. It appears as clear and colourless gummy solid. Poly-isobutene is produced through the polymerization of isobutene monomer. The polymerization reaction combines isobutene in the presence of aluminium chloride or boron trifluoride catalyst. Poly-isobutene chemical formula is $(C_4H_8)_n$, where "n" is 180-650 isobutene units in the polymer chain and is shown in Figure 2.30 [175].
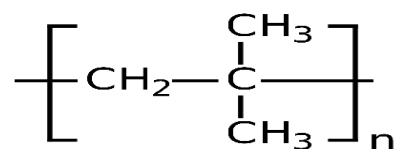
Figure 2.30: Chemical Structure of Poly-isobutene (Poly-isobutylene)

Poly-isobutene remains as a single polymer chain and cannot be cross-linked. This polymer is considered a covalent bond and contains hydrogen (H) and carbon (C) that have similar electro-negativity values. Poly-isobutene is impermeable and does not allow liquid or gas to go through. Due to these elastomeric properties, poly-isobutene flows and fills into the irregularities of the substrate even at low temperature. Viscoelastic poly-isobutene has some special features such as low temperature resistance without getting brittle, low surface tension and adheres on substrates at a molecular level, surface tolerant and no blasting required, self-healing of small dents, voids and cracks, cold flow into the irregular shapes and finest pores of the substrate.

Viscoelasticity was examined in the nineteenth century for synthetic polymers. Viscosity is the property of a fluid and elasticity is the property of a solid. When stress is applied, deformation of elastic materials is instantaneous i.e., independent of time and is totally recovered. But when stress is applied, viscous materials resist strain and shear flow linearly with time. Deformation of viscous materials exhibits time-dependent strain and is not recoverable. At sufficiently high temperature, thermally activated process takes place i.e. in viscous condition, the diffusion of atoms or molecules occurs inside an amorphous polymer, whereas in elastic

condition, bond stretching occurs along crystallographic planes in an ordered solid. This is described by an Arrhenius-type equation and is shown below by the following Equation (2-21) [176, 177]:

$$\eta = A \cdot e^{(Q/RT)} \ldots\ldots\ldots\ldots (2\text{-}21)$$

Where,

η = Viscosity in Newton-second per square meter (N·s/m^2) or Pascal-second (Pa·s)

A = Pre-exponential factor or Arrhenius factor or frequency factor

Q= Energy Activation

R = Gas-Constant Universal

T = Temperature Absolute, ^{0}K

Viscoelastic materials behave like a glass at low temperature, a rubbery solid at intermediate temperature i.e., above glass transition temperature (T_g) and a viscous liquid when the temperature is raised. A rubbery solid at intermediate temperature exhibits the combined mechanical properties of these two properties.

A viscoelastic polymer has two components - an elastic component and a viscous component. For purely elastic material, heat energy is not dissipated during application of load and then its removal. But for viscous material, heat energy is dissipated during application of load and then its removal. The elastic components and the viscous components of viscoelastic polymers can be given by the Equation (2-22) and Equation (2-23) respectively:

$$\sigma = E \cdot \varepsilon \ldots\ldots\ldots\ldots\ldots\ldots (2\text{-}22)$$
$$\sigma = \eta \cdot (d\varepsilon/dt) \ldots\ldots\ldots\ldots (2\text{-}23)$$

Where,

σ = Stress, E = Elastic modulus of the material, ε = Strain under the given stress,

η = Viscosity of the material, $d\varepsilon/dt$ = Time derivative of strain.

In 1867, a Scottish physicist, James Clerck Maxwell represented a model for viscoelastic material. This model is known as the "Maxwell model "as shown in Figure 2.31 [176, 177]. The model is represented by the following Equation (2-24). Most polymers are accurately predicted

by this model. The limitation of this model is that viscoelastic material under constant stress or creep cannot be predicted.
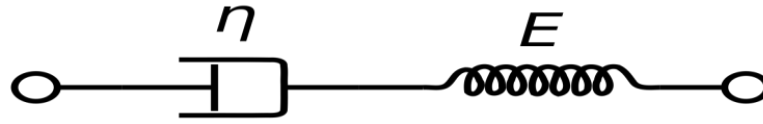
Figure 2.31: Maxwell Model for Viscoelastic Material

$$d\varepsilon/dt = 1/E \, . \, (d\sigma/dt) + (\sigma/\eta) \, \ldots\ldots\ldots\ldots \, (2\text{-}24)$$

There is another model known as the "Voigt model" (or the "Kelvin-Voigt model")as shown in Figure 2.32 [176, 177]. The model is represented by the following Equation (2-25). It accurately predicts creep behaviour of materials, but it also has limitations. This model is less regards to relaxation.
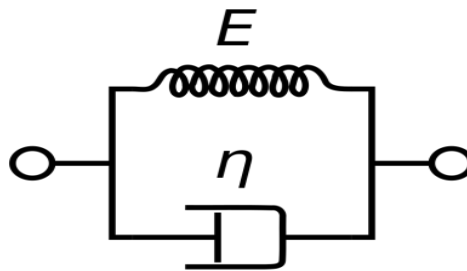
Figure 2.32: Voigt Model for Viscoelastic Material

$$\sigma = \eta . \, (d\varepsilon/dt) + E. \, \varepsilon \, \ldots\ldots\ldots\ldots \, (2\text{-}25)$$

Viscoelastic polymer can be categorized linear viscoelasticity and non-linear viscoelasticity based on the change of strain rate versus stress inside a material. For linear viscoelasticity, the stress is linearly proportional to the strain rate and represented as Newtonian material. Linear viscoelasticity is applicable only for small deformations. Non-linear viscoelasticity happens when the material changes its properties under deformations or when the deformations are large.

2.3.5.5 Liquid Epoxy (LE)

This coating system is Solvent-Free. This is high-build novolac epoxy. This coating system conforms to the requirements as per ISO 21809-3. After thoroughly mixing part A and part B (usually 3.5:1 ratio in volume), the coating is applied by using heated plural component airless equipment to the blast-cleaned pipe surface to achieve thickness of 800-1500 μ. - 20°C to 80°C is the operating temperature range for this coating system. A carbon steel pipeline coated with solvent-free liquid-applied epoxy is shown in Figure 2.33.

Figure 2.33: Solvent-Free Liquid-Applied Epoxy Coated Steel Pipeline

Novolac resins are manufactured in acidic condition polymerizing phenol by substituting formaldehyde on the aromatic ring of phenol via a condensation reaction [178]. Phenol (benzenol, or carbolic acid or phenolic acid) is an aromatic, volatile, white crystalline solid organic compound. The chemical formula of phenol is C_6H_5OH, where phenyl group ($-C_6H_5$) is bonded with hydroxyl group (-OH). Phenol is mildly acidic with pH=6.6. Phenol is greatly soluble in water. As phenol is highly reactive, many groups can be attached to an aromatic ring.

Formaldehyde (methanal) is a naturally occurring organic compound. The chemical formula of formaldehyde is CH_2O and the structure is H-CHO. It is a pungent, colourless gas. As it polymerizes spontaneously, it is stored by dissolving in water and the aqueous solution is known as formalin. The reaction between phenol and formaldehyde produces methylene glycol, where formaldehyde exists in equilibrium with methylene glycol in aqueous solution. The reaction is shown in Figure 2.34.
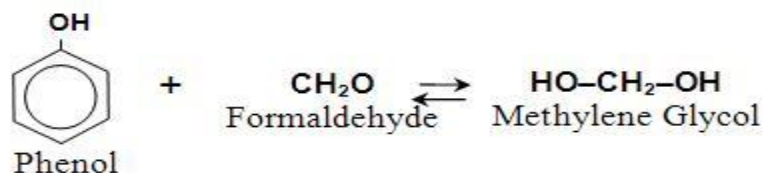
Figure 2.34: Reaction between Phenol and Formaldehyde

Novolac resins are also typically manufactured by a mixture of para-cresol and meta-cresol with formaldehyde in the presence of an acidic catalyst and in a condition where the molar excess of phenol to formaldehyde exists. Oxalic acid is preferred as an acidic catalyst and is removed by decomposition subsequently. Cresols (hydroxytoluene, toluenol, benzol or cresylic acid) are categorized as methyl-phenols (a group of aromatic organic compounds) either natural or synthetic. As their melting points are close to room temperature, they occur as either solids or liquids.

The initial reaction occurs between phenol and methylene glycol, and it continues with additional phenol, and splitting off of water. Novolac resins have a degree of polymerization (about 20-40). The chemical reactions are shown in Figure 2.35 [179].
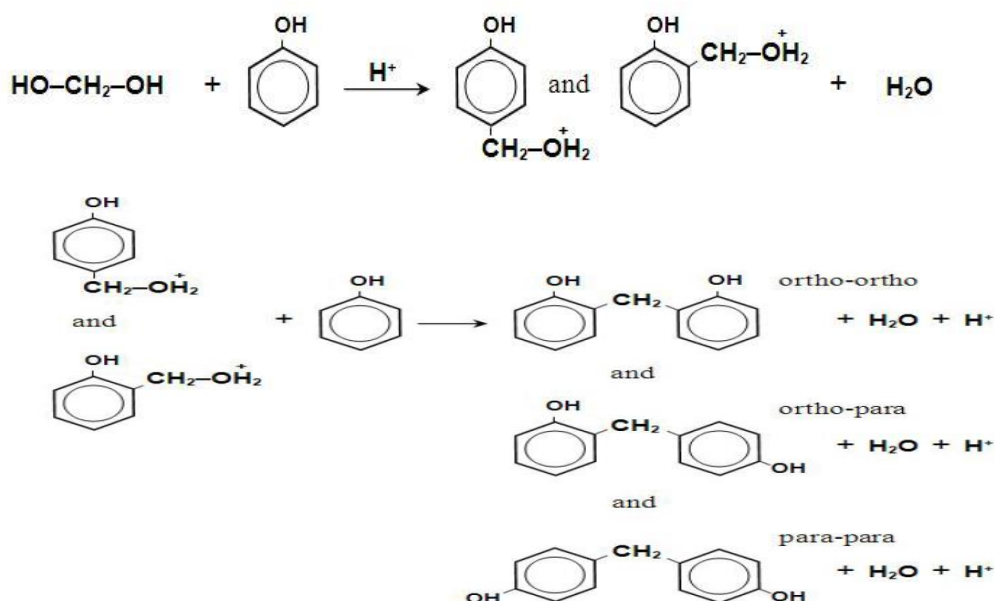
Figure 2.35: Production of Novolac Resin

To cure novolac resin completely, additional agent i.e. Hexa-Methylene Tetra-Amine (HMTA) is added to the phenolic resin to cross-linking novolac resin. HMTA reacts directly with resin and phenol in presence of heat without producing significant amount of formaldehyde. HMTA cures novolac resin by cross-linking and polymerization of the molecule. The final

novolac resin produced does not remain a long straight polymer chain, but remain a complex three-dimensional network with high molecular weight. Such cured novolac resin yields high hardness, stability, chemical resistant properties at high temperatures. A schematic Illustration of cured novolac resin is shown in Figure 2.36 [180].
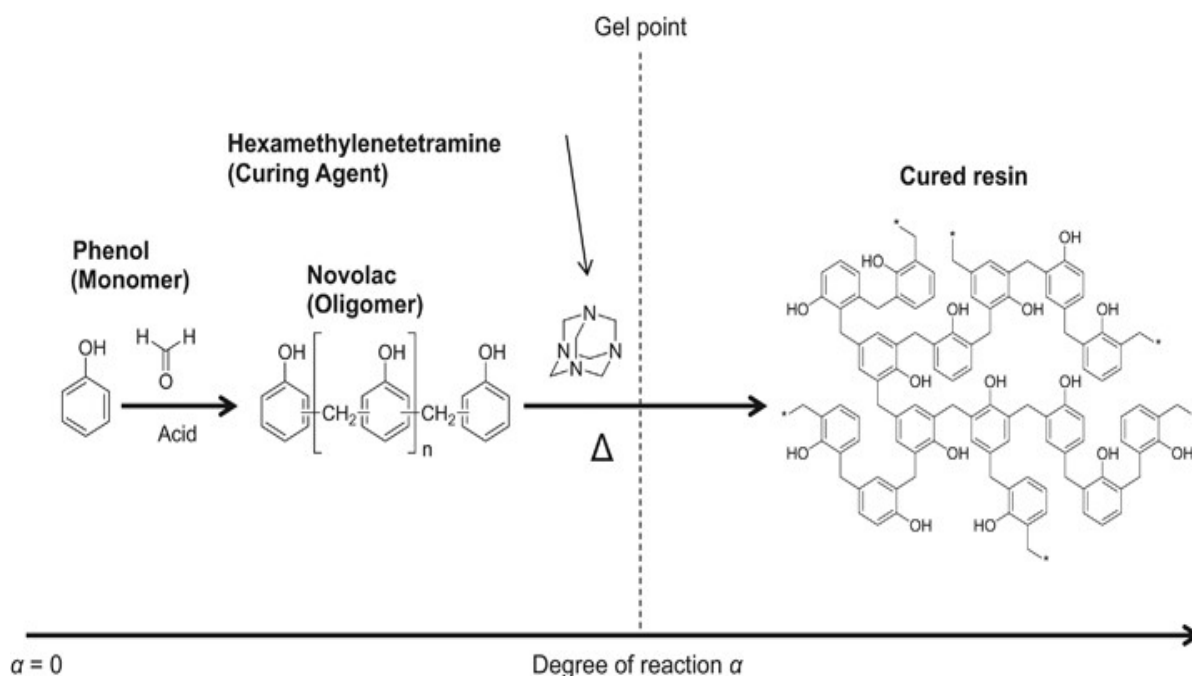
Figure 2.36: A Schematic Illustration of Cured Novolac Resin

Solvent-free (100% volume solid) novolac epoxy resin has some special features such as no presence of volatile organic compound (VOC), resistant to many corrosive chemicals. This coating needs minimum surface preparation. It has excellent and high level of adhesion to steel and fusion bonded epoxy (FBE) coating.

2.3.5.6 Heat-Shrink Sleeve (HSS)

This coating system is 3-layer system and conforms to the requirements as per ISO 21809-3. 1st layer - epoxy primer (200-220 μ), 2nd layer - adhesive (200-225μ), and 3rd layer - UV stabilized HDPE (cross-linked) (2000-2500 μ). The blast-cleaned pipe surface is heated at about 80°C and solvent-free two component liquid epoxy primer is applied to the pipe surface. Heat-Shrinkable Sleeve is wrapped around immediately over the wet epoxy. The sleeve is then heated with a propane torch until it shrinks and fits tightly around the joint as shown in Figure 2.37. The joints between the pipes are welded in the field. The weld joints of the buried pipelines are protected by HSS. Maximum 80°C is the operating temperature for this coating system.

Figure 2.37: Application of PE-based HSS wrap on a Pipeline Bend Joint

HSS materials or HSPs (Heat Shrink Polymers) commonly known as 'Shrink Wrap' are available commercially over the past six decades. These materials are part of SMPs (Shape Memory Polymers) and have the abilities to change from permanent (original) shape to temporary (deformed) shape by the process of programming. By the process of recovery, they back to their permanent (original) shape on exposure to an external stimulus i.e., heat. Heating up this polymer above T_{trans}(transition temperature) induces the shape memory effect. A schematic representation of thermally induced shape memory effect is shown in Figure 2.38 [181].
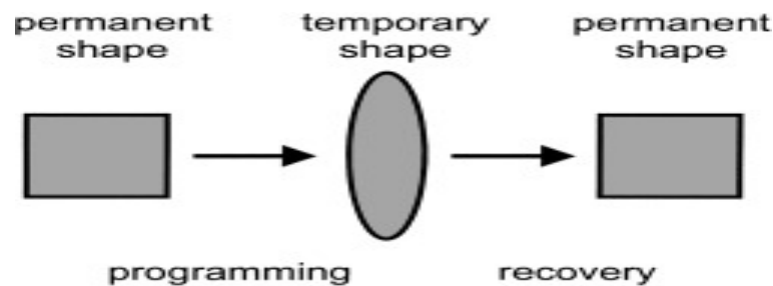
Figure 2.38: Schematic Representation of Thermally Induced Shape-Memory Effect

HSPs possess crystalline and amorphous regions. The crystalline regions represent a reversible transition (rigid) component and the amorphous polymer chains represent an elastic component [182]. The material will not possess heat shrink qualities without rigid and elastic components [183]. Original HSP is exposed to an electron beam (crosslinking agent) to crosslink polymer chains. After crosslinking, HSP is heated to above its melting temperature and deformed radially (mechanically expanded) and then quickly cooled to room temperature. The elastic

57

components of amorphous regions are stretched in the expanded state and give a new temporary shape, which is known as programming. With subsequent heating above its melting temperature, the elastic components of amorphous regions are stretched and strained to return to its original shape. This process is known as recovery. A schematic representation of original, programming and recovery of HSS material is shown in Figure 2.39 A, B, C [184].

A
Original

B
Expanded: Programming

C
Recovery
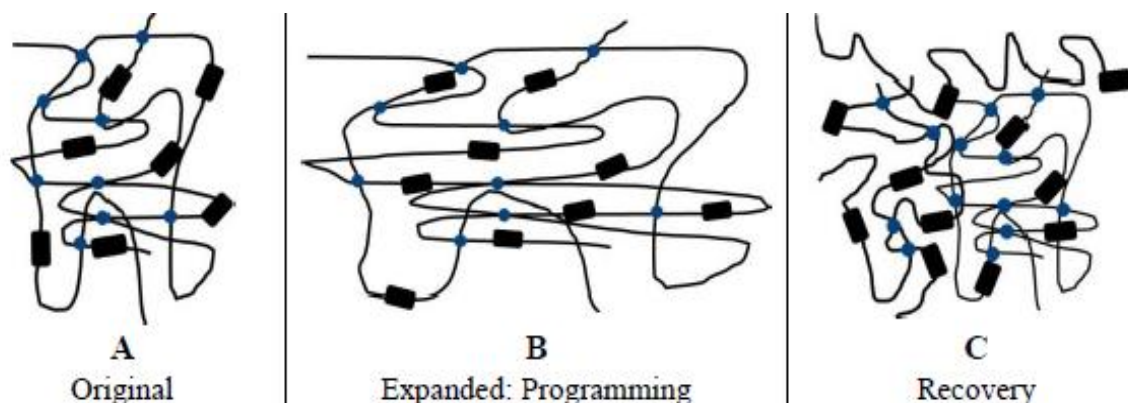
Figure 2.39: Schematic Representation of Original, Programming and Recovery of HSS

HSS materials are almost always crosslinked to enhance their heat shrinkable properties. Crosslinking can be done either by radiation using electron beam or using chemical additives. But radiation crosslinking is cheaper than chemical additives and hence, the former is the preferred method of crosslinking. Ionizing radiation under vacuum or in an inert atmosphere induces crosslinking. Radiation cross-linking of polyethylene-based HSS polymer chains is shown in Figure 2.40 A, B [184]. Radiation cross-linked HSS has greater strength at higher temperatures than non-cross-linked HSS [185].
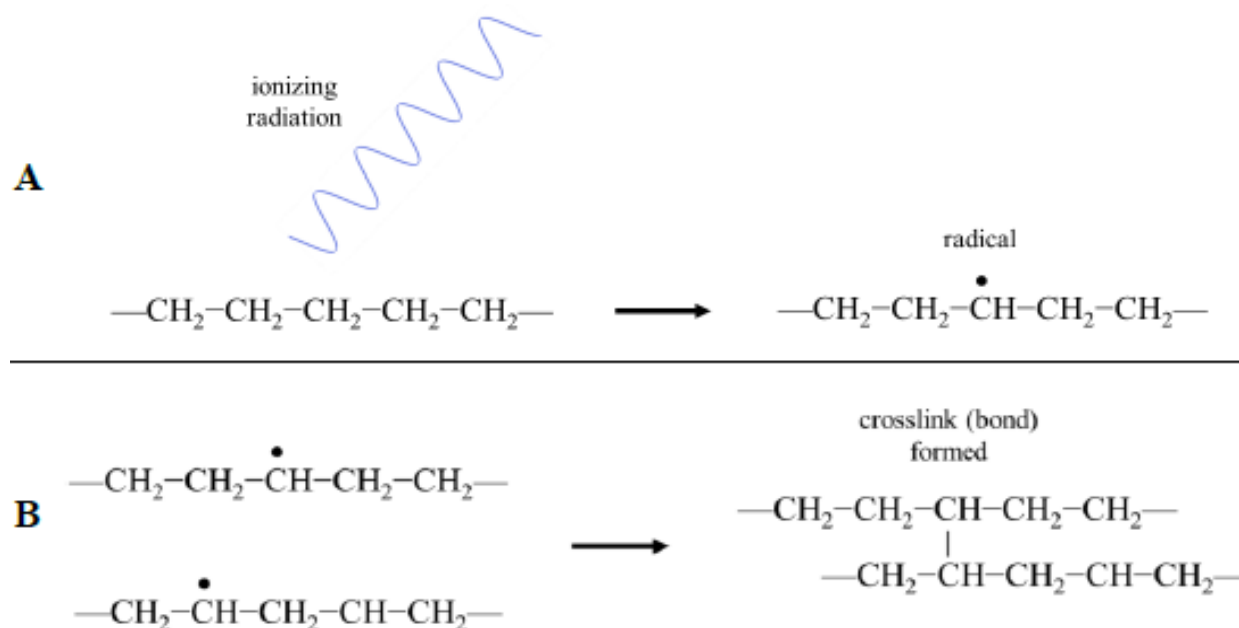
Figure 2.40: Radiation Cross-Linking of PE-based HSS Polymer Chains

The important feature of HSS is heat shrink ratio. Though some HSS materials produce a ratio of 6:1, but many HSS materials cannot produce such large ratios. The heat shrinkage ratio can be determined either by the Equation (2-26) or Equation (2-27):

$$\text{Heat shrinkage [\%]} = [L_{str} - L_s / L_{str} - L_0] \times 100 \quad \dots\dots\dots\dots\dots (2\text{-}26)$$

$$\text{Heat shrinkage [\%]} = [L_{str} - L_s / L_{str} (1 - \lambda^{-1})] \times 100 \quad \dots\dots\dots\dots (2\text{-}27)$$

Where,

L_{str} = Sample length in stretched condition

L_s = After shrinkage, sample length

L_0 = Sample length (original)

λ = Ratio of shrinkage.

Besides ratio of shrinkage, HSS final dimension is an important consideration. Though HSS is expanded radially, but there is likely some longitudinal shrinkage in addition to the circumferential shrinkage. Another important consideration of HSS is the environment such as chemical and temperature before selecting this material. HSS materials are great boon to the oil and gas industries to be used as anti-corrosion protective external coatings for weld-joints of buried or submerged 3LPE coated pipelines.

2.4 References

[1] Donald-Peckner, I.M. Bernstein, "Handbook of Stainless Steels", McGraw-Hill New York, 1977

[2] H. M. Cobb, "The History of Stainless Steel", Edition 2010, ASM International, Materials Park, Ohio, USA

[3] P. Marshall, "Austenitic Stainless Steels: Microstructure and Mechanical Properties", Springer Science & Business Media, 1984

[4] B.R. Kumar, S. Sharma, P. Munda, R. Minz, "Structure and Microstructure Evolution ofA Ternary Fe–Cr–Ni Alloy Akin to Super Martensitic Stainless Steel", Materials & Design, 50 (2013) 392-398

[5] A. Kisko, A. Hamada, J. Talonen, D. Porter, L. Karjalainen, "Effects of Reversion and Recrystallization on Microstructure and Mechanical Properties of Nb-Alloyed Low-Ni

High-Mn Austenitic Stainless Steels", Materials Science and Engineering: A, 657 (2016) 359-370

[6] I. Calliari, M. Zanesco, M. Dabala, K. Brunelli, E. Ramous, "Investigation of Microstructure and Properties of a Ni–Mo Martensitic Stainless Steel", Materials & Design, 29 (2008) 246-250

[7] H.Nakagawa, T.Miyazaki, H.Yokota, "Effects of Aging Temperature on the Microstructure and Mechanical Properties of 1.8Cu-7.3Ni-15.9Cr-1.2Mo-low C, N Martensitic Precipitation Hardening Stainless Steel", Journal of Materials Science, 35 (2000) 2245-2253

[8] H.-Y.Ha, T.-H.Lee, J-H.Bae, D.Chun, "Molybdenum Effects on Pitting Corrosion Resistance of FeCrMnMoNC Austenitic Stainless Steels", Metals, 8 (2018), p. 653

[9] LvJinlong, T.X. Liang, C. Wang, "Surface Enriched Molybdenum Enhancing the Corrosion Resistance of 316L Stainless Steel", Materials Letters, 171, February (2016), p.38-41.

[10] W. Tobler, S. Virtanen, "Effect of Mo Species on Metastable Pitting of Fe-18Cr alloys - A Current Transient Analysis", Corrosion Science, 48 (2006) p.1585-1607

[11] A.F. Padilha, I.F. Machado, R.L. Plaut, "Microstructures and Mechanical Properties of Fe–15%Cr–15%Ni Austenitic Stainless Steels Containing Different Levels of Niobium Additions Submitted to Various Processing Stages", Journal of Materials Processing Technology, 170 (2005), p.89-96.

[12] M. Aksoy, V. Kuzucu, M. Korkut, M. Yildirim, "The Effect of Niobium and Homogenization on the Wear Resistance and Some Mechanical Properties of Ferritic Stainless Steel Containing 17–18 wt.% Chromium", Journal of Materials Processing Technology, 91 (1999), p.172-177

[13] M. Tendo, Y. Tadokoro, K. Suetsugu, T. Nakazawa, "Effects of Nitrogen, Niobium and Molybdenum on Strengthening of Austenitic Stainless Steel produced by Thermo-Mechanical Control Process", ISIJ International, 41 (2001), p.262-267

[14] E. El-Kashif, K. Asakura, T. Koseki, K. Shibata, "Effects of Boron, Niobium and Titanium on Grain Growth in Ultra High Purity 18% Cr Ferritic Stainless Steel", ISIJ International, 44 (2004), p.1568-1575

[15] V. Kuzucu, M. Aksoy, M. Korkut, M. Yildirim, "The Effect of Niobium on the Microstructure of Ferritic Stainless Steel", Materials Science and Engineering: A, 230 (1997), p.75-80

[16] M. Fujikura, K. Takada, K. Ishida, "Effect of Manganese and Nitrogen on the Mechanical Properties of Fe-18%Cr-10%Ni Stainless Steels", Transactions of the Iron and Steel Institute of Japan, 15 (1975), p.464-469

[17] V. Muthupandi, P.B. Srinivasan, V. Shankar, S. Seshadri, S. Sundaresan, "Effect of Nickel and Nitrogen addition on the Microstructure and Mechanical Properties of Power Beam Processed Duplex Stainless Steel (UNS 31803) Weld Metals", Materials Letters, 59 August (2005), p.2305-2309

[18] J.W. Simmons, "Mechanical Properties of Isothermally Aged High-Nitrogen Stainless Steel", Metallurgical and Materials Transactions A, 26 (1995), p.2579-2595

[19] J. Simmons, "Overview: High-Nitrogen Alloying of Stainless Steels", Materials Science and Engineering: A, Vol.207, Issue 2 (1996), p.159-169

[20] H.B. Li, Z.H. Jiang, Z.R. Zhang, Y. Yang, "Effect of Grain Size on Mechanical Properties of Nickel-free high Nitrogen Austenitic Stainless Steel", Journal of Iron and Steel Research International, 16 (2009) 58-61

[21] D.W. Kim, "Influence of Nitrogen-Induced Grain Refinement on Mechanical Properties of Nitrogen Alloyed Type 316LN Stainless Steel", Journal of Nuclear Materials, 420 (2012), p.473-478

[22] H. Li, Z. Jiang, H. Feng, S. Zhang, L. Li, P. Han, R. Misra, J. Li, "Microstructure, Mechanical and Corrosion Properties of Friction Stir Welded high Nitrogen Nickel-free Austenitic Stainless Steel", Materials &Design, 84 (2015), p.291-299

[23] T. Xi, M.B. Shahzad, D. Xu, Z. Sun, J. Zhao, C. Yang, M. Qi, K. Yang, "Effect of Copper addition on Mechanical Properties, Corrosion Resistance and Antibacterial Property of 316L Stainless Steel", Materials Science and Engineering: C, 71 (2017), p.1079-1085

[24] B.M. Gonzalez, C.S.B. Castro, V.T.L. Buono, J.M.C. Vilela, M.S. Andrade, J.M.D. Moraes, M.J. Mantel, "The Influence of Copper addition on the formability of AISI 304 Stainless Steel", Materials Science and Engineering: A, 343 (2003), p.51-56

[25] S.H. Jeon, S.T. Kim, IS. Lee, J.H. Park, K.T. Kim, J.S. Kim, Y.S. Park, "Effects of Copper addition on the formation of Inclusions and the Resistance to Pitting Corrosion of high performance Duplex Stainless Steels", Corrosion science, 53 (2011), p.1408-1416

[26] M. Gurram, K. Adepu, R.R. Pinninti, M.R. Gankidi, "Effect of Copper and Aluminium addition on Mechanical Properties and Corrosion Behaviour of AISI 430 Ferritic Stainless Steel Gas Tungsten Arc Welds", Journal of Materials Research and Technology, 2 (2013), p.238-249

[27] D. Uzunsoy, "The characterisation of PM 304 Stainless Steel sintered in the presence of a Copper based additive", Materials Letters, 61 (2007), p.10-15

[28] A. Sharon, D. Itzhak, "Mechanical properties of sintered Austenitic Stainless Steel -effect of Silicon addition", Materials Science and Engineering: A, 157 (1992), p.145-149

[29] M. Youseffi, K. Chong, "Enhanced sintering and mechanical properties of 316L Stainless Steel with Silicon additions as sintering aid", Powder Metallurgy, 46 (2003), p.30-38

[30] S. Lal, G. Upadhyaya, "Effect of Phosphorus and Silicon addition on the sintered properties of 316L Austenitic Stainless Steel and its composites containing 4 vol% Yttria", Journal of Materials Science, 24 (1989), p.3069-3075

[31] A. Hermas, I. Hassab-Allah, Microstructure, Corrosion And Mechanical Properties of 304 Stainless Steel containing Copper, Silicon And Nitrogen, Journal of Materials Science, 36 (2001), p.3415-3422

[32] W. Wang, Y.L. Su, "Liquid phase sintering of Austenitic Stainless Steel powders with Silicon additions", Powder Metallurgy, 29 (1986), p.269-275

[33] A. Reichardt, R.P. Dillon, J.P. Borgonia, A.A. Shapiro, B.W. McEnerney, T. Momose, P. Hosemann, "Development and Characterization of Ti-6Al-4V to 304L Stainless Steel gradient components fabricated with laser deposition additive manufacturing", Materials & Design, 104 (2016), p.404-413

[34] J. Cotton, R. Knutsen, C. Lang, "The influence of Niobium and Vanadium on the Microstructure and Mechanical Properties of a high Nitrogen Stainless Steel", Materials Science Forum, (1999), p.271-280

[35] S.Abbasi, A.Shokuhfar, "Improvement of Mechanical Properties of Cr-Ni-Mo-Cu-Ti Stainless Steel with addition of Vanadium", Journal of Iron and Steel Research International, 14 (2007), p.74-78

[36] Davis, Joseph R, "Stainless Steels", ASM Specialty Handbook, Edition 1994, p.3, ASM International, Materials Park, Ohio, USA

[37] C-O-A Olsson, D-Landolt, "Passive Films on Stainless-Steels - Chemistry, Structure and Growth", Electrochimica Acta, April 2003, p.1093-1104

[38] Y. Lakhtin, "Engineering Physical Metallurgy", p. 347, Mir Publisher, Moscow, Russia

[39] A. B. Kinzel, "Chromium Carbide in Stainless Steel", JOM, 4 (1952), p.469-488

[40] ASM Handbook, Vol.13,"Corrosion", fourth printing (1992),p.96, ASMInternational, Materials Park, Ohio, USA

[41] E. McCafferty, "Introduction to Corrosion Science", Chapter 9: Passivity, Edition (2010), p.212

[42] R.P. Reed, "Nitrogen in Austenitic Stainless Steels", JOM, 41 (1989), p.16-21

[43] T. Oshima, Y. Habara, K. Kuroda, "Efforts to save Nickel in Austenitic Stainless Steels, ISIJ international, 47 (2007), p.359-364

[44] A. Di Schino, J. Kenny, M. Mecozzi, M. Barteri, "Development of high Nitrogen, low Nickel, 18% Cr Austenitic Stainless Steels", Journal of Materials Science, 35 (2000), p. 4803-4808

[45] N. Ohkubo, K. Miyakusu, Y. Uematsu, H. Kimura, "Effect of Alloying Elements on the Mechanical Properties of the Stable Austenitic Stainless Steel", ISIJ international, 34 (1994), p.764-772

[46] D. Llewellyn, "Work hardening effects in Austenitic Stainless Steels, Materials Science and Technology, 13 (1997), p.389-400

[47] NACE Group Committee T-1, "Corrosion Control in Petroleum Production", TPC Publication No.5, Chapter 6 - Metallurgy, p.70, NACE International, Houston, Texas, USA

[48] G.S. Was, S. Ukai, "Austenitic Stainless Steels, Structural Alloys for Nuclear Energy Applications", Elsevier, (2019) 293-347

[49] A.F. Padilha, P.R. Rios, "Decomposition of Austenite in Austenitic Stainless Steels", ISIJ international, 42 (2002) 325-327.

[50] G. Michal, F. Ernst, H. Kahn, Y. Cao, F. Oba, N. Agarwal, A. Heuer, "Carbon Supersaturation due to Para-Equilibrium Carburization: Stainless Steels with Greatly Improved Mechanical Properties", Acta Materialia, 54 (2006) 1597-1606.

[51] A. Pardo, M. Merino, A. Coy, F. Viejo, R. Arrabal, E. Matykina, Pitting corrosion behaviour of austenitic stainless steels–combining effects of Mn and Mo additions, Corrosion 37 Science, 50 (2008) 1796-1806

[52] NiDI Handbook Series N9014, "Design Guidelines for the Selection and Use of Stainless Steel", p.1, Nickel Development Institute (NiDI): Toronto, ON, Canada

[53] Michael Mcguire, "Stainless Steels for Design Engineers" Edition (2008), ASM International, Materials Park, Ohio, USA

[54] ASM Handbook, Vol.6 (1993), "Welding, Brazing, and Soldering",p.1543, ASM International, Materials Park, Ohio, USA

[55] D. Hamm, K. Ogle, C.O.A. Olsson, S. Weber, D. Landolt, "Passivation of Fe-Cr alloys studied with ICP-AES and EQCM", Corrosion Science, 44 (2002), p.1443-1456.

[56] I. Olefjord, L. Wegrelius, "Surface Analysis of Passive State", Corrosion Science, 31 (1990), p.89-98.

[57] V. Maurice, P. Marcus, "Passive Films at the Nanoscale", Electrochimica Acta, 84 (2012), p.129-138

[58] V. Maurice, P. Marcus, "Progress in Corrosion Science at Atomic and Nanometric Scales", Progress in Materials Science, 95 (2018), p.132-171

[59] A. Brooks, C. Clayton, K. Doss, Y. Lu, "On the role of Cr in the Passivity of Stainless Steel", Journal of the Electrochemical Society, 133 (1986), p.2459-2464

[60].H. H. Uhlig, "Passivity in metals and alloys", Corrosion science, Vol.19, Issue 7 (1979), p.777-791, Elsevier, ScienceDirect

[61] N. Sato, "An overview on the passivity of metals", Corrosion science, Vol.31 (1990), p.1-19, Elsevier, ScienceDirect

[62] J.W. Schultze, M.M. Lohrengel, "Stability, reactivity and breakdown of passive films. Problems of recent and future research",Electrochimca Acta, Vo.45, Issue 15-16 (2000), p. 2499-2513, Elsevier, ScienceDirect

[63] I. Olefjord, "The Passive State of Stainless Steels", Materials Science and Engineering, 42 (1980), p.161-171

[64] P. Schmuki, "From Bacon to Barriers: A Review on the Passivity of Metals and Alloys", Journal of Solid State Electrochemistry, 6 (2002), p.145-164

[65] I. Olefjord, L. Wegrelius, "Surface Analysis of Passive State", Corrosion Science, 31 (1990), p.89-98

[66] R. Kirchheim, B. Heine, H. Fischmeister, S. Hofmann, H. Knote, U. Stolz, "The Passivity of Iron-Chromium Alloys", Corrosion Science, 29 (1989), p.899-917

[67] K. Asami, K. Hashimoto, S. Shimodaira, "An XPS Study of the Passivity of aseries of Iron-Chromium Alloys in Sulphuric Acid", Corrosion Science, 18 (1978), p.151-160

[68] V. Maurice, H. Peng, L.H. Klein, A. Seyeux, S. Zanna, P. Marcus, "Effects of Molybdenum on the Composition and Nanoscale Morphology of Passivated Austenitic Stainless Steel Surfaces", Faraday Discussions, 180 (2015), p.151-170

[69] S. Haupt, H.-H. Strehblow, "A Combined Surface Analytical and Electrochemical Study of the Formation of Passive Layers on FeCr Alloys in 0.5 M H_2SO_4", Corrosion Science, 37 (1995), p.43-54

[70] H.W. Hoppe, S. Haupt, H.H. Strehblow, "Combined Surface Analytical and Electrochemical Study of the Formation of Passive Layers onFe/Cr Alloys In 1 M NaOH", Surface and Interface Analysis, 21 (1994) 514-525.

[71] R. Kirchheim, B. Heine, S. Hofmann, H. Hofsäss, "Compositional Changes of Passive Films due to Different Transport Rates and Preferential Dissolution", Corrosion Science, 31 (1990), p.573-578

[72] I. Olefjord, B.O. Elfstrom, "The Composition ofthe Surface During Passivation Of Stainless Steels", Corrosion, 38 (1982) 46-52.

[73] V. Maurice, W. Yang, P. Marcus, "XPS and STM Study of Passive Films Formed on Fe-22Cr (110) Single-Crystal Surfaces", Journal of the Electrochemical Society, 143 (1996), p.1182-1200

[74] N. Hara, K. Sugimoto, "The Study of the Passivation Films on Fe-Cr Alloys by Modulation Spectroscopy", Journal of the Electrochemical Society, 126 (1979), p.1328

[75] P. Marcus, I. Olefjord, "Round Robin on combined Electrochemical and AES/ESCA Characterization of the Passive Films on Fe-Cr and Fe-Cr-Mo Alloys", Surface and Interface Analysis, 11 (1988), p.569-576

[76] D. Mitchell, M. Graham, "Comparison of Auger and SIMS Analysis of a Thin Passive Oxide Film on Iron-25% Chromium, Surface and Interface Analysis, 10 (1987), p.259-261

[77] V. Maurice, W. Yang, P. Marcus, "XPS and STM Investigation of the Passive Film Formed on Cr (110) Single-Crystal Surfaces", Journal of the Electrochemical Society, 141 (1994), p.3016-3027

[78] D. Marijan, M. Gojić, "Electrochemical Study of the Chromium Electrode Behaviour in Borate Buffer Solution", Journal of Applied Electrochemistry, 32 (2002), p.1341-1346

[79] N. Sato, T. Noda, K. Kudo, "Thickness and Structure of Passive Films on Iron in Acidic and Basic Solutions", Electrochimica Acta, 19 (1974), p.471-475

[80] Z. Wang, F. Di-Franco, A. Seyeux, S. Zanna, V. Maurice, P. Marcus, "Passivation-Induced Physicochemical Alterations of the native Surface Oxide Film on 316L Austenitic Stainless Steel", Journal of The Electrochemical Society, 166 (2019), p.C3376-C3388

[81] Z. Wang, E.-M. Paschalidou, A. Seyeux, S. Zanna, V. Maurice, P. Marcus, "Mechanisms of Cr and Mo Enrichments in the Passive Oxide Film on 316L Austenitic Stainless Steel", Frontiers in Materials, 6 (2019), p.232

[82] I. Olefjord, B. Brox, U. Jelvestam, "Surface Composition of Stainless Steels during Anodic Dissolution and Passivation Studied by ESCA", Journal of the Electrochemical Society, 132 44 (1985), p.2854-2861

[83] J. Lumsden, R. Staehle, "Application of Auger Electron Spectroscopy to the Determination of the Composition of Passive Films on Type 316 SS", Scripta Metallurgica, 6 (1972), p.1205-1208

[84] N. Hakiki, M.D.C. Belo, A. Simoes, M. Ferreira, "Semiconducting Properties of Passive Films Formed on Stainless Steels: Influence of the Alloying Elements", Journal of the Electrochemical Society, 145 (1998), p.3821

[85] V. Maurice, W. Yang, P. Marcus, "X-Ray Photoelectron Spectroscopy and Scanning Tunnelling Microscopy Study of Passive Films Formed on (100) Fe-18Cr-13Ni Single-Crystal Surfaces" Journal of the Electrochemical Society, 145 (1998), p.909-920

[86] J. Castle, J. Qiu, "The Application of ICP-MS and XPS to Studies of Ion Selectivity during Passivation of Stainless Steels", Journal of the Electrochemical Society, 137 (1990), p.2031

[87] L. Ma, F. Wiame, V. Maurice, P. Marcus, "New insight on early oxidation stages of austenitic stainless steel from in situ XPS analysis on single-crystalline Fe-18Cr-13Ni", Corrosion Science, 140 (2018), p.205-216

[88] A. Mishra, D. Shoesmith, P. Manning, "Materials Selection for use in Concentrated Hydrochloric Acid", Corrosion, 73 (2017), p.68-76

[89] K. Hashimoto, K. Asami, A. Kawashima, H. Habazaki, E. Akiyama, "The Role of Corrosion-Resistant Alloying Elements in Passivity", Corrosion Science, 49 (2007), p.42-52

[90] J. Park, T. Suter, H. Bohni, "Role of Manganese Sulphide Inclusions on Pit Initiation of Super Austenitic Stainless Steels", Corrosion, 59 (2003), p.59-67

[91] P. Schmuki, H. Hildebrand, A. Friedrich, S. Virtanen, "The Composition of the Boundary Region of MnS Inclusions in Stainless Steel and its Relevance in Triggering Pitting Corrosion", Corrosion Science, 47 (2005), p.1239-1250

[92] H. Krawiec, V. Vignal, O. Heintz, R. Oltra, "Influence of the Dissolution of MnS Inclusions under free Corrosion and Potentiostatic Conditions on the Composition of Passive Films and the Electrochemical Behaviour of Stainless Steels", Electrochimica Acta, 51 (2006), p.3235-3243

[93] E. Webb, T. Suter, R.C. Alkire, "Micro-electrochemical Measurements of the Dissolution of Single MnS Inclusions, and the Prediction of the Critical Conditions for Pit Initiation on Stainless Steel", Journal of the Electrochemical Society, 148 (2001), p. B186-B195

[94] D.E-Williams, M.R-Kilburn, J. Cliff, G.I.N. Waterhouse, "Composition Changes around Sulphide-Inclusions in Stainless Steels, and Implications for the Initiation of Pitting Corrosion", Corrosion Science 52 (2010), p.3702-3716

[95] ASM Handbook, Vol. No.13C,"Corrosion: Environments and Industries", First printing (November 2005), p.16, ASM International, Ohio, USA

[96] H. Bohni, "Breakdown of Passivity and Localized Corrosion Process", Langmuir 3(6)(1987), p.924-930

[97] D. E. Williams, R. C. Newman, Q. Song and R. G. Kelly, "Passivity Breakdown and Pitting Corrosion of Binary Alloys", Nature350 (1991), p.216-219

[98] P.C. Pistorius, G.T. Burstein, "Growth of Corrosion Pits on Stainless Steel in Chloride Solution Containing Dilute Sulphate", Corrosion Science 33(1992), p.1885-1897

[99] P. Ernst, N.J. Laycock, M.H. Moayed, R.C. Newman, "The Mechanism of Lacy Cover Formation in Pitting", Corrosion Science 39 (1997), p.1133-1136

[100] G.S. Frankel, "Pitting Corrosion of Metals: A Review of the Critical Factors", J. Electrochemical Society 145 (1998), p.2186-2198

[101C.Wagner and W.Traud, "On the Interpretation of Corrosion Processes through the Superposition of Electrochemical Partial Processes and on the Potential of Mixed Electrodes", CORROSION (October 2006), Vol. 62, No. 10, NACE International, Houston, Texas, USA

[102] F. Mansfeld, "Classic Paper in Corrosion Science and Engineering with a Perspective", Corrosion (October 2006), Vol. 62, No. 10, NACE International, Houston, Texas, USA

[103] Herbert H. Uhlig, R. Winston Revie, "Corrosion and Corrosion Control", fourth Edition, John Wiley & Sons, Inc., Hoboken New Jersey, 2008, p.96 and p.352

[104] ASM Metal Handbook, Vol.13, "Corrosion", (1992), p.242, ASM International

[105] U.R. Evans, Corrosion, Vol. 7, No. 238, 1951

[106] R. Winston Revie, "Uhlig's Corrosion Handbook", Third Edition (2011), p.166, A John Wiley & Sons, Inc. Publication, Hoboken New Jersey

[107] Mars G Fontana, "Corrosion Engineering", Third Edition, Chapter 3 (1987), p.66-67, McGraw-Hill Book Company

[108] A. John-Sedriks, "Corrosion of Stainless-Steels", Second Edition (1996), Chapter 4, p.102, John Wiley & Sons, Inc., Hoboken New Jersey

[109] ASM Hand-book, Vol.13B, "Corrosion: Materials", First Printing (November 2005), p.62, ASM International, Ohio, USA

[110] D. A. Jones, "Principles and Prevention of Corrosion, Chapter 7: Pitting and Crevice Corrosion", p.198, Macmillan Publishing Company, New York

[111] J. Soltis, "Passivity Breakdown, Pit Initiation and Propagation of Pits in Metallic Materials – Review", Corrosion Science 90 (2015), p.5-22

[112] Robert G-Kelly, John R-Scully, David W-Shoesmith, and Rudolph G. Buchheit, "Electrochemical Techniques in Corrosion Science and Engineering", Chapter 3, p.55, Marcel Dekker, Inc. New York

[113] D. C. Silverman, "Practical Corrosion Prediction Using Electrochemical Techniques", Chapter 85, Uhlig's Corrosion Handbook, Third Edition

[114] S. Esmailzadeh, M. Aliofkhazraei, H. Sarlak, "Interpretation of Cyclic Potentiodynamic Polarization Test Results for Study of Corrosion Behaviour of Metals: A Review", Protection of Metals and Physical Chemistry of Surfaces, 54 (2018), p.976-989

[115] A. Sara, Y. Yongsun, C. Pyungyeon, J. Changheui, B. Philip, "Passivity Breakdown of 316L Stainless Steel during Potentiodynamic Polarization in NaCl Solution", Corrosion Science 111 (2016), p.720-727

[116] Y. T. Sun, J. M. Wang, Y. M. Jiang, J. Li, "A Comparative Study on Potentiodynamic and Potentiostatic Critical Pitting Temperature of Austenitic Stainless Steels", Materials and Corrosion, 69 (2018), p.44-52

[117] R A Cottis, M J Graham, R Lindsay, S B Lyon, J A Richardson, J D Scantlebury, F H Stott, "Shreir's Corrosion", Vol.1, Fourth Edition, p.44, Elsevier B.V, Amsterdam, The Netherlands

[118] Perez N, "Electrochemistry and Corrosion Science", Kluwer Academic Publishers, Boston, 2004, p.83-105

[119] Roberge P-R, "Corrosion-Engineering: Principle and Practice", McGraw-Hill, New York, 2008, p.112-114

[120] L. L. Shreir, G. T. Burstein, R. A. Jarman, "Corrosion: Metal/Environmental Reactions", Vol.1, Third Edition 1994, Butterworth-Heinemann, Oxford, Reprinted 2000, p.92

[121] Badea G.E, Caraban A, Sebesan M, Dzitac S, Cret P, Setel A, "Polarization Measurements used for Corrosion Rates Determination", Journal of Sustainable Energy, Vol. 1, No. 1, March 2010

[122] E. McCafferty, "Validation of Corrosion Rates Measured by the Tafel Extrapolation Method", Corrosion Science, Vol. 47, Issue 12, (December 2005), p.3202-3215

[123] P.C-Pistorius, G.T-Burstein, "Metastable Pitting Corrosion of Stainless-Steel and the Transition to Stability", Philosophical Transactions of The Royal Society A Mathematical Physical and Engineering Sciences, 341(1992), p.531-559

[124] Gerald S Frankel, L. Stockert, Fritz Hunkeler, H. Boehni, "Metastable Pitting of Stainless Steel", CORROSION, July 1987, Vol.43, No.7, p.429-436, NACE International, Houston, Texas, USA

[125] Wenming Tian, Nan Du, Songmei Li, Sibing Chen, Qunying Wu, "Metastable Pitting Corrosion of 304 Stainless Steel in 3.5% NaCl Solution", Corrosion Science, Vol. 85, August 2014, p.372-379

[126] P.C. Pistorius, G.T. Burstein, "Aspects of the Effects of Electrolyte Composition on the Occurrence of Metastable Pitting on Stainless Steel", Corrosion Science, Vol. 36, Issue 3, March 1994, p.525-538

[127] David E. Williams, John Stewart, Peter H. Balkwill, "The Nucleation, Growth and Stability of Micro pits in Stainless Steel", Corrosion Science, Vol. 36, Issue 7, July 1994, p.1213-1235

[128] R A Cottis, M J Graham, R Lindsay, S B Lyon, J A Richardson, J D Scantlebury, F H Stott, "Shreir's Corrosion", Vol.3, fourth Edition, p.2170, Elsevier B.V, Amsterdam, The Netherlands

[129] N.J. Laycock, R.C. Newman, "Temperature Dependence of Pitting Potentials for Austenitic Stainless Steels above their Critical Pitting Temperature", Corrosion Science, Vol.40, Issue 6, (June 1998), p.887-902

[130] Nihal U. Obeyesekere, "Chapter 9: Pitting Corrosion", Trends in Oil and Gas Corrosion Research and Technologies: Production and Transmission, Woodhead Publishing series in Energy (2017), p.215-248

[131] Béla Leffler, "STAINLESS-Stainless Steel and their Properties", Outokumpu, p.12-13

[132] C.P. Dillion, "Corrosion Resistance of Stainless Steels", "Aqueous Corrosion: Corrosion by Soil", 1995, p.93, Marcel Dekker Inc., 270, Madison Avenue, New York, USA

[133] M. Romanoff, "Underground Corrosion", National Bureau of Standards, Circular 579. US Government Printing Office, Washington, 1957

[134] W. F. Gerhold, E. Escalante, B. Sanderson, "The Corrosion Behaviour of Selected Stainless Steels in Underground Soil Environments", Report No. NBSIR 81-2228, National Bureau of Standards, Washington, 1981

[135] R. Winston Revie and Herbert H. Uhlig, "Corrosion and Corrosion Control", "Chapter 10, Corrosion in Soils", 2008, p.205-213, John Wiley & Sons, Inc.

[136] M. J. Wilmott, T. R. Jack, "Chapter 20, Corrosion by Soils", Uhlig's Corrosion Handbook", Second Edition, 2000, p.329-348,Edited by R. Winston Revie, John Wiley & Sons, Inc.

[137] Slessarev, Eric-W.; Lin, Yuan; Bingham, Nina-L.; Johnson, Jennifer E.; Dai, Yongjiu; Schimel, Joshua P.; Chadwick, Oliver A, "Water Balance Creates A Threshold in Soil pH at the Global Scale", Nature 540 (7634), 21 November 2016, p.567

[138] W. Stumm, J. J. Morgan, "Aquatic Chemistry: Chemical Equilibria and Rates inNatural Waters", 3rd edition, Wiley, New York,1996

[139] L. Sjogren, G. Camitz, J. Peultier, S. Jacques, V. Baudu, F. Barrau, B. Chareyre, A. Bergquist, A. Pourbaix and P. Carpentiers, "Corrosion Resistance of Stainless Steel Pipes in Soil", Materials and Corrosion 2011, Vol. 62, No. 4, p.1-11

[140] Japan Stainless Steel Association, (JSSA) and Nickel Development Institute (NiDI), "A Report on the Performance of Stainless Steel Pipe for Water Supply in Underground Soil Environments", Volume 1, 2, 3, 1988-1997, Nickel Institute, Brookfield Place, 161 Bay, Street, Suite 2700, Toronto, Ontario, Canada

[141] Lissel Pilcher, "Guidelines for Use of Stainless Steel in the Ground, April 2018, Australian Stainless Steel Development Association (ASSDA), Level 9, 307 Queen Street, Brisbane QLD 4000, Australia

[142] Pierre-Jean Cuna, "Corrosion Resistance of Stainless Steels in Soils and in Concrete", October 2001, p.1-12, Ceocor, Biarritz(Paper presented at the Plenary Days of the Committee on the Study of Pipe Corrosion and Protection)

[143] Pierre R. Roberge, Handbook of Corrosion Engineering, Chapter 2: Environments", (2000), p.150, McGraw-Hill, 11 West 19th Street, New York, NY 10011

[144] Fuente, D. d. l., Chico, B., Morcillo, M., "The Effects of Soluble Salts at the Metal/Paint Interface: Advances in Knowledge",Portugaliae Electrochimica Acta 24 (2006), p.191-206

[145] Ukpaka, C.P., "Detrimental Effect of Water Soluble Contaminant on Steel/Paint Interface", AMIRJ 2:2 (2014), p.1–4

[146] Kenneth B-Tator, "Soluble Salts and Coatings- an Overview, Part 1: A Summary of Recent Research on Allowable Amounts of Salts Tolerated beneath Coatings", JPCL(2010), p.50-63

[147] Victor Elias, P.E., Kenneth L. Fishman, Ph.D., P.E., Barry R. Christopher, Ph.D., P.E. and Ryan R. Berg, P.E., "Corrosion/Degradation of Soil Reinforcements for Mechanically Stabilized Earth Walls and Reinforced Soil Slopes"' U. S. Department of Transportation

Federal Highway Administration Publication No. FHWA-NHI-09-087, November (2009), Chapter 2, p.18

[148] Al Tayyib A.J., Khan M.S., "Effect of Sulphate Ions on the Corrosion Rebars Embedded in Concrete", Cement and Concrete Composites, Vol.13, Issue 2 (1991), p.123-127

[149] B.J. Little, R. Ray, P. Wagner, Z. Lewandowski, W.C. Lee, W.C. Characklis,"Biofouling 3" (1991), p.43.

[150] B.J. Little, P.A. Wagner, K.R. Hart, R.I. Ray, "Spatial Relationships Between Bacteria and Localized Corrosion", CORROSION (1996), paper no. 278, NACE International, Houston, Texas, USA

[151] Zaki Ahmad, "Principles of Corrosion Engineering and Corrosion Control," First edition (2006), Chapter 2, p.13, Butterworth-Heinemann, Oxford

[152] Michael J. Szeliga, "Stray current Corrosion: Chapter 11, Peabody's Control of Pipeline Corrosion", p.211-236, Second Edition (2001), Edited by Ronald L. Bianchetti, NACE International, Houston, Texas, USA

[153] Dwight G. Weldon, "Failure Analysis of Paints and Coatings", Revised Edition (2009), Chapter 2, p.14, John Wiley & Sons Ltd, The Atrium, Southern Gate, Chichester, West Sussex, PO19 8SQ, United Kingdom

[154] Z. Makama, I. Doble, D. Nicolson, M. E. Webb, I. B. Beech, S. A. Campbell, J. R. Smith, "Surface Preparation of Stainless Steel 316L,Bronze CW451K and Titanium Ti6Al4V for bonding to Polyurethane in Marine Cable Connector Assemblies", Transactions of the Institute of Materials Finishing, Vol.89 (2001), No. (5), p.237-243

[155] British Stainless Steel Association, "Paint Coating Stainless Steels", (2018), p.1-2, BSSA, Regus, Blades Enterprise Centre, John Street, Sheffield S2 4SW

[156] Stefan Schafföner, Christin Dietzea, Steffen Möhmelb, Jens Fruhstorfera, Christos G. Aneziris, "Refractories containing Fused and Sintered Alumina Aggregates: Investigations on Processing, Particle Size Distribution and Particle Morphology", Ceramics International, Vol. 43, Issue 5, April 2017, p.4252-4262

[157] Richard N. Sloan Pipeline Coatings: Chapter 2, Peabody's Control of Pipeline Corrosion", p.7-20, Second Edition (2001), Edited by Ronald L. Bianchetti, NACE International, Houston, Texas, USA

[158] Mohammad Ijaz , "Comparing Powder and Liquid Coatings for Pipeline Applications" Paint and Coating Industry, 2401 W. Big Beaver Rd., Suite 700, Troy, MI

[159] "Aldrich 188050" Sigma-Aldrich Chemical Private Limited Industrial Area, Anekal Taluka, Plot No. 12, 12 Bommasandra - Jigani Link Road, Bangalore, India

[160] Priyank Purohit, Akanksha Bhatt, Ravi K. Mittal, Magda H. Abdellatti, and Thoraya A. Farghaly, "Polymer Grafting and its Chemical Reactions", Frontiers in Bioengineering and Biotechnology, January 2023, p.1-23

[161] Kirk M. Cantor, Patrick Watts, "Chapter 1: Plastics Materials", Applied Plastics Engineering Handbook, Processing and Materials, (2011), p.3-5, William Andrew Publisher

[162] Amy Forsgren, "Chapter 6: Weathering and Aging of Paints", Corrosion Control through Organic Coatings, Edition (2006),p.99-101, Taylor & Francis Group, 6000 Broken Sound Parkway NW, Suite 300 Boca Raton, FL,USA

[163] K. Alfaramaw, "Optical and Dielectric Dispersion Parameters of General Purpose Furnace (GPF) Carbon Black Reinforced Butyl Rubber", Polymer Bulletin, Vol. 75 (2018), p.5713-5730, Springer-Verlag GmbH Germany

[164] James M. Sloan, "Butyl Rubber: Compound Development and Characterization", Army Research Laboratory, Report No. ARL-TR-2224, April 2000

[165] "Butyl Rubber: A Techno-commercial Profile", Chemical Weekly, November 3, 2009, Vol. 55, No.12, p.207-211

[166] Thomas Rehberg, Michael Schad, "Corrosion Protective Coating Technology for Transit Pipelines in Europe", 3R International, No.2 (2010), p. 62-69, 3R International Special Edition

[167] "Innowrap Application Procedures", (2017), p.22-23, Innochem Company Limited, 199-17, Bangkkoji-gil, Seotan-myeon Pyeongtaek-city, Gyeonggi-do South Korea 17704

[168] Janik H., Sienkiewicz M., Kucinska, Lipka J, "Polyurethanes. In Handbook of Thermoset Plastics", Third edition (2014), p.253–295, Dodiuk H., Goodman, S. H., Eds. William Andrew Publishing: Boston

[169] Felipe M. de Souza, Pawan K. Kahol, Ram K. Gupta, "Chapter 1: Introduction to Polyurethane Chemistry" (2021), p.1-24, American Chemical Society (ACS), Washington, DC, USA

[170] Kurt C. Frisch Jr., "Chapter 16 - Chemistry and Technology of Polyurethane Adhesives", Adhesion Science and Engineering-1,The Mechanics of Adhesion, Edited By D.A. Dillard and A.V. Pocius, Volume 2 (2002), Elsevier Science B.Y, p.759-812

[171] John O. Akindoyo, M. D. H. Beg, Suriati Ghazali, M. R. Islam, Nitthiyah Jeyaratnam, A. R. Yuvaraj, "Polyurethane Types, Synthesis and Applications - A Review", RSC Advances, Issue 115 (2016), p.114453-114482

[172] Shiwei William Guan, "100% Solid Polyurethane and Polyurea Coatings Technology", Coatings World, March 2003, p.49-58

[173] Chy Hyung Kim, "A Comparison of the Dielectric Behaviour of Aromatic and Aliphatic Polyurethanes in Relation to Transitional Phenomena", Transactions on Electrical and Electronic Materials, Vol. 18, No. 4, (August 25, 2017), p. 211-216

[174] Jan Frederik Doddema, "Use of 100% Self-Healing Fully Amorphous Visco-Elastic Coating Against Corrosion" Paper No.10042, NACE Conference, CORROSION 2010, NACE International, 15835 Park Ten Place, Houston, Texas 77084, USA

[175] Kenneth S. Whiteley; T. Geoffrey Heggs; Hartmut Koch; Ralph L. Mawer; Wolfgang Immel (2005). "Polyolefins". Ullmann's Encyclopaedia of Industrial Chemistry. Weinheim: Wiley-VCH

[176] Marc Andre Meyers and Krishan Kumar Chawla, "Mechanical Behaviour of Materials", (2009), p.98-103, Cambridge University Press, The Edinburgh Building, Cambridge CB2 8RU, UK

[177] John D Ferry, "Viscoelastic Properties of Polymers", Third Edition (1980),Chapter 3, p.56-58, John Wiley & Sons Inc., New York, USA

[178] D.J. Allen and H. Ishida, "Thermosets: Phenolics, Novolacs, and Benzoxazine", Encyclopaedia of Materials: Science and Technology, p.9226-9229

[179] Ralph Dammel Chapter 3: "Basic Chemistry of Novolaks". Diazo naphthoquinone-based Resists. Fifth Printing (1993), p.29, International Society for Optical Engineering (SPIE),Bellingham, Washington, USA.

[180]Yasuyuki-Shudo, Atsushi-Izumi, Takeshi-Takeuchi, Toshio-Nakao & Mitsuhiro Shibayama, "Dynamic Light Scattering Study of the Curing Mechanisms of Novolac-Type Phenolic Resins", Polymer Journal (2015) Vol. 47, p. 428-433, The Society of Polymer Science, Japan (SPSJ)

[181] Andreas Lendlein, Steffen Kelch, "Shape-Memory Polymers" Angew and te Chemie International Edition (2002), 41, p.2034-2057, WILEY-VCH Verlag GmbH, 69451 Weinheim, Germany

[182] Xuelian Wu, Wei Min Huang, Yong Zhao, Zheng Ding, Cheng Tang and Jiliang Zhang, " Mechanisms of the Shape Memory Effect in Polymeric Materials", Polymers (2013), Vol.5, p.1169-1202

[183] Tao Xie, "Recent Advances in Polymer Shape Memory", Polymer 52 (2011), p.4985-5000, Elsevier Ltd

[184] Kevin J. Bigham, "Heat Shrink Technology and Applications: An Overview", RESINATE , No.6, April 2019, p. 1-11, Zeus Industrial Products, Inc., 3737 Industrial Blvd. Orangeburg, SC 29118 USA

[185] R.L. Clough, "High-energy radiation and polymers: A review of commercial processes and emerging applications", Nuclear Instruments and Methods in Physics Research Section B: Beam Interactions with Materials and Atoms,185 (2001), p.8-33

Chapter - 3
Scope of Work

Chapter - 3: Scope of work

3. Introduction

Austenitic stainless steel resists dry corrosion in atmospheric exposure and hence, it does not need any protective coating in above-ground. But it cannot resist wet corrosion. Uncoated austenitic stainless steel pipeline in buried condition is doubtful when the resistance of soil is low enough and there is presence of corrosive halides like chlorides and also there is a deficiency in oxygen content in soil. Chlorides attack passive film and as a result, numerous pits are formed on austenitic stainless steel surfaces. After initiation of pitting in the localized area, growth of the pits are rapid. The penetration of pits into the austenitic stainless steel has resulted in a tiny perforation in the structure in a short time. In such phenomenon, metal weight loss is not noticeable. It is, therefore, extremely important to apply external polymeric (organic) protective coating on austenitic stainless steel pipeline in buried condition for longevity and reliability. In this chapter, the scope of work explains evaluation of six coatings on stainless steel pipes in various conditions. Corrosion prevention is crucial in marine environments and under thermal insulation for above-ground conditions.

3.1 Scope of Work

Research papers and literature have shown various protective coatings for carbon steel pipelines in buried or submerged condition. A large number of papers has revealed that several studies have been conducted by the researchers to protect austenitic stainless steel structures from pitting in marine atmosphere and corrosion under insulation. But the researchers perhaps have not paid much attention hitherto to study on suitable protective coatings for austenitic stainless steel pipelines in buried or submerged condition. There is an opportunity for studying and finding out answer to this problem. To deal and solve this problem for austenitic stainless steel pipelines in buried or submerged condition, six generic polymeric coatings commonly used for buried carbon steel pipelines in the petroleum, petrochemical and natural gas industries will be chosen for austenitic stainless steel pipelines. Each type of coating will be applied separately on each austenitic stainless steel pipe external surface after surface preparation. Samples will be extracted from the coated austenitic stainless steel pipes and will be subjected to relevant tests to investigate the coatings mechanical properties, coatings electrical and electrochemical properties, barrier, or degradation properties. The experimental data will be evaluated in comparing the coatings performances.

No coating is usually applied on austenitic stainless steel pipeline external surface in above-ground condition because austenitic stainless steel is a corrosion resistant material in atmospheric exposure. However, for austenitic stainless steel pipeline in above-ground condition, one coating will be selected among six coatings for one mechanical test to evaluate resistance to damage that may occur during transportation and storage of pipeline.

Austenitic stainless steel pipeline sometimes can pass through the areas being exposed to a condition which is similar to a splashed condition. In splashed condition, six coatings will be subjected to the salt spray test to evaluate probable deterioration in coatings materials or coatings properties.

3.2 Salient Points of Scope of Work

The scope of the study includes the following:

3.2.1 Selection of austenitic stainless steel pipe/grade, and plate/type.

3.2.2 Characterization of austenitic stainless steel pipe.

    3.2.2.1 Extraction of samples from austenitic stainless steels pipe.

    3.2.2.2 Chemical composition analysis.

    3.2.2.3 Mechanical testings.

    3.2.2.4 Microstructural analysis.

    3.2.2.5 Corrosion testings.

3.2.3 Surface preparation of austenitic stainless steel pipe and plate.

3.2.4 Selection of generic polymeric coatings.

3.2.5 Application of six coatings

    3.2.5.1 Application of each coating separately on each austenitic stainless steel pipe.

    3.2.5.2 Application of one coating on austenitic stainless steel plate.

3.2.6 Testing of samples for austenitic stainless steel pipeline in buried condition.

    3.2.6.1 Extraction of samples from coated austenitic stainless steel pipes.

    3.2.6.2 Mechanical testing.

    3.2.6.3 Electrical, electrochemical and corrosion testings.

3.2.7 Testing of samples for austenitic stainless steel pipeline in above-ground condition.

    3.2.7.1 Extraction of samples from coated austenitic stainless steel plate.

    3.2.7.2 One mechanical testing.

3.2.8 Testing of samples for austenitic stainless steel pipeline in splashed condition.

    3.2.8.1   Extraction of samples from coated austenitic stainless steel pipes.

    3.2.8.2   Samples exposed to corrosive (salt spray test) environment.

    3.2.8.3   Qualitative analysis of samples, before and after the salt spray tests.

    3.2.8.4   One mechanical testing, before and after the salt spray tests.

3.2.9   Analyse and correlate the data collected from above testings.

3.2.10 Correlate the coatings performances with basic parameters.

3.2.11 Evaluate ranking based on the coatings performances.

3.2.12 Develop modeling based on ranking from numerical methods/statistical analysis or modeling based on cost aspect/availability/productivity.

3.2.13 Draw conclusions of the study and recommend future scope of work.

Chapter - 4

Methodology

Chapter - 4: Methodology

4. Introduction

This chapter provides the comprehensive steps that will be followed in the process of conducting the laboratory experiments on the samples extracted from coated austenitic stainless steel pipe/plate in order to achieve the objective of the study. The results of the experiments will facilitate to evaluate the performances and ranking of the coatings. The effectiveness of the study will be addressed by a modeling based on ranking from numerical methods/statistical analysis or a modeling based on cost aspect/availability/productivity.

4.1 Methodology

The methodology of the research will be as follows:

4.1.1 Selection of Austenitic Stainless Steels

Austenitic stainless steels materials (pipe/grade and plate/type) will be selected to conduct the testing in the laboratories.

4.1.2 Characterization of Austenitic Stainless Steel Pipe

Three samples extracted from austenitic stainless steel pipe will be subjected to the following tests in the laboratory for characterization of austenitic stainless steel pipe material:

4.1.2.1 Chemical-Composition

4.1.2.2 Mechanical-Properties

4.1.2.3 Microstructure

4.1.2.4 Cyclic Potentiodynamic Polarization

4.1.2.5 Pitting Corrosion and Critical Pitting Temperature

4.1.2.1 Chemical-Composition

This test will be performed to determine carbon, chromium, manganese, nickel, molybdenum, silicon, sulphur, phosphorous and nitrogen of austenitic stainless steel pipe. The results will conform to the chemical composition of austenitic stainless steel pipe and grade.

4.1.2.2 Mechanical-Properties

This test will be conducted to determine the mechanical properties i.e. ultimate tensile strength, yield strength, % elongation and hardness of austenitic stainless steel pipe. The results will conform to the mechanical properties of austenitic stainless steel pipe and grade.

4.1.2.3 Microstructure

In this test, the samples will be electrolytic etched by 10% aqueous oxalic acid solution and the etched surfaces will be examined on a metallurgical microscope in order to evaluate the microstructural features of austenitic stainless steel pipe.

4.1.2.4 Cyclic Potentiodynamic Polarization

This test will be conducted on the samples in 3.5% sodium chloride (NaCl) solution at 23-25⁰C to determine susceptibility to localized pitting corrosion. Corrosion potential, corrosion current density, and critical pitting potential will be evaluated from the cyclic potentiodynamic polarization plots on semilogarithmic papers. These plots will represent polarization curves of potentials (ordinate) versus current densities (abscissa).After completion of the polarization test, localized pitting corrosion on SS316L bold surface will be investigated by scanning electron microscopy (SEM).

4.1.2.5 Pitting Corrosion Test and Evaluation of Critical Pitting Temperature

This test will be conducted on the samples in reagent grade 6% ferric chloride ($FeCl_3$) solution at 22-24⁰C for the determination of mass loss corrosion rate and critical pitting temperature that indicate significant pitting corrosion of austenitic stainless steel pipe.

4.1.3 Surface Preparation of Austenitic Stainless Steel Pipe and Plate

The external surfaces of austenitic stainless steel pipe and plate will be prepared by fused alumina (Al_2O_3) fine particles. Surfaces will be made dry and free from contamination prior to the application of coatings.

4.1.4 Selection of Polymeric Coatings

Six generic polymeric coatings commonly used for buried carbon steel pipeline in the petroleum, petrochemical and natural gas industries will be selected for austenitic stainless steel pipe and plate.

4.1.5 Application of Coatings

The standard practices for the application of coatings on carbon steel pipes in the petroleum, petrochemical and natural gas industries will be adopted for austenitic stainless steel pipe and plate:

4.1.5.1 Six coatings will be applied separately to the external surfaces of austenitic stainless steel pipes.

4.1.5.2 One coating among six coating will be chosen and applied to austenitic stainless steel plates

4.1.6 Testing of Samples in the Laboratories

The samples will be subjected to various relevant testings in the laboratories as per suitable conditions arising out of the industrial application in India and will cover the following areas:

4.1.6.1 Testing of samples extracted from six coated pipes for austenitic stainless steel pipeline in buried condition.

4.1.6.2 Testing of samples extracted from one coated plate for austenitic stainless steel pipeline in above-ground condition.

4.1.6.3 Testing of samples extracted from six coated pipes for austenitic stainless steel pipeline in splashed condition.

4.1.6.1 Testing of Samples for Austenitic Stainless Steel Pipeline in Buried Condition

The samples will be extracted from six coated austenitic stainless steel pipes and will be subjected to the following tests in the laboratories:

4.1.6.1.1 Thickness Measurement

4.1.6.1.2 Holiday Detection

4.1.6.1.3 Type D Shore Durometer Hardness

4.1.6.1.4 Impact Resistance

4.1.6.1.5 Indentation Resistance

4.1.6.1.6 Water Absorption (WA)

4.1.6.1.7 Cathodic Disbondment (CD)

4.1.6.1.8 Peel Strength

4.1.6.1.9 Pull-Off Adhesion

4.1.6.1.10 Hot Water Immersion (HWI)

4.1.6.1.11 Specific Electrical Insulation Resistance (SEIR)

4.1.6.1.12 Electrochemical Impedance Spectroscopy (EIS)

4.1.6.1.1 Thickness Measurement

This test will be carried out to measure the dry film thicknesses (DFT) of the coatings using PosiTector 6000, DeFelsko at eight points on each pipe surface. The coatings measured thicknesses will be recorded. An arithmetic mean value of thickness for each coating will be evaluated.

4.1.6.1.2 Holiday Detection

This test will be carried out on coatings by Model Nos.DC-05, SD-120 of Associate Electronics applying voltages based on type and thickness to ensure the coating free from holidays. The range of voltages applied to each coating and the test results will be reported.

4.1.6.1.3 Type-D Shore Durometer Hardness

This test will be performed to measure Shore hardness on coatings by Model No. EDHT-DII, STECH, Model No. DD-D, PCE Instruments. The hardness values of the coatings will be recorded. An arithmetic mean value of hardness for each coating will be evaluated.

4.1.6.1.4 Impact Resistance

This test will be carried out to verify the strengths of coatings by the impact of a punch of Drop Weight Testing Machine, Mech-Cad Services. A hemispherical head steel punch will be dropped from a fixed height and at a fixed temperature on the coated surface perpendicularly. Ten impacts will be carried out with the required impact energy based on the type of the coating. Immediately after the test, the holiday detection on each coating will be undertaken. The impact energy and the holiday detection result of each coating will be reported.

4.1.6.1.5 Indentation Resistance

This test will be performed to measure the indentation resistances of coatings under Thermostatically Controlled Chamber, DSH equipment. The sample with a cylindrical indenter will be placed in this chamber at a defined temperature for a particular duration. In this condition, the dial gauge reading with the indenter and without the mass will be recorded. After taking this initial reading, a weight mounted on the top of a cylindrical indenter will be applied on the sample being kept in thermostatically controlled chamber at a defined temperature for duration of 24 hours. This assembly will produce a pressure on the sample. In this pressurized condition, the dial gauge reading (final) with the indenter plus with the applied mass will be recorded. From the difference between the initial and final dial gauge readings, the indentation

depth will be computed and recorded. An arithmetic mean value of indentation depth for each coating will be evaluated.

4.1.6.1.6 Water Absorption

This test will be carried out to determine the amount of water absorbed by a flat coating sample. Before the test, the sample will be dried in an oven and weighed. This will be recorded as initial weight. Then the sample will be immersed in distilled water at a defined temperature for 28 days. After completion of the test, the sample will be taken out. With the help of a dry cloth, water will be cleaned off from each coating surface. Then the weight measurement will be performed for each coating by Weighing Balance Model No. HTR-220F, Vibra/Essae. This will be recorded as final weight. The amount of water absorbed by a coating will be determined from the difference between final weight and initial weight. The change will be expressed as a percentage of water absorbed by the coating with respect to the initial weight and recorded. An arithmetic mean value of the percentage of water absorbed by each coating will be evaluated.

4.1.6.1.7 Cathodic Disbondment

This test will be conducted to evaluate the disbondment resistance to a coating exposed to cathodic polarization, Potentiostat Model No.75-091-024, Coesfeld GmbH & Co. An artificial defect of a defined diameter, an intentional holiday will be created on the sample and subjected to cathodic disbondment test at 23-25°C for 28 days in a three-electrode system with 3% NaCl solution. The potential of the working electrode equals to -1500 mV with respect to the saturated calomel reference electrode (SCE) will be maintained. After completion of the test, four radial cuts will be made through the coating at the intentional holiday to the substrate and attempted to lift coating away from substrate. The measured disbondment of coating will be recorded. An arithmetic mean value of disbondment for each coating will be evaluated.

4.1.6.1.8 Peel Strength

This test will be carried out to determine the peel strengths of the coatings except liquid-applied coatings. This test will be performed to measure each coating peel strength with a universal tensile testing machine, Model No. H10KT, Tinius Olsen, at ambient condition and at a defined temperature. A coating strip will be cut in the circumferential direction into a desired shape. The peel force will be applied to the strip perpendicular to the test sample axis. The peel force will be evaluated from the arithmetic mean over 100 mm length of coating. The peel

strength will be computed based on the average peel force & the width of the coating and recorded. An arithmetic mean value of the peel strength for each coating will be evaluated.

4.1.6.1.9 Pull-off Adhesion

This test will be carried out to determine the pull-off adhesion strengths of liquid-applied coatings, Model No. PosiTest AT-A20, Make: DeFelsko Inspection Instruments. Steel dollies will be bonded directly to the coatings surfaces. A portable adhesion tester will be used to pull-off each dolly attached to each coating surface. Each pull-off force will be recorded. Each coating pull-off strength will be computed based on the surface area of the sample and recorded. The type of failure of the sample i.e. adhesive or cohesive will be recorded. An arithmetic mean value of the pull-off adhesion strength for each coating will be evaluated.

4.1.6.1.10 Hot Water Immersion

This test will be carried out to evaluate the loss of adhesion of coating due to hot water immersion (HWI), Water Oven, Model No. LECT 4852, Lubi, Shivam Enterprises. Before HWI, first set of samples will be subjected to the peel strength and pull-off adhesion tests at room temperatures based on coating types. Second set of samples will be subjected to HWI in a heated vessel for 100 days. After completion of the hot water immersion test, the samples will be subjected to the peel strength and pull-off adhesion tests at room temperatures based on the types of the coatings. The peel strength ratios and the pull-off adhesion strength ratios of the coatings will be computed based on the data obtained before and after the hot water immersion tests and will be recorded. An arithmetic mean value of the peel strength ratio and an arithmetic mean value of the pull-off adhesion strength ratio will be evaluated to compare coatings adhesion performances.

4.1.6.1.11 Specific Electrical Insulation Resistance

This test will be conducted for measuring the specific electrical insulation resistance (SEIR) of a coating by applying a direct current (DC), Model No. SISR-05, Caltech Engineering. The samples will be immersed in 0.1 mol/litre of NaCl solution over a period of 100 days. The specific electrical resistance of a coating will be measured at periodic intervals in relation to the surface area of the sample and will be recorded. A comparison of coatings performances will be drawn based on the coatings specific electrical insulation resistance values.

4.1.6.1.12 Electrochemical Impedance Spectroscopy

      This test will be carried out for measuring impedance of a coating by applying an alternating current (AC), Model 600+, GAMRY Instruments. The impedance of the coating will be measured with the attached cell to the coated sample using 3.5% NaCl solution. The measurements will be carried out at periodic intervals with an applied AC voltage of 100 mV$_{rms}$ in amplitude and in the frequency range of 100 kHz-10 mHz. The data will be represented by the Bode plots. A comparison of coatings performances will be drawn based on the coatings impedance values obtained from the Bode plots at 100 mHz (0.1Hz).

4.1.6.1.13 Analysis of Test Results and Graphs

      The test results and graphs obtained from all the above experiments will be thoroughly analysed. A comparison of coatings performances will be drawn, and the best coating will be identified.

4.1.6.2 Testing of Samples for Austenitic Stainless Steel Pipeline in Above-ground Condition

      Three plates will be extracted from an austenitic stainless steel plate. One coating among six coatings will be chosen and applied on these plates after surface preparation. The following tests will be conducted:

4.1.6.2.1 Chemical Composition of Austenitic Stainless Steel Plate.
4.1.6.2.2 Abrasion Resistance on the coated Austenitic Stainless Steel Plate.

4.1.6.2.1 Chemical Composition

      This test will be performed to determine carbon, chromium, manganese, nickel, molybdenum, silicon, sulphur, phosphorous and nitrogen of austenitic stainless steel plate. The results will conform to the chemical composition of austenitic stainless steel plate and type.

4.1.6.2.2 Abrasion Resistance

      This test will be conducted on the coated samples to determine the resistance of coating to abrasion produced by the Taber Abraser. Prior to abrasion testing, a hole of 6.3 mm will be drilled through the centre of each coated sample to allow fixturing to the Taber Abraser equipment. The sample will be mounted. Weighted abrading wheels (CS 17) will be placed on

the sample. A load of 1000g on each wheel will be applied for1000 cycles. The abrasion resistance of the coating will be computed as loss in weight in mg per 1000 cycles and will be recorded. The wear index of a coating i.e. average mass loss per 1000 cycles of abrasion will also be computed. An arithmetic mean value of weight loss and wear index for each coating will be evaluated.

4.1.6.3 Testing of Samples for Austenitic Stainless Steel Pipeline in Splashed Condition

The samples extracted from six coated austenitic stainless steel pipes will be subjected to the following tests in the laboratory:

4.1.6.3.1Fourier Transform Infrared Spectroscopy (FTIR)
4.1.6.3.2Type D Shore Durometer Hardness
4.1.6.3.3 Salt Spray

4.1.6.3.1 Fourier Transform Infrared Spectroscopy (FTIR)

The FTIR test will be conducted on the virgin coating and the coating exposed to the salt spray tests for a defined period. This method will cover the spectral range from 4000 – 500 cm^{-1} wave number. This analysis will be done based on the recording spectrum, which is a plot of transmittance in percentage (Y-axis, ordinate) versus wave number in cm^{-1} (X-axis, abscissa).

4.1.6.3.2 Type D Shore Durometer Hardness

This test will be performed to measure type-D Shore Durometer hardness of the virgin coating and the coating exposed to the salt spray tests for a defined period. The measured hardness values of the coatings will be recorded. An arithmetic mean value of hardness for each coating, before and after the salty spray test, will be evaluated.

4.1.6.3.3 Salt Spray

This test will be conducted on the coated pipe samples exposed in a salt spray test chamber for a defined period. The samples will be subjected to the salt spray environment, which is 5% NaCl solution at 35°C in the pH range from 6.5 to 7.2. Before atomizing the solution, it will be ensured that there would be no suspended solids in the solution. The effect of the salt spray test on the coating material will be studied.

4.1.6.3.4 Analysis of Test Results and Graphs

The test results and graphs obtained from the FTIR, and hardness tests, before and after the salty spray test, will be analysed. A comparison of coatings performances will be drawn and the best coating will be identified.

4.2 Comparisons of Coatings to Optimize Use in Different Conditions

The comparisons of coatings will be made based on the analysis of data collected from each test. For the purpose of ranking, the coatings will be rated on a scale of 1 to 6 in each test, where "1" will be the highest performance or highest corrosion resistance property of a coating. Other coatings will follow according to their values. The arithmetic mean of all the ratings for all the tests applicable for coatings will be written from lowest to highest order. The lowest order will be the coating highest performance or corrosion resistance property and will be ranked "1". Thus, the rankings for the coatings will be found out from the technological viewpoint to optimize coatings for austenitic stainless steel pipeline in buried and splashed condition.

4.3 Modeling

An attempt will be made to develop a model based on ranking from numerical methods/statistical analysis or a model based on cost aspect/availability/productivity.

4.4 Conclusions and Future Scope of Work

The conclusion will be drawn from the analysis of the study. Some aspects will be recommended in this thesis in which future studies of optimization of coating on austenitic stainless steel may be undertaken.

Chapter - 5

Materials and Methods

Chapter - 5: Materials and Methods

5. Introduction

The techniques and the different apparatuses used to investigate the properties of the anti-corrosive polymeric coatings applied on the external surfaces of austenitic stainless steels pipes and plates are described because the experimental set-up is essential to record the data precisely and accurately that influence to draw a proper conclusion of the study. In this chapter, the scope of each test along with the apparatus or instrumentation cell being used, information on sample preparation, the compositions of electrolytes and the description of each experimental procedure are presented. Tests have been conducted at 23-25°C and 50-60°C for water, oil/gas industries.

5.1 Materials and Methods

The details of materials and the relevant methods are described.

5.1.1 Selection of Austenitic Stainless Steel Material

Austenitic Stainless Steels, SS316L pipes (each pipe: 4-inch sch. 40s, 6.1 meter length, 6.0 mm thick) and SS316L plate (one plate: 400x400x2 mm) in solution-annealed conditions were selected. Low carbon grades were chosen to avoid any chromium carbide precipitation (i.e. sensitization) in the grain boundary. SS316L has higher pitting index no. than usual SS like 304, 304L.

5.1.2 Characterization of SS316L Pipe

Three samples extracted from SS316L pipe were subjected to the following tests in the laboratory:

5.1.2.1 Chemical-Composition

5.1.2.2 Mechanical-Properties

5.1.2.3 Microstructure

5.1.2.4 Cyclic Potentiodynamic Polarization

5.1.2.5 Pitting Corrosion and Critical Pitting Temperature

5.1.2.1 Chemical-Composition

5.1.2.1.1 Scope

The purpose of this test is to determine Carbon (C), Chromium (Cr), Manganese (Mn), Nickel (Ni), Molybdenum (Mo), Silicon (Si), Sulphur (S), Phosphorous (P), and Nitrogen (N). This test conforms to the chemical composition of SS316L pipe.

5.1.2.1.2 Apparatus

The following apparatuses used for chemical composition analysis are shown in Figure 5.1 a), b):

1) LECO Model 836 Series Combustion Analyzers, Make: LECO, USA
2) SPECTROLAB Model Spark Metal Analyzer, Make: Spectro Analytical Instruments GmbH, Germany

Figure 5.1: a) LECO Combustion Analyzer, b) SPECTROLAB Analyzer

5.1.2.1.3 Sample Preparation

For the determination of C, S, N, chips of about 1.0 mm thick were removed from SS316L pipe by drilling. For analysis of Cr, Mn, Ni, Mo, Si, P, the sample pieces were removed from SS316L pipe, and the sample surfaces were made flat by grinding.

5.1.2.1.4 Experimental Procedure

For C, S, N, samples were analysed by the combustion technique as per ASTM E-1019 [1].For the determination of Cr, Mn, Ni, Mo, Si, P, the samples were analysed by the spark atomic emission spectrometry according to ASTM E-1086 [2].The chemical composition analysis of SS316L pipe was recorded.

5.1.2.2 Mechanical Properties

5.1.2.2.1 Scope

The purpose of the mechanical tests is to determine the ultimate tensile strength, yield strength, % elongation and hardness of SS316L pipe.

5.1.2.2.2 Apparatus

The following apparatuses used for mechanical tests are shown in Figure 5.2 a), b):

1) UTS Machine Model WAW-C, Make: Jinan Precision Testing Equipment Co., Ltd., Shandong, China

2) Rockwell Hardness Tester Model RASNE-3, Make: Fuel Instruments & Engineers Pvt. Ltd., Kolhapur, Maharashtra, India

Figure 5.2: a) UTS Machine, b) Rockwell Hardness Tester

5.1.2.2.3 Sample Preparation

The standard 12.5 mm diameter round test samples with gauge lengths of 50 mm was prepared for tension testing. For hardness testing, the sample surface areas were prepared by removing surface irregularities.

5.1.2.2.4 Experimental Procedure

The tension and hardness testing were performed on the samples at room temperature in accordance with ASTM A-370 [3]. The ultimate tensile strength and 0.2% proof stress (yield strength) were evaluated from the stress-strain diagrams. The percentage elongations were computed fitting the ends of the fractured samples together and measuring the distances between

the gauge marks to the nearest 0.25 mm for gauge lengths of 50 mm. Rockwell B-scale hardness was measured applying first 10 kg minor load for a short time and then applying 100 kg major load to obtain depth of penetration by a 1.588 mm steel ball. The ultimate tensile strength, yield strength, % elongation and hardness in Rockwell B-scale of three samples were recorded. An arithmetic mean value of three samples was computed.

5.1.2.3 Microstructure

5.1.2.3.1 Scope

This test method covers a procedure for conducting the oxalic acid etch test to evaluate the microstructure of SS316L pipe.

5.1.2.3.2 Apparatus

The following apparatuses used for the microstructural examination are shown in Figure 5.3 a), b):

1) Carl Zeiss Model Primostar1, Make: Carl Zeiss Microscopy Deutschland GmbH, Germany

2) Leica Model DM500 Make: Leica Microsystems GmbH, Germany

a)   b)

Figure 5.3: Optical Microscope - a) Carl Zeiss, b) Leica

5.1.2.3.3 Sample Preparation

The samples were cut from SS316L pipe by shearing and the sample surfaces were prepared by polishing for electrolytic etching. The polished samples were etched by an aqueous 10% oxalic acid solution (COOHCOOH.2H$_2$O) at 1 ampere per cm^2 current density for about 1.5 minutes. After etching, the samples were rinsed in hot water and acetone.

5.1.2.3.4 Experimental Procedure

The etched surfaces of the samples were thoroughly examined on the metallurgical microscopes at 100x magnification. The microstructural features were recorded. All the photomicrographs of the samples were taken.

5.1.2.4 Cyclic Potentiodynamic Polarization

5.1.2.4.1 Scope

This test is performed to find out potential at which stable pitting occurs on SS316L pipe sample surface in chloride bearing atmosphere. The potential at which the anodic current increases rapidly indicates the initiation of localized corrosion. After the cyclic potentiodynamic polarization test, localized corrosion is investigated by the Scanning Electron Microscopy (SEM). Localized corrosion in the forms of pits is seen on SS316L bold surface.

5.1.2.4.2 Apparatus

The following apparatuses used for cyclic potentiodynamic polarization measurements are shown in Figure 5.4 a), b):

1) Gill AC Potentiostat with 5 channels, Make: ACM Instruments, UK
2) Polarization Cell, Thermometer, Luggin-Probe Salt Bridge, one Saturated Calomel Electrode (SCE), one Platinum Rod
3) SEM Machine, Model No. EVO 40, Make: Carl Zeiss AG, Germany
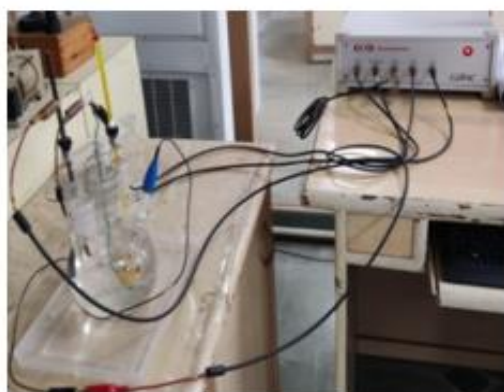
a)   b)

Figure 5.4: a) 3-electrode system, b) SEM Model No. EVO 40

5.1.2.4.3 Sample Preparation

SS316L samples were machined into flat 14-mm diameter disks. Coarse scratches of the samples were removed by wet grind and wet polish with Silicon Carbide (SiC) papers. Then the sample surfaces were rinsed thoroughly in distilled water and were made dry.

5.1.2.4.4 Experimental Procedure

The Cyclic Potentiodynamic Polarization test was conducted on SS316L samples at 25°C using three-electrode system within a glass cell according to ASTM G-61 [4]. In these three electrodes system, SS316L samples as working electrodes, a platinum rod as the counter electrode and SCE as the reference electrode, were used. The sample was mounted in the electrode holder and tightened the assembly with TEF-fluorocarbon gasket to avoid leakage. The platinum rod, Luggin-probe salt bridge and other components were placed in the glass cell. The cell was filled up with 3.5% NaCl solution. The Luggin probe-salt bridge separated the bulk solution from SCE. The probe tip was adjusted so that it was brought into close proximity with the working electrode.

After 1 hour of immersion, scanning was started at the corrosion potential (E_{corr}) and was continued in the noble direction at a rate of 10 mV/minute with a potential range from - 400 mV to + 600 mV. Current after reaching to 0.005 ampere, reverse scanning was done toward active potentials and continued until the corrosion potential was reached. From the potentiodynamic polarization plots i.e., potential in the vertical Y-axis (ordinate) and current density in the horizontal X-axis (abscissa) on semilogarithmic paper, the critical pitting potential (E_{pit}), the corrosion potential (E_{corr}), and the corrosion current density (i_{corr}) were evaluated. The significant pitting corrosion on sample (SS316L) surface was noticed by Scanning Electron Microscopy (SEM).

5.1.2.5 Pitting Corrosion and Critical Pitting Temperature
5.1.2.5.1 Scope

This test method covers a procedure to determine the resistance of SS316L pipe to pitting corrosion when exposed to oxidizing chloride environments. This test also evaluates the minimum temperature known as the critical pitting temperature to produce pitting attack on the bold surface of SS316L pipe.

Apparatus

The following weighing balance used for pitting corrosion measurement is shown in Figure 5.5:

1) Weighing Balance Model No. CY 124C, Make: Aczet Private Ltd., Mumbai

Figure 5.5: Weighing Balance Model No. CY 124C

5.1.2.5.3 Sample Preparation

The samples were cut from SS316L pipe by shearing and the sample surfaces were prepared by removing surface irregularities. Coarse scratches of the samples were removed by wet grind and wet polish with abrasive papers. Then the sample surfaces were rinsed thoroughly in distilled water and were made dry.

5.1.2.5.4 Experimental Procedure

Pitting corrosion test was conducted in $FeCl_3$ solution at ambient temperature for 72 hours. The test method is ASTM G-48 [5]. The samples were weighed before pitting corrosion tests. Samples were immersed in $FeCl_3$ solution. Using Equation (5-1), the initial temperature was evaluated to begin the test.

$$CPT \ (°C) = (2.5 \ x \ \% \ Cr) + (7.6 \ x \ \% \ Mo) + (31.9 \ x \ \% \ Ni) - 41.0 \ \dots\dots\dots\dots \ (5\text{-}1)$$

After completion of the test, the samples were weighed and recorded. Mass loss corrosion rate of a sample in g/cm^2 was computed based on the mass loss after pitting corrosion test and area of the sample. The critical pitting temperature (CPT) was evaluated from the minimum temperature that produced pits on the bold surfaces of SS316L pipe samples.

5.1.3 Surface Preparation of SS316L Pipe and Plate

External surfaces of SS316L pipe and plate were prepared by fused alumina (Al_2O_3) fine particles. Surfaces were made dry and free from contamination prior to the application of coatings.

5.1.4 Selection of Polymeric Coatings

Following six generic polymeric coatings were selected for SS316L material:

1) 3-Layer Poly-Ethylene (**3LPE**)
2) 3-ply/2-ply Cold-Applied Tape (**3p/2p CAT**)
3) Polyurethane (**PU**)
4) Visco-Elastic (**VE**)
5) Liquid Epoxy (**LE**)
6) Heat-Shrink Sleeve (**HSS**).

5.1.5 Application of Coatings

After surface preparation, the following coatings were applied on SS316L pipe and SS316L plate:

5.1.5.1 Six coatings were applied separately on the external surfaces of 4-inch SS316L pipes.

5.1.5.2 One coating i.e. solvent-free liquid-applied epoxy (LE) was applied to 2.0 mm thick SS316L plate.

5.1.6 Testings of Samples in the Laboratories

The testings of samples were conducted in the laboratories to cover the following areas:

5.1.6.1 Testings of samples extracted from six coated SS316L pipes for SS316L pipeline in buried condition.

5.1.6.2 Testings of solvent-free liquid-applied epoxy (LE) coated SS316L plate for SS316L pipeline in above-ground condition.

5.1.6.3 Testings of samples extracted from six coated SS316L pipes for SS316L pipeline in splashed condition.

5.1.6.1 Testing of Samples extracted from Six Coated SS316L Pipes for SS316L Pipeline in Buried Condition

The samples were subjected to the following tests:

5.1.6.1.1 Thickness Measurement

5.1.6.1.2 Holiday Detection

5.1.6.1.3 Type D Shore Durometer Hardness

5.1.6.1.4 Impact Resistance

5.1.6.1.5 Indentation Resistance

5.1.6.1.6 Water Absorption (WA)

5.1.6.1.7 Cathodic Disbondment (CD)

5.1.6.1.8 Peel Strength

5.1.6.1.9 Pull-Off Adhesion

5.1.6.1.10 Hot Water Immersion (HWI)

5.1.6.1.11 Specific Electrical Insulation Resistance (SEIR)

5.1.6.1.12 Electrochemical Impedance Spectroscopy (EIS)

5.1.6.1.1 Thickness Measurement

5.1.6.1.1.1 Scope

This test method covers a procedure to measure the thickness of the coating by the digital ultrasonic measuring instrument calibrated for the range of coating thickness being measured.

5.1.6.1.1.2 Apparatus

The following apparatus used for thickness measurement of the coatings is shown in Figure 5.6:

1) PosiTector 6000, Make: DeFelsko Inspection Instruments, USA

Figure 5.6: DeFelsko PosiTector 6000

5.1.6.1.1.3 Sample Preparation

The coated samples were prepared after cold cutting about 200 mm long, 4-inch pipe sections from the coated 4-inch SS316L pipes to conduct thickness measurement in the laboratory.

5.1.6.1.1.4 Experimental Procedure

The thickness measurement of each coating was performed by the digital ultrasonic thickness gauges in accordance with ISO: 21809-3 [6] Annex B. Thickness gauges were calibrated before measurements. At eight points on each pipe surface, thicknesses were measured by the digital gauge. Total of eight measurements were carried out on each coated sample. The measured thicknesses of coatings were recorded. An arithmetic mean of thickness for each coating was computed.

5.1.6.1.2 Holiday Detection
5.1.6.1.2.1 Scope

This test method covers a procedure for detecting coating holiday (i.e., porosity or pinhole) using high voltage sparking. The detector contains either light or sound signal.

5.1.6.1.2.2 Apparatus

The following apparatuses used for holiday detection of the coatings are shown in Figure 5.7 a), b):

1) Model No.DC-05, Sr. No.91 (up to 5 kV), Make: Associate Electronics, India
2) Model No.SD-120, Sr. No.515 (8-30 kV), Make: Associate Electronics, India

Figure 5.7: a) Model No.DC-05, b) Model No.SD-120

5.1.6.1.2.3 Sample Preparation

The coated samples were prepared after cold cutting about 200 mm long, 4-inch pipe sections from the coated 4-inch SS316L pipes to conduct holiday detection testing in the laboratory.

5.1.6.1.2.4 Experimental Procedure

The entire surface of each coating was subjected to a holiday test by the holiday detector. Holiday detector and earths were connected to the coated pipes. A metal brush as a scanning electrode was passed over the entire surface of the coated pipe at room temperature. At the time of the test, a range of voltage was applied to the coating based on the type of coating and thickness as per ISO: 21809-3 Annex C/NACE SP-0274 [6,7]. For liquid coatings (LE, PU), holiday detection is at 5kV/mm and for tape or tape-like (layer) coatings (3p/2p CAT, VE, 3LPE, HSS), holiday detection is at 5kV/mm+5kV and maximum 25 kV. The applied voltage and the holiday detection result for each coating were recorded.

5.1.6.1.3 Type D Shore Durometer Hardness

5.1.6.1.3.1 Scope

This test method specifies a procedure for the determination of the indentation hardness of the coating using Shore Durometer in D-scale. The indentation depth is measured.

5.1.6.1.3.2 Apparatus

The following apparatus used for hardness measurement of the coatings is shown in Figure 5.8:

    1) Model No. EDHT-DII, Make: STECH Engineers, India

Figure 5.8: Model No. EDHT-DII

5.1.6.1.3.3 Sample Preparation

The coated samples were prepared after cold cutting about 200 mm long, 4-inch pipe sections from the coated 4-inch SS316L pipes to conduct hardness measurement in the laboratory.

5.1.6.1.3.4 Experimental Procedure

Type D Shore Durometer hardness was measured on the sample at room temperature according to the ISO: 868 [8]. Each sample was placed on a hard flat surface and the pressure was applied. Five measurements of hardness readings were taken. An arithmetic mean of hardness for each coating was computed.

5.1.6.1.4 Impact Resistance

5.1.6.1.4 .1 Scope

This test method covers a procedure to verify the strength of the coating by the impact of hard steel punch with a hemispherical head. This punch falls perpendicularly on coating surface from a height of 1.0 metre at room temperature.

5.1.6.1.4.2 Apparatus

The following apparatus used for impact resistance of the coatings is shown in Figure 5.9:

1) Drop Weight Testing Machine Make: Mech-Cad Services, India

Figure 5.9: Drop Weight Testing Machine

5.1.6.1.4.3 Sample Preparation

      The coated samples were prepared after cold cutting about 200 mm long, 4-inch pipe sections from the coated 4-inch SS316L pipes to conduct impact resistance testing in the laboratory.

5.1.6.1.4.4 Experimental Procedure

      Before carrying out the test, the samples were checked by holiday detectors to ascertain the coatings free from porosity or pinhole. The impact resistance tests on the samples were carried out in accordance with ISO: 21809-3 Annex D. A steel punch of long 6 mm diameter rod attached to a hemispherical head of 25 mm diameter was dropped from a height of 1 metre on the coated surface perpendicularly. Ten impacts were carried out on each coating sample with the required impact energy evaluated based on the type and thickness of coating. Immediately after impact test, the samples were checked by holiday detectors. The impact energy and holiday detection result for each coating were recorded.

5.1.6.1.5 Indentation Resistance

5.1.6.1.5.1 Scope

      This test method covers a procedure to measure indentation resistance of a coating exposed to 55-60°C temperature.

5.1.6.1.5.2 Apparatus

      The following apparatuses used for indentation resistances of the coatings are shown in Figure 5.10:

1) Dial Gauges Model Nos. 3161, 3644, 1768, Make: KANN, India
2) Thermostatically controlled chamber, Make: DSH equipment

Figure 5.10: Thermostatically Controlled Chamber

5.1.6.1.5.3 Sample Preparation

The coated samples were prepared after cold cutting about 200 mm long, 4-inch pipe sections from the coated 4-inch SS316L pipes to conduct testing in the laboratory.

5.1.6.1.5.4 Experimental Procedure

This test was conducted in accordance with ISO: 21809-3Annex E. The samples with penetrometer were placed in thermostatically controlled chamber at 55-60°C. A penetrometer was comprised of a cylindrical indenter of 1.80 mm diameter. The dial gauge reading with the indenter without the mass was recorded. Then, on the top of indenter, 2.5 kg load was mounted. This assembly, indenter plus weight, produced a pressure of 10 N/mm^2 perpendicularly on coating. This pressure was kept for 24 hour. After 24 hours, the dial gauge reading with the indenter with the mass applied was recorded. From the initial and final gauge readings, the indentation depth of each coating was determined. An arithmetic mean of the indentation depth for each coating was computed.

5.1.6.1.6 Water Absorption
5.1.6.1.6.1 Scope

This test method covers a procedure for determining the amount of water absorbed by the polymeric coatings, when immersed in distilled water at 23-25°C for defined periods of time.

5.1.6.1.6.2 Apparatus

The following apparatus used for weight measure measurements of the coatings is shown in Figure 5.11:

1) Weighing balance Model No. HTR-220F, Make: Vibra/Essae, India

Figure 5.11: Weighing Balance Model No. HTR-220F

5.1.6.1.6.3 Sample Preparation

The square-shaped samples (60 by 60 mm) from the coatings were dried in an oven for 24 h at 50°C and then were cooled in desiccators.

5.1.6.1.6.4 Experimental Procedure

After initial drying and before immersion, the samples were weighed and recorded as initial weights. The samples were then immersed in distilled water at 23-25°C for 28 days and test was conducted in accordance with ASTM D-570 [9] / ISO: 62 [10]. After completion of 28 days, the samples were taken out. With the help of a dry cloth, water was cleaned off from each coating surface. Then the weight measurement was performed for each coating. This was recorded as final weight. The amount of water absorbed by a coating was determined from the difference between final weight and initial weight. The change (C) was expressed as a percentage of the initial weight using the following Equation (5-2). An arithmetic mean value of the percentage of water absorbed by each coating was evaluated.

$$C = [(M_2 - M_1) / M_1] \times 100\% \dots\dots\dots\dots\dots (5\text{-}2)$$

Where,

M_1 = Initial weight of the sample in mg or g, after initial drying and before immersion

M_2= Final weight of the sample in mg or g, after immersion and wiping out surface water.

5.1.6.1.7 Cathodic Disbondment

5.1.6.1.7.1 Scope

The test method specifies a procedure to determine cathodic disbondment of a coating at ambient temperature. An artificial defect of a defined size is made on the coated sample.

5.1.6.1.7.2 Apparatus

The following apparatuses used for cathodic disbondment (CD) of the coatings are shown in Figure 5.12:

1) Potentiostat Model No. 75-091-024, Make: Coesfeld GmbH & Co., Germany

2) Saturated Calomel Electrode (SCE) as Reference Electrode

Figure 5.12: Cathodic Disbondment Test Assembly

5.1.6.1.7.3 Sample Preparation

The coated samples were prepared after cold cutting about 200 mm long, 4-inch pipe sections from the coated 4-inch SS316L pipes to conduct cathodic disbondment test. A 6.0 mm diameter hole through the coating was carefully made by drilling in the centre of each sample so that the depth of the hole in SS316L did not exceed 0.5 mm.

5.1.6.1.7.4 Experimental Procedure

This test was performed at 23-25ºC for 28 days in accordance with ASTM G-8 [11]. The samples were subjected to holiday testings before cathodic disbondment tests to ensure the coatings free from pinholes or porosities. The plastic pipe forming the electrolytic cell was placed

at the top of the sample with the artificial defect in the centre of the cell. The surface between the sample and the electrolytic cell was sealed with silicone sealant. The electrolytic cell was filled with 3% NaCl solution and the solution pH in the range of 6 to 9 was maintained during testing. The height of the electrolyte in the cell was maintained about 80mm.Saturated Calomel Electrode (SCE) as a reference electrode and platinum wire of 1 mm diameter as an auxiliary electrode were immersed in the electrolyte. A negative potential i.e., -1500 mV was applied between the reference electrode and the sample. After 28 days, the cell with the electrolyte was removed. The sample was rinsed with water and was made dry. Evaluation of the sample was performed making 4 radial cuts through the coating at the intentional holidays and attempting to lift the coating away from the substrate. The arithmetic mean value of cathodic disbondment for each coating was computed.

5.1.6.1.8 Peel Strength

5.1.6.1.8.1 Scope

This test method covers a procedure to measure peel strength of a coating. The adhesion test by peel strength method is performed with a universal tensile testing machine at ambient condition or at the desired temperature based on the type of coating.

5.1.6.1.8.2 Apparatus

The following apparatuses used for peel strength measurements of the coatings are shown in Figure 5.13 a), b):

1) Universal testing machine Model No. H10KT, Make: Tinius Olsen, UK
2) A temperature controlled box

a)   b)

Figure 5.13: a) UTS Model No. H10KT, b) Temperature Controlled Box

5.1.6.1.8.1.3 Sample Preparation

The coated samples were prepared after cold cutting about 200 mm long, 4-inch pipe sections from the coated 4-inch SS316L pipes to conduct peel strength testing in the laboratory.

5.1.6.1.8.1.4 Experimental Procedure

This test was performed as per ISO: 21809-3 Annex H. A coating strip of 160 mm long and 25 - 50 mm wide was cut in the circumferential direction of each layer/tape coating sample. The tests were performed at 23-25°C and at 55±5°C. During testing, the peel-force against extension length graph was generated for the sample. The peel strength of the sample was evaluated from the average force over 100 mm extension length. An arithmetic mean value of the peel strength for each coating was computed.

5.1.6.1.9 Pull-off Adhesion
5.1.6.1.9.1 Scope

This test method covers a procedure to measure pull-off adhesion strength of a coating. Dollies are bonded directly to the coated surfaces. The adhesion test by pull-off method is performed with a portable adhesion tester to break the dollies from the coated surfaces at ambient condition or at the desired temperature based on the type of coating.

5.1.6.1.9.2 Apparatus

The following apparatus used for pull-of adhesion strength measurements of the coatings is shown in Figure 5.14:

1) Model No. PosiTest AT-A20, Make: DeFelsko Inspection Instruments, USA

Figure 5.14: Adhesion Tester Model No. PosiTest AT-A20

5.1.6.1.9.3 Sample Preparation

The coated samples were prepared after cold cutting about 200 mm long, 4-inch pipe sections from the coated 4-inch SS316L pipes to conduct pull-of adhesion testing in the laboratory.

5.1.6.1.9.4 Experimental Procedure

The tests were performed as per ISO: 4624 [12] using three steel dollies of 20 mm diameters.

The rigid flat faces of steel dollies were bonded directly to the coatings surfaces. A portable adhesion tester was used to pull-off each dolly attached to each coating surface at 23-25°C and at 55±5°C temperatures. The measurement of each pull-off force was recorded. Each coating pull-off strength was computed based on the surface area of the sample and recorded. The type of failure of the sample i.e. adhesive or cohesive was recorded. For each coating, an arithmetic mean of pull strength was evaluated.

5.1.6.1.10 Hot Water Immersion
5.1.6.1.10.1 Scope

This test method covers a procedure for evaluating the coating to loss of adhesion due to hot water immersion for a specified duration. This test also helps in comparing the adhesion performances of the coatings.

5.1.6.1.10.2 Apparatus

The following apparatus used for hot water immersion (HWI) test of the coatings is shown in Figure 5.15:

1) Water Oven, Model No. LECT 4852, Make: Lubi, Shivam Enterprises, India

Figure 5.15: Hot Water Oven Model No. LECT 4852

5.1.6.1.10.3 Sample Preparation

The coated samples were prepared after cold cutting about 200 mm long, 4-inch pipe sections from the coated 4-inch SS316L pipes to conduct testing in the laboratory.

5.1.6.1.10.4 Experimental Procedure

3LPE, 3p/2p CAT, VE, HSS samples were initially subjected to the peel strength tests at 23°C. Likewise, LE and PU samples were initially subjected to the pull-off adhesion strength tests at 23°C. The adhesion values of the coatings obtained by these tests were recorded as P_0.

To carry out the HWI test, each sample bottom cut edge was sealed by sealant so that water cannot enter from bottom side. The coated pipe samples were immersed in warm service water kept in a vessel. The vessel was placed in an oven heated to 55±5°C for a period of 100 days. The HWI test was carried out as per ISO: 21809-3 Annex I. After completion of the hot water test, the samples were taken out and cooled at room temperature. 3LPE, 3p/2p CAT, VE, HSS samples and LE, PU samples were subjected to the peel strength tests at 23°C and pull-off adhesion strength tests at 23°C respectively. The adhesion values of the coatings obtained after HWI test were recorded as P_{100}. The ratio, P_{100}/P_0 for each coating of three samples was computed. An arithmetic mean of ratio for each coating was evaluated in comparing the adhesion performances of the coatings.

5.1.6.1.11 Specific Electrical Insulation Resistance
5.1.6.1.11.1 Scope

This test method covers a procedure for measuring the specific electrical insulation resistance of a coating quantitatively by applying a Direct Current (DC). The test samples are immersed vertically in 0.1 mol/litre of NaCl solution for a period of 100 days. The specific electrical resistance is measured in relation to the surface area of the coated sample.

5.1.6.1.11.2 Apparatus

The following apparatus used for electrical insulation resistance measurement of the coatings is shown in Figure 5.16:

1) Specific Electrical Insulation Resistance Tester, Model No. SISR-05, Make: Caltech Engineering Services, Mumbai, India

Figure 5.16: Model No. SISR-05

5.1.6.1.11.3 Sample Preparation

       The coated samples were prepared after cold cutting about 200 mm long, 4-inch pipe sections from the coated 4-inch SS316L pipes to conduct specific electrical insulation resistance testing in the laboratory.

5.1.6.1.11.4 Experimental Procedure

       The samples were immersed vertically in 0.1 mol/litre of NaCl solution in the plastic container. The submerged end of the sample was sealed with non-conductive sealant so that there was no contact with NaCl solution. A counter electrode, a copper rod of 10 cm^2 was immersed in NaCl solution in the plastic container. The test was carried out according to ISO: 21809-3 Annex F. Positive pole and negative pole of power supply were connected to top end of the sample and counter electrode respectively, during each measurement. 100V was applied during measurement and current & voltage were measured after 1 minute. Then, the measurements were continued at intervals for a total of 100 days. The specific electrical insulation resistance (Rs) in ohm square metre was calculated using the following Equation (5-3):

$$Rs = U \times A/I = R1 \times A \quad \text{............................ (5-3)}$$

Where,

R1 = Measured electrical resistance of the submerged sample in Ohm,

U = Voltage between counter electrode and test sample in Volt,

A = Submerged surface area of coating, expressed in Square Metre,

I = Measured current, expressed in Amperes.

110

For each coating, a graph of specific electrical insulation resistance against time was plotted. A comparison of coatings performances with respect to their specific electrical insulation resistance values against a total of 100 days was drawn.

5.1.6.1.12 Electrochemical Impedance Spectroscopy (EIS)

5.1.6.1.12.1 Scope

This test method covers a procedure to measure impedance of the coating quantitatively by applying an Alternating Current (AC). The results are represented by the Bode plots. This test also helps to investigate the electrical and electrochemical properties, barrier or degradation properties of the coating.

5.1.6.1.12.2 Apparatus

The following apparatus used for impedance measurements of the coatings is shown in Figure 5.17:

1) GAMRY Model Reference 600+, Make: GAMRY Instruments, USA

Figure 5.17: GAMRY Model Reference 600+

5.1.6.1.12.3 Sample Preparation

The coated samples were prepared after cold cutting about 200 mm long, 4-inch pipe sections from the coated 4-inch SS316L pipes to conduct electrochemical impedance spectroscopy testing in the laboratory.

5.1.6.1.12.4 Experimental Procedure

The impedances of the samples were measured with the attached cell methods. Each cell consisted of glass tube was cemented to each sample surface. The coated pipe surface acted

as WE (Working-Electrode). CE (Counter-Electrode) and RE (Reference-Electrode) were a Graphite rod and a Saturated Calomel Electrode (SCE) respectively. Cell was filled with 3.5% NaCl solution. EIS test was performed as per ASTM G-106 [13] using GAMRY Instruments Reference 600+ model at 23°C-25°C for an immersion period of 14 days. During testing, the samples with the attached cells were placed inside the Faraday cage to avoid noise. The measurements were carried out on 1st day, 7th day and 14th day at corrosion potential. During measurement, 100 mV in amplitude AC voltage with 100 kHz to 10 mHz frequency was applied. The data generated for the coatings during EIS measurement were represented by the Bode plots as impedance magnitudes, |Z| and phase angles, Φ (in the vertical Y-axes) versus the measured frequencies in Hertz (Hz) (in the horizontal X-axis). From the Bode plots, the impedances values of the coatings were evaluated. A comparison of coatings performances with respect to their impedance values at 0.1 Hz (100 mHz) frequency against a total of 14 days was drawn.

5.1.6.2 Testings of Solvent-Free Liquid-Applied Epoxy (LE) Coated SS316L Plate for SS316L Pipeline in Above-ground Condition

The samples were subjected to the following tests:

5.1.6.2.1 Chemical Composition of SS316L plate
5.1.6.2.2 Abrasion Resistance of coated plates

5.1.6.2.1 Chemical Composition of SS316L plate
5.1.6.2.1.1 Scope

The purpose of this test is to determine carbon (C), chromium (Cr), manganese (Mn), nickel (Ni), molybdenum (Mo), silicon (Si), sulphur (S), phosphorous (P), and nitrogen (N). This test conforms to the chemical composition of SS316L plate.

5.1.6.2.1.2 Apparatus

The following apparatuses used for chemical composition analysis have already been shown in Figure 5.1 a), b) under clause no. 5.1.2.1.2:

1) LECO Model 836 Series Combustion Analysers, Make: LECO, USA
2) SPECTROLAB Model Spark Metal Analyzer, Make: Spectro Analytical Instruments GmbH, Germany

5.1.6.2.1.3 Sample Preparation

For the determination of C, S, N, chips of about 1.0 mm thick were removed from SS316L pipe by drilling. For analysis of Cr, Mn, Ni, Mo, Si, P, the sample pieces were removed from SS316L pipe, and the sample surfaces were made flat by grinding.

5.1.6.2.1.4 Experimental Procedure

For C, S, N, samples were analysed by combustion technique as per ASTM E-1019. For the determination of Cr, Mn, Ni, Mo, Si, P, the samples were analysed by spark atomic emission spectrometry according to ASTM E-1086. The chemical composition analysis of SS316L plate was recorded.

5.1.6.2.2 Abrasion Resistance of coated plates

5.1.6.2.2.1 Scope

This test method specifies a procedure to determine the abrasion resistance of coating by the Taber Abraser.

5.1.6.2.2.2 Apparatus

The following apparatus used for abrasion resistance measurement of the coated samples is in Figure 5.18:

1) Taber Abraser, Model No.5135, Make: Taber Industries, USA

Figure 5.18: Taber Abraser Model No.5135

5.1.6.2.2.3 Sample Preparation

Three SS316L square plates with dimensions of 100 mm X 100 mm X 2.0 mm and with rounded corners were prepared for abrasion testing. A 6.5 mm hole was made at the centre of each plate. SS316L plates' surfaces were prepared by fused Al_2O_3 fine particles. Surfaces were

made dry and free from contamination prior to the application of coatings. Solvent-free liquid-applied epoxy (LE) coating of 900-950 microns was applied uniformly on these plates. The coated plates were cured properly before testing.

5.1.6.2.2.4 Experimental Procedure

This test was conducted as per ASTM D-4060 [14] using CS17 abrasive wheels with 1000g load for 1000 cycles. The test sample was mounted vertically on a turntable platform against the sliding rotation of two abrading wheels of the Taber Abraser. During testing, loose debris was removed by a vacuum system. Abrasion resistance was calculated as loss in weight (in mg) per 1000 cycles. An arithmetic mean of abrasion resistance for LE coating was evaluated.

5.1.6.3 Testings of Samples extracted from Six Coated SS316L Pipes for SS316L Pipeline in Splashed Condition

The samples were subjected to the following tests:

5.1.6.3.1 Fourier Transform Infrared Spectroscopy (FTIR)

5.1.6.3.2 Type D Shore Durometer Hardness

5.1.6.3.3 Salt Spray

5.1.6.3.1 FTIR

5.1.6.3.1.1 Scope

This test method covers a procedure for qualitative analysis of solid coating samples by infrared spectrometric technique. This technique is used to determine the functional groups in an organic molecule of the protective coating, to identify fingerprinting of coating, to identify contaminants in a coating, to determine improper mixing of coatings etc. This technique is useful for recording spectrum, which is a plot of measured infrared intensity (% transmittance) versus wave number (or frequency) of light. This method covers the spectral range from 4000 to 500 cm^{-1} wave number.

5.1.6.3.1.2 Apparatus

The following apparatus used for FTIR of the coatings is shown in Figure 5.19:

1) FTIR Spectrometer, Model No. ALPHA II with Opus 7.8 software, Make: Bruker, USA

Figure 5.19: FTIR Bruker Model No. ALPHA II

5.1.6.3.1.3 Sample Preparation

Solid samples were extracted from virgin coatings and from six coated SS316L pipes exposed to the salt spray test. The samples were placed on the anvil tip of the diamond crystal.

5.1.6.3.1.4 Experimental Procedure

This test was conducted according to the ASTM E-1252 [15] with ATR (Attenuated Total Reflection) technique. Before carrying out the salt spray test, the virgin coatings samples were analysed by FTIR technique. The samples absorbed some of the energy of the IR source depending on the functional groups present in the coatings and their characteristic vibration frequencies, which were transformed into unique spectrums. Similarly, FTIR analysis was carried out on the coatings samples being exposed to the saltwater test for 3000 hours and the spectrums were recorded. The spectrums obtained by FTIR techniques in both these conditions were studied.

5.1.6.3.2 Type D Shore Durometer Hardness

5.1.6.3.2.1 Scope

This test method specifies a procedure for the determination of the indentation hardness of the coating using Shore Durometer in D-scale. The indentation depth is measured.

5.1.6.3.2.2 Apparatus

      The following apparatus used for hardness measurement of the coatings is shown in Figure 5.20.

      1) Model No. DD-D, Make: PCE Instruments, UK

Figure 5.20: PCE Model No. DD-D

5.1.6.3.2.3 Sample Preparation

      The coated samples were prepared after cold cutting about 200 mm long, 4-inch pipe sections from the coated 4-inch SS316L pipes to conduct hardness measurement in the laboratory.

5.1.6.3.2.4 Experimental Procedure

      Type D Shore Durometer hardness was measured at room temperature according to the ISO: 868 on the virgin coatings and the coatings exposed to the saltwater test. Each coating sample was placed on a hard flat surface and the pressure was applied. Five measurements of hardness on each coating were taken. An arithmetic mean of hardness for each coating was computed.

5.1.6.3.3 Salt Spray

5.1.6.3.3.1 Scope

      This test covers a procedure to maintain the salt spray test environment in a given test chamber. This practice provides information on corrosion resistance of the coating exposed to a controlled corrosive environment(salt solution) for a specified duration.

5.1.6.3.3.2 Apparatus

The following apparatus used for the salt spray test of the coatings is shown in Figure 5.21.

1) Salt Spray Chamber Model No. SF/450, Make: C&W Specialist Equipment, Industrial Physics, UK

Figure 5.21: Salt Spray Chamber Model No. SF/450

5.1.6.3.3.3 Sample Preparation

The coated samples were prepared after cold cutting about 200 mm long, 4-inch pipe sections from the coated 4-inch SS316L pipes to conduct the salt spray test in the laboratory.

5.1.6.3.3.4 Experimental Procedure

Six coated samples were subjected to the salt spray test in 5% NaCl solution in accordance with ASTM B-117 [16] for a minimum period of 3000 hours. The solution pH was maintained in the range of 6.5 to 7.2 at 35°C.After completion of the salt spray test, six coatings were gently washed in distilled water to remove salt deposits from the coatings surfaces and then dried immediately. These coatings were subjected to FTIR and Type D Shore Durometer hardness tests.

5.1.7 References

[1] ASTM E-1019, "Standard Test-Methods for Determination of Carbon, Sulphur, Nitrogen, and Oxygen in Steel, Iron, Nickel, and Cobalt Alloys by Various Combustion and Inert Gas Fusion Techniques", ASTM International, 100 Barr Harbor Drive, P.O. Box C700, West Conshohocken, PA19428-2959, USA

[2] ASTM E-1086, "Standard Test-Method for Analysis of Austenitic Stainless Steel by Spark Atomic Emission Spectrometry", ASTM International, USA

[3] ASTM A-370, "Standard Test-Methods and Definitions for Mechanical Testing of Steel Products", ASTM International, USA

[4] ASTM G-61,"Standard Test-Method for Conducting Cyclic Potentiodynamic Polarization Measurements for Localized Corrosion Susceptibility of Iron, Nickel, or Cobalt-Based Alloys", ASTM International, USA

[5] ASTM G-48, "Standard Test-Methods for Pitting and Crevice Corrosion Resistance of Stainless Steels and Related Alloys by Use of Ferric Chloride Solution", ASTM International, USA

[6] ISO: 21809-3, "Petroleum and natural gas industries - External coatings for buried or submerged pipelines used in pipeline transportation-systems -Part 3:Field joint-coatings", ISO office, Chemin de Blandonnet8, CP 401, CH-1214 Vernier, Geneva, Switzerland

[7] NACE SP-0274, "High-Voltage Electrical Inspection of Pipeline Coatings", 15835 Park Ten Place, NACE International, Houston, Texas 77084, USA

[8] ISO: 868, "Plastics and ebonite - Determination of Indentation-Hardness by means of a Durometer (Shore-hardness)", ISO office, Switzerland

[9] ASTM D-570, "Standard Test-Method for Water Absorption of Plastics", ASTM International, USA

[10] ISO: 62, "Plastics - Determination of water absorption" ISO office, Switzerland

[11] ASTM G-8, "Standard Test-Methods for Cathodic Disbonding of Pipeline Coatings", ASTM International, USA

[12] ISO: 4624, "Paints and varnishes - Pull-off test for adhesion" ISO office, Switzerland

[13] ASTM G-106, "Standard Practice for Verification of Algorithm and Equipment for Electrochemical-Impedance Measurements", ASTM International, USA

[14] ASTM D-4060, "Standard Test-Method for Abrasion Resistance of Organic Coatings by the Taber Abraser", ASTM International, USA

[15] ASTM E-1252, "Standard Practice for General Techniques for Obtaining Infrared Spectra for Qualitative-Analysis", ASTM International, USA

[16] ASTM B-117, "Standard Practice for Operating Salt-Spray (Fog) Apparatus", ASTM International, USA.

Chapter - 6

Results and Discussion

Chapter - 6A

Characterization of SS316L Pipes

Chapter - 6A: Characterization of SS316L Pipes

6A Introduction

It is very safe, reliable and economical to dispatch petroleum products to distant places through SS316L pipelines. A major portion of a pipeline remains buried in soil for a safe operation and without public interruption. Only a small portion of a pipeline remains in above-ground and splashed conditions. An uncoated SS316L pipeline in buried condition can suffer localized pitting corrosion in aquatic soil in the presence of chlorides ions. Pitting corrosion can perforate buried SS316L pipeline within short duration. For that reason, protective polymeric coatings are needed to prevent leaks and to maintain the integrity & longevity of SS316L pipeline in buried condition.

Based on the above view, more attention has been paid to SS316L pipeline in buried condition in the present study. Six generic polymeric coatings were selected and applied separately on4-inch SS316L pipes external surfaces to represent coatings for SS316L pipelines in buried conditions. Before carrying out extensive testing for coatings, it was judiciously decided at the beginning of the proposed study to extract three samples from SS316L pipes for chemical composition analysis, mechanical properties, microstructure, and corrosion testing to represent the whole lot of SS316L pipes. It is because the factory made SS316L pipes may not remain uniform or homogeneous composition throughout and there may be small variations in composition and process. Moreover, the results of three SS316L samples obtained by the above-mentioned testing provide very reliable and authentic data. The average of the three results i.e. an arithmetic mean estimates a very realistic effect on arriving at more accurate and correct result to characterize SS316L pipes.

In this chapter, the results obtained by the chemical composition analysis, mechanical testing, microstructural examination, and corrosion testing of SS316L pipes, and the subsequent discussions are presented.

6A.1 Results and Discussion on Chemical, Mechanical, and Microstructure of SS316L Pipes

The chemical composition analysis, mechanical testing, and microstructural examination were carried out on SS316L samples.

6A.1.1 Results of Chemical Composition Analysis

Three samples were drawn from 4-inch SS316L pipes and were analysed for chemical composition. Carbon (C), Sulphur (S) in weight percentages (%) and Nitrogen (N) in ppm were determined by the combustion technique as per ASTM E-1019 [1]. Other elements such as Chromium (Cr), Manganese (Mn), Nickel (Ni), Molybdenum (Mo), Silicon (Si), Phosphorous (P) in weight percentages (%) were determined by the spark atomic emission spectrometry according to ASTM E-1086 [2]. The chemical composition analysis of three samples is shown in Table 6A.1.

Table 6A.1: Chemical Composition Analysis of SS316L Pipes (in wt%)

Sample no.	C	Mn	S	P	Si	Cr	Ni	Mo	N (ppm)*	Fe
Sample 1	0.021	1.24	0.005	0.042	0.26	16.32	10.05	2.03	380	Balance
Sample 2	0.022	1.25	0.004	0.043	0.27	16.08	10.06	2.03	395	Balance
Sample 3	0.018	1.27	0.004	0.043	0.20	16.29	10.05	2.04	440	Balance

(**ppm** - parts per million)

6A.1.2 Discussion on Chemical Composition Analysis

In the chemical composition analysis of the samples, C, Mn, Si, Cr, Ni, Mo in wt% and N in ppm have been found to be in the range of 0.018-0.022, 1.24-1.27, 0.20-0.27, 16.08-16.32, 10.05-10.06, 2.03-2.04, and 380-440 respectively. Very low level of S and P has been found to be in the range of 0.004-0.005 and 0.042-0.045 respectively in the chemical analysis. The chemical composition analysis of three samples has shown minor variations in wt% of the elements. The chemical composition conforms to austenitic stainless steel pipe grade SS316L intended for high-temperature and general corrosion service applications in accordance with ASTM A-312 [3].

6A.1.3 Results of Mechanical Testing

The tension and hardness testing were performed on the three samples at room temperature in accordance with ASTM A-370 [4]. Three samples of standard sizes with gauge lengths of 50 mm were prepared for tension testing. Ultimate tensile strength and 0.2% proof stress (yield strength) were evaluated from the stress-strain diagrams. The percentage elongations were computed fitting the ends of the fractured samples together and measuring the distances between the gauge marks to the nearest 0.25 mm for gauge lengths of 50 mm.

For hardness testing, the subjected surface areas of the samples were prepared by removing surface irregularities Rockwell B-scale hardness was measured applying first 10 kg minor load for a short time and then applying 100 kg major load to obtain depth of penetration by a 1.588 mm steel ball.

The ultimate tensile strength in MPa, 0.2% proof stress in MPa, % elongation and hardness in Rockwell B-Scale of three samples are shown in Table 6A.2.

Table 6A.2: Mechanical Properties of SS316L Pipes

Sample no.	Ultimate Tensile Strength (MPa)	0.2% Proof Stress (MPa)	% Elongation in 50 mm	Average Rockwell Hardness (B Scale)
Sample 1	578	323	54	81, 82, 83
Sample 2	579	323	54	81, 82, 83
Sample 3	579	321	52	81, 82, 83

6A.1.4 Discussion on Mechanical Testing

The ultimate tensile strength, 0.2% proof stress, and elongation have been found to be 578-579 MPa, 321-323 MPa, and 52-54% respectively. The mechanical properties are found to be almost identical for the three samples. The hardness values are also found to be identical for the three samples, in the range of 81-83 HRB. Therefore, all the three SS316L samples are virtually found to be identical. The mechanical properties conform to pipe grade SS316L intended for high-temperature and general corrosion service applications in accordance with ASTM A312.

6A.1.5 Results of Microstructural Examination

Three samples were sheared from SS316L pipes. The samples surfaces were polished for electrolytic etching. The polished surfaces were etched by an aqueous 10% oxalic acid solution (COOHCOOH.2H$_2$O) at 1 ampere per cm^2 current density for about 1.5 minutes. Acetone and hot water were used to rinse the sample after etching. The microstructural features were observed under metallurgical microscope at a magnification of 100x. The photo-micrographs of the samples are shown in Figure 6A.1.

Sample 1   Sample 2   Sample 3
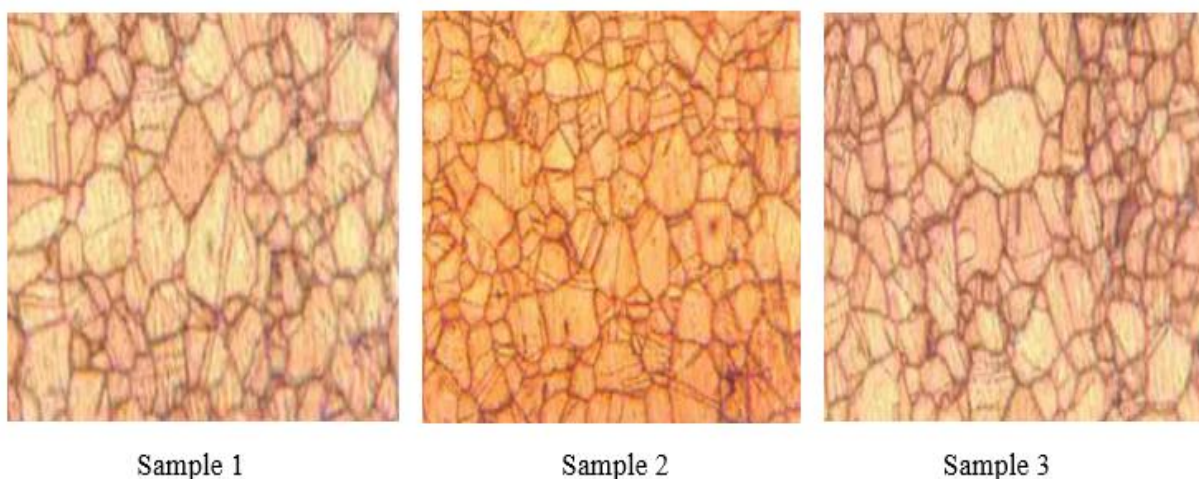
Figure 6A.1: Microstructures of SS316L Samples

6A.1.6 Discussion on Microstructural examination

The microstructures of three SS316L samples are found to be identical. It has been observed austenitic equiaxed grains, characteristic annealing twins, and grain boundaries free from carbide precipitation. From the microstructural analysis, it is inferred that SS316L pipes are supplied in solution-annealed conditions and are not susceptible to intergranular corrosion or attack.

6A.1.7 Overall Discussion on Chemical, Mechanical and Microstructure of SS316L Pipes

It has been found that there are minor variations in the chemical compositions between the samples. It has also been found from the mechanical properties that the results of UTS, proof stress and elongation are almost same for all the three samples. The hardness values and the microstructures are found to be identical for all these samples. Therefore, the minor variation in the chemical composition between the samples does not influence the mechanical properties and microstructures. It can be interpreted that such minor variation in the chemical composition is possible because the factory made SS316L pipe may not remain homogeneous composition throughout or may be due to some marginal errors introduced during testing. Therefore, it can be logically concluded from the repeatability of the results that the samples are virtually identical, represent basically the only one sample for the entire lot of SS316L pipes and three different data from different testings are highly reproducible.

6A.2 Results and Discussion on Corrosion Testing of SS316L Pipes

The cyclic potentiodynamic polarization, pitting corrosion, and critical pitting temperature tests were carried out on SS316L samples.

6A.2.1 Results of Cyclic Potiodynamic Polarization Test

The Cyclic Potentiodynamic Polarization test was conducted on SS316L samples at 25⁰C using 3-electrode system within a glass cell with 3.5% NaCl solution according to ASTM G-61 [5]. SS316L samples, a platinum rod and SCE were utilized as working electrodes, counter electrode and reference electrode respectively. After 1 hour of immersion, scanning was done at a rate of 10mV/minute with a potential range of - 400 mV to + 600 mV. The cyclic potentiodynamic polarization plots (i.e., potential versus current density) were obtained after completion of the test. The cyclic potentiodynamic polarization plots of three SS316L samples are shown in Figure 6A.2 [6-8]. After the cyclic potentiodynamic polarization test, significant pitting corrosion has been observed on SS316L surfaces under Scanning Electron Microscopy (SEM) examination. The SEM photographs of pitting corrosion are shown in Figure 6A.3.
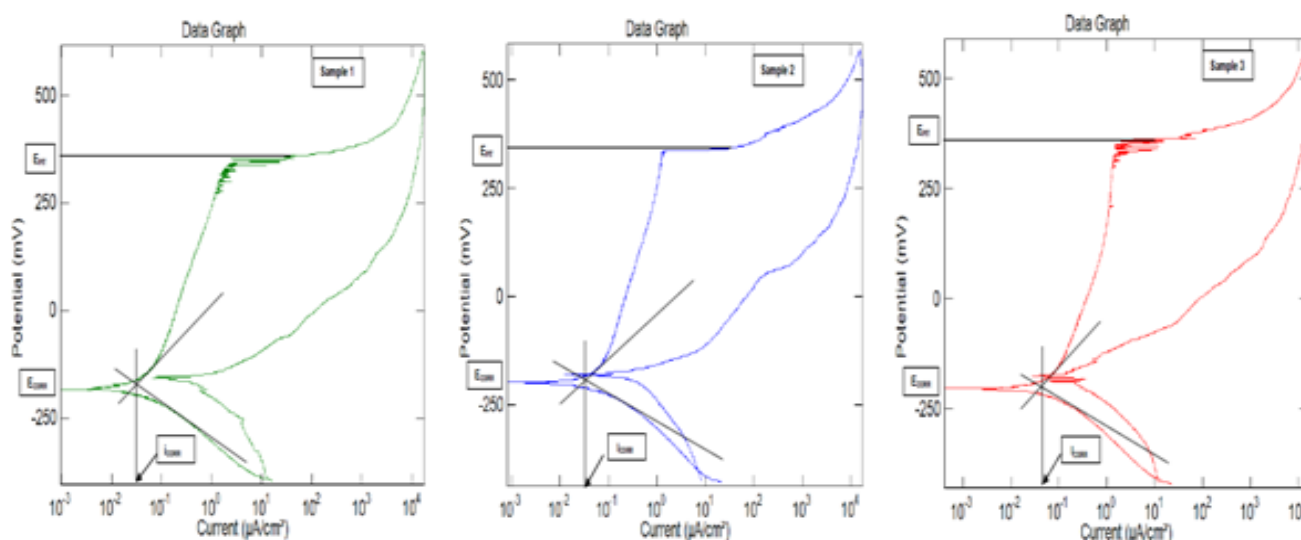
Figure 6A.2: Cyclic Potentiodynamic Polarization Plots of SS316L Samples
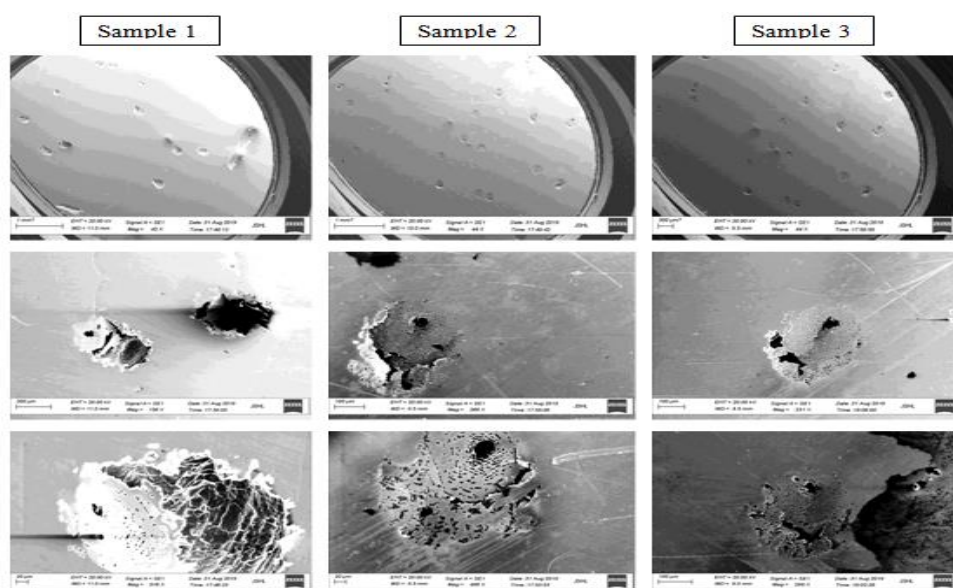
Figure 6A.3: SEM Photographs of Pitting Corrosion on SS316L Surfaces

Table 6A.3: E_{corr}, i_{corr}, and E_{pit} of SS316L Pipes

Sample no.	E_{pit} (mV) vs. SCE*	E_{corr}(mV) vs. SCE*	i_{corr} (μA/cm^2)
Sample 1	361	- 195	0.05
Sample 2	363	- 200	0.06
Sample 3	380	- 205	0.07

(* SCE- Saturated Calomel Electrode as the reference electrode)

The critical pitting potential (E_{pit}), corrosion potential (E_{corr}), and corrosion current density (i_{corr}) are evaluated from these cyclic potentiodynamic polarization plots. E_{corr}, i_{corr}, and E_{pit} are shown in Table 6A.3.

6A.2.2 Discussion on Cyclic Potentiodynamic Polarization Test

It can be observed from the potential versus current density semi-logarithmic plot that the current density increases steeply from the corrosion potential (E_{corr}) to the critical pitting potential (E_{pit}), which indicates the onset of stable pits formation from the transient metastable pitting [9-10]. After stable pit formation in the localized areas, the Cr_2O_3 passive film cannot remain continuous and protective. The values of E_{pit} are found to be in the range of 361-380 mV versus the SCE reference electrode. Open circuit potential and its corresponding current density are found out from the polarization diagram linear section by the Tafel extrapolation method. The values of E_{corr} and i_{corr} are found to be in the range of 195-205 mV versus SCE reference electrode, and 0.05-0.07 μA/cm^2 respectively. Scanning Electron Microscopy (SEM) examination has revealed localized pitting on SS316L surface. It is inferred that SS316L material suffers localized pitting corrosion in chloride bearing environment.

6A.2.3 Results of Pitting Corrosion and Critical Pitting Temperature Tests

The pitting corrosion test was conducted as per ASTM G-48 [11] at 22-24°C in reagent grade 6% ferric chloride ($FeCl_3$) solution for 72 hours for the determination of the resistance of SS316L to pitting corrosion when exposed to oxidizing chloride environments [12-13]. The samples were weighed before and after pitting corrosion test. Mass loss corrosion rate has been computed in g/cm^2 based on the mass loss after pitting corrosion test and area of the sample.

Table 6A.4: Pitting Corrosion and CPTs of SS316L Pipes

Sample no.	Mass loss corrosion rate (g/cm^2)	CPT (^{o}C)
Sample 1	0.02071	16
Sample 2	0.02598	15
Sample 3	0.01519	16

The Critical Pitting Temperature (CPT) has been found out the minimum temperature that produced pitting attack on bold surface of SS316L samples. Pitting corrosion (i.e., mass loss corrosion rate), and CPTs are shown in Table 6A.4.

6A.2.4 Discussion on Pitting Corrosion and Critical Pitting Temperature Tests

It has been reported in literature/standard that when mass loss corrosion rate is > or = 0.0001 g/cm^2, noticeable pitting occurs on SS316L surface [11]. Therefore, from mass loss corrosion rates found to be in the range of 0.015-0.026 g/cm^2, it can be concluded that SS316L surface has suffered from noticeable pitting. It has also been found out that critical pitting temperature of SS316L material is 15-16°C [14].

6A.2.5 Conclusion

The chemical compositions, mechanical properties and microstructures of SS316L pipes represent basically the only one sample for the entire lot of SS316L pipes. From corrosion testing, it has been found that SS316L material suffers localized pitting corrosion in chloride bearing environment and the critical pitting temperature of SS316L material is 15-16°C.

6A.3 References

[1] ASTM E-1019, "Standard Test-Methods for Determination of Carbon, Sulphur, Nitrogen, and Oxygen in Steel, Iron, Nickel, and Cobalt Alloys by Various Combustion and Inert Gas Fusion Techniques", ASTM International, 100 Barr Harbor Drive, P.O. Box C700, West Conshohocken, PA19428-2959, USA

[2] ASTM E-1086, "Standard Test-Method for Analysis of Austenitic Stainless Steel by Spark Atomic Emission Spectrometry", ASTM International, USA

[3] ASTM A-312, "Standard Specification for Seamless, Welded, and Heavily Cold Worked Austenitic Stainless Steel Pipes", ASTM International, USA

[4] ASTM A-370, "Standard Test-Methods and Definitions for Mechanical Testing of Steel Products", ASTM International, USA

[5] ASTM G-61, "Standard Test-Method for Conducting Cyclic Potentiodynamic Polarization Measurements for Localized Corrosion Susceptibility of Iron, Nickel, or Cobalt-Based Alloys", ASTM International, USA

[6] P.C-Pistorius, G.T-Burstein, "Metastable Pitting Corrosion of Stainless-Steel and the Transition to Stability", Philosophical Transactions of The Royal Society A Mathematical Physical and Engineering Sciences, 341(1992), p.531-559

[7] Gerald S Frankel, L. Stockert, Fritz Hunkeler, H. Boehni, "Metastable Pitting of Stainless Steel", CORROSION, July 1987, Vol.43, No.7, p.429-436, NACE International, Houston, Texas, USA

[8] Wenming Tian, Nan Du, Songmei Li, Sibing Chen, Qunying Wu, "Metastable Pitting Corrosion of 304 Stainless Steel in 3.5% NaCl Solution", Corrosion Science, Vol. 85, August 2014, p.372-379

[9] P.C. Pistorius, G.T. Burstein, "Aspects of the Effects of Electrolyte Composition on the Occurrence of Metastable Pitting on Stainless Steel", Corrosion Science, Vol. 36, Issue 3, March 1994, p.525-538

[10] David E. Williams, John Stewart, Peter H. Balkwill, "The Nucleation, Growth and Stability of Micro pits in Stainless Steel", Corrosion Science, Vol. 36, Issue 7, July 1994, p.1213-1235

[11] ASTM G-48, "Standard Test-Methods for Pitting and Crevice Corrosion Resistance of Stainless Steels and Related Alloys by use of Ferric Chloride Solution", ASTM International, USA.

[12] R A Cottis, M J Graham, R Lindsay, S B Lyon, J A Richardson, J D Scantlebury, F H Stott, "Shreir's Corrosion", Vol.3, fourth Edition, p.2170, Elsevier B.V, Amsterdam, The Netherlands

[13] N.J. Laycock, R.C. Newman, "Temperature Dependence of Pitting Potentials for Austenitic Stainless Steels above their Critical Pitting Temperature", Corrosion Science, Vol.40, Issue 6, (June 1998), p.887-902

[14] Nihal U. Obeyesekere, "Chapter 9: Pitting Corrosion", Trends in Oil and Gas Corrosion Research and Technologies: Production and Transmission, Woodhead Publishing series in Energy (2017), p.215-248.

Chapter - 6B

Coating for SS316L Pipeline

in Buried Condition

Chapter - 6B: Coating for SS316L Pipeline in Buried Condition

6B. Introduction

The petrochemical products are transported via buried SS316L pipelines to distant places because the pipelines are the safe, reliable, and economical. The pipelines are installed mostly in buried condition to avoid external damage and spillage. But an uncoated SS316L pipeline in buried condition can suffer localized pitting corrosion in moist soil in the presence of chlorides ions. Therefore, polymeric coating is applied on the external surface of SS316L pipeline as primary corrosion protection. Polymeric coating attributes integrity and longevity of the buried pipeline. For the present study, generic six types of polymeric coatings have been selected and applied separately on 4-inch SS316L pipes external surfaces. The coatings have been subjected to various relevant testing to optimize their uses for SS316Lpipelines in buried condition.

In this chapter, surface preparation of SS316L pipes, generic six types of polymeric coatings, the results of various testing conducted on the coated samples and the subsequent discussions are presented.

6B.1 SS316L Pipes - Surface Preparation

Al_2O_3 (Alumina) fine particles in fused condition were used as abrasive blasting to prepare the external surfaces of 4-inch SS 316L pipes. Such blasted and cleaned surface facilitates good bonding and adhesion of coating to SS316L pipe. Before applying coating, S316L pipe surface was made dry. Alumina fine particles in fused condition, pipe surface - original, and pipe surface - after blasting are shown in Figure 6B.1.

(a)   (b)   (c)
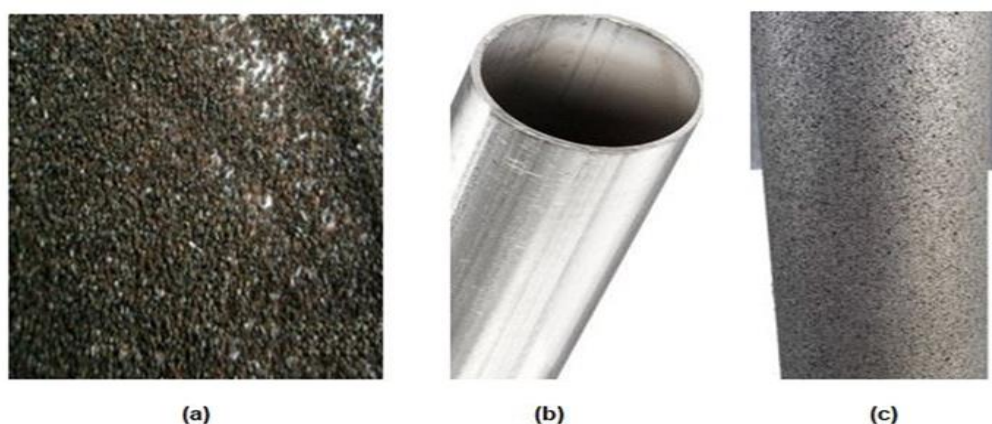
Figure 6B.1: Surface preparation of SS316L pipe - a) Alumina fine particles in fused condition, b) pipe surface - original, c) pipe surface - after blasting

6B.2 Selection and Application of Polymeric Coatings on SS316L Pipes

Generic six types of external polymeric coatings commonly used for buried carbon steel pipelines in the petroleum, petrochemical and natural gas industries were selected for SS316L pipelines:

1) 3-Layer Poly-Ethylene (**3LPE**)
2) 3-ply/2-ply Cold-Applied Tape (**3p/2p CAT**)
3) Polyurethane (**PU**)
4) Visco-Elastic (**VE**)
5) Liquid Epoxy (**LE**)
6) Heat-Shrink Sleeve (**HSS**).

Among these coatings, 3LPE, 3p/2p CAT, VE, HSS were layer/tape coatings, whereas PU and LE were liquid-applied coatings. 3LPE, 3p/2p CAT, VE, HSS, PU and LE coatings were applied separately to 4-inch SS316L pipes.

6B.3 Samples Preparation for Testing

The samples were prepared after cold cutting 4-inch pipe sections of about 200 mm long from the main and lengthy coated 4-inch SS316L pipes to conduct relevant testings in the laboratories. Each test was carried out on the three samples of every coating.

6B.4 Results and Discussion

The following tests were conducted on the samples in the laboratories:

6B.4.1 Thickness Measurement

6B.4.2 Holiday Detection

6B.4.3 Type D Shore Durometer Hardness

6B.4.4 Impact Resistance

6B.4.5 Indentation Resistance

6B.4.6 Water Absorption

6B.4.7 Cathodic Disbondment

6B.4.8 Peel Strength

6B.4.9 Pull-off Adhesion

6B.4.10 Hot Water Immersion

6B.4.11 Specific Electrical Insulation Resistance

6B.4.12 Electrochemical Impedance Spectroscopy

6B.4.1 Results of the Thickness Measurement

The thickness measurements were performed on the samples by the ultrasonic digital thickness gauge in accordance with ISO: 21809-3 Annex B. The ultrasonic digital thickness gauge with ±10 % reading accuracy was calibrated for the range of coating thickness being measured. Thickness was measured at eight points on each sample. The measured values at eight points were recorded. The measured thickness values and an arithmetic mean i.e. the average of eight values for each coating are shown in Figure 6B.2. The thickness measurements conducted on the samples are shown in Figure 6B.3.
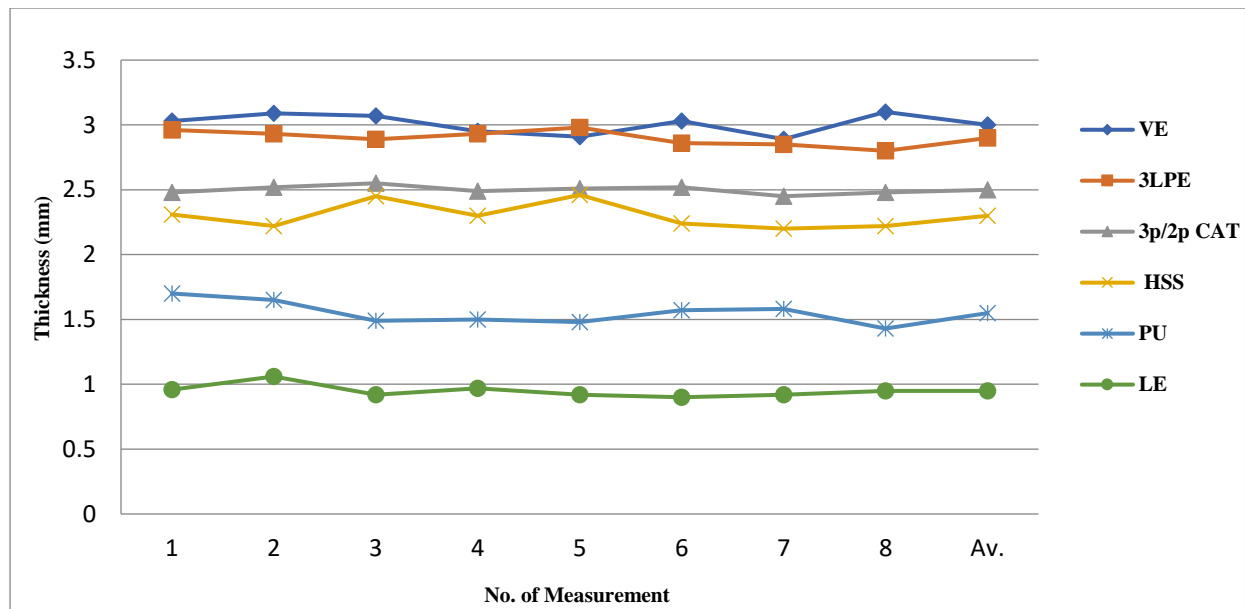
Figure 6B.2: Measured Thicknesses of Coatings
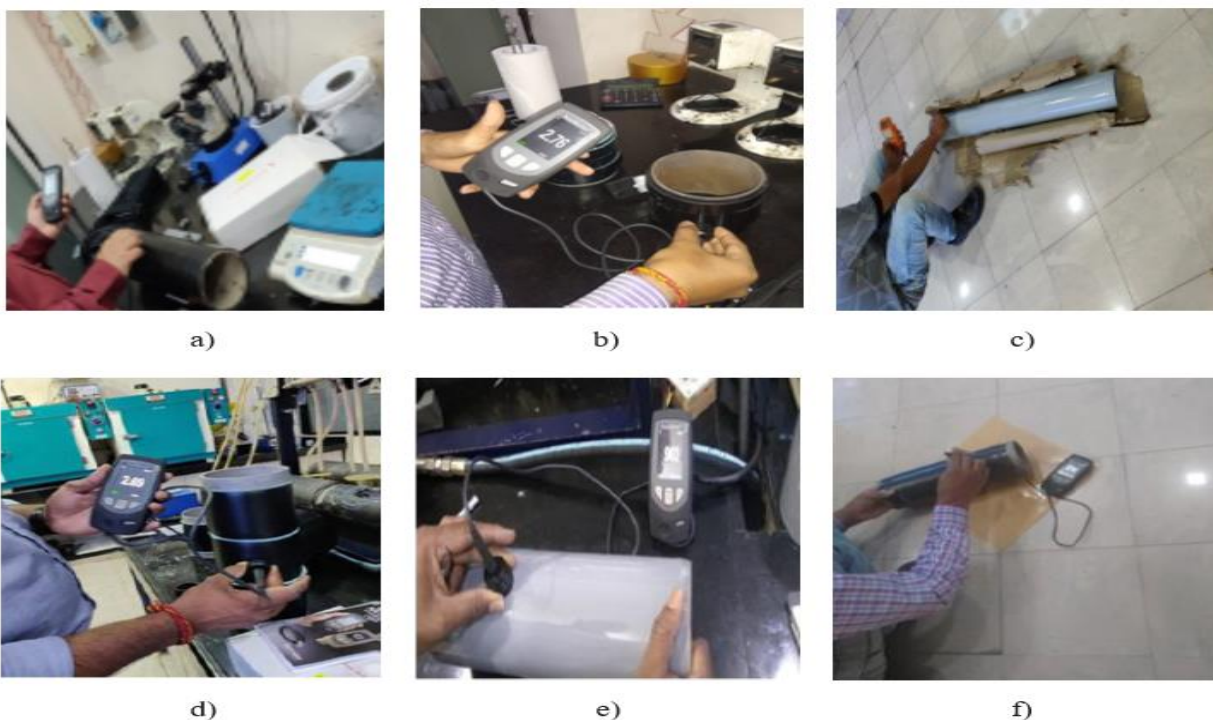
Figure 6B.3: Thickness Measurement - a) 3LPE, b) 3p/2p CAT, c) PU, d) VE, e) LE, f) HSS

6B.4.1.1 Discussion on the Thickness Measurement

The average thicknesses of 3LPE, 3p/2p CAT, PU, VE, LE, and HSS have been found to be 2.9 mm, 2.5 mm, 1.55 mm, 3.0 mm, 0.95 mm, and 2.3 mm respectively. Among the coatings, VE has the highest thickness, whereas PU and LE have lower thickness and lowest thickness respectively. Solvent-free liquid-applied coatings have less thickness in comparison with layer/tape coatings (3LPE, 3p/2p CAT, VE, HSS). Such trends in thickness are prevalent among these coatings in the petroleum and natural gas industries to protect buried or submerged pipelines external surfaces.

6B.4.2 Results of the Holiday Detection Test

The entire surfaces of the samples were subjected to the holiday detection by the high-voltage holiday detectors as per NACE SP-0274 to ensure the coatings free from porosities or pinholes. The holiday detector i.e. a scanning electrode in the form of a metal brush equipped with a sound and light signal was calibrated before testing. During testing, sample was connected to earth and to the detector. The whole surface of the sample was scanned by the detector at room temperature. At the time of the test, minimum and maximum voltages were applied to the samples based on the types of coatings and their thicknesses. The minimum and maximum voltages applied to the coatings during the holiday detection are shown in Figure 6B.4. The

results of the holiday detection are shown in Table 6B.1. The holiday detection performed on the samples are shown in Figure 6B.5.
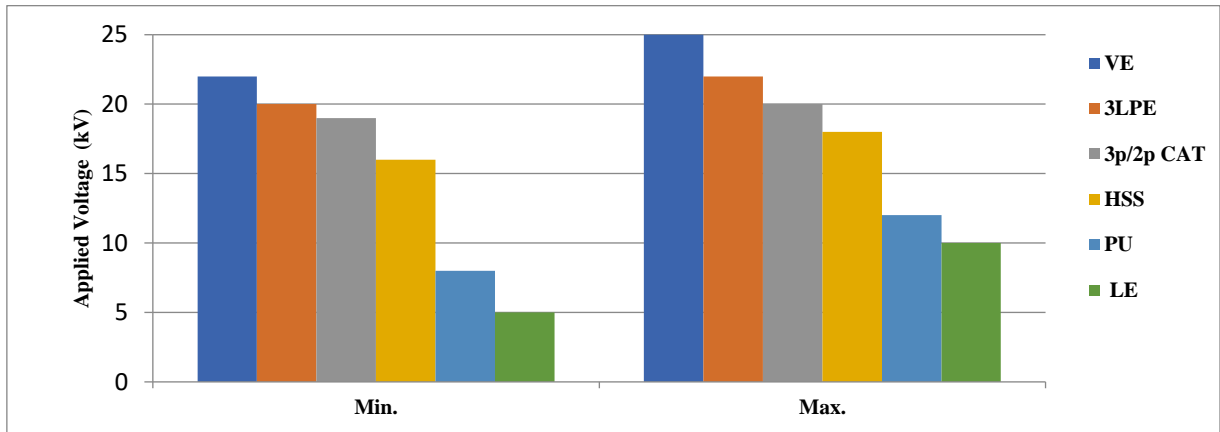
Figure 6B.4: Minimum and Maximum Voltages applied during Holiday Detection

Table 6B.1: Results of Holiday Detection

Type of Coating	No. of Holidays
3LPE	Nil
3p/2p CAT	Nil
PU	Nil
VE	Nil
LE	Nil
HSS	Nil

Figure 6B.5: Holiday Detection - a) 3LPE, b) 3p/2p CAT, c) PU, d) VE, e) LE, f) HSS

6B.4.2.1 Discussion on the Holiday Detection Test

The entire surfaces of all the coatings have been found to be free from pinholes or porosities. Among the coatings, VE has been found to withstand the maximum voltage of 25 kV due to its highest thickness, whereas LE has been found to withstand the least voltage of 10 kV due to its lowest thickness.

6B.4.3 Results of the Type D Shore Durometer Hardness Measurement

The Type D Shore Durometer hardness measurement were carried out on the samples at room temperature according to the ISO 868. The sample was placed on a hard flat surface and the specified indenter was forced into the coating material with the applied pressure. The indentation hardness values were measured at five different points on a sample and recorded. The measured hardness values and an arithmetic mean i.e. the average of five values for each coating are shown in Figure 6B.6. The Type D Shore Durometer hardness measurements of the samples are shown in Figure 6B.7.
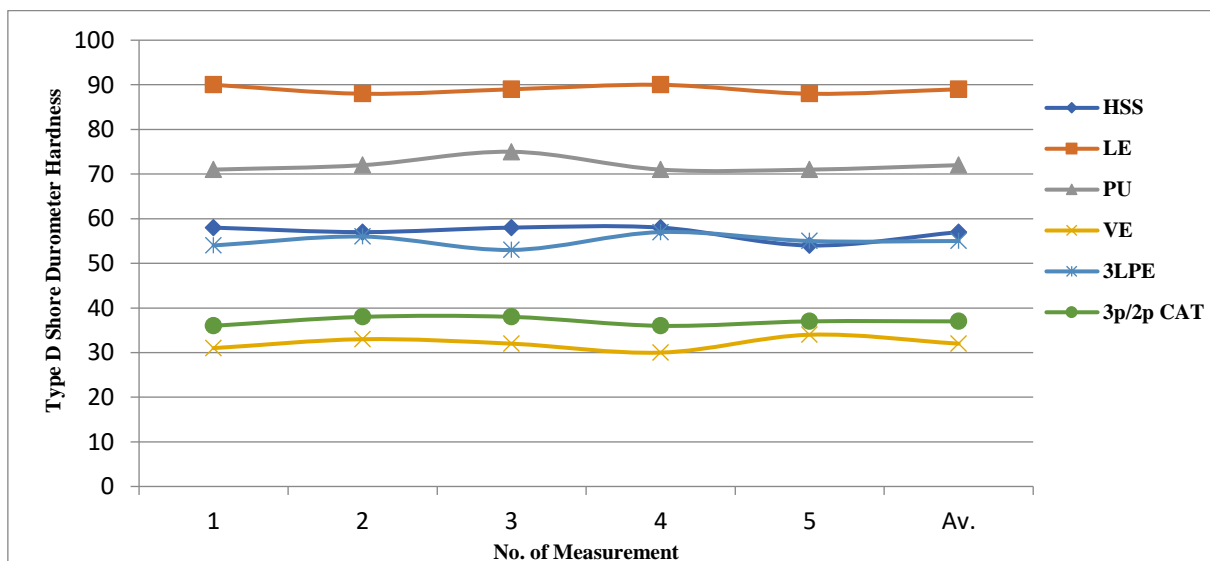
Figure 6B.6: Measured Hardness Values of Coatings
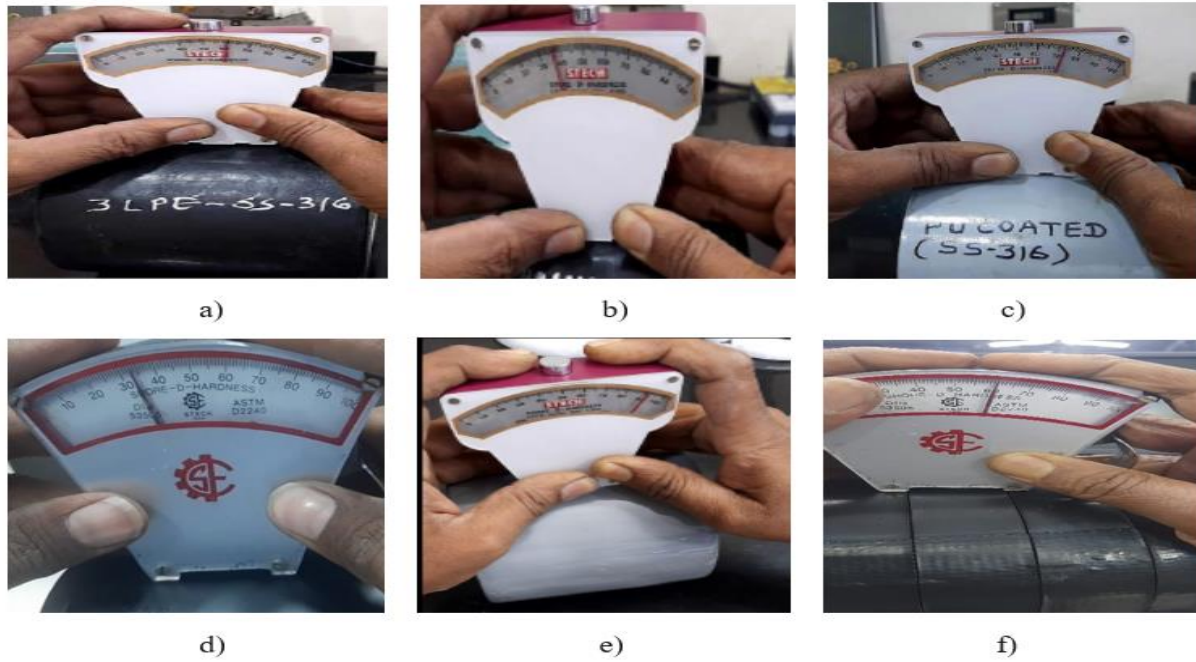
Figure 6B.7: Hardness Measurement- a) 3LPE, b) 3p/2p CAT, c) PU, d) VE, e) LE, f) HSS

6B.4.3.1 Discussion on the Type D Shore Durometer Hardness Measurement

The average Type D Shore Durometer hardness values of 3LPE, 3p/2p CAT, PU, VE, LE, and HSS have been found to be 55, 37, 72, 32, 89 and 57 respectively. It has been found that among the coatings, LE has the highest hardness, whereas 3p/2p CAT&VE have the lower hardness and lowest hardness respectively. It appears that LE is very hard material and 3p/2p CAT & VE are soft materials. LE can give highest resistance to penetration when it is encountered by sharp particles during pipe laying and backfilling the trench.

6B.4.4 Results of the Impact Resistance Test

The impact resistance tests were carried out on the samples at room temperature in accordance with ISO: 21809-3 Annex D. The strength of the coating was verified by the impact of hard steel punch with a hemispherical head falling perpendicularly onto the sample. Before carrying out the test, each sample was subjected to the holiday detection test to ensure the coating free from porosity or pinhole. A steel punch of long 6 mm diameter rod attached to a hemispherical head of 25 mm diameter was dropped from a height of 1 metre on the coated surface perpendicularly at room temperature. Ten impacts were carried out on each sample with the specified impact energy calculated based on type of coating and its thickness, with a minimum value of 5J/mm. A uniform value of 15J was applied to layer/tape coatings, whereas 8J and 5J were applied to PU and LE respectively [1]. After the impact resistance test, each

sample was subjected again to the holiday detection. The impact energies applied to the coatings are shown in Figure 6B.8. The samples under the impact resistance tests are shown in Figure 6B.9. The holiday detection results are shown in Table 6B.2.
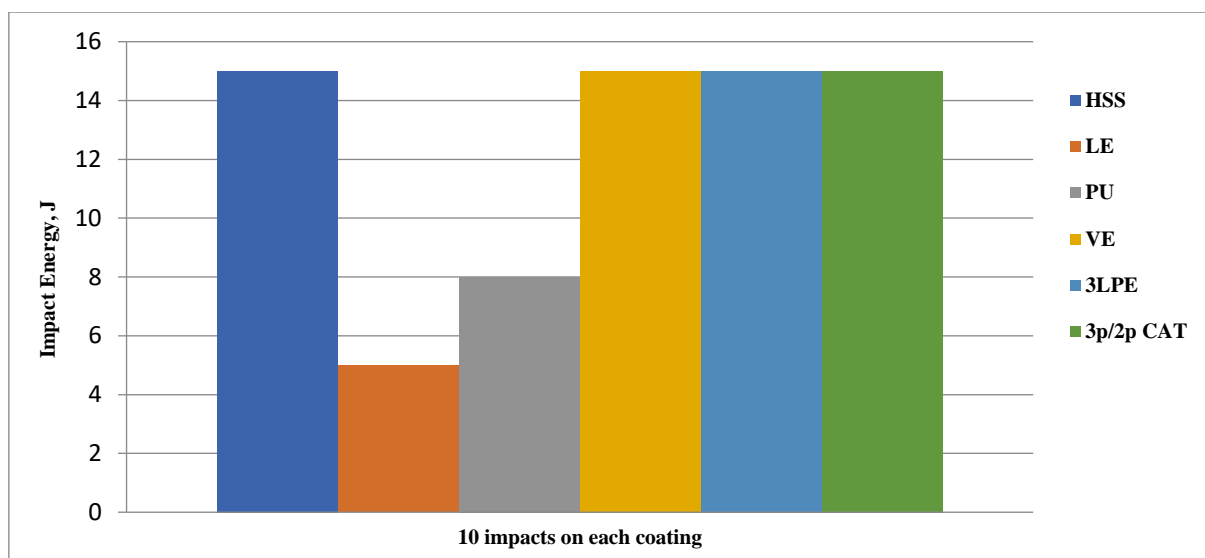
Figure 6B.8: Impact Energies applied to the Coatings

Table 6B.2: Results of Holiday Detection after Impact Resistance Tests

Type of Coating	No. of Holidays
3LPE	Nil
3p/2p CAT	Nil
PU	Nil
VE	Nil
LE	Nil
HSS	Nil
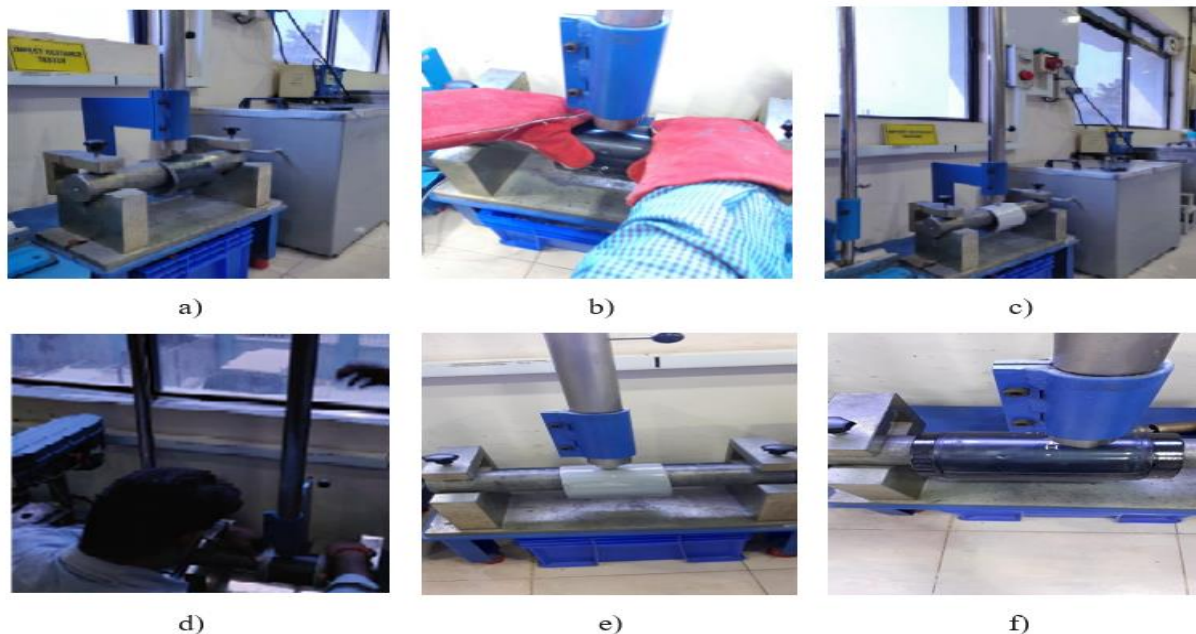
Figure 6B.9: Impact Resistance - a) 3LPE, b) 3p/2p CAT, c) PU, d) VE, e) LE, f) HSS

6B.4.4.1 Discussion on the Impact Resistance Test

The entire surfaces of all the coatings after the impact resistance tests have been found to be free from pinholes or porosities. 3LPE/3p-2p CAT/VE/HSS have been found to withstand 15 Joule due to their high thicknesses, whereas PU and LE have been found to withstand 8J and 5J respectively. It appears that layer/tape coatings (3LPE, 3p/2p CAT, VE, HSS) can provide high impact resistances to physical or mechanical damage during shipping, installation, or service in the field in comparison with liquid-applied coatings (PU, LE).

6B.4.5 Results of the Indentation Resistance Test

The indentation resistance tests were performed on the samples in accordance with ISO: 21809-3 Annex E to measure the indentation of a punch into the coating under a specified load and controlled conditions. The samples with penetrometer were placed in thermostatically controlled chamber at 55±5°C. A penetrometer was comprised of a cylindrical indenter of 1.80 mm diameter, on the top of which 2.5 kg weight was mounted. The indenter plus weight of the assembly is shown in Figure 6B.10. The indentation resistance tests on the samples are shown in Figure 6B.11.

Figure 6B.10: Weight of the Assembly ≈ 2.5 kg (2525.69 g)
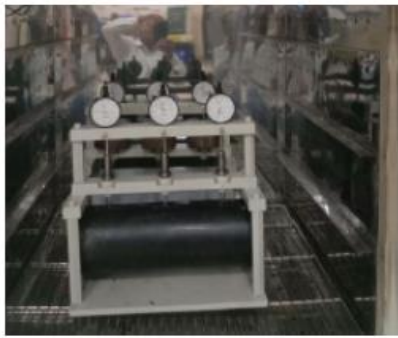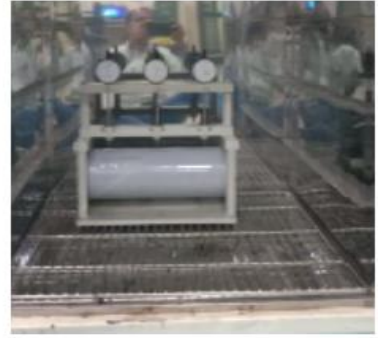
Figure 6B.11: Indentation Resistance - a) 3LPE, b) 3p/2p CAT, c) PU, d) VE,

e) LE, f) HSS

At first, the dial gauge reading with the cylindrical indenter (without the weight) positioned centrally over the sample was recorded. Then the assembly i.e. the cylindrical indenter with the weight was positioned centrally over the sample. This assembly had produced a pressure of 10 N/mm^2 on the sample surface. This pressure was kept for 24 hours. After 24 hours, the dial gauge reading with the cylindrical indenter plus the weight positioned centrally over the sample was recorded. The test was performed three times on each coating sample. The indentation of each coating was evaluated using the Equation (6B-1):

$$t_3 = t_1 - t_2 \quad .... \text{(6B-1)}$$

140

Where,

t_1 = Dial gauge reading (in mm) with indenter and without applying weight to the sample

t_2 = Dial gauge reading (in mm) with indenter and with applying weight to the sample and after keeping load for 24 hours.

t_3 = Indentation of coating (in mm)

The indentation of each coating and an arithmetic mean i.e. the average of the three results for each coating are shown in Figure 6B.12.
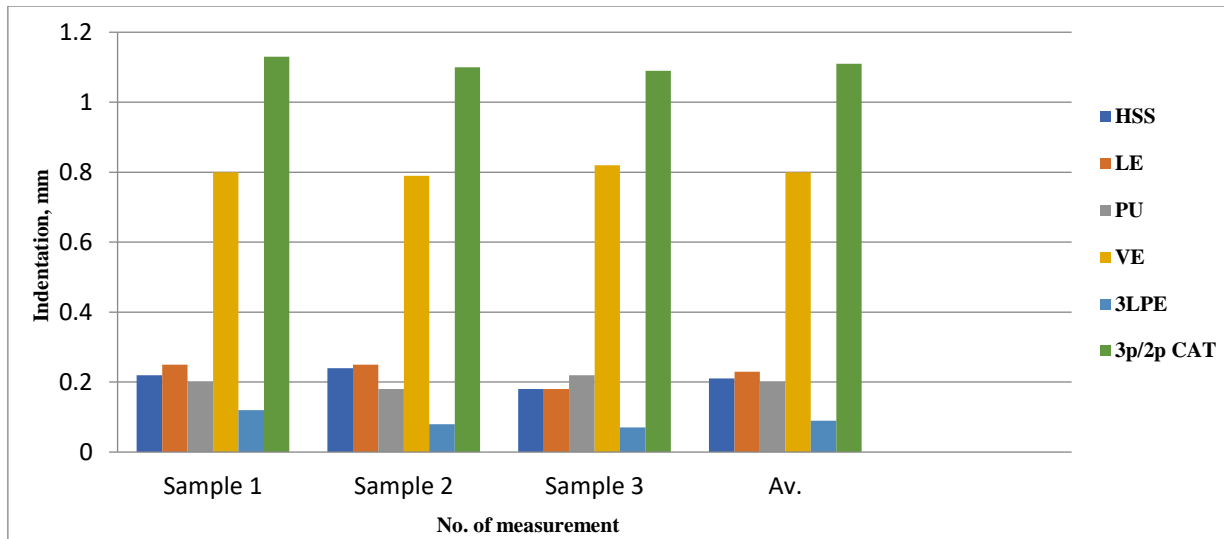
Figure 6B.12: Indentation of Coating

6B.4.5.1 Discussion on the Indentation Resistance Test

The average indentation of 3LPE, 3p/2p CAT, PU, VE, LE, and HSS have been found to be 0.09 mm, 1.11 mm, 0.20 mm, 0.80 mm, 0.23 mm, and 0.21 mm respectively. 3LPE coating has shown best performance in this test because the outer layer is of 3LPE coating is high density polyethylene (HDPE) for mechanical protection. HDPE possesses high strength-to-density ratio that gives stronger intermolecular forces and tensile strength. It enhances impact, indentation, and abrasion resistance and hence, 3LPE gives least depth of indentation or highest indentation resistance to withstand the deformation force exerted by the weight of the pipe or the backfill during installation. Therefore, the order of the coatings with respect to the highest to the lowest indentation resistance is found to be 3LPE, PU, HSS, LE, VE, and 3p/2p CAT.

6B.4.6 Results of the Water Absorption Test

The water absorption tests in accordance with ASTM D-570 and ISO:62 were carried out on the coatings (60 mm by 60 mm in dimension) extracted from the samples in order to determine the amount of water absorbed by the coatings [2].The coatings were made dry in an oven

at 50°C for 24 hours. After 24 hours, the coatings were removed from the oven and cooled in the desiccator. After initial drying and before immersed in distilled water, the coatings were weighed. These measured weights were recorded as initial weights. Then the coatings were immersed in distilled water at 23-25°C and were kept for 28 days. The water absorption tests of the coatings are shown in Figure 6B.13.

After completion of the test, the coatings were taken out. Dry cloth was used to clean off water from coatings surfaces. Then weight measurements were done. These measured weights were recorded as final weights. The amounts of water absorbed by the coatings were determined by measuring their change in weights i.e. the difference between final weights and initial weights. The percentage change in weight of a coating relative to its initial weight was computed using the Equation (6B-2):

$$C = [(m_2-m_1) / m_1] \times 100\% \ldots\ldots\ldots\ldots (6B- 2)$$

Where,

C = Percentage change in weight relative to the initial weight,

m_1 = Initial weight of the sample (in mg or g), after initial drying and before immersion,

m_2 = Final weight of the sample (in mg or g), after immersion and after final drying.
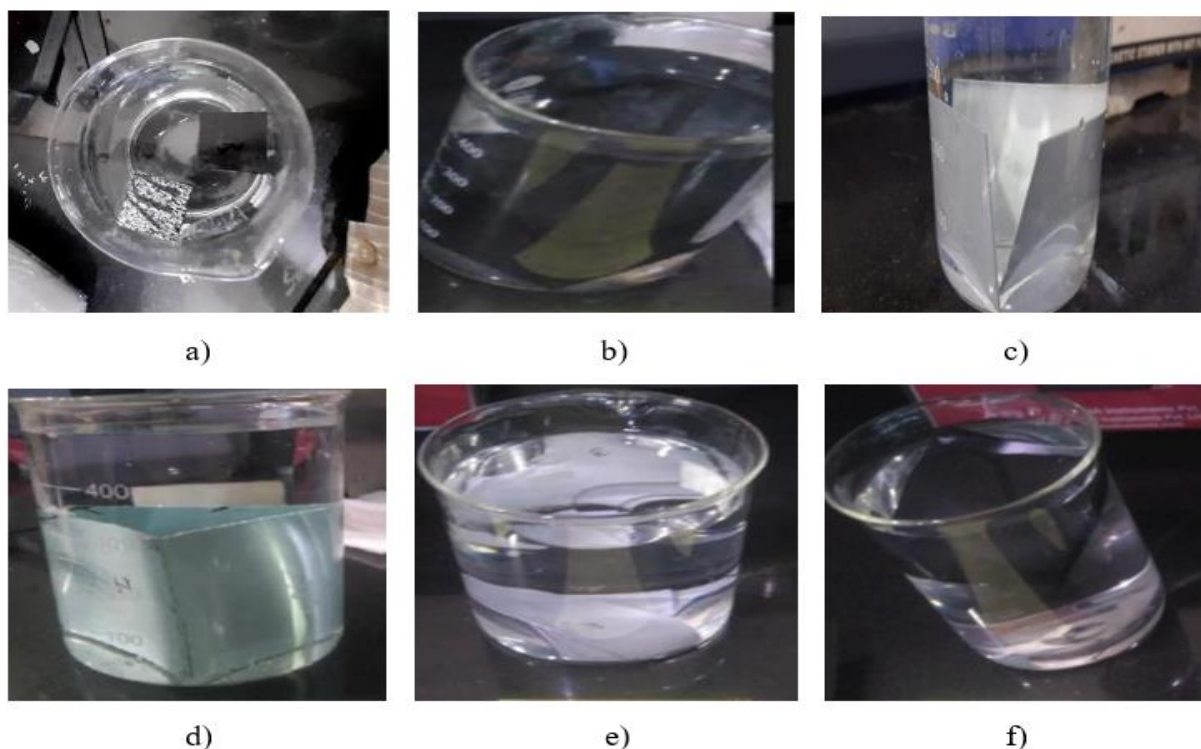
Figure 6B.13: Water Absorption - a) 3LPE, b) 3p/2p CAT, c) PU, d) VE, e) LE, f) HSS

The percentage water absorbed by each coating and an arithmetic mean i.e. the average of the three results for each coating are shown in Figure 6B.14.
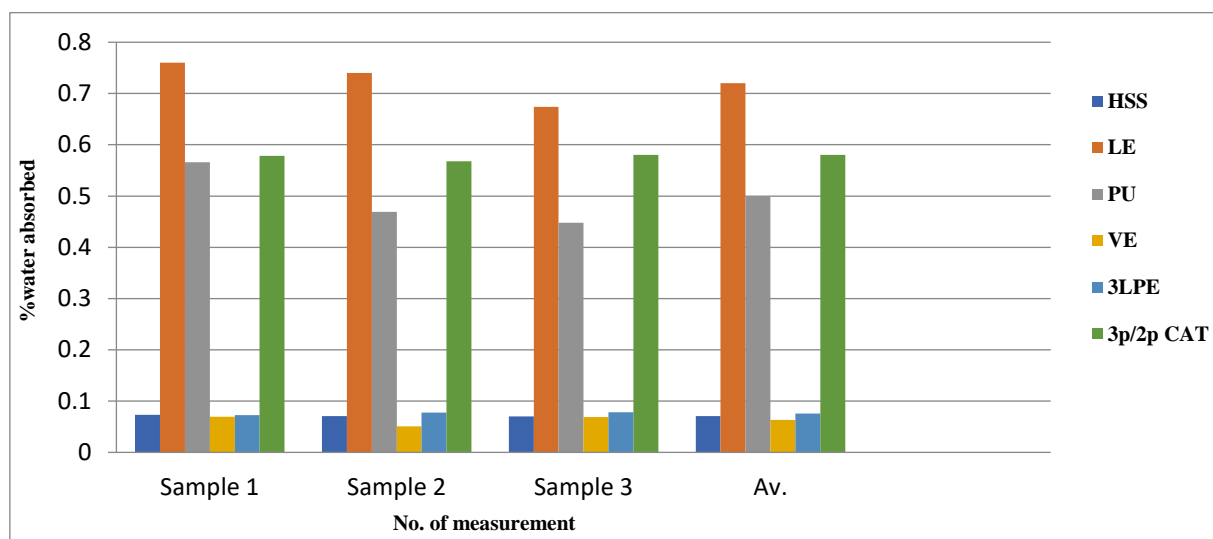
Figure 6B.14: Percentage Water Absorbed by Coating

6B.4.6.1 Discussion on the Water Absorption Test

The average water absorbed by 3LPE, 3p/2p CAT, PU, VE, LE, and HSS have been found to be 0.076%, 0.580%, 0.5%, 0.063%, 0.720%, and 0.071% respectively. VE coating has shown best performance in this test because the chemical composition of VE coating is Poly-isobutene (or Poly-isobutylene, PIB), which is non-crystalline, non-cross-linked and non-reactive and has uniform structure. Poly-isobutylene is a hydrophobic polymer. The polymer chains make compact structure that repels water. Therefore, the order of the coatings in respect of the highest to the lowest performances is found to be VE, HSS, 3LPE, PU, 3p/2p CAT, LE.

6B.4.7 Results of the Cathodic Disbondment Test

The cathodic disbondment tests were performed on the samples at 23-25ºC for 28 days in accordance with ASTM G-8 to determine the resistance to disbondment of damage to the coating when exposed to cathodic polarization [3]. The samples were subjected to the holiday detection tests before cathodic disbondment tests. An artificial defect i.e. a 6.0 mm diameter hole through the coating was made by drilling in the centre of each sample carefully. Plastic pipe forming electrolytic-cell was placed at the top of the sample with the artificial defect in the centre of the cell. The surface between the sample and the cell was sealed with silicone sealant. The cell was filled with 3% sodium chloride (NaCl) solution. Solution pH = 6-9 was maintained. The Saturated Calomel Electrode (SCE) and platinum wire of 1 mm diameter were immersed in the solution as reference electrode and an auxiliary electrode respectively. A cathodic polarization potential (E) equivalent to -1500 mV versus SCE was applied between the reference electrode

and the sample (working electrode). After 28 days, plastic pipe forming electrolytic-cell was taken out. Each sample after cathodic disbondment test was evaluated after making 4 radial cuts through the coating at the intentional holidays and attempting to lift the coating away from the substrate. The measured disbondment and an arithmetic mean i.e. the average of the three results for each coating are shown in Figure 6B.15. The cathodic disbondment measurements of the samples are shown in Figure 6B.16.
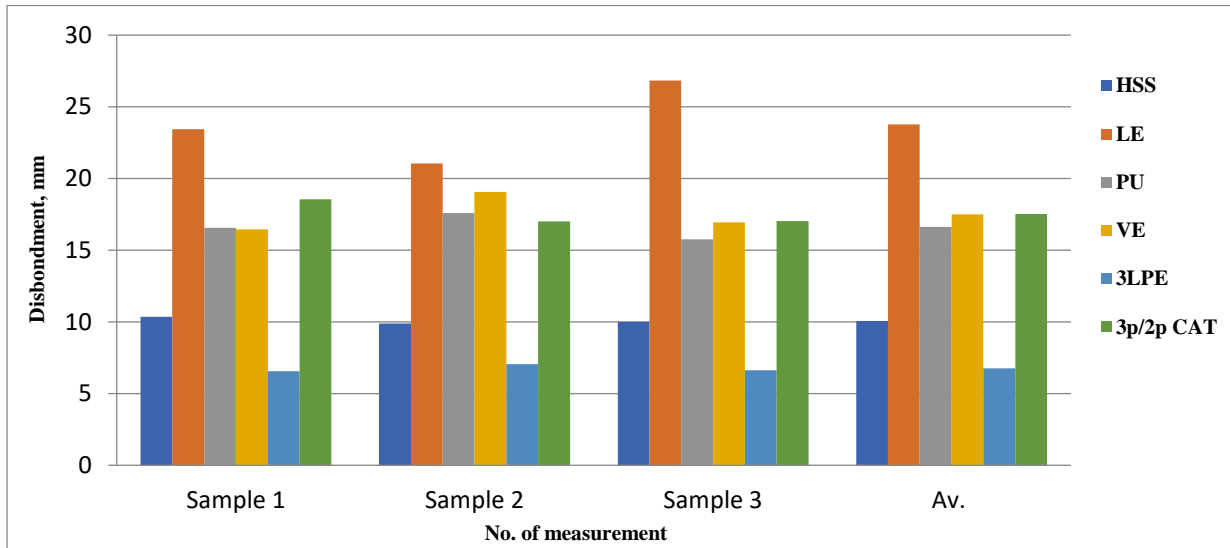
Figure 6B.15: Cathodic Disbondment of Coating
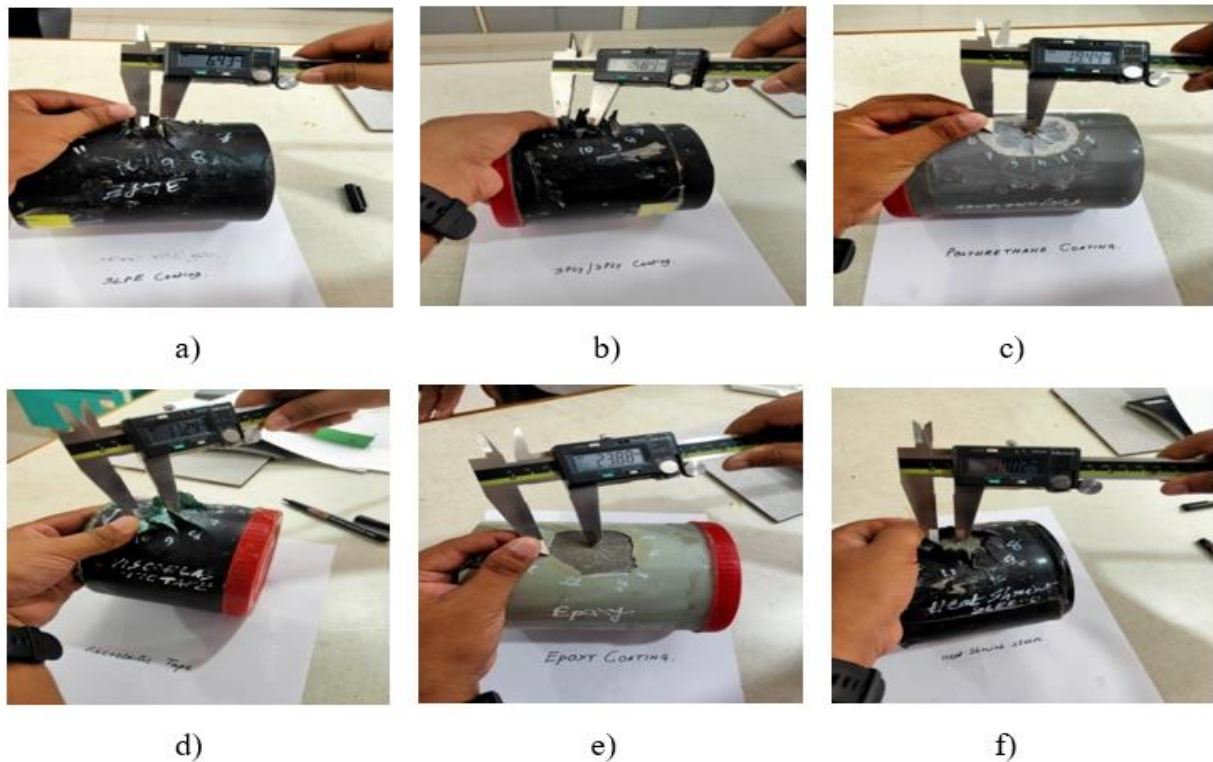
Figure 6B.16: Disbondment Measurements- a) 3LPE, b) 3p/2p CAT, c) PU, d)VE, e) LE, f)HSS

144

6B.4.7.1 Discussion on the Cathodic Disbondment

The average cathodic disbondments of 3LPE, 3p/2p CAT, PU, VE, LE, and HSS have been found to be 6.76 mm, 17.52 mm, 16.64 mm, 17.49 mm, 23.77 mm and 10.07 mm respectively. 3LPE coating has shown best performance in this test because the inner layer is fusion bonded epoxy (FBE), an epoxy-based powder coating, (a thermosetting and cross-linked polymer) used to protect steel from corrosion due to ingress of water and salt by osmosis, electroosmosis and electrophoresis processes. FBE resists strong alkaline solution generated by the cathodic protection system, which is the primary cause of cathodic disbonding. The order of the coatings with respect to the highest to the lowest resistances to cathodic disbondment of damages is found to be 3LPE, HSS, PU, VE, 3p/2p CAT, and LE.

6B.4.8 Results of the Peel Strength Test

The peel strength tests were performed on the samples at 23-25°C and 55±5⁰C with a universal tensile testing machine as per ISO: 21809-3 Annex H to determine the adhesion strengths of layer/tape coatings (i.e. 3LPE, 3p/2p CAT, VE, HSS). Figure 6B.17 a), b) have shown peel-strength testing schematically and UTS machine respectively.
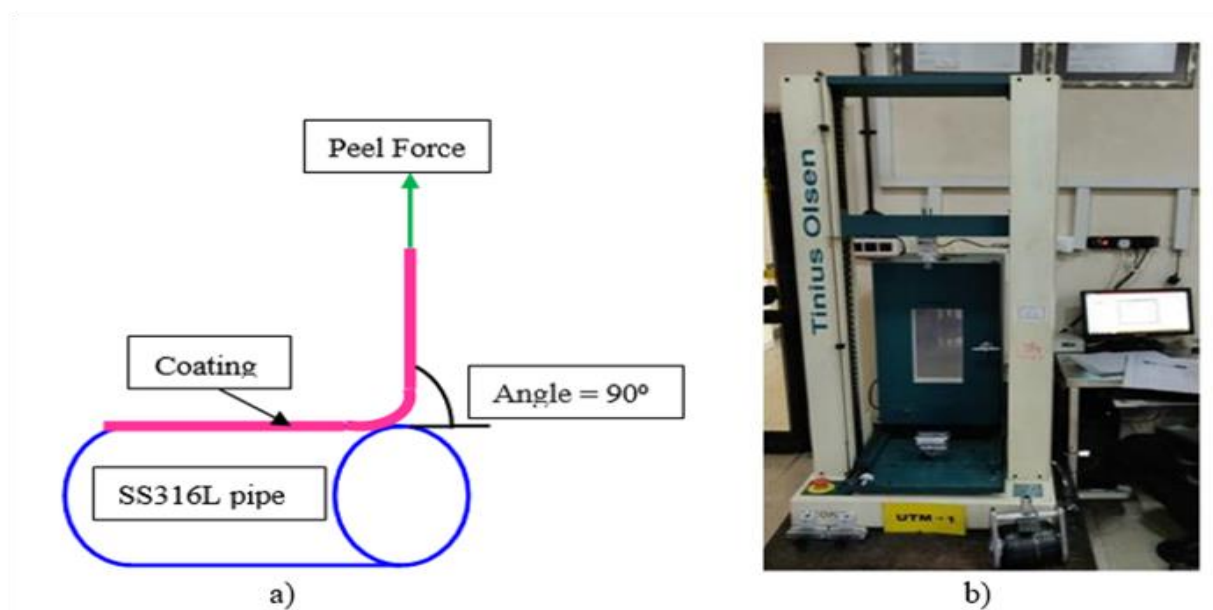
Figure 6B.17: a) Schematic Diagram of Peel Strength Test, b) UTS Machine

A coating strip of 160 mm long and 25 mm-50 mm wide was cut in the circumferential direction of each sample. During testing, the peel-force against extension length graph was generated. The peel-force against extension length graphs of 3LPE, 3p/2p CAT, VE, HSS at 23-25°C and 55±5⁰C are shown in Figures 6B.18, 19, 20, 21 respectively. From these graphs, the peel strengths of the coatings were evaluated from the average forces over 100 mm extension lengths using the Equation (6B-3).

$$P_{peel} = F/w\ldots\ldots\ldots\ldots\ldots\ldots (6B-3)$$

F = Peel-Force (in Newton or Pound)

w = Coating width (in mm or in)

P_{peel} = Peel-Strength (in N/mm or lb/in)

a)   b)
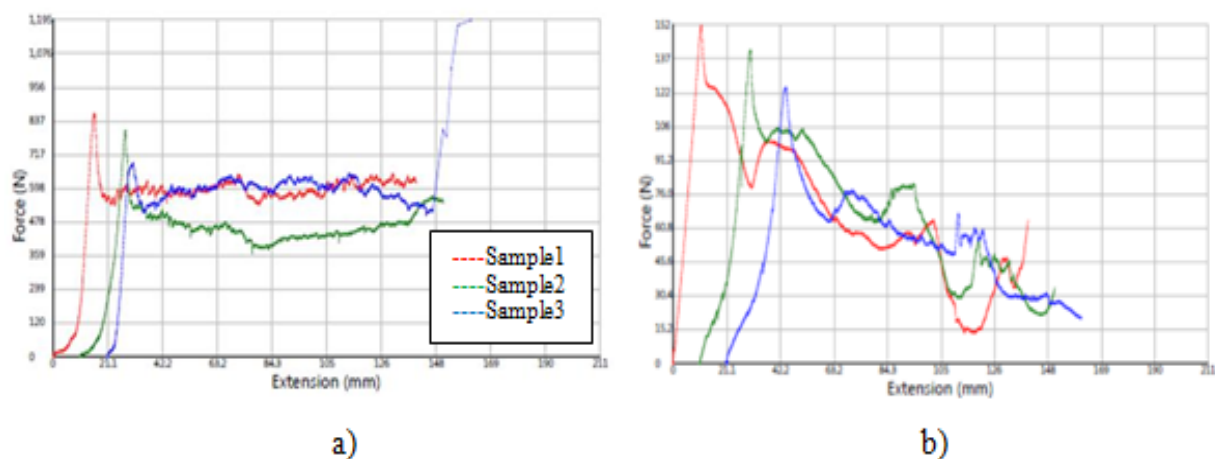
Figure 6B.18: Peel Strength Graphs of 3LPE - a) at 23-25°C, b) at 55±5⁰C

a)   b)
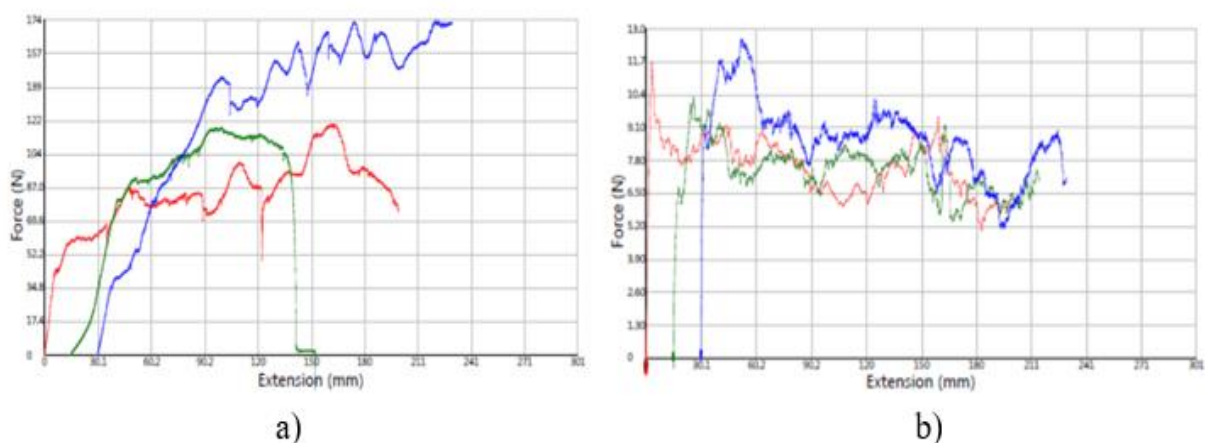
Figure 6B.19: Peel Strength Graphs of 3p/2p CAT - a) at 23-25°C, b) at 55±5⁰C

a)   b)
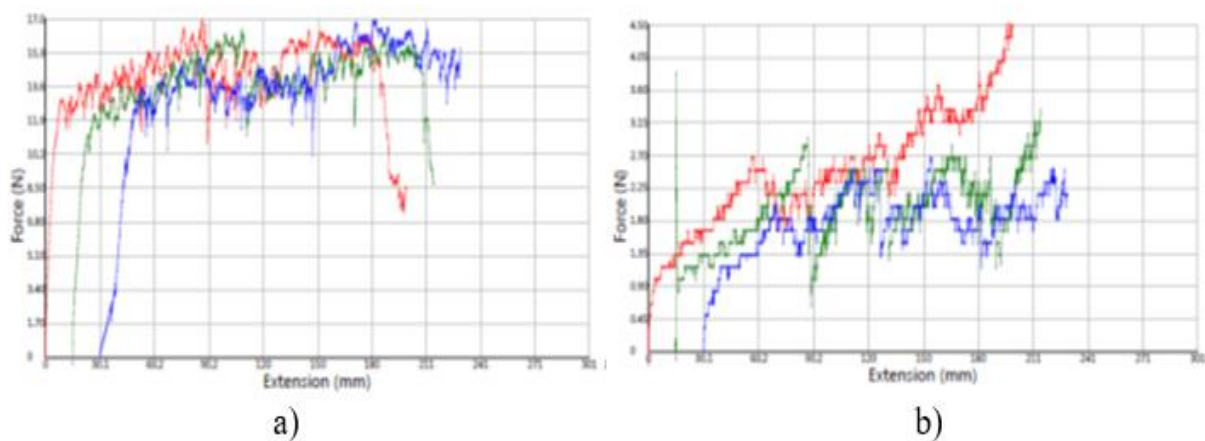
Figure 6B.20: Peel Strength Graphs of VE - a) at 23-25°C, b) at 55±5⁰C
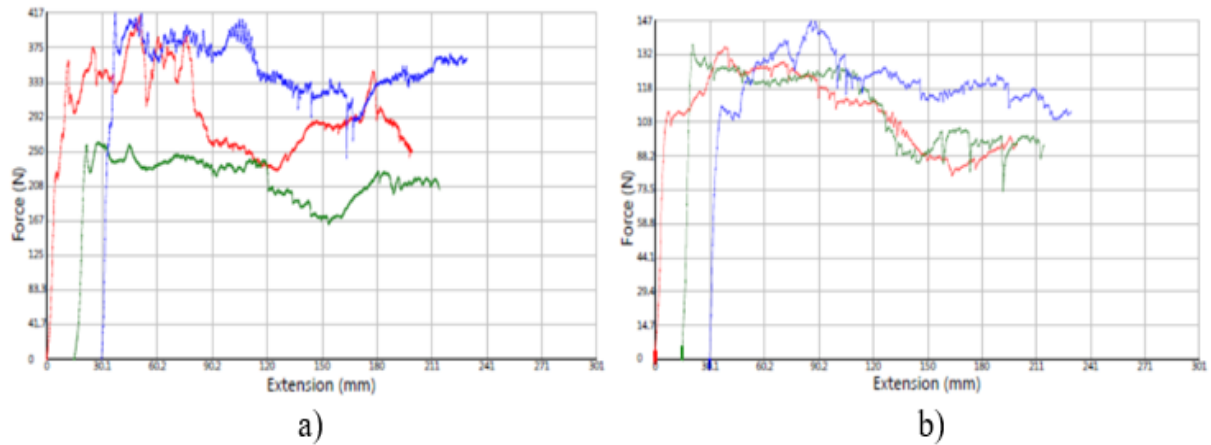
Figure 6B.21: Peel Strength Graphs of HSS - a) at 23-25°C, b) at 55±5⁰C

The peel strengths of the coatings and an arithmetic mean i.e. the average of the three results for each coating are shown in Figure 6B.22. The samples after the peel strength tests are shown in Figure 6B.23.
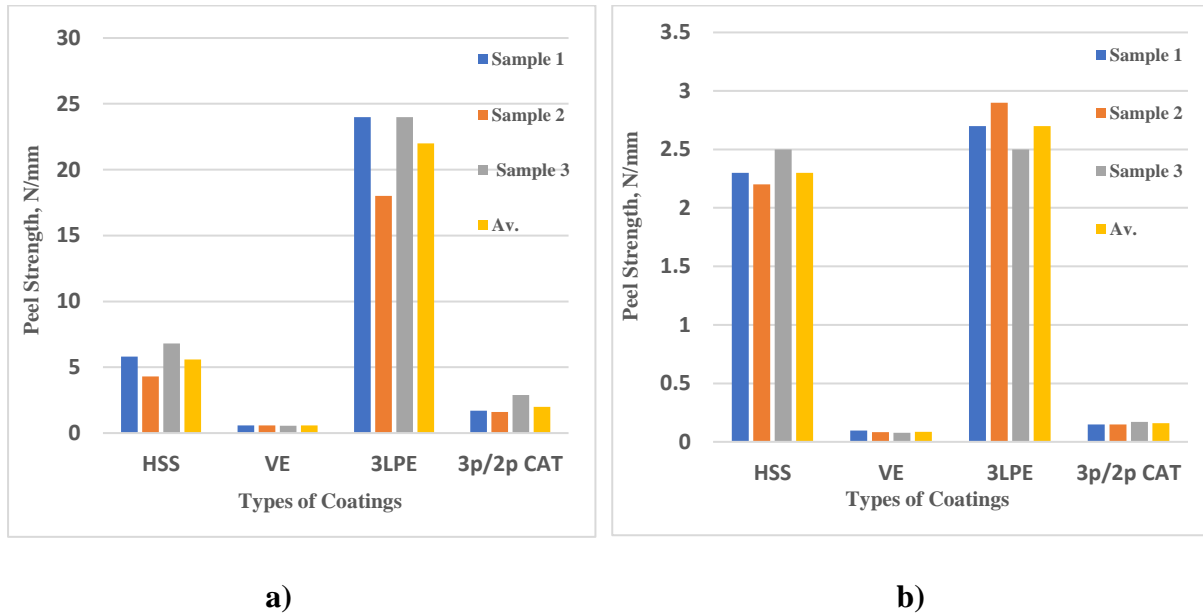
Figure 6B.22: Peel Strength of Coating - a) at 23-25ᵒC, b) at 55±5ᵒC
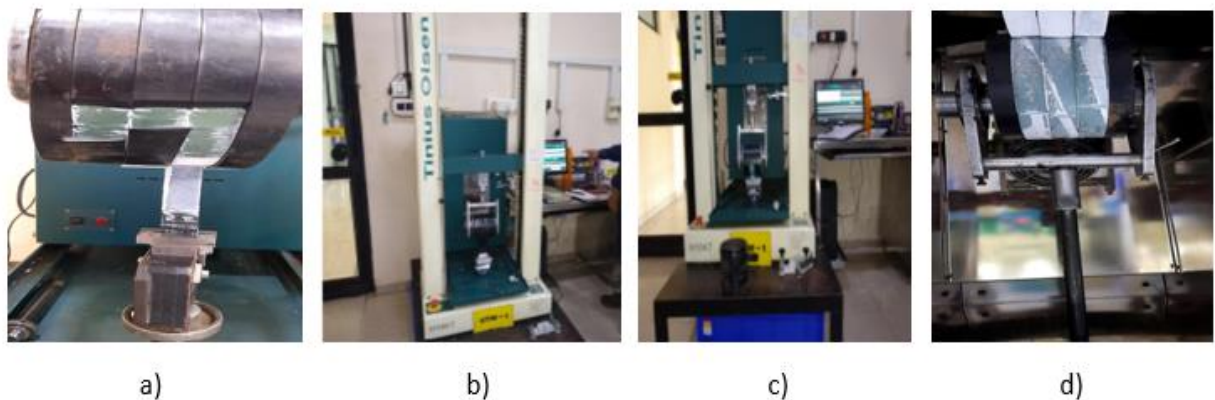
Figure 6B.23: Samples after Peel Strength Test - a) 3LPE, b) 3p/2p CAT, c) VE, d) HSS

6B.4.8.1 Discussion on the Peel Strength Test

The average peel strengths of 3LPE, 3p/2p CAT, VE, and HSS at 23-25°C have been found to be 22 N/mm, 2 N/mm, 0.58 N/mm, and 5.6 N/mm respectively. The average peel strengths of 3LPE, 3p/2p CAT, VE, and HSS at 55±5⁰C have been found to be 2.7 N/mm, 0.16 N/mm, 0.086 N/mm, and 2.3 N/mm respectively. The significant reductions in the adhesion strengths of 3LPE, 3p/2p CAT, VE, and HSS at 55±5⁰C are found to be 88%, 92%, 85%, and 59% respectively in relation to their respective adhesion strengths at 23-25°C. Among the coatings, HSS has shown the least reduction in adhesion strength and best adhesion performance, whereas 3p/2p CAT has shown the greatest reduction in adhesion strength and least adhesion performance. The order of the coatings in respect of the highest to the lowest adhesion performances is found to be HSS, VE, 3LPE, 3p/2p CAT.

6B.4.9 Results of the Pull-off Adhesion Test

The adhesion strengths of solvent-free liquid-applied coatings (i.e., PU, LE) were determined by the pull-off adhesion tests. The pull-off adhesion tests were performed on the samples at 23-25°C and 55±5⁰C with a portable adhesion tester as per ISO 4624. Figure 6B.24 a), b) have shown pull-off testing schematically and Adhesion tester respectively.
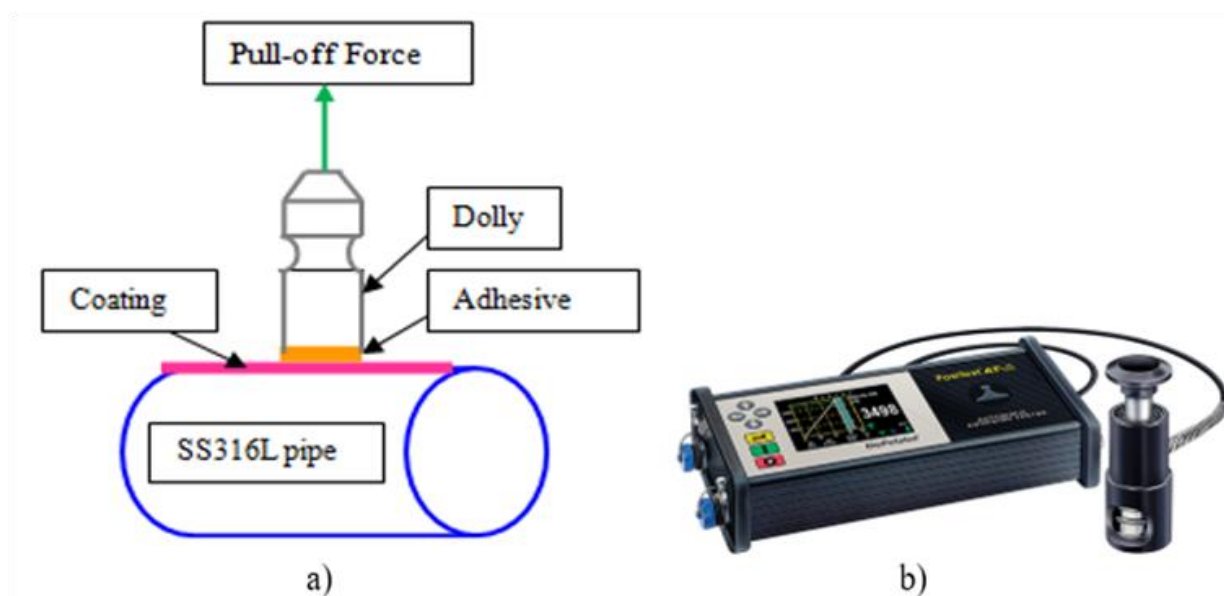
Figure 6B.24: a) Schematic Diagram of Pull-off Adhesion Test, b) Adhesion Tester

The rigid flat faces of three steel dollies of 20 mm diameters were bonded directly to the sample surfaces by adhesive. Each dolly attached to coating was pulled-off by adhesion tester. Pull-off force at which each dolly broke from the coated surface was measured. The fracture was

found to be cohesive in nature. The pull-off adhesion strength of the coating was evaluated from the tensile stress using the Equation (6B-4).

$$P_{pull} = 4F/\pi D^2 \ \ldots\ldots\ldots\ldots\ldots \ (6B\text{-}4)$$

F = Force for detaching dollies (in Newton or Pound)

D = Diameter of surface area (in mm or in)

P_{pull} = Pull-off Strength (in N/mm^2 or Psi)

The pull-off adhesion strengths of the coatings and an arithmetic mean i.e. the average of the three results for each coating are shown in Figure 6B.25. The samples after the pull-off adhesion tests are shown in Figure 6B.26.

a)   b)
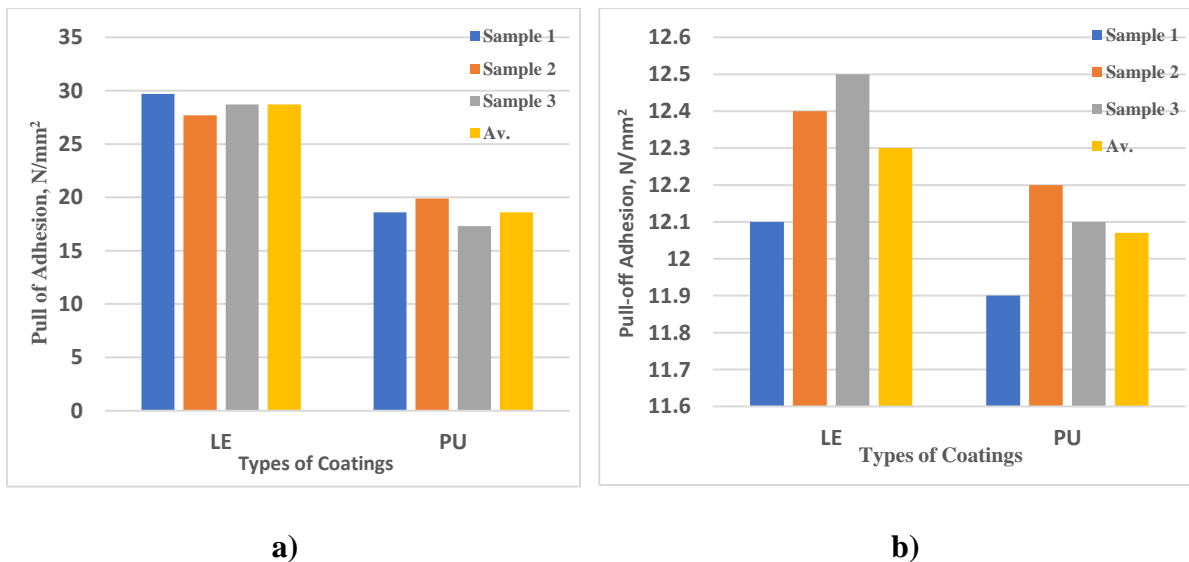
Figure 6B.25: Pull-off Adhesion Strength of Coatings - a) at 23-25ºC, b) at 55±5ºC

Figure 6B.26: Samples after Pull-off Adhesion Test -a) PU, b) LE

6B.4.9.1 Discussion on the Pull-off Adhesion Test

The average pull-off adhesion strengths of PU, LE at 23-25°C have been found to be 18.6 N/mm^2, 28.7 N/mm^2 respectively. The average pull-off adhesion strengths of PU, LE at 55±5ºC have been found to be 12.07 N/mm^2, 12.3 N/mm^2 respectively. The significant

reductions in the adhesion strengths of PU and LE at 55±5⁰C are found to be 35%, and 57% in relation to their respective adhesion strengths at 23-25°C. PU has shown the least reduction in adhesion strength and best adhesion performance, whereas LE has shown the greatest reduction in adhesion strength and least adhesion performance. The order of the coatings in respect of the highest to the lowest adhesion performances is found to be PU, LE.

6B.4.10 Results of the Hot Water Immersion (HWI) Test

The HWI tests were performed on the samples to assess loss of adhesion of the coatings due to hot water immersion for a specific duration [6]. Two sets of samples were prepared after cold cutting 4-inch pipe sections of about 200 mm long from the main and lengthy coated 4-inch SS316L pipes due to the destructive nature of the adhesion tests. Before and after the HWI tests, the peel strength tests for 3LPE, 3p/2p CAT, VE, HSS and the pull-off adhesion strength test for PU, LE were carried out.

Before conducting the HWI test and for the first set of the samples, the adhesion tests of 3LPE, 3p/2p CAT, VE and HSS were performed at 23-25°Cby the peel strength methods with a universal tensile testing machine in accordance with ISO: 21809-3. At the time of testing, the peel-forces against extension lengths graphs were generated. From these graphs, the peel strengths of the coatings were evaluated from the average forces over 100 mm extension lengths using the Equation (6B-3) aforementioned. The peel-forces against extension lengths graphs of 3LPE, 3p/2p CAT, VE and HSS at 23-25°C are shown in Figure 6B.27. The peel strengths of the coatings and the arithmetic mean, i.e. the average of the three results for each coating are shown in Figure 6B.28 a). These peel strength values of the coatings before the HWI test were considered initial peel strengths and were termed as Peel (P_0). The peel tested samples before the HWI test are shown in Figure 6B.29.

Similarly, before conducting the HWI test and for the first set of the samples, the adhesion tests of PU and LE were performed at 23-25°C by the pull-off adhesion strength methods with a portable adhesion tester in accordance with ISO 4624. The pull-off adhesion strengths of PU and LE were evaluated from the tensile stresses using the Equation (6B-4) aforementioned. The pull-off adhesion strengths of the coatings and the arithmetic mean, i.e. the average of the three results for each coating are shown in Figure 6B.28 b). These pull-off adhesion strength values of the coatings before the HWI test were considered initial pull-off adhesion strengths and were termed

as Pull (P_0). Before the HWI test, the pull-off adhesion tested samples with values in Psi units are shown in Figure 6B.30.
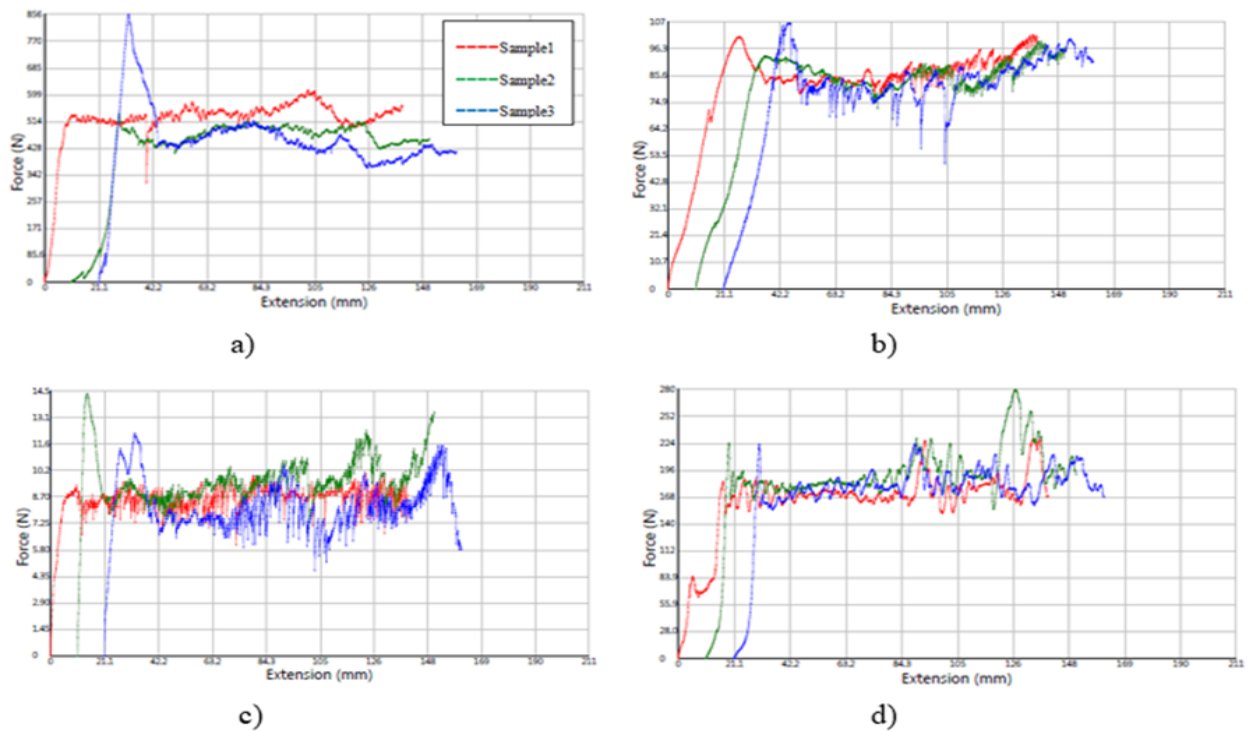
Figure 6B.27: Peel-Force Graphs - a) 3LPE, b) 3p/2p CAT, c) VE, d) HSS

a)   b)
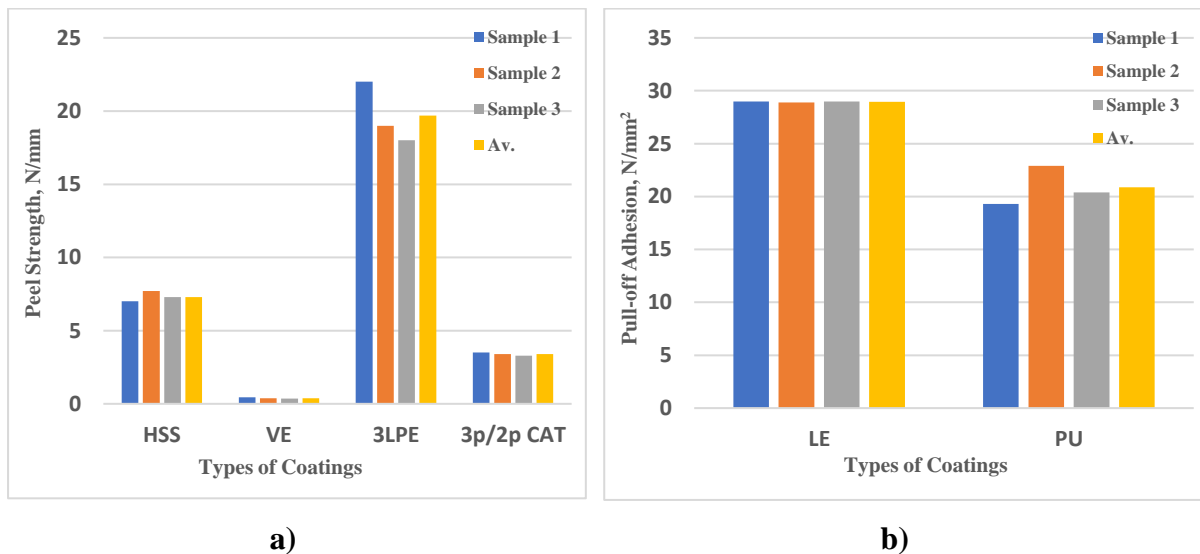
Figure 6B.28: Before HWI Test - a) Peel (P_0), b) Pull (P_0)

Figure 6B.29: Peel Tested Samples - a) 3LPE, b) 3p/2p CAT, c) VE, d) HSS

Figure 6B.30: Pull-off Adhesion Tested Samples (before HWI Test) - a) LE, b) PU

HWI tests were carried out on the second set samples in accordance with ISO: 21809-3 Annex I. The samples were immersed in warm tap (service) water in a vessel. The vessel was placed in an oven for 100 days. The temperature was maintained about 55 ± 5°C. Figure 6B- 31 a) , b), C) have shown an oven and test samples. After 100 days, samples were taken out and cooed in ambient temperature.
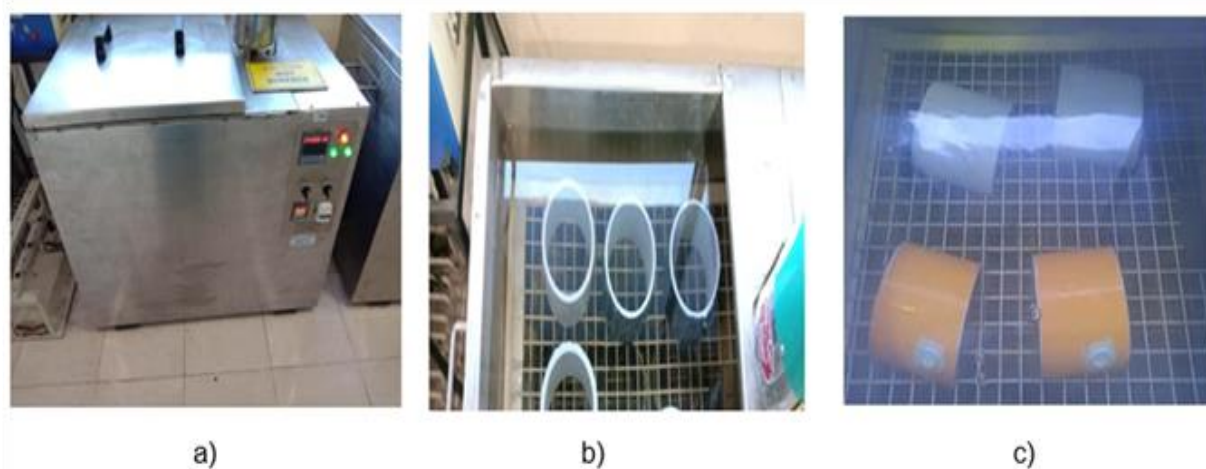
Figure 6B.31: a) A thermostatically controlled oven, b) & c): Samples for HWI test

After the HWI test and for the second set of the samples, the adhesion tests of 3LPE, 3p/2p CAT, VE and HSS were conducted at 23-25°C by the peel strength methods with a universal tensile testing machine in accordance with ISO 21809-3. The peel strengths of 3LPE, 3p/2p CAT, VE, HSS at 23-25°C were evaluated from the peel-forces against extension lengths graphs and are shown in Figure 6B.32. The peel strengths of the coatings and the arithmetic mean, i.e. the average of the three results for each coating are shown in Figure 6B.33 a). These peel strength values of the coatings after the HWI test were considered final peel strengths and were termed as Peel (P_{100}). The peel tested samples, after HWI test, are shown in Figure 6B.34.
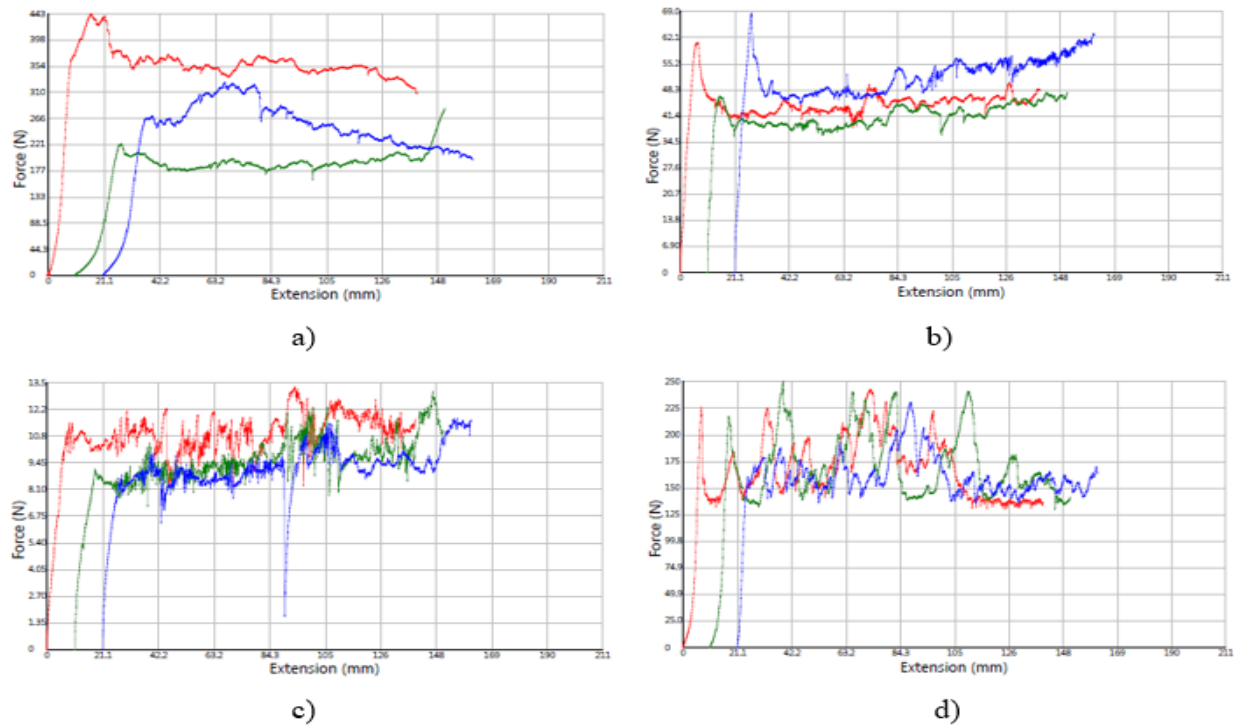
Figure 6B.32: Peel-Force Graphs - a) 3LPE, b) 3p/2p CAT, c) VE, d) HSS

Similarly, after the HWI test and for the second set of the samples, the adhesion tests of PU and LE were carried out at 23-25°C by the pull-off adhesion strength methods with a portable adhesion tester in accordance with ISO 4624.The pull-off adhesion strengths of PU and LE were evaluated from the tensile stresses. The pull-off adhesion strengths of the coatings and the arithmetic mean, i.e. the average of the three results for each coating are shown in Figure 6B.33 b). These pull-off adhesion strength values of the coatings after the HWI tests were considered final pull-off adhesion strengths of the coatings and were termed as Pull (P_{100}). The pull-off adhesion tested samples with values in Psi units are shown in Figure 6B.35.

a)

b)
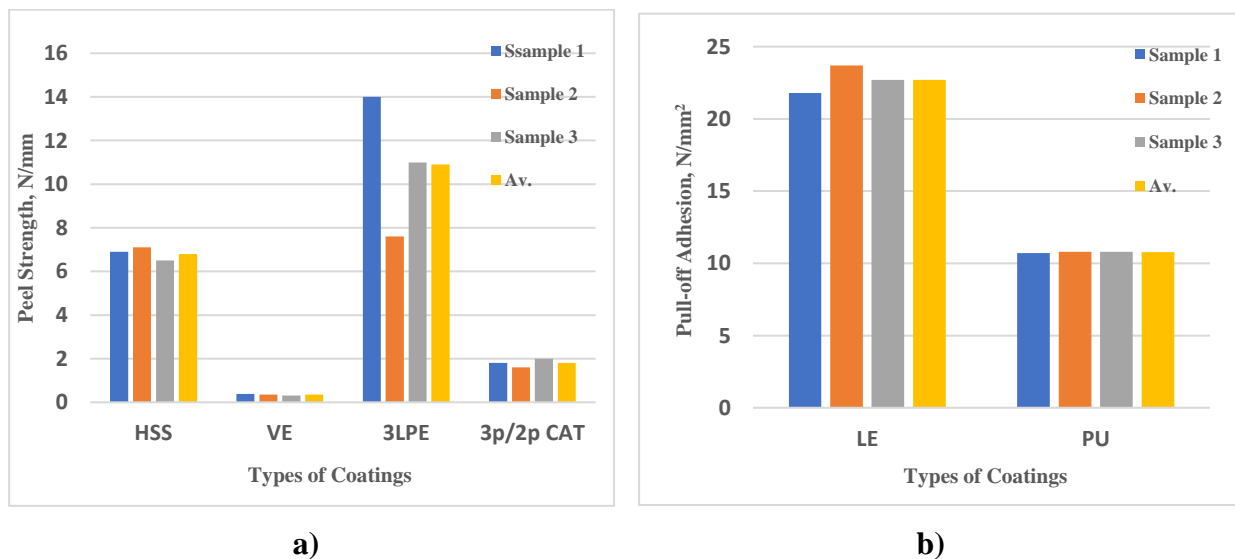
Figure 6B.33: After HWI Test - a) Peel (P_{100}), b) Pull(P_{100})

153
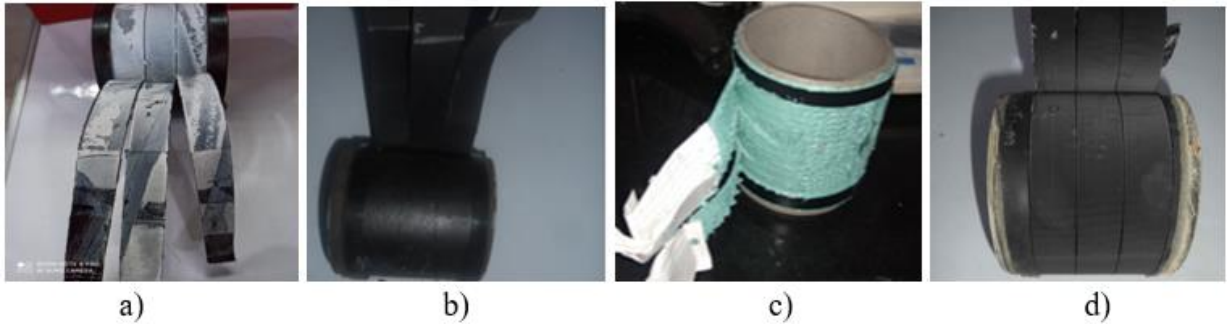
Figure 6B.34: Peel Tested Samples - a) 3LPE, b) 3p/2p CAT, c) VE, d) HSS
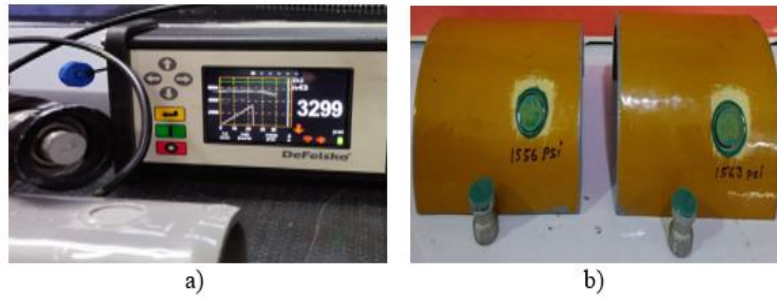
Figure 6B.35: Pull-off Adhesion Tested Samples (after HWI Test) - a) LE, b) PU

The ratios (P_{100}/P_0) of the coatings and the arithmetic mean, i.e. the average of the three results for each coating were computed and are shown in Figure 6B.36.
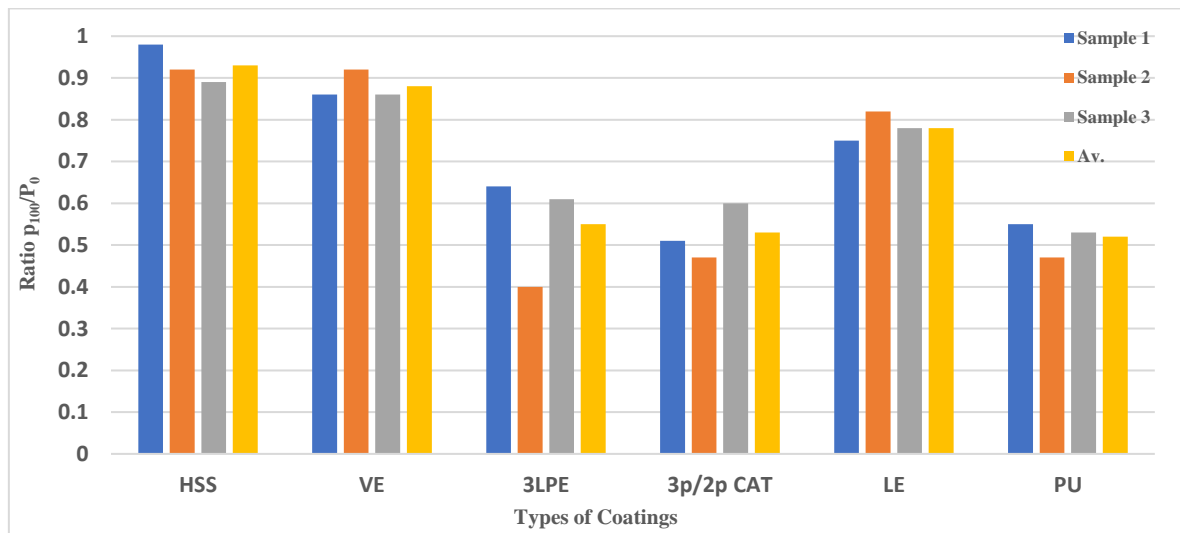
Figure 6B.36: Comparison of Adhesion Performances - Ratio (P_{100}/P_0)

6B.4.10.1 Discussion on the HWI Test

The average initial peel strengths [i.e., Peel (P_0)] of 3LPE, 3p/2p CAT, VE, HSS, before the HWI test and from Figure 6B-28 a), have been found to be 19.7 N/mm, 3.4 N/mm, 0.39 N/mm, 7.3 N/mm respectively. After the HWI test and from Figure 6B.33 a), the average final peel strengths [i.e., Peel (P_{100})] of 3LPE, 3p/2p CAT, VE, HSS have been found to be 10.9 N/mm, 1.8 N/mm, 0.35 N/mm, 6.8 N/mm respectively. It is observed that adhesion strength of

3LPE after HWI test has been reduced to a greater extent, whereas adhesion strengths of HSS and VE after HWI test have been reduced to a lesser extent.

The average initial pull off adhesion strengths [i.e., Pull (P_0)] of LE, PU before the HWI test and from Figure 6B-28 b), were found to be 28.97 N/mm^2, 20.87 N/mm^2 respectively. After the HWI test and from Figure 6B.33 b), the average final pull-off adhesion strengths [i.e., Pull (P_{100})] of LE, PU were found to be 22.7 N/mm^2, 10.77 N/mm^2 respectively. It is apparent that adhesion strength of PU after HWI test has been reduced to a greater extent, whereas adhesion strength of LE after HWI test has been reduced to a lesser extent.

Peel-strength units of 3LPE, 3p/2p CAT, VE, HSS are in N/mm, whereas Pull-off strength units of LE, PU are N/mm^2 . It is, therefore, not possible to make comparison between coatings performances. A dimensionless number based on P_{100}/P_0 ratio for each coating has been calculated. This ratio is termed as the "Coating Bond Index" in this study. Each ratio for each coating gives coating adhesion performance. Ratio with highest value gives coating best adhesion performance. This means that bonding between coating and SS316L will stay long.

The average ratio for 3LPE, 3p/2p CAT, PU, VE, LE, HSS has been found to be 0.55, 0.53, 0.52, 0.88, 0.78, 0.93 respectively. HSS coating has shown best performance in this test because it contains electron beam radiation cross-linking of high density polyethylene (HDPE) to enhance heat shrinkable properties. Radiation cross-linked HDPE polymer chain has greater strength and adhesion properties at higher temperatures than linear version of HDPE. The order of the coatings with respect to the highest to the lowest adhesion performances is found to be HSS, VE, LE, 3LPE, 3p/2p CAT, PU.

6B.4.11 Results of Specific Electrical Insulation Resistance (SEIR) Test

The SEIR test was conducted in accordance with ISO: 21809-3 Annex-F for measuring the specific electrical insulation resistance of a coating in 0.1 mol/litre of NaCl solutions over a period of 100 days and by applying a Direct Current (DC). Three samples of each coating were immersed vertically in NaCl solution in the plastic container as shown in Figure 6B.37. The submerged ends of the samples were sealed with silicone sealants so that these ends were prevented from contacting with NaCl solutions. During measurement, the other ends of the samples not immersed in NaCl solutions were connected to the positive poles of DC power supply and the negative pole was connected to a copper rod (counter electrode). The counter

electrode with an area of 10 cm^2 was immersed in NaCl solution. A schematic diagram of SEIR test and a sample under the SEIR testing are shown in Figure 6B.38 a) and b) respectively.

The SEIR test was performed at 23-25°C for 100 days. During each measurement, 100V was applied and after 1 minute, voltage and current were recorded. The first measurement was taken after three days i.e., on the 4th day. Then, the measurements were taken at intervals for a total of 100 days. The specific electrical resistance was calculated using the Equation (6B-5):

$$Rs = U \times A/I = R1 \times A \ldots\ldots\ldots\ldots\ldots\ldots\ldots.(6B\text{-}5)$$

Where,

Rs = Specific electrical resistance (ohm.m^2), I = Measured current (amperes)

R1 = Measured electrical resistance of the submerged sample (ohm),

U = Voltage between the counter electrode and the sample (volt),

A = Submerged surface area of the coating (m^2),

The SEIR values of 3LPE, 3p/2p CAT, PU, VE, LE, HSS are shown in Figure 6B.39. A comparison was drawn based on the coatings SEIR values obtained over 100 days immersion in 0.1mol/litre of NaCl solution at 23-25°C and is shown in Figure 6B.40.
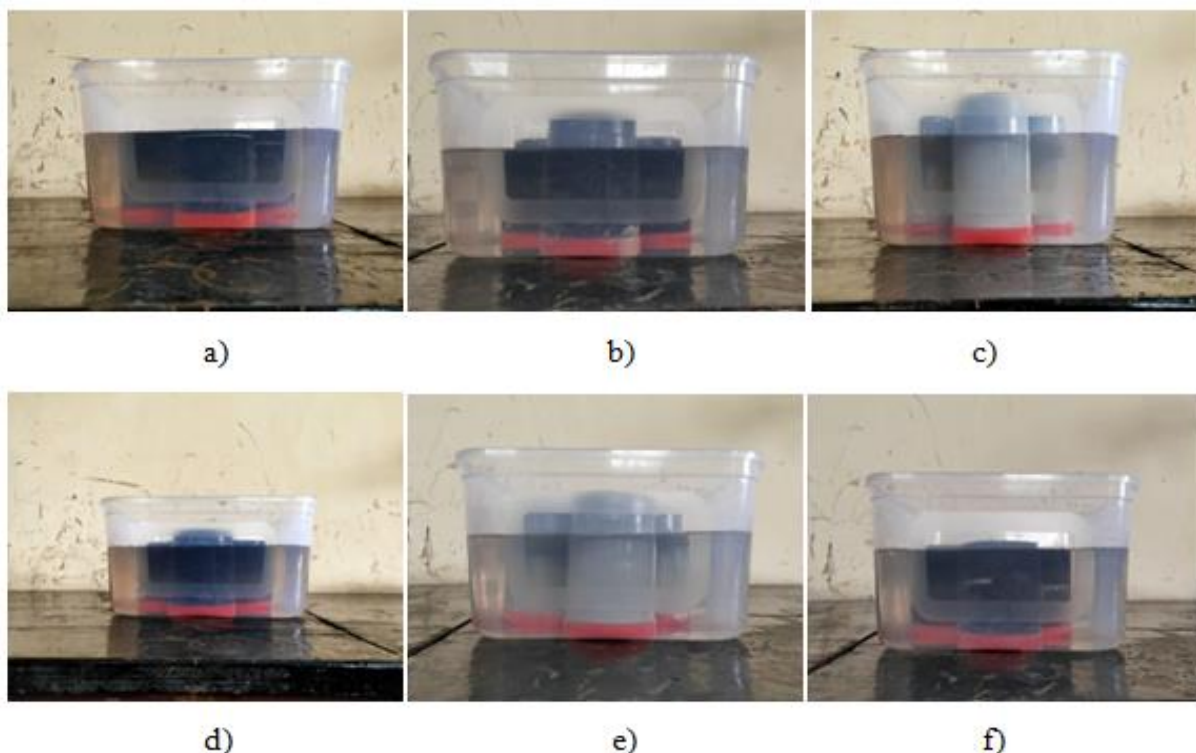
Figure 6B.37: Test Samples - a) 3LPE, b) 3p/2p CAT, c) PU, d) VE, e) LE, f) HSS
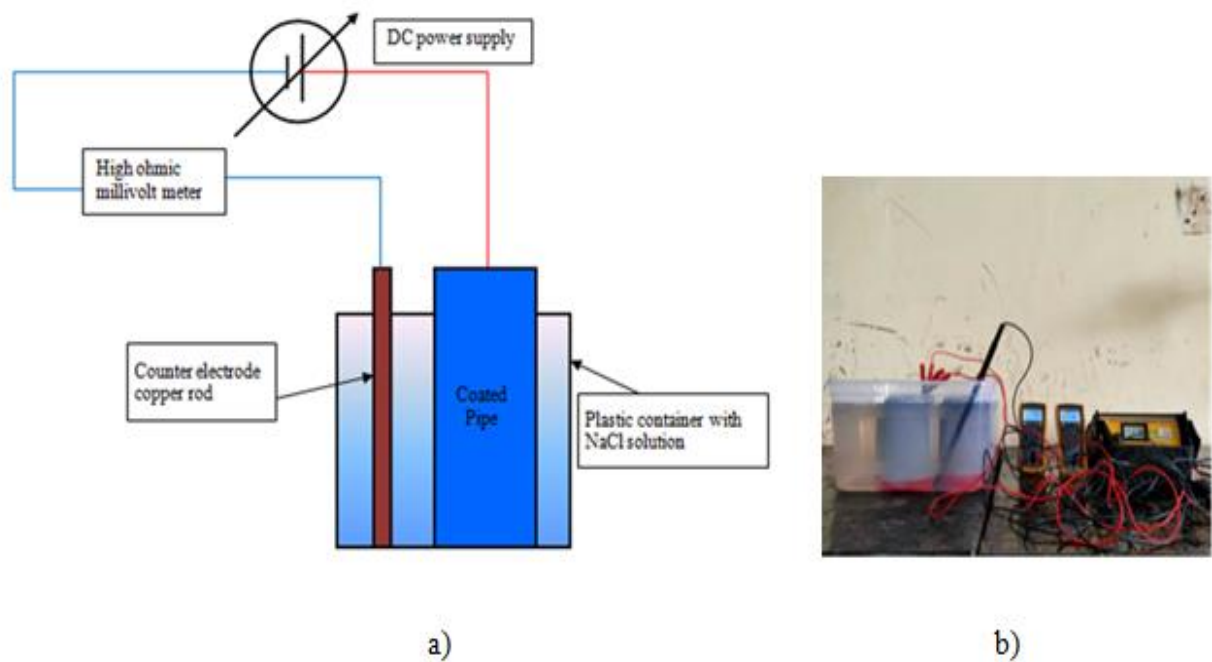
Figure 6B.38: a) Schematic Diagram of SEIR test, b) A Sample under SEIR Testing

6B.4.11.1 Discussion on SEIR Test

The initial SEIR values of 3LPE, PU, LE have found to be greater than 10^9 ohm.m^2, whereas the initial SEIR values of 3p/2p CAT, VE, HSS have been found to be greater than 10^8 ohm.m^2. Six coatings with such high initial SEIR values reveal them perfect insulators that yield highest corrosion protection. After 100 days of immersion, the SEIR values of all the coatings have been found to be reduced. This phenomenon is likely to happen due to exposure of a coating to a corrosive environment over a period of time and due to water absorption by the coating on metal substrate resulting in loss of insulating properties and corrosion protection efficiency.
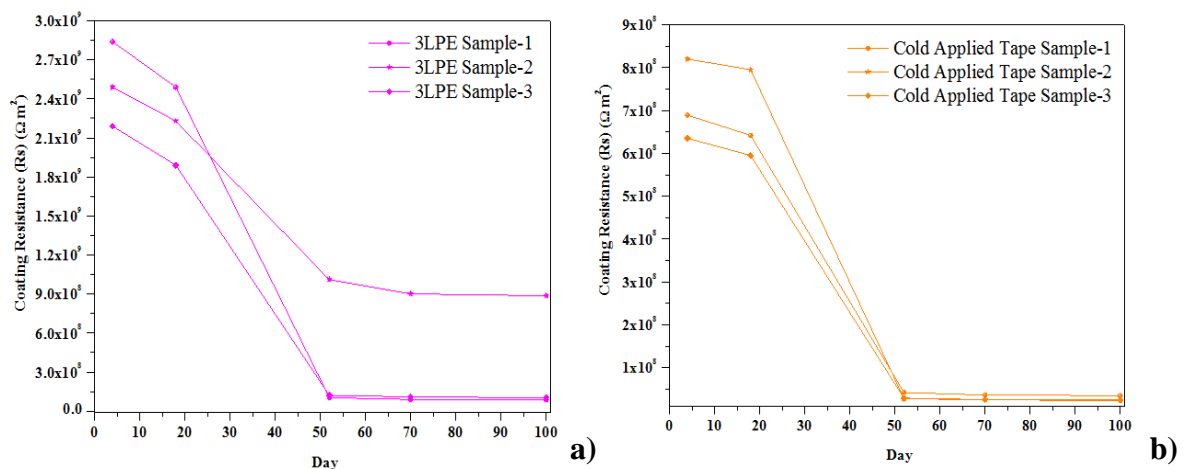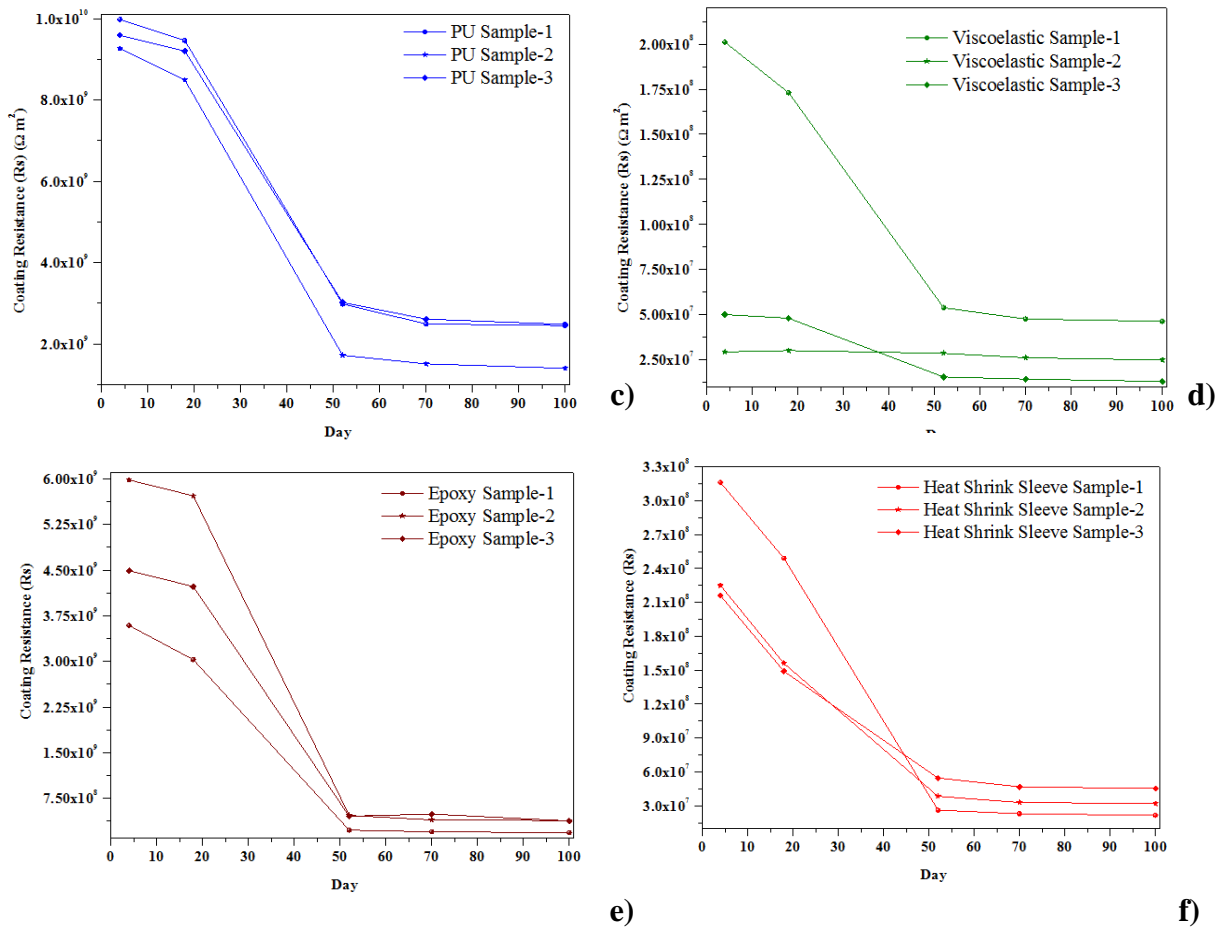
Figure 6B.39: SEIR Values - a) 3LPE, b) 3p/2p CAT, c) PU, d)VE, e) LE, f) HSS

To differentiate the performances of the coatings in the SEIR tests, a comparison has been drawn based on the SEIR values of the coatings versus 100 days of immersion in 0.1mol/litre of NaCl solution at 23-25°C and is shown in Figure 6B-40.
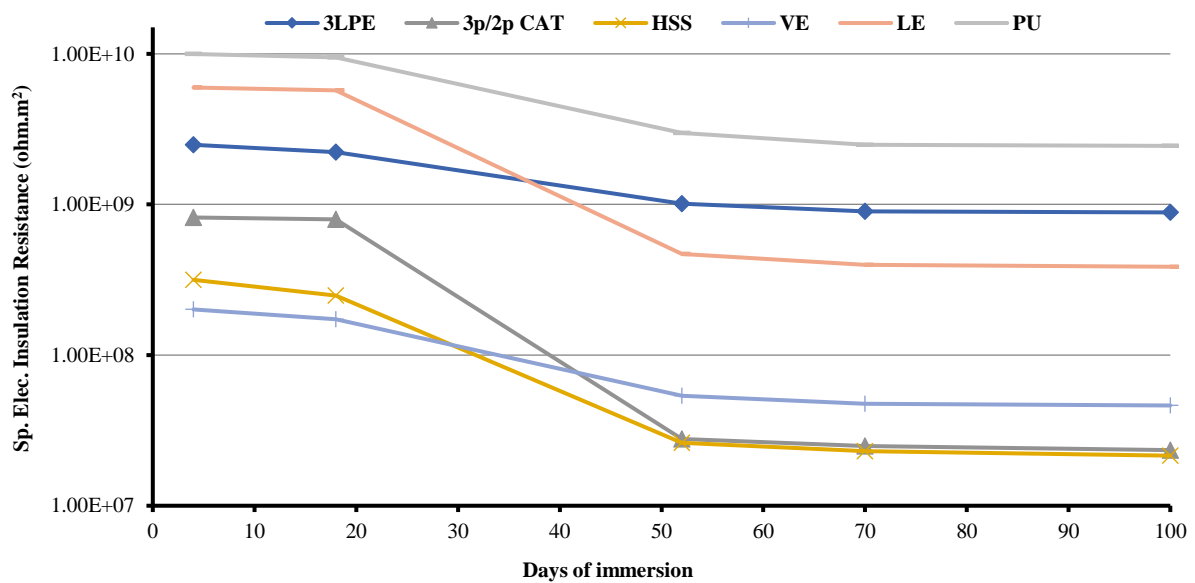
Figure 6B.40: Comparison of Coatings SEIR Values for 100 Days of Immersion in 0.1mol/litre of NaCl Solution at 23-25°C

158

The SEIR values (ohm.m^2) of 3LPE, 3p/2p CAT, PU, VE, LE and HSS after 100 days of immersion are found to be 8.86×10^8, 2.34×10^7, 2.45×10^9, 4.63×10^7, 3.86×10^8 and 2.15×10^7 respectively. PU coating has shown best performance in this test because it is an aromatic and thermoset polyurethane, where aromatic methylene diphenyl diisocyanate (MDI) reacts with polyol for curing of PU. As the aromatic isocyanate proportion is more than polyol, such PU is hydrophobic. It acts as an effective barrier and gives resistance to water permeability through coating and maintains high electrical insulation resistance. The order of the coatings with respect to the highest to the lowest specific electrical insulation resistances is found to be PU, 3LPE, LE, VE, 3p/2p CAT, and HSS.

6B.4.12 Results of Electrochemical Impedance Spectroscopy (EIS) Test

The EIS test was conducted to measure the electrochemical impedances of the coatings by the Alternating Current (AC) impedance method. The EIS test generates data within short testing times and is more reliable to predict the long-term performances of the coatings. The experiments for collecting electrochemical impedance data were performed in accordance with ASTM Standard Practice G106 with the attached cells consisting of glass tubes cemented to the samples. The samples with attached cells are shown in Figure 6B.41. A coated pipe surface, a graphite rod and a Saturated Calomel Electrode (SCE) were used as WE (Working Electrode), CE (Counter Electrode), and RE (Reference Electrode) respectively. The attached cell was filled with 3.5% NaCl solution. CE and RE were inserted into the solution. A schematic diagram of the EIS test and a sample under the EIS testing are shown in Figure 6B.42 a) and b) respectively.
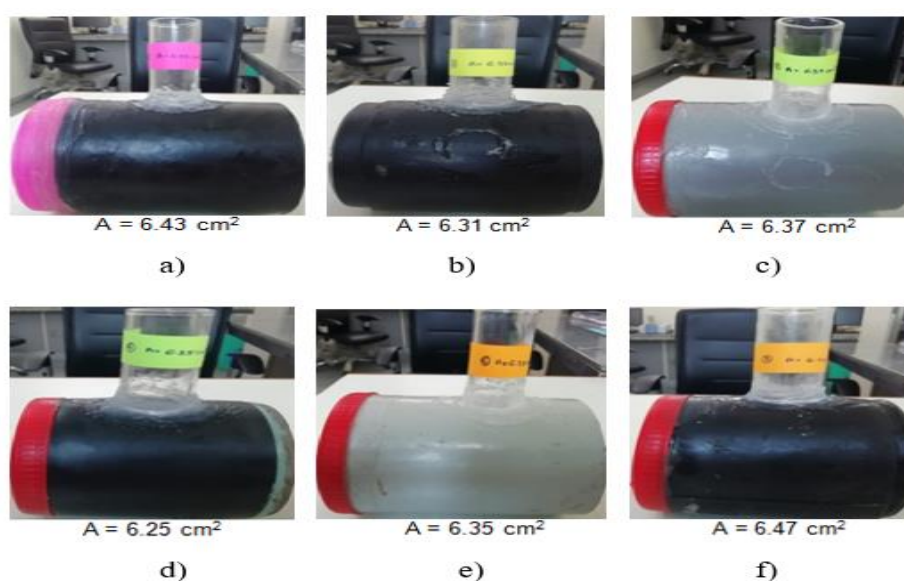
Figure 6B.41: Samples with Attached Cells - a) 3LPE, b) 3p/2p CAT, c) PU, d) VE, e) LE, f) HSS (A= cell area in cm^2)
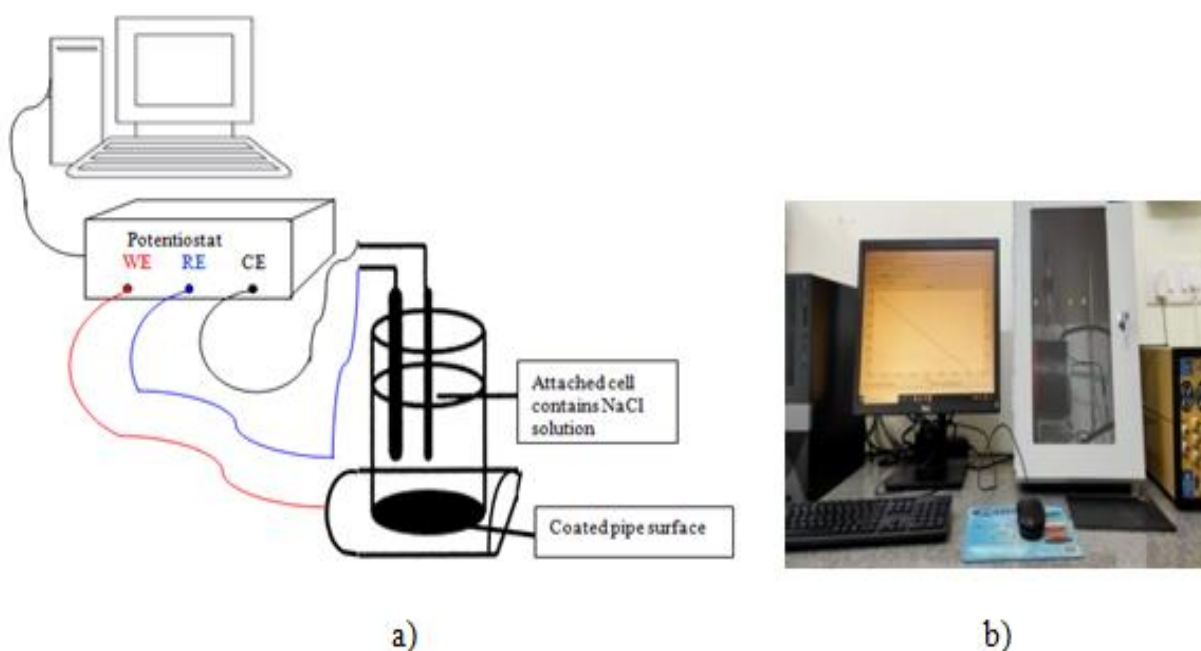
Figure 6B.42: a) Schematic Diagram of EIS Test, b) A Sample under EIS Test

The EIS tests were conducted on the samples by GAMRY Model 600+ at 23-25°C for 14 days of immersion. The measurements were carried out on the 1st day, 7th day, and 14th day at open circuit potential with an applied AC voltage of 100 mV$_{rms}$ in amplitude in the frequency range of 100 kHz -10 mHz. During data collection of electrochemical impedances, the samples were placed inside the Faraday cage to minimize electromagnetic interference and noise. A sample inside the Faraday cage under the EIS testing is shown in Figure 6B.42b).

During EIS tests, the data and spectra of the Bode plots were generated. These plots were interpreted as impedance magnitudes, |Z| in ohm.cm^2 (left side Y1 vertical axis in log scale) and phase angles, Φ in degree (right side Y2 vertical axis) versus the measured frequencies in Hertz (Hz) (horizontal X axis in log scale) [7-8]. A common legend was used for the Bode plots of six types of coatings and is shown in Figure 6B.43. The Bode plots of the coatings are shown in Figures 6B-44, 45. From these plots, the electrochemical impedance values of the coatings were evaluated
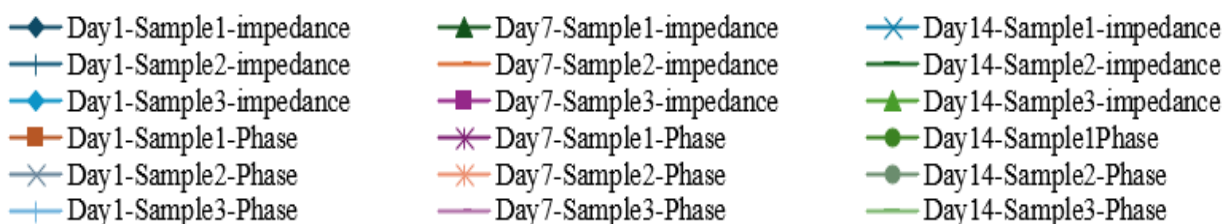
Figure 6B.43: Common Legend used for the Bode Plots of Six Coatings
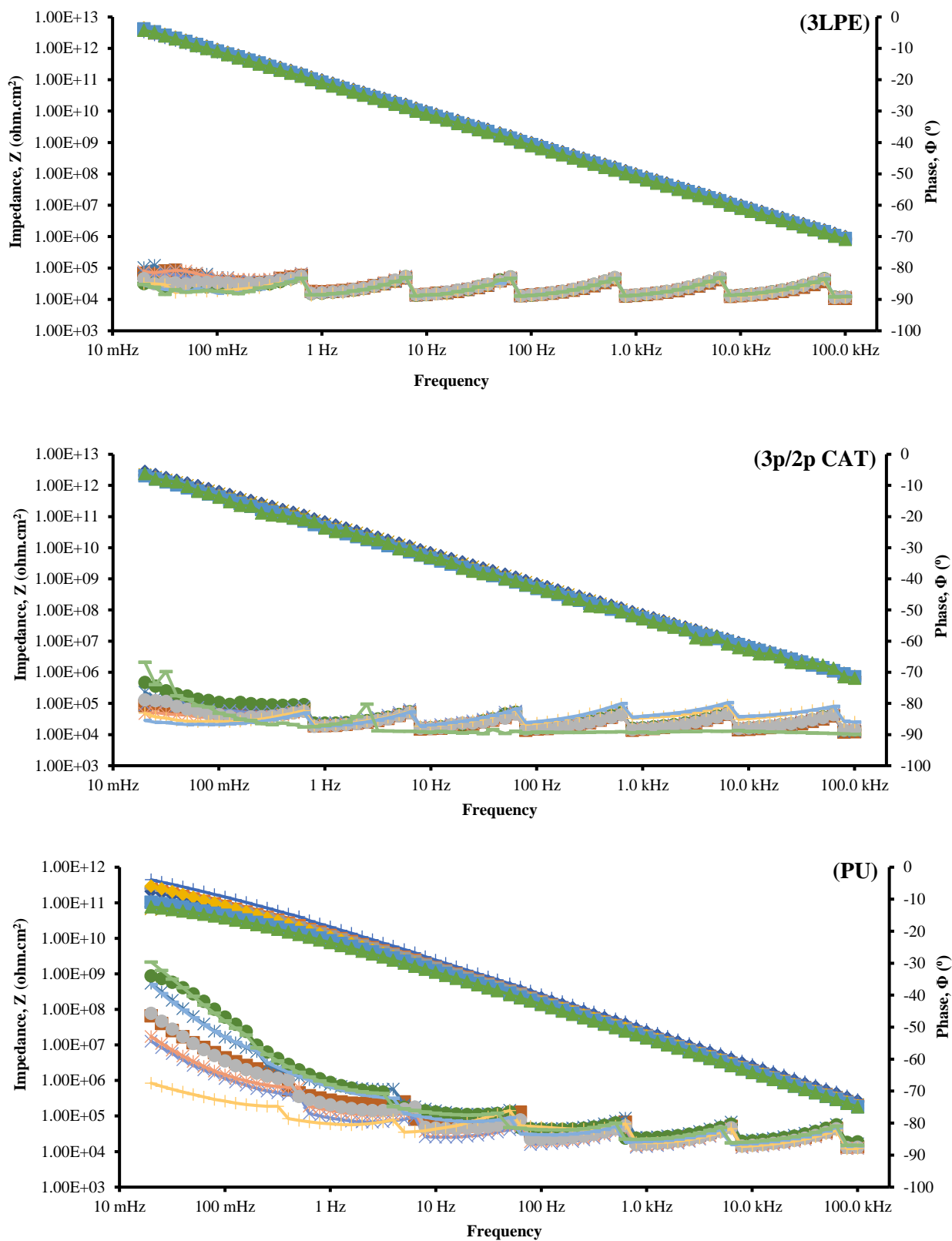
Figure 6B.44: Bode plots of 3LPE, 3p/2p CAT, PU
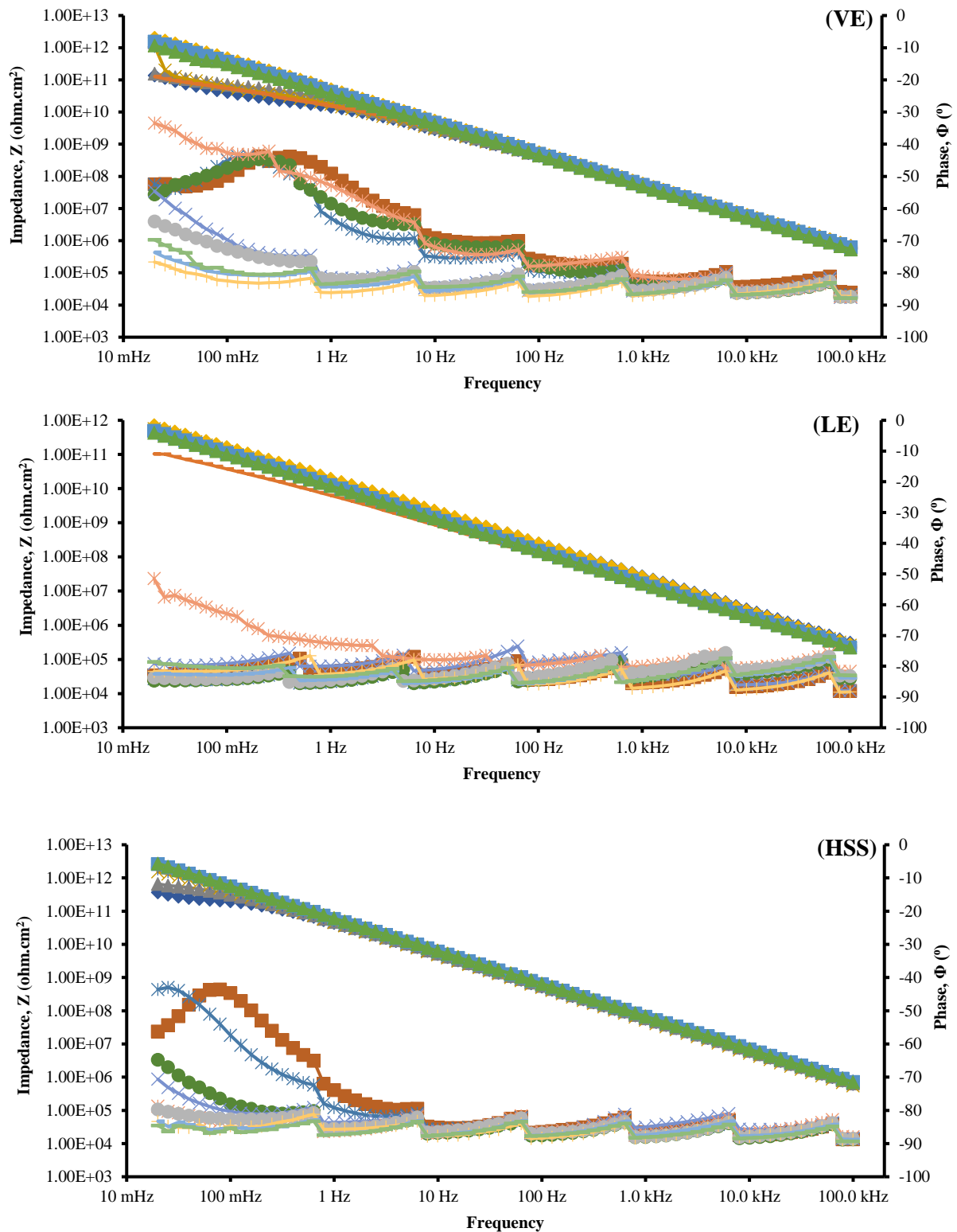
Figure 6B.45: Bode plots of VE, LE, HSS

6B.4.12.1 Discussion on EIS Test

It has been observed from the Bode plots of the coatings that the electrochemical impedances versus frequencies are diagonal and their slopes are -1. All the coatings have shown the high impedance values at the lowest frequencies, which are found to be greater than 10^{11}

ohm.cm^2, although little variations in impedance values are observed for HSS, VE, and LE. The impedance values of the coatings are also found to be greater than 10^5 ohm.cm^2 at higher frequencies. Overall, all the coatings are found to be good insulators.

The phase angles of 3LPE and 3p/2p CAT versus frequencies are found to be -90° and a little less than -90° respectively. It appears that 3LPE and 3p/2p CAT behave as better capacitors. The variations of the phase angles at lower frequencies have been observed on PU, VE, LE, HSS. These phenomena indicate that there was a likelihood of permeating water, oxygen, ions and corrosive species through the coatings into the metal substrates beneath over a period of time. The diffusion of water is a prime mechanism of water absorption in polymeric coating and is played a significant role on water uptake. It has been reported in the literature that there are four different stages for water uptake by the coating. The four stages are (1) water absorption rapidly in the initial days, (2) increased water uptake with a slower rate, (3) saturation of water, and (4) lastly, a further increase in water absorption. Water causes swelling by transporting ions into the coating. When water uptake is low, the coating resistance is high because of low permeation of oxygen, ions and corrosive species into the coating.
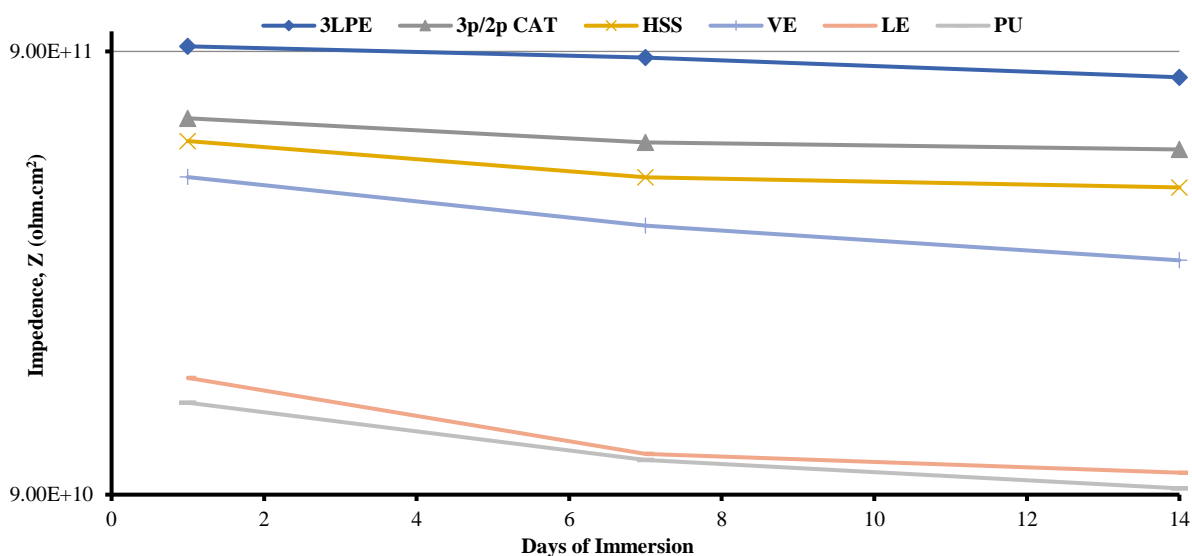
Figure 6B.46: Comparison of Coatings Impedance Values with respect to Cell Areas of 1 cm^2 with an Applied AC voltage of 100 mVrms at 100 mHz (0.1 Hz) for 14 Days of Immersion in 3.5% NaCl Solution at 23-25°C

To distinguish the performances of the coatings in the EIS tests, a comparison [9] has been drawn based on the impedance values of the coatings in respect of cell areas of 1 cm^2 with

an applied AC voltage of 100 mV$_{rms}$ in amplitude at frequency of 100 mHz (0.1 Hz) versus 14 days of immersion in 3.5% NaCl solution at 23-25°Cand is shown in Figure 6B.46**.**

The electrochemical impedance values (ohm.cm^2) of 3LPE, 3p/2p CAT, PU, VE, LE, HSS after 14 days of immersion are found to be 7.87x10^{11}, 5.41x10^{11}, 9.30x10^{10}, 3.04x10^{11}, 1.01x10^{11}, 4.44x10^{11} respectively. 3LPE coating has shown best performance in this test. Electrochemical and water-dependent phenomenon occurs when there is presence of an aqueous film on the surface of the polymer. Moisture and ionic contamination can cause ionic migration on the surface of polymeric materials reducing the electrochemical impedance and insulation resistance properties. 3LPE insulate the polymer surface to acquire sufficient moisture and resists ionic conduction in the presence of an electrical potential with high electrochemical impedance values. The order of the coatings in respect of the highest to the lowest impedances is found to be 3LPE, 3p/2p CAT, HSS, VE, LE, PU [10].

6B.4.13 Conclusion

3LPE coating has shown best performance in the indentation resistance test. VE coating has shown best performance in the water absorption test. 3LPE coating has shown best performance in the cathodic disbondment test. HSS coating has shown best performance in the hot water immersion test. PU coating has shown best performance in the specific electrical insulation resistance test. 3LPE coating has shown best performance in the electrochemical impedance spectroscopy test.

6B.5 References

[1] Richard E. Ricker, 'Advanced Coatings R&D for Pipelines and Related Facilities' NIST Special Publication 1044, June 9-10, 2005, Impact Resistance of Coatings, Table-23, p.83
[2] B De'Nèv et al., Water absorption by an epoxy resin and its effect on the mechanical properties and infra-red spectra, Polymer, Vol. 34, Issue 24, December 1993, p.5099-5105
[3] Min Xu et al., Evaluation of the cathodic disbondment resistance of pipeline coatings - A review, Progress in Organic Coatings, Vol.146, September 2020, 105728
[4] Denise S. de Freitas et al., Long-term cathodic disbondment tests in three-layer polyethylene coatings - Materials and Corrosion Materials and Corrosion, August 2023, Vol. 74, Issue 8, p.1129-1262
[5] Ole Øystein Knudsen, Cathodic Disbonding of Epoxy Coatings - Effect of Test Parameters, Paper No. 08005, Corrosion 2008, p.1-16
[6] Enrique Vaca-Cortés et al., Adhesion Testing of Epoxy Coating, Chapter-4, Hot Water test, Texas Department of Transportation, Research Report No.1265-6, September 1998, p.77
[7] M. Mirzaee1 et al., Investigation of Corrosion Properties of Modified Epoxy and Polyurethane Organic Coating on Steel Substrate, Prog. Color Colorants Coat. 15 (2022), p.25-36
[8] Bobbi Jo Merten, Coating Evaluation by EIS Research and Development Office U.S. Department of the Interior, Bureau of Reclamation, p.1-32
[9] Linda G.S. Gray et al., KTA-Tator (Canada) EIS: A Tool to Predict Remaining Coating Life, JPCL February 2003, p.66-74
[10] E.Akbarinezhad et al., Another approach for ranking and evaluating organic paint coatings via EIS, Elsevier, Corrosion Science 51 (2009), p.356-363

Chapter - 6C

Coating for SS316L Pipeline in Above-ground Condition

Chapter - 6C: Coating for SS316L Pipeline in Above-ground Condition

6C Introduction

The uncoated SS316L is most prevalent for SS316L pipeline marginally exposed in above-ground condition in the petroleum, petrochemical and natural gas industries. No coating is usually applied on external surface of SS316L pipeline in above-ground condition because SS316L is a corrosion resistant material due to the presence of a thin chromium oxide (Cr_2O_3) passive layer in atmospheric exposure. But, in marine atmosphere or under thermal insulation, corrosion on SS316L can be prevented by applying coating. Hence, one liquid coating (i.e. solvent free liquid epoxy) commonly used has been tested for Above-ground condition. The abrasion resistance test has been conducted to represent resistance to abrasion of the coated pipes during transportation and storage. LE has been selected because it possesses highest hardness among six coatings and liquid coating can be applied in the field at ease. It has been assumed that due to its highest hardness, LE can give highest resistance to damage that may be caused practically during transportation and storage. LE has been applied on three SS316L square plates and after curing, these coated plates have been subjected to the Taber abrasion resistance test.

In this chapter, the results obtained by the chemical composition analysis of a SS316L plate, the abrasion resistances of LE coated SS316L plates, and the subsequent discussions are presented.

6C.1 Results and Discussion on Chemical, and Abrasion Resistance Tests of SS316L Plates

The chemical composition analysis of a SS316L plate and the abrasion resistance tests of LE coated SS316L plates were carried out.

6C.1.1 Results of Chemical Composition Analysis

One sample was extracted from SS316L plate and was subjected to chemical composition analysis. Carbon (C), Sulphur (S) in weight percentages (wt%) and Nitrogen (N) in ppm were determined by the combustion technique as per ASTM E-1019 [1]. Other elements such as Chromium (Cr), Manganese (Mn), Nickel (Ni), Molybdenum (Mo), Silicon (Si), Phosphorous (P) in weight percentages (wt%) were determined by the spark atomic emission spectrometry according to ASTM E-1086 [2]. The chemical composition analysis of three SS316L samples is shown in Table 6C.1.

Table 6C.1: Chemical Composition Analysis of SS316L Plate (wt%)

Sample no.	C	Mn	S	P	Si	Cr	Ni	Mo	N (ppm)*	Fe
Sample 1	0.02	1.48	0.019	0.028	0.62	16.68	11. 09	2.39	405	Balance

(**ppm** - parts per million)

6C.1.2 Discussion on Chemical Composition Analysis

In the chemical composition analysis of SS316L plate, C, Mn, Si, Cr, Ni, Mo in wt% and N in ppm have been found to be 0.02, 1.48, 0.62, 16.68, 11.09, 2.39 and 405 respectively. Very low level of S and P in wt% has been found 0.019 and 0.028 respectively in the chemical analysis. The chemical composition conforms to austenitic stainless steel plate type SS316L intended for pressure vessels and for general applications in accordance with ASTM A-240 [3].

6C.1.3 Results of the Abrasion Resistance Tests

Three square plates of 100 mm X 100 mm X 2 mm were cut out from a 400 mm X 400 mm X 2 mm SS316L plate. A 6.3 mm hole was made in the centre of each square plate. The surfaces of the plates were prepared by fused aluminium oxide (Al_2O_3) fine particles. After adequate surface preparation, solvent-free liquid-applied epoxy (LE) coating of 1000 microns was applied uniformly on each plate. After curing, the coated plates were subjected to the Taber abrasion resistance tests. Abrasion resistance testing of LE coated SS316L plates were conducted by the Taber Abraser CS 17 abrasive wheels with 1000g load per wheel and 1000 cycles in accordance with ASTM D-4060 [4].The sample was mounted vertically on a turntable platform with the side to be abraded facing up and against the sliding rotation of two abrading wheels of the Taber Abraser. Loose debris was taken off by a vacuum system.

The abrasion resistances of LE coated plates have been computed as weight loss (L) using the following Equation (6C-1):

$$L = A - B \quad \text{......................} \quad (6C\text{-}1)$$

Where,

A = Weight of LE coated plates in mg, before abrasion resistance test,

B = Weight of LE coated plates in mg, after abrasion resistance test for 1000 cycles.

The wear indexes (I) of LE coated plates have been computed using the following Equation (6C-2):

$$I = \frac{(A-B)1000}{C} \quad \dots \dots \dots \dots \dots \dots \quad (6C\text{-}2)$$

Where,

C = Number of cycles of abrasion.

An arithmetic mean of weight loss in mg and wear index of three samples has been computed and recorded. The abrasion results are shown in Table 6C-2. The results of weight loss and wear index have been found to be identical because number of cycles of abrasion is 1000. Before and after the abrasion resistance test, the samples are shown in Figure 6C.1 and Figure 6C.2 respectively.

Table 6C.2: Abrasion Resistance of LE Coated SS316L Plates

Sample no.	Wheel type	Applied load to wheels, g (per arm)	No. of cycles, C	Weight loss, L (mg)	Arithmetic mean of weight loss (mg)	Wear index, I = 1000 L/C	Arithmetic mean of wear index
S-1	CS-17	1000	1000	30.9	31.9	30.9	31.9
S-2	CS-17	1000	1000	31.5		31.5	
S-3	CS-17	1000	1000	33.4		33.4	

S-1   S-2   S-3
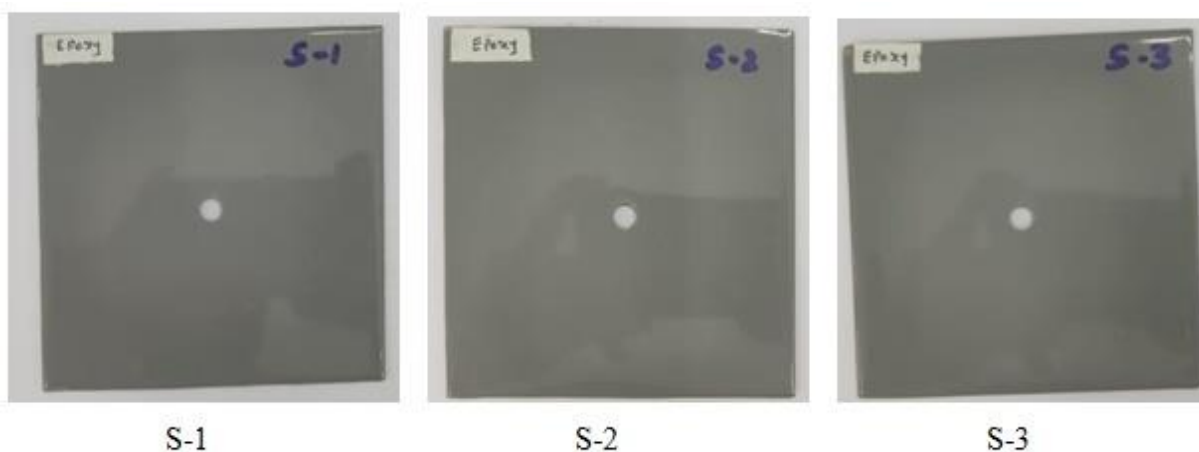
Figure 6C.1: LE Coated Samples before the Abrasion Resistance Test
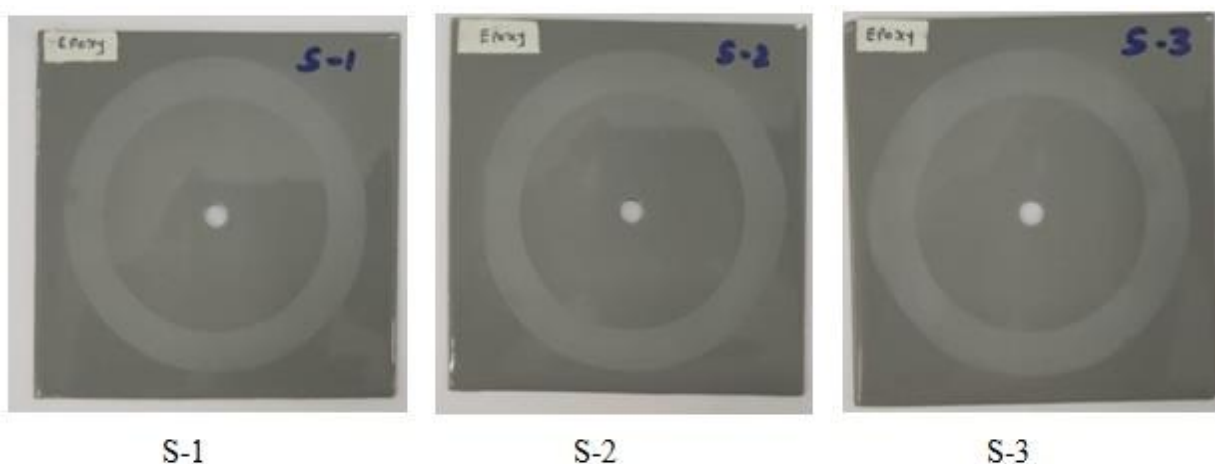
Figure 6C.2: LE Coated Samples after the Abrasion Resistance Test

6C.1.4 Discussion on the Abrasion Resistance Tests

From the results of the abrasion resistance tests, the weight loss and the wear index values of LE coating have been found to be identical for 1000 cycles of abrasion. LE coated samples have shown weight losses in the range of 30.9 - 33.4 mg [5]. An arithmetic mean of weight loss is found to be 31.9 mg. Such minimal weight loss is found to be an indication of insignificant abrasion of LE. It appears from the test results that LE is excellent resistant to abrasion and is expected to be least damaged by handling or during transportation and storage.

6C.1.5 Conclusion

LE has shown a minimal weight loss in the Taber Abrasion Resistance Test. Due to high resistance to abrasion, LE would be least affected during transportation and storage at site.

6C.2 References

[1] ASTM E-1019, "Standard Test-Methods for Determination of Carbon, Sulphur, Nitrogen, and Oxygen in Steel, Iron, Nickel, and Cobalt Alloys by Various Combustion and Inert Gas Fusion Techniques", ASTM International, 100 Barr Harbour Drive, P.O. Box C700, West Conshohocken, PA19428-2959, USA

[2] ASTM E-1086, "Standard Test-Method for Analysis of Austenitic Stainless Steel by Spark Atomic Emission Spectrometry", ASTM International, USA

[3] ASTM A-240, "Standard Specification for Chromium and Chromium-Nickel Stainless-Steel Plate, Sheet, and Strip for Pressure Vessels and for General Applications", ASTM International, USA

[4] ASTM D-4060, "Standard Test-Method for Abrasion Resistance of Organic Coatings by the Taber Abraser", ASTM International, USA.

[5] Richard E. Ricker, "Advanced Coatings R&D for Pipelines and Related Facilities" NIST Publication 1044, June 9-10, 2005, Abrasion Resistance of Coatings, Table-22, p.82

Chapter - 6D

Coating for SS316L Pipeline

in Splashed Condition

Chapter - 6D: Coating for SS316L Pipeline in Splashed Condition

6D Introduction

The pipeline sometimes traverses through the areas exposed to splashed condition. A splashed condition is defined as the state originated by dropping continuously a small amount of water in the form of droplet on the surface of the structure. To simulate and represent coatings for SS316L pipeline in splashed conditions,six coated samples extracted from the coated SS316L pipes have been subjected to the salt spray tests. Before carrying out the salt spray tests, virgin six coatings extracted from the coated SS316L samples have been subjected to FTIR (Fourier Transform Infrared Spectroscopy) analysis and Type D Shore Durometer hardness test. FTIR has been conducted by FTIR Spectrometer (Model No. ALPHA II with Opus 7.8 software, make: Bruker, USA) using ATR (Attenuated Total Reflection) technique according to the ASTM E1252. Then six coated SS316L samples have been subjected to the salt spray test in 5% NaCl solution at 35°C with salt solution pH range from 6.5 to 7.2 in accordance with ASTM B117 for a period of 3000 hours. After completion of the salt spray test, six coatings extracted from the coated SS316L samples have been subjected to FTIR analysis and Type D Shore Durometer hardness test. The FTIR spectrums and Type D Shore Durometer hardness values of virgin coatings as well as coatings exposed to the salt spray tests have been recorded.

In this chapter, the results of FTIR analysis and Type D Shore Durometer hardness tests of virgin coatings, and coatings exposed to the salt spray tests, and the subsequent discussions are presented.

6D.1 Results and Discussion

6D.1.1 Results of Coating FTIR Testings

The solid samples of virgin coatings and the coatings exposed to the salt spray tests have been analysed by FTIR-ATR technique using the Bruker FTIR Spectrometer. The coating sample has been placed on the anvil tip of the diamond crystal. The test has been performed by an infrared (IR) signal through a monochromatic controller with the specified wavelengths. Infrared has been passed through the polymeric coating to cause the functional groups to vibrate at specific frequencies. The organic compounds of the coating have absorbed at these characteristic frequencies and produced a unique FTIR spectrum. The FTIR spectrum is a plot of the frequency

(or wave number) of infrared light versus infrared light transmitted through (or absorbed by) the sample. The spectrums have been represented as infrared transmittances (Y-axis) in percentages versus wave numbers (horizontal X-axis) from 4000 to 500 cm^{-1} [1]. The FTIR spectrums of 3LPE [1], 3p/2p CAT [3], PU [5], VE [7], LE [9], and HSS [11] for virgin coatings and coatings after the salt spray tests are shown below in Figure 6D.1 a), b), Figure 6D.2 a), b), Figure 6D.3 a), b), Figure 6D.4 a), b), Figure 6D.5 a), b) and Figure 6D.6 a), b) respectively.
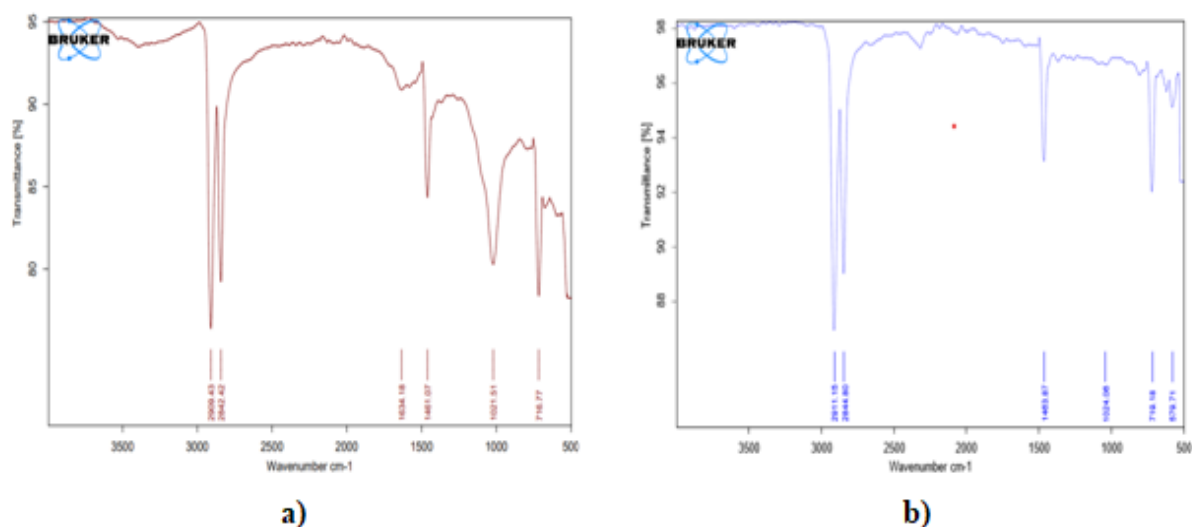
Figure 6D.1: FTIR Spectrums - a) Virgin 3LPE, b)3LPE after Salt Spray Test
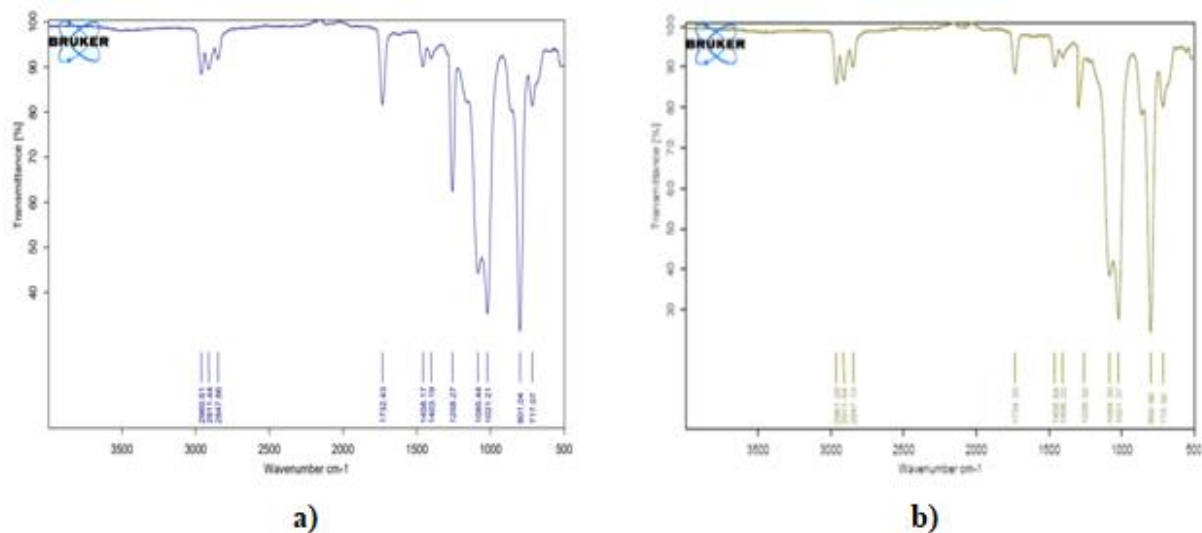
Figure 6D.2: FTIR Spectrums - a) Virgin 3p/2p CAT, b)3p/2p CAT after Salt Spray Test

Figure 6D.3: FTIR Spectrums - a) Virgin PU, b) PU after Salt Spray Test

Figure 6D.4: FTIR Spectrums - a) Virgin VE, b) VE after Salt Spray Test

Figure 6D.5: FTIR Spectrums - a) Virgin LE, b) LE after Salt Spray Test

Figure 6D.6: FTIR Spectrums - a) Virgin HSS, b) HSS after Salt Spray Test

6D.1.2 Discussion on Coatings FTIR Spectrums

The spectrums of 3LPE [2] have shown two strong intensity bands of virgin coating before salt spray at 2909 cm^{-1} due to C-H asymmetric stretching and 2842 cm^{-1} due to C-H symmetric stretching vibrations. After the salt spray test of coating, these vibrations are noticed at 2911 cm^{-1} and 2844 cm^{-1} respectively. Before salt spray, medium intensity bands observed at 1461 cm^{-1} and 716 cm^{-1} of virgin coating attribute to C-H scissoring and C-H rocking vibrations respectively. After the salt spray test of coating, C-H scissoring and C-H rocking vibrations are identified at 1463 cm^{-1}, 719 cm^{-1} respectively. Before salt spray, medium intensity band observed at 1021 cm^{-1} of virgin coating is due to C-O-C stretching vibration from the aromatic co-polymer adhesive compound. After the salt spray test of coating, very weak intensity band at 1024 cm^{-1}, C-O-C stretching vibration has been found to be almost disappearing.

The spectrums of 3p/2p CAT [4] have shown weak intensity bands of virgin coating before salt spray at 2960 cm^{-1}, and after the salt spray test of coating at 2961 cm^{-1} due to C-H asymmetric stretching vibrations. Before salt spray, weak intensity bands observed at 2911 cm^{-1}, 2847 cm^{-1} of virgin coating and after the salt spray test of coating at 2911 cm^{-1}, 2847 cm^{-1} attribute to C-H symmetric stretching vibrations. Before salt spray, medium intensity bands identified at 1732 cm^{-1} of virgin coating and after the salt spray test of coating at 1734 cm^{-1} attribute to C=O stretching vibrations. Before salt spray, weak intensity bands observed at 1458 cm^{-1}, 717 cm^{-1} of virgin coating are assigned to C-H scissoring and C-H rocking vibrations respectively. After the salt spray test of coating, C-H scissoring and C-H rocking vibrations are noticed at 1458 cm^{-1} and 715 cm^{-1} respectively. Before salt spray, very sharp and strong intensity bands at 1258 cm^{-1}, 1085 cm^{-1}, 1021 cm^{-1}, 801 cm^{-1} of virgin coating are found due to C-H bending, C-C stretching, aromatic C-H bending, C-H stretching vibrations respectively. After the salt spray test of coating, these vibrations are identified at 1258 cm^{-1}, 1084 cm^{-1}, 1021 cm^{-1}, 800 cm^{-1} respectively.

The spectrums of PU [6] have shown weak to medium intensity bands of virgin coating before salt spray at 3321 cm^{-1} due to N-H stretching, 2923 cm^{-1} due to C-H asymmetric stretching, 2856 cm^{-1} due to C-H symmetric stretching vibrations. After the salt spray test of coating, these vibrations are noticed at 3322 cm^{-1}, 2920 cm^{-1}, 2853 cm^{-1} respectively. Before salt spray, medium intensity bands identified at 1715 cm^{-1}, 1598 cm^{-1}, 1411 cm^{-1}, 1308 cm^{-1} of virgin coating attribute to C=O stretching, aromatic C-C stretching, C=C stretching, C-N stretching vibrations respectively. After the salt spray test of coating, these vibrations are observed at 1709 cm^{-1}, 1598 cm^{-1}, 1411 cm^{-1}, 1307 cm^{-1} respectively. Before salt spray, very sharp and strong intensity bands observed at 1522 cm^{-1}, 1048 cm^{-1}, 600 cm^{-1} of virgin coating are due to C-N stretching & N-H scissoring, C-O-C stretching, C-H bending vibrations of aromatic compound respectively. After the salt spray test of coating, bands at 1520 cm^{-1}, 1073 cm^{-1}, 604 cm^{-1} have shown these vibrations respectively.

The spectrums of VE [8] have shown medium intensity bands of virgin coating before salt spray at 2919 cm^{-1}, 2860 cm^{-1}, 2352 cm^{-1} due to C-H asymmetric stretching, C-H symmetric stretching vibrations, C ≡ C stretching vibration respectively. After the salt spray test of coating, these vibrations are observed at 2920 cm^{-1}, 2857 cm^{-1}, 2343 cm^{-1} respectively. Before salt spray, strong intensity bands of virgin coating are identified at 1721 cm^{-1} due to C=O stretching, 1427 cm^{-1} due to C-H bending, 1259 cm^{-1} due to C-H bending, 1069 cm^{-1} due to C-C stretching, 956 cm^{-1} due to C-H out-of-plane bending, 615 cm^{-1} due to C-H wagging vibrations. After the salt spray test of coating, these vibrations are observed at 1722 cm^{-1}, 1427 cm^{-1}, 1258 cm^{-1}, 1072 cm^{-1}, 960 cm^{-1}, 614 cm^{-1} respectively. Before salt spray, sharp intensity bands of virgin coating at 1582 cm^{-1}, 738 cm^{-1}, 690 cm^{-1} attribute to aromatic C=C stretching, C-H rocking, C-H bending respectively. After the salt spray test of coating, these vibrations are identified at 1584 cm^{-1}, 741 cm^{-1}, 687 cm^{-1} respectively. Before salt spray, sharp intensity band observed at 1119 cm^{-1} of virgin coating is due to C-H deformation in aromatic compound ring. After the salt spray test of coating, C-H deformation in aromatic compound ring has been found to be disappearing.

The spectrums of LE [10] have shown weak intensity bands of virgin coating before salt spray at 2917 cm^{-1}, and after the salt spray test of coating at 2910 cm^{-1} due to C-H asymmetric stretching vibrations. Before salt spray, weak intensity band of virgin coating at 2853 cm^{-1} attributes to C-H symmetric stretching vibration. This band after the salt spray test of coating has been found to be disappearing. Before salt spray, medium to weak intensity bands of virgin coating observed at 1598 cm^{-1}, 1171 cm^{-1}, 551 cm^{-1} are due to N-H bending, C=C stretching, C-O & C-C out-of-plane bending vibrations respectively. After the salt spray test of coating, these vibrations are noticed at 1596 cm^{-1}, 1173 cm^{-1}, 552 cm^{-1} respectively. Before salt spray, strong intensity bands of virgin coating are identified at 1418 cm^{-1} due to C-H in-plane bending, 1234 cm^{-1} due to C-O stretching, 1020 cm^{-1} due to aromatic compound C-H in-plane bending, 866 cm^{-1} & 750 cm^{-1} due to C-O-C symmetric stretching vibrations. After the salt spray test of coating, these vibrations are identified at 1425 cm^{-1}, 1234 cm^{-1}, 1022 cm^{-1}, 875 cm^{-1}, 752 cm^{-1}

respectively. Before salt spray, sharp intensity bands of virgin coating at 1499 cm^{-1}, 911 cm^{-1}, 700 cm^{-1} are found due to C-C stretching in aromatic compound ring, C-O-C asymmetric stretching in aromatic compound ring, C-C out-of-plane bending vibrations respectively. After the salt spray test of coating, C-C stretching in aromatic compound ring, C-O-C asymmetric stretching in aromatic compound ring, C-C out-of-plane bending vibrations have been found to be disappearing.

The spectrums of HSS [12] have shown two strong intensity bands of virgin coating before salt spray at 2911 cm^{-1} due to C-H asymmetric stretching, 2845 cm^{-1} due to C-H symmetric stretching vibrations. After the salt spray test of coating, these vibrations are noticed medium intensity bands at 2909 cm^{-1}, 2841 cm^{-1} respectively. Before salt spray, weak intensity bands at 1738 cm^{-1} of virgin coating and after the salt spray test of coating at 1741 cm^{-1} are due to C=O stretching vibrations. Before salt spray, the sharp intensity bands occurring at 1462 cm^{-1}, 721 cm^{-1} of virgin coating attribute to C-H scissoring and C-H rocking vibrations respectively. After the salt spray test of coating, C-H scissoring and C-H rocking vibrations are observed at 1460 cm^{-1}, 715 cm^{-1} respectively. Before salt spray, weak intensity band of virgin coating observed at 1030 cm^{-1} is due to C-O-C stretching vibration from the aromatic co-polymer adhesive compound. After the salt spray test of coating, very weak intensity band at 1028 cm^{-1}, C-O-C stretching vibration has been found to be almost disappearing.

The characteristic bands in the FTIR spectrums of the virgin coatings before salt spray and exposed coatings after salt spray are analysed qualitatively based on strong intensity band, less strong intensity band, weak intensity band, more weak intensity band, about to disappearing band and disappeared bands. In this work, transmittance (%) is taken as a comparison of characteristic bands of virgin coatings before salt spray and exposed coatings after salt spray and are indexed on a scale of 1 to 6, where 1 = strong intensity band, 2 = less strong intensity band, 3 = weak intensity band, 4 = more weak intensity band, 5 = about to disappearing band and 6 = disappeared band and ranking of coating has been made accordingly.

Based on the detailed analysis of the functional groups in the FTIR spectrums of the coatings, it has been found that all the characteristic bands of 3p/2p CAT, PU virgin coatings as well as coatings exposed to the salt spray test are distinctly visible. It can be concluded that 3p/2p CAT, PU have been remained to be unaffected by the salt spray tests. In the case of 3LPE and HSS spectrums, C-O-C stretching vibrations from the aromatic co-polymer adhesive compounds have been found to be very weak intensity bands or almost disappearing after the salt spray tests. For VE, C-H deformation in aromatic compound ring has been found to be disappearing after

the salt spray test. It can be concluded that VE is more affected by the salt spray test than 3LPE and HSS, which are less affected by the salt solutions. For LE, C-H symmetric stretching, C-C stretching in aromatic compound ring, C-O-C asymmetric stretching in aromatic compound ring, C-C out-of-plane bending vibrations have been found to be disappearing after the salt spray test. It can be concluded that LE among all the coatings is greatly affected by the salt spray test.

Therefore, the order of the coatings with respect to the analysis of the FTIR spectrums of virgin coatings and coatings after the salt spray test is found to be 3p/2p CAT/PU, 3LPE/HSS, VE, and LE.

6D.1.3 Results of Type D Shore Durometer Hardness Test

The hardness of virgin coatings and coatings after the salt spray test are shown in Figure 6D.7 a) and b) respectively. A comparison of coatings hardness values has been drawn and is shown in Table 6D.1.

a)   b)
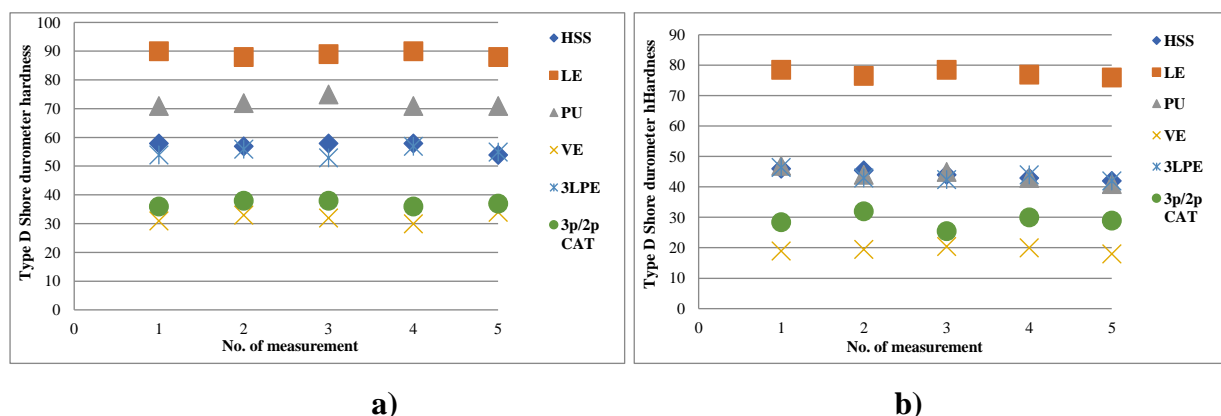
Figure 6D.7: Hardness Values - a) Virgin Coatings, b) Coatings after the Salt Spray Test
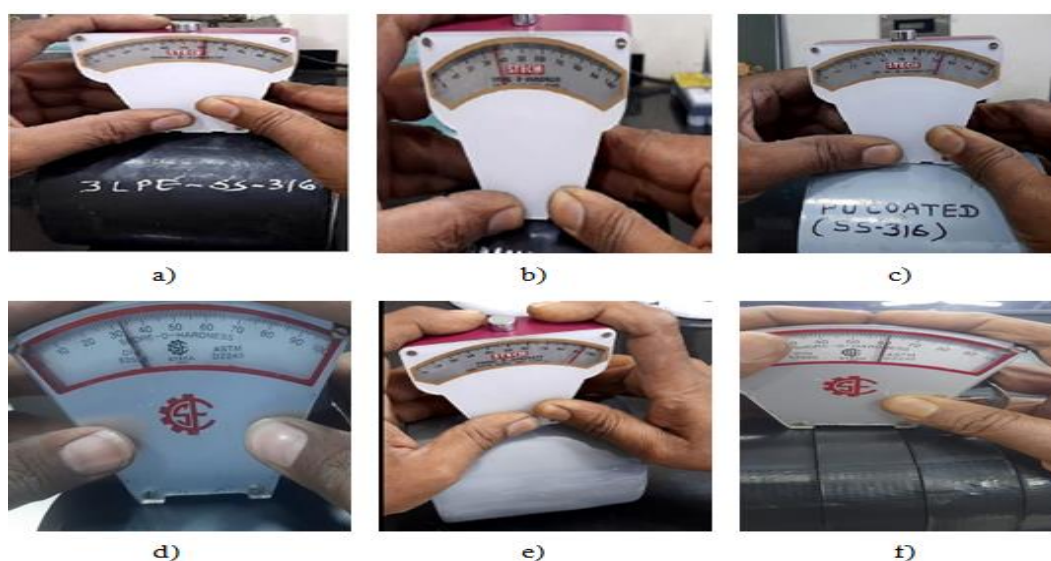
Figure 6D.8: Hardness Measurements on Samples before the Salt Spray Test - a) 3LPE, b) 3p/2p CAT, c) PU, d) VE, e) LE, f) HSS
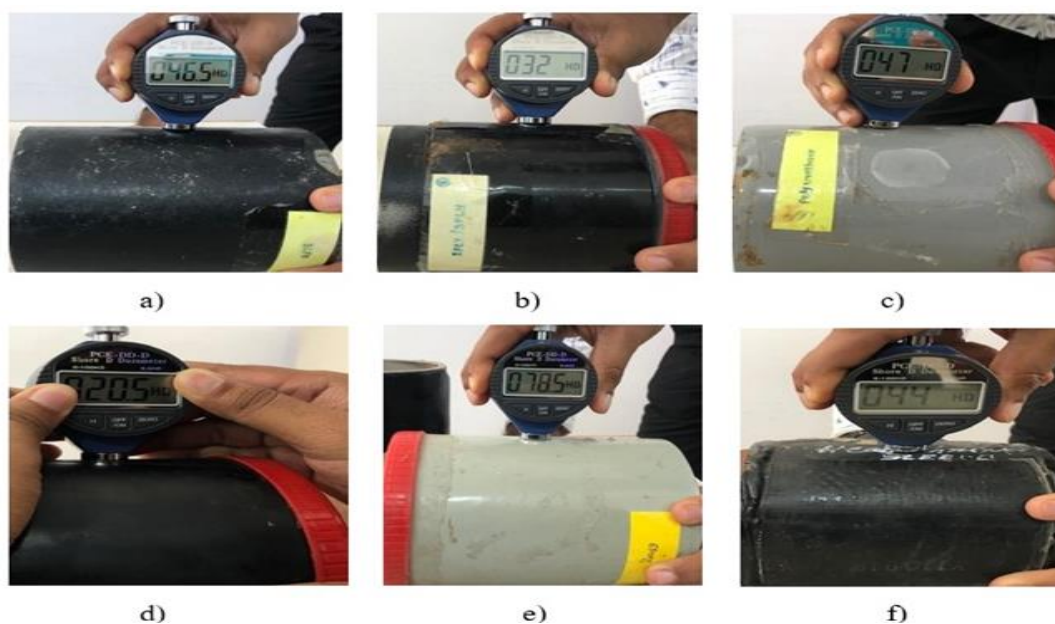
Figure 6D.9: Hardness Measurements on Samples after the Salt Spray Test - a) 3LPE, b) 3p/2p CAT, c) PU, d) VE, e) LE, f) HSS

Table 6D.1:Comparison of Coating Hardness

Type of Coating	Arithmetic Mean of Hardness (Type D Shore Durometer)		Reduction in Hardness in Percentage (%)
	Virgin Coating	Coating after the Salt Spray Test	
3LPE	55	44	20
3p/2p CAT	37	29	22
PU	72	46	36
VE	32	19	40
LE	89	77	13
HSS	57	44	23

6D.1.4 Discussion on Type D Shore Durometer Hardness Test

Virgin LE has shown the highest hardness of the order of 89 in Type D Shore Durometer hardness test. Next to LE, virgin PU has shown the higher hardness of the order of 72. The hardness values of virgin HSS and 3LPE are found to be 57 and 55 respectively. The hardness values of virgin 3p/2p CAT and VE are found to be 37 and 32 respectively. It appears from the results that virgin VE has the lowest hardness among six virgin coatings.

After the salt spray test, LE has shown highest hardness of the order of 77. The hardness values of HSS, 3LPEafter the salt spray test are found to be identical i.e., 44. The hardness of PU after the salt spray test is found to be 46. The hardness values of 3p/2p CAT and VE after the salt spray test are found to be 29 and 19 respectively.

A significant reduction in hardness of each coating has been observed after the salt spray test. A percentage reduction in hardness of each coating after the salt spray with respect to its original hardness has been computed to compare the coatings mechanical properties and is shown in Table 6D.1.

It has been found from Table 6D-1 that the least reduction to highest reduction in hardness measurements of coatings are 13%, 20%, 22%, 23%, 36% and 40% for LE, 3LPE, 3p/2p CAT, HSS, PU, and VE respectively. Therefore, the order of the coatings in respect of the highest to the lowest performances in hardness testing after the salt spray test is found to be LE, 3LPE, 3p/2p CAT, HSS, PU, and VE.

6D.1.5 Conclusion

3p/2p CAT/PU have shown best performance in FTIR analysis after salt spray test. LE has shown the best performance in hardness testing after the salt spray test.

6D.2 References

[1] J.V. Gulmine et. al, "Polyethylene characterization by FTIR", Elsevier, Polymer testing 21 (2002), p.567-563
[2] Julie Charles and G.R. Ramkumaar, "Qualitative Analysis of High Density Polyethylene Using FTIR Spectroscopy", Asian Journal of Chemistry Vol. 21, No. 6 (2009), p.4477-4484
[3] Shin-Ichiro Goto et al., "Novel Gas-Barrier Elastomer Composed of Butyl Rubber and Polyamide", Journal of Applied Polymer Science, Vol. 74, (1999), p.3548–3552
[4] Julie Charles, "Comparative Study of Butyl Rubber (IIR) and Bromobutyl Rubber (BIIR) based on FTIR, Dielectric and Thermal Studies", Journal of Applied Science and Engineering Methodologies, Vol.2 (2016), No.1, p.206-211
[5] Brian C. Smith, "Infrared Spectroscopy of Polymer XIII: Polyurethanes", Spectroscopy July 2023, Volume 38, Issue 7, p.14-16
[6] Dr. J.TennisAnthuvan, "Applications of IR Spectroscopy for Two Component Polyurethane Coatings", IJSR,Vol.2, Issue 9, September (2013), p.405-406
[7] Anatoly Lisovskii et al., "Polymerization of isobutylene and copolymerization of isobutylene with isoprene promoted by methylalumoxane", Inorganica Chimica Acta, 334 (2002), p.243-252
[8] Kees C. J. Camphuysen et al., "Seabirds in the North Sea Demobilized and Killed by Polyisobutylene (C4H8)n (PIB), Marine Pollution Bulletin", Science Ltd., Vol. 38 (1999), No. 12, p. 1171-1176
[9] Hemant Kumar et al., Synthesis, "Characterization & Application of Coatings based on Epoxy, Epoxy novolac and Liquid Rubber Blend", Chemistry (2009), 6(4), p.1253-1259
[10] Guoyuan PAN, "Effect of Structure of Bridging Group on Curing and Properties of Bisphenol-A Based Novolac Epoxy Resins", Polymer Journal (2007), The Society of Polymer Science, Japan, Vol. 39, No. 5, p. 478–487
[11] Marisa Cristina Guimarães Rochaa et al., "Thermal and Mechanical Properties of Vinyltrimethoxysilane (VTMOS) Crosslinked High Molecular Weight Polyethylene (HMWPE)", Materials Research (2017), p.1-8
[12] H. G. Harish Kumar, "Electron-Beam-Induced Modifications in High-Density Polyethylene", Braz J Phys (2011), Springer, Vol. 41, p.7-14.

Chapter - 6E

Comparison between Test Results of Coatings for SS316L Pipeline in Buried, Above-ground and Splashed Condition

Chapter - 6E: Comparison between Test Results of Coatings for SS316L Pipeline in Buried, Above-ground and Splashed Condition

6E Introduction

A comparison of coatings performances has been carried out based on the analysis of data obtained from the relevant tests in buried and splashed conditions. The relevant tests of the coatings in buried conditions are the indentation resistance, the water absorption, the cathodic disbondment, the hot water immersion, the specific electrical insulation resistance, the electrochemical impedance. The relevant tests of the coatings in splashed conditions are FTIR and the Type D Shore Durometer hardness of the virgin coatings as well as the coatings exposed to the salt spray test for a specific duration.

No coating is generally applied on external surface of SS316L pipeline in above-ground condition because SS316L is a corrosion resistant material in atmospheric exposure. Still, only one coating from solvent-free liquid-applied coatings has been selected and subjected to a mechanical test (i.e. the Taber Abrasion Resistance test) to verify the resistance to damage that may cause practically during transportation and storage. Therefore, the performance of one coating from one test for pipeline in above-ground condition is not considered for comparison with the performances of all coatings for pipeline in buried and splashed conditions.

A ranking system has been followed for coatings for pipeline in buried and splashed conditions separately based on their performances or corrosion resistance properties in the relevant tests mentioned above. For the purpose of ranking, the coatings has been rated on a scale of 1 to 6 in each test, where "1" is the highest performance or highest corrosion resistance property of the coating. Other coatings have followed according to their performances or corrosion resistance properties. The arithmetic mean of all the ratings obtained by the above mentioned tests has been written from lowest to highest order. The lowest order is the coating highest performance or highest corrosion resistance property and is identified as overall rank "1". Thus, the coatings have been found out from the technological viewpoint for optimization of coatings for austenitic stainless steel pipeline in buried and splashed conditions.

In this chapter, the ranking of each coating in each test and the overall rankings of the coatings for austenitic stainless steel pipeline in buried and splashed conditions are presented.

6E.1 Coating for SS316L Pipeline in Buried Condition

6E.1.1 Indentation Resistance Test

The rankings of the coatings with respect to the highest to the lowest indentation resistance are shown in Table 6E.1. The absolute data are given in Chapter-6B under Clause No. 6B.4.5.1.

Table 6E.1: Rankings of Coatings in Indentation Resistance Test

Type of Coating	Ranking
3LPE	Highest
PU	Higher
HSS	High
LE	Low
VE	Lower
3p/2p CAT	Lowest

6E.1.2 Water Absorption Test

The rankings of the coatings in respect of the highest to the lowest performances are shown in Table 6E.2.The absolute data are given in Chapter-6B under Clause No. 6B.4.6.1.

Table 6E.2: Rankings of Coatings in Water Absorption Test

Type of Coating	Ranking
VE	Highest
HSS	Higher
3LPE	High
PU	Low
3p/2p CAT	Lower
LE	Lowest

6E.1.3 Cathodic Disbondment (CD) Test

The ranking of the coatings in respect of the highest to the lowest resistances to disbondment of damages are shown in Table 6E.3.The absolute data are given in Chapter-6B under Clause No. 6B.4.7.1.

Table 6E.3: Rankings of Coatings Cathodic Disbondment (CD) Test

Type of Coating	Ranking
3LPE	Highest
HSS	Higher
PU	High
VE	Low
3p/2p CAT	Lower
LE	Lowest

6E.1.4 Hot Water Immersion (HWI) Test

The rankings of the coatings in respect of the highest to the lowest adhesion performances are shown in Table 6E.4. The absolute data are given in Chapter-6B under Clause No. 6B.4.10.1.

Table 6E.4: Rankings of Coatings in Hot Water Immersion (HWI) Test

Type of Coating	Ranking
HSS	Highest
VE	Higher
LE	High
3LPE	Low
3p/2p CAT	Lower
PU	Lowest

6E.1.5 Specific Electrical Insulation Resistance (SEIR) Test

The ranking of the coatings in respect of the highest to the lowest specific electrical insulation resistances are shown in Table 6E.5.The absolute data are given in Chapter-6B under Clause No. 6B.4.11.1.

Table 6E.5: Rankings of Coatings in SEIR Test

Type of Coating	Ranking
PU	Highest
3LPE	Higher
LE	High
VE	Low
3p/2p CAT	Lower
HSS	Lowest

6E.1.6 Electrochemical Impedance Spectroscopy (EIS) Test

The rankings of the coatings in respect of the highest to the lowest impedances are shown in Table 6E.6. The absolute data are given in Chapter-6B under Clause No. 6B.4.12.1.

Table 6E.6: Rankings of Coatings in EIS Test

Type of Coating	Ranking
3LPE	Highest
3p/2p CAT	Higher
HSS	High
VE	Low
LE	Lower
PU	Lowest

6E.1.7 Summary of Rankings of Coatings for SS316L Pipeline in Buried Condition

The rankings of the coatings for SS316L pipeline in buried condition are summarised and are shown in Table 6E.7.

Table 6E.7: Summary of Rankings of Coatings for Pipeline in Buried Condition

Type of Coating	Ranking based on rating						Arithmetic Mean	Total Rank
	IND. RES.	WA	CD	HWI	SEIR	EIS		
3LPE	1	3	1	4	2	1	2.0	1
3p/2p CAT	6	5	5	5	5	2	4.7	6
PU	2	4	3	6	1	6	3.7	4
VE	5	1	4	2	4	4	3.3	3
LE	4	6	6	3	3	5	4.5	5
HSS	3	2	2	1	6	3	2.8	2

Overall Ranking: 1 to 6 (1 being the highest performance or highest corrosion resistance property)

It appears from the rankings of the coatings that 3LPE is the best coating among six coatings. Next to 3LPE, HSS is the best coating. After 3LPE and HSS, VE is the better coating. The order of coatings with respect to their performances in buried condition is found to be 3LPE, HSS, VE, PU, LE, 3p/2p CAT.

6E.2 Coating for SS316L Pipeline in Above-ground Condition

Generally, no coating is applied on external surface of SS316L pipeline in above-ground condition as S316L is corrosion-resistant material in atmospheric environment. Still, one coating i.e., solvent-free liquid-applied epoxy (LE) has been selected and one mechanical test (the Taber Abrasion Resistance) has been conducted to evaluate coating for SS316L pipeline in above-ground condition.

From the test results of the Taber Abrasion Resistance as per Chapter - 6C Table 6C.2, LE coated samples have shown weight losses in the range of 30.9-33.4 mg. An arithmetic mean of weight loss is found to be 31.9 mg. Such minimal weight loss is found to be an indication of insignificant abrasion of LE. It appears from the test results that LE is excellent resistant to abrasion and is expected to be least damaged by handling or during transportation and storage.

6E.3 Coating for SS316L Pipeline in Splashed Condition

6E.3.1 FTIR Test

The rankings of the coatings in respect of the highest to the lowest performances are shown in Table 6E.8. The analysis of the FTIR spectrums of the is given in Chapter-6D under Clause No. 6D.1.2.

Table 6E.8: Rankings of Coatings in FTIR Test

Type of Coating	Ranking
3p/2p CAT	Highest
PU	
3LPE	High
HSS	
VE	Lower
LE	Lowest

6E.3.2 Type D Shore Durometer Hardness Test

The rankings of the coatings in respect of the highest to the lowest performances are shown in Table 6E.9. The absolute data are given in Chapter-6D under Clause No. 6D.1.4.

Table 6E.9: Rankings of Coatings in Type D Shore Hardness Test

Type of Coating	Ranking
LE	Highest
3LPE	Higher
3p/2p CAT	High
HSS	Low
PU	Lower
VE	Lowest

6E.3.3 Summary of Rankings of Coatings for SS316L Pipeline in Splashed Condition

The rankings for the coatings for SS316L pipeline in splashed condition are summarised and are shown in Table 6E.10.

Table 6E.10: Summary of Rankings of Coatings for Pipeline in Splashed Condition

Type of Coating	Ranking		Arithmetic Mean	Total Rank
	FTIR	RED. HRD.		
3LPE	3	2	2.5	2
3p/2p CAT	1	3	2.0	1
PU	1	5	3.0	3
VE	5	6	5.5	6
LE	6	1	3.5	4
HSS	3	4	3.5	4

Overall Ranking: 1 to 6 (1 being the highest performance or highest corrosion resistance property)

It appears from the rankings for the coatings that 3p/2p CAT is the best coating among six coatings and 3LPE, PU are better coatings than others in splashed condition. The order of coatings with respect to their performances in splashed condition is 3p/2p CAT, 3LPE, PU, LE/HSS, and VE.

6E.4 Summary of Rankings of Coatings for SS316L Pipeline in all Conditions

The rankings of the coatings for SS316L pipeline in all conditions are summarised and are shown in Table 6E.11.

Table 6E.11: Summary of Rankings of Coatings for Pipeline in all Conditions

Type of Coating	Ranking		Arithmetic Mean	Overall Rank
	Buried	Splashed		
3LPE	1	2	1.5	1
3p/2p CAT	6	1	3.5	3
PU	4	3	3.5	3
VE	3	6	4.5	5
LE	5	4	4.5	5
HSS	2	4	3.0	2

Ranking Scale: 1 to 6 (1 being the highest performance or highest corrosion resistance property)

From the results obtained by a simplified arithmetic mean system, it has been found in this study that 3LPE is the best coating for SS316L pipeline in all conditions .After 3LPE, HSS and 3p/2p CAT/PU are found to be the better coatings than others. The rankings of the coatings are shown in Table 6E.12.

Table 6E.12: Rankings of Coatings for Pipeline in all Conditions

Type of Coating	Ranking
3LPE	1
HSS	2
3p/2p CAT/ PU	3
VE/LE	5

Chapter - 6F

Validation of the Rankings of the Coatings Using Mathematical Modeling

Chapter - 6F: Validation of the Rankings of the Coatings using Mathematical Modeling

6F Introduction

It is necessary to build a decision making system through a model from the statistical analysis so that the model can address the objective and effectiveness of the study. This model can also help in determining the best coating for SS316L pipeline taking into consideration both buried and splashed conditions. In this research, a scientific numerical method namely 'TOPSIS' has been used. 'TOPSIS' is the abbreviation for 'Technique for Order of Preference by Similarity to Ideal Solution' [1-6]. This method has been applied to solve Multi-Criteria Decision Making (MCDM) problems. MCDM supports decision makers to make an optimal decision among numerous and conflicting alternatives [7,8].

TOPSIS is very suitable for practical application and is applied with a mathematical model in the last four decades [9,10]. The best alternative (i.e. the best coating among six coatings) is determined using mathematical formulas in a series of 9 steps. The advantage of this method is the ability to identify the best alternative from multiple alternatives with multiple criteria.

In this chapter, the methodology along with the computation for the selection of the best coating among six types of coatings are presented.

6F.1 Methodology

This method evaluates the alternative by considering the positive and the negative ideal solutions. The basic of the method is to determine best alternative, which will be nearest to ideal solution positive (+) and furthest from ideal solution negative (-). Computation is expressed in a series of steps. The steps are mentioned below:

Step 1:

If there are 'm' alternatives and each alternative has 'n' criteria, they can be expressed as A_1.......... A_m, and X_1.............X_n, respectively. Positive numbers are allotted for criteria. Among these criteria, X_1........X_k are considered with a monotonous increase (i.e. benefit criteria), and X_{k+1}...........X_n are considered with a monotonous decrease (i.e. non-benefit criteria). Each criterion has weight, which may be considered equal or in proportion so that weights 'w_j' of the criteria X_j comply the following Equation (6F-1):

$$\sum_{j=1}^{n} (w_j) = 1 \quad \ldots\ldots\ldots\ldots\ldots \text{ (6F-1)}$$

The alternatives, criteria and weights can be arranged (i.e. pay-off matrix) in a table as shown in the following Table 6F.1:

Table 6F.1: Pay-off Matrix

Criteria		X_1	X_2	...	X_n
Weights		w_1	w_2	...	w_n
Alternatives	A_1	X_{11}	X_{12}	...	X_{1n}
	A_2	X_{21}	X_{22}	...	X_{2n}
	:	:	:	:	:
	:	:	:	:	:
	A_m	X_{m1}	X_{m2}	...	X_{mn}

Step 2:

The numbers 'X_{ij}' present values of different criteria (X_j) with different measuring units and so the pay-off matrix is needed to be balanced and normalized. In place of 'X_{ij}', 'R_{ij}' will be taken to determine normalized pay-off matrix using the following Equation (6F-2) and are shown in Table 6F.2:

$$R_{ij} = \frac{X_{ij}}{\sqrt{\sum_{i=1}^{m} X_{ij}^{2}}} \quad \ldots\ldots\ldots\ldots \text{ (6F-2)}$$

Table 6F.2: Normalized Pay-off Matrix

Criteria		X_1	X_2	...	X_n
Weights		w_1	w_2	...	w_n
Alternatives	A_1	R_{11}	R_{12}	...	R_{1n}
	A_2	R_{21}	R_{22}	...	R_{2n}
	:	:	:	:	:
	:	:	:	:	:
	A_m	R_{m1}	R_{m2}	...	R_{mn}

Step 3:

The weighted normalized pay-off matrix for numbers (a_{ij}) will be obtained multiplying weights 'w_j' of the criteria X_j by 'R_{ij}' using the following Equation (6F-3) and are shown in Table 6F.3:

$$a_{ij} = w_j \frac{X_{ij}}{\sqrt{\sum_{i=1}^{m} X_{ij}^2}} \quad \dots\dots\dots\dots (6F\text{-}3)$$

Table 6F.3: Weighted Normalized Pay-off Matrix

Criteria	X_1	X_2	......	......	X_n
A_1	a_{11}	a_{12}	......	......	a_{1n}
:	:	:	:	:	:
A_m	a_{m1}	a_{m2}	......	......	a_{mn}

Step 4:

The coordinates $a_j *$ of the positive ideal solution(A*) are chosen using the following Equation (6F-4)

$$a_j * = \text{Maximum } a_{ij} \text{ for } j = 1\dots\dots k \text{ and Minimum } a_{ij} \text{ for } j = k+1\dots\dots n \quad \dots\dots\dots (6F\text{-}4)$$

Step 5:

The coordinates $a_j **$ of the negative ideal solution (A**) are chosen using the following Equation (6F-5)

$$a_j ** = \text{Minimum } a_{ij} \text{ for } j = 1\dots\dots k \text{ and Maximum } a_{ij} \text{ for } j = k+1\dots\dots n \quad \dots\dots\dots (6F\text{-}5)$$

Step 6:

The distances, from the alternatives to the positive ideal solution (A*), are calculated using the following Equation (6F-6)

$$d_i^* = \sqrt{\sum_{j=1}^{n} (a_{ij} - a_j^*)^2} \dots\dots\dots\dots (6F\text{-}6)$$

Step 7:

The distances, from the alternatives to the negative ideal solution (A**) are calculated using the following Equation (6F-7)

$$d_i^{**} = \sqrt{\sum_{j=1}^{n}(a_{ij} - a_j^{**})^2} \ldots\ldots\ldots\ldots \text{ (6F- 7)}$$

Step 8:

The positive ideal solutions C_i^+ are calculated using the following Equation (6F-8)

$$C_i^+ = \frac{d_i^{**}}{d_i^* + d_i^{**}} \ldots\ldots\ldots\ldots \text{ (6F-8)}$$

Step 9:

The ranking of the alternative C_i^+ sorted from largest value to the smallest valueis evaluated. Alternative with largest value of C_i^+ is acceptable as the best solution and is ranked first i.e., rank =1.Other alternatives follow the ranking according to their C_i^+ values.

6F.2 Selection of the Best Coating using the above Method

In the present study, the best coating is selected based on the computation results obtained by using the above method.

The alternatives are six types of coatings, and they are as follows:
1) **3-LPE,** 2) **3-p/2-p CAT,** 3) **PU,** 4) **VE,** 5) **LE,** 6) **HSS.**

The criteria are seven types of tests, and they are as follows:
1) Indentation Resistance (**IND. RES.**), 2) Water Absorption (**WA**), 3) Cathodic Disbondment (**CD**), 4) Hot Water Immersion (**HWI**), 5) Specific Electrical Insulation Resistance (**SEIR**), 6) Electrochemical Impedance (**EIS**), 7) Reduction in Hardness (**RED. HRD.**) after the Salt Spray test.

Six alternatives with seven criteria are shown as 'Pay-off Matrix 'in Table 6F.4. The weights of the criteria are considered equal i.e. 0.143.

Table 6F.4:Pay-off Matrix of Six Alternatives with Seven Criteria

Type of Coating	IND. RES.	WA	CD	HWI	SEIR	EIS	RED. HRD.
Weight	0.143	0.143	0.143	0.143	0.143	0.143	0.143
3LPE	0.09	0.076	6.76	0.55	8.86E+8	7.87E+11	20
3p/2p CAT	1.11	0.58	17.52	0.53	2.34E+7	5.41E+11	22
PU	0.20	0.50	16.64	0.52	2.45E+9	9.30E+10	36
VE	0.80	0.063	17.49	0.88	4.63E+7	3.04E+11	40
LE	0.23	0.72	23.77	0.78	3.86E+8	1.01E+11	13
HSS	0.21	0.071	10.07	0.93	2.15E+7	4.44E+11	23

Using the equations (2) to (8), the values of C_i^+ for the six coatings are found out and the best coating is selected. C_i^+ values are shown in Figure 6F.1.
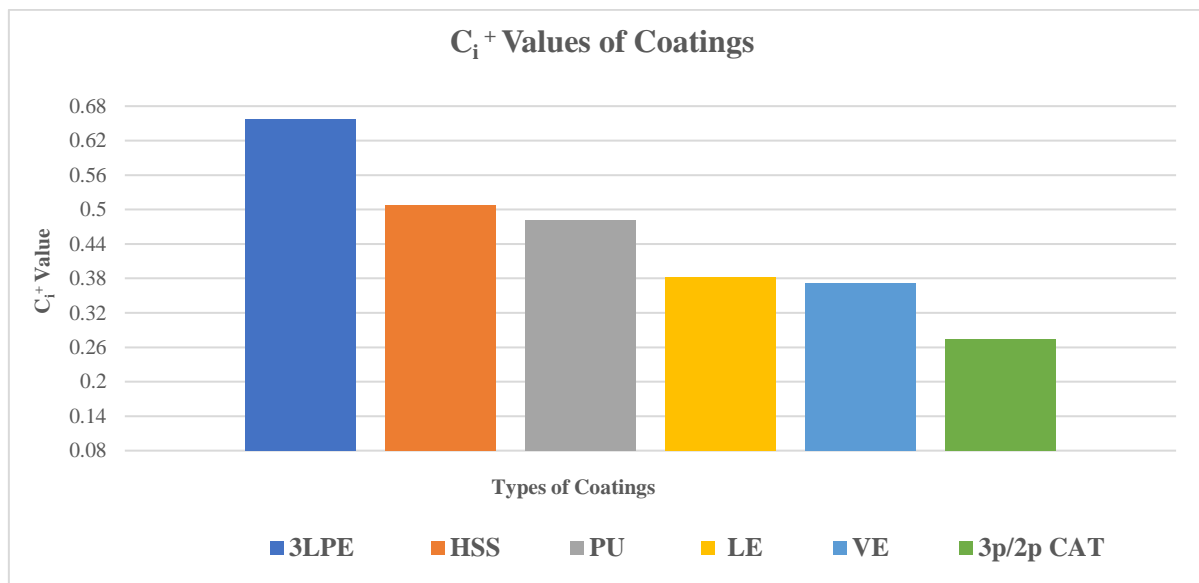
Figure 6F.1: Selection Process of the Best Coating

The detailed computations are presented in Appendix-I. The results support the validity of the approach adopted in this study. Based on the C_i^+ values obtained by the above method, the rankings of the coatings are evaluated in the present study. The highest C_i^+ value gives the highest performance of the coating and is represented by rank =1. The rankings of the coatings are shown in Table 6F.5.

Table 6F.5: Ranking of Six Coatings

Type of coating	Rank
3LPE	1
HSS	2
PU	3
LE	4
VE	5
3p/2p CAT	6

Based on the above results, 3LPE is found to be the best coating among six coatings for all conditions. HSS is the better coating after 3LPE. Next to 3LPE and HSS, PU is the better coating. The order of coatings with respect to the highest performance to the lowest is found to be 3LPE, HSS, PU, LE, VE, 3p/2p CAT.

It has been found out from the present study that the rankings of 3LPE, HSS and PU evaluated by a simplified arithmetic mean system have been adequately validated by this mathematical modeling. Therefore, 3LPE, HSS and PU is found to be suitable for SS316L pipeline in all conditions.

6F.3 References

[1] Robbi-Rahim, S Supiyandi, A P U Siahaan et al., "TOPSIS-Method Application for Decision Support System in Internal Control for Selecting Best Employees", 2nd International Conference on Statistics, Journal of Physics, 1028 (2018) 012052

[2] David-L-Olson, "Comparison of Weights in TOPSIS-Models", Mathematical and Computer Modelling, Elsevier, 40 (2004), p.721-727

[3] Hepu-Deng, Chung-Hsing Yeh, Robert J. Willis, "Inter-Company Comparison using Modified-TOPSIS with Objective Weights", Computers & Operations Research, PERGAMON, Elsevier, 27 (2000), p.963-973

[4] Hsu-Shih-Shiha, Huan-Jyh Shyurb, E. Stanley Leec, "An Extension-of-TOPSIS for Group Decision-Making", Mathematical and Computer Modelling, Elsevier, 45 (2007), p.801-813

[5] Zlatko-Pavić1, Vedran-Novoselac, "Notes-on TOPSIS-Method", International Journal of Research in Engineering and Science (IJRES), Vol.1, Issue 2, June (2013), p.05-12

[6] Vasiliki-Balioti, Christos Tzimopoulos, Christos Evangelides, "Multi-Criteria-Decision-Making Using TOPSIS-Method Under Fuzzy Environment. Application in Spillway Selection", MDPI Proceedings, (2018), 2(11), p.637

[7] David-L-Olsen, "Comparison of Three-Multicriteria- Methods to Predict Known Outcomes", European Journal of Operational research, Elsevier, 130 (2001), p.576-587

[8] Gwo-Hshiung Tzeng, Jih-Jeng Huang, "Multiple-Attribute-Decision-Making Methods and Application, (2011) Chapter 5, p.69-76, CRC Press, Taylor & Francis Group, 6000 Broken Sound Parkway NW, Suite 300 Boca Raton, FL

[9] C-L-Hwang, Y. J. Lai, and T. Y. Liu, "A New Approach for Multiple-Objective-Decision-Making", Computers and Operational Research 20 (1983), p.889-899

[10] C-L-Hwang, and K. Yoon, "Multiple-Attribute-Decision-Making: Methods and Applications", (1981), Springer-Verlag, Berlin Heidelberg.

Chapter - 7

Conclusions and Future Scope-of-Work

Chapter - 7: Conclusions and Future Scope-of-Work

7. Conclusions

Through both experimental procedures and mathematical modeling, the performances of the coatings for SS316L pipeline in buried, above-ground and splashed conditions have been investigated. The results obtained by the experiments have successfully fulfilled the objectives of the study. Based on the research outcomes in this study, the primary conclusions are drawn and listed as below:

- It is concluded from the repeatability of the results that the SS316L samples are virtually identical, represent basically the only one sample for the entire lot of SS316L pipes and three different data from different testing procedures are highly reproducible.

- The critical pitting potentials (E_{pit}) of SS316L samples are found to be 361-380 mV versus SCE. The corrosion potential (E_{corr}) and corrosion current density (i_{corr}) are found to be 195-205 mV versus SCE and 0.05-0.07 µA/cm^2 respectively.

- Significant pitting corrosion along with mass loss of 0.015-0.026 g/cm^2 for SS316L samples are found in chloride-bearing environments. The critical pitting temperatures of SS316L samples have been found to be in the range of 15-16ºC. It is reasonably concluded that SS316L is vulnerable to attack by aggressive halides like chlorides at lower temperature (15-16ºC) than usual ambient temperature.

- The thicknesses of 3LPE, 3p/2p CAT, PU, VE, LE and HSS are found to be 2.9 mm, 2.5 mm, 1.55 mm, 3.0 mm, 0.95 mm, and 2.3 mm respectively. The entire surface of each coating is found to be free from pinholes or porosities in the Holiday Detection Tests.

- The order of the coatings in respect of the highest hardness value to the lowest is found to be LE, PU, HSS, 3LPE, 3p/2p CAT and VE. It is concluded that LE can offer the highest resistance to penetration when it is encountered by sharp particles during backfilling the trench.

- From the results of the Impact Resistance Tests, it is concluded that 3LPE, 3p/2p CAT, VE, HSS possess high impact resistances and can resist physical or mechanical damage during shipping, installation,

- The order of the coatings in respect of the least indentation depth to the highest indentation depth in the Indentation Resistance Tests is found to be 3LPE, PU, HSS, LE, VE, 3p/2p CAT. It is concluded that 3LPE, PU, HSS can withstand the deformation force when it is subjected to concentrated pressure exerted by the weight of the pipe or the backfill during installation.

- The order of the coatings with respect to the least percentage of water absorbed by the coatings to the highest percentage of water absorbed in the Water Absorption Tests is found to be VE, HSS, 3LPE, PU,3p/2p CAT,LE.

- The order of the coatings in respect of the highest resistances to cathodic disbondments to the lowest in the Cathodic Disbondment Tests is found to be 3LPE, HSS, PU, VE, 3p/2p CAT, and LE. It is inferred that 3LPE has the highest and LE has the least resistance to disbondment of damage when exposed to cathodic polarization.

- The order of the coatings in respect of the peel strength at $55\pm5^{\circ}C$ in comparison with the peel strength at room temperature ($23^{\circ}C$) in the Peel Strength Tests is found to be HSS, VE, 3LPE, 3p/2p CAT.

- The order of the coatings in respect of the pull-off adhesion strength at $55\pm5^{\circ}C$ in comparison with the pull-off adhesion at room temperature ($23^{\circ}C$) in the Pull-off Adhesion Strength Tests is found to be PU, LE.

- The order of the coatings with respect to the best adhesion performances in the Hot Water Immersion Tests is found to be HSS, VE, LE, 3LPE, 3p/2p CAT, PU.

- The order of the coatings with respect to the highest electrical resistances to the lowest in the Specific Electrical Insulation Resistance Tests is found to be PU, 3LPE, LE, VE, 3p/2p CAT, and HSS.

- The order of the coatings with respect to their highest impedances to the lowest in the Electrochemical Impedance Spectroscopy Tests is found to be 3LPE, 3p/2p CAT, HSS, VE, LE, and PU.

- For SS 316L pipeline in above-ground condition, no coating is usually applied on the external surface of SS316L pipeline due to its corrosion resistance in atmospheric exposure. Still, one coating i.e., solvent-free liquid-applied epoxy (LE) has been selected because it possesses high hardness, and this coating can be applied at ease in the field. One mechanical test (the Taber Abrasion Resistance) has been conducted to evaluate coating for SS316L pipeline in above-ground condition. LE is found to be excellent resistant to abrasion and is expected to be least damaged by handling or during transportation and storage.

- For SS 316L pipeline in splashed condition, from the detailed analysis of the functional groups in the FTIR spectrums of the coatings, it is concluded that 3p/2p CAT, PU have been remained to be unaffected by the salt spray tests. In the case of 3LPE and HSS spectrums, C-O-C stretching vibrations from the aromatic co-polymer adhesive compounds have been found to be very weak intensity bands or almost disappearing after the salt spray tests. For VE, C-H deformation in aromatic compound ring has been found to be disappearing after the salt spray test. It is concluded that VE is more affected by the salt spray test than 3LPE and HSS. For LE, C-H symmetric stretching, C-C stretching in aromatic compound ring, C-O-C asymmetric stretching in aromatic compound ring, C-C out-of-plane bending vibrations have been found to be disappearing after the salt spray test. It is concluded that LE among all the coatings is greatly affected by the salt spray test. Therefore, the order of the coatings with respect to the analysis of the FTIR spectrums of virgin coatings and coatings after the salt spray test is found to be 3p/2p CAT/PU, 3LPE/HSS, VE, and LE.

A significant reduction in hardness properties of the coatings has been observed after the Salt Spray Tests. The order of the coatings with respect to the least reduction in hardness to the highest after the salt spray tests is found to be LE, 3LPE, 3p/2p CAT, HSS, PU, and VE.

- Taking into consideration SS 316L pipeline in all conditions and from the analysis of the results obtained by a simplified arithmetic mean system in determining the overall performances of all the coatings, 3LPE is found to be the best coating among all coatings in the present study. After 3LPE, HSS and PU are found to be the better coatings than others. The rankings of the coatings are found to be 3LPE, HSS, PU/3p/2p CAT, VE/LE.

- For the selection of the best coating for SS 316L pipeline in all conditions, C_i^+ value of each coating has been evaluated using the established mathematical modeling. The highest C_i^+ value gives the highest performance of the coating and is represented by rank = 1. Accordingly, based on the values of C_i^+, the rankings of the coatings are found to be 3LPE, HSS, PU, LE, VE, 3p/2p CAT.

Taking into consideration the objective of this research, which is evaluation of six coatings on stainless steel pipes in various conditions representing buried and splashed conditions, and corrosion prevention being crucial in marine environments and under thermal insulation for above-ground conditions, it is deduced after analysing the experimental results and findings that 3LPE is the best coating among six coatings in all conditions. Next to 3LPE, HSS and PU are found to be better coatings. The rankings of 3LPE, HSS and PU evaluated by a simplified arithmetic mean system have also been validated by a mathematical modeling. For SS316L pipeline in above-ground condition, bare or uncoated SS316L is normally used. But the pipeline short section, which is in transition from buried to above-ground, LE is found to be appropriate as it is compatible with best coating (3LPE) and it can be applied at ease in the field. For above-ground condition, LE coating is also suitable for marine atmosphere or corrosion under thermal insulation on austenitic stainless steel pipeline. Therefore, it is concluded from the present study that 3LPE, HSS and PU are found to be suitable coatings for SS316L pipeline in all conditions.

7.1 Future Scope-of-Work

The present research evaluates the performances of six polymeric coatings and their optimization for SS316L pipeline in buried, above-ground and splashed condition in the petroleum, petrochemical and natural gas industries. The following fundamental aspects could be selected as future scope-of-work for the pursuit of certain important phases in this study in order to improve the applicability of the research findings in practice:

- Capacitance measurements of coatings applied on SS316L pipes
- Evaluation of water absorbed by the coatings from the capacitance values
- Make a comparison of water absorbed by the coatings by the gravimetric method and water absorbed by the coatings evaluated by the capacitance measurements, and their significance to corrosion protection for buried SS316L pipelines
- Cathodic Disbondment (CD) tests of the coatings at 23°C and 60°C
- Make a comparison of CD values of the coatings obtained at 23°C and 60°C, and their significance to corrosion protection for buried SS316L pipelines.

Appendix

Appendix - I

Mathematical Computation to validate the Rankings of the Coatings

Appendix - I

Mathematical Computation to validate the Rankings of the Coatings

A-I.1 Objective

The objective of the model is to select the best coating by the computational method of a MCDM technique - TOPSIS to validate rankings of coatings evaluated by simplified arithmetic mean. The computational analysis has been made following the procedure of the above method and is given below in this Appendix.

A-I.2 Alternatives

The types of the coatings are the alternatives of this model:

- 3-Layer Poly-Ethylene (**3LPE**)
- 3-ply/2-ply Cold-Applied Tape (**3p/2p CAT**)
- Polyurethane (**PU**)
- Visco-Elastic (**VE**)
- Liquid Epoxy (**LE**)
- Heat-Shrink Sleeve (**HSS**).

A-I.3 Criteria

The electro-chemical, corrosion and physical tests of the coatings represent the criteria of this model and are as follows:

- Indentation Resistance (**IND. RES.**)
- Water Absorption (**WA**)
- Cathodic Disbondment (**CD**)
- Hot Water Immersion (**HWI**)
- Specific Electrical Insulation Resistance (**SEIR**)
- Electrochemical Impedance (**EIS**)
- Reduction in Hardness (**RED. HRD.**) after the salt spray test.

A-I.4 Benefit and Non-Benefit Criteria

The **HWI, SEIR, EIS** are the benefit criteria. The maximum (highest) values of these test results demonstrate the best performances of the coatings. The **IND.RES, WA, CD, RED. HRD** are non-benefit criteria. The minimum (lowest) values of these test results show the best performances of the coatings. The coordinates of the positive and negative ideal solutions have been decided accordingly from the test results.

A-I.5 Weights of the Criteria

The weights of the criteria are considered equal (i.e. 0.143). Therefore, all the above criteria are at least of equal importance in determining the best coating among six coatings and the rankings of the coatings.

A-I.6 Payoff Matrix

The "Payoff Matrix" for six alternatives with seven criteria is shown in Table A-I.1.

Table A-I.1: Payoff Matrix of Six Alternatives with Seven Criteria

Type of Coating	IND. RES.	WA	CD	HWI	SEIR	EIS	RED. HRD.
Weight	0.143	0.143	0.143	0.143	0.143	0.143	0.143
3LPE	0.09	0.076	6.76	0.55	8.86E+8	7.87E+11	20
3p/2p CAT	1.11	0.58	17.52	0.53	2.34E+7	5.41E+11	22
PU	0.20	0.50	16.64	0.52	2.45E+9	9.30E+10	36
VE	0.80	0.063	17.49	0.88	4.63E+7	3.04E+11	40
LE	0.23	0.72	23.77	0.78	3.86E+8	1.01E+11	13
HSS	0.21	0.071	10.07	0.93	2.15E+7	4.44E+11	23
$\sqrt{\sum_{i=1}^{m} x_{ij}^{2}}$	1.420	1.058	40.023	1.761	2.481 E+9	1.105E+12	66.918

A-I.7 Normalized Payoff Matrix

The 'Normalized Payoff Matrix" for coatings is shown in Table A-I.2.

Table A-I.2: Normalized Payoff Matrix

Type of Coating	IND. RES.	WA	CD	HWI	SEIR	EIS	RED. HRD.
3LPE	0.064	0.072	0.169	0.313	0.358	0.7125	0.299
3p/2p CAT	0.782	0.549	0.438	0.301	0.0095	0.490	0.329
PU	0.141	0.473	0.416	0.296	0.988	0.0842	0.538
VE	0.563	0.060	0.437	0.500	0.0187	0.275	0.598
LE	0.162	0.681	0.594	0.443	0.156	0.0913	0.195
HSS	0.148	0.067	0.252	0.529	0.0087	0.402	0.344

A-I.8 Weighted Normalized Payoff Matrix

The "Weighted Normalized Payoff Matrix" for coatings is shown in Table A-I.3.

Table A-I.3: Weighted Normalized Payoff Matrix

Type of Coating	IND. RES.	WA	CD	HWI	SEIR	EIS	RED. HRD.
3LPE	0.0091	0.0103	0.0242	0.0447	0.0511	0.1019	0.0428
3p/2p CAT	0.1118	0.0784	0.0626	0.0430	0.0014	0.0700	0.0470
PU	0.0202	0.0676	0.0595	0.0422	0.1412	0.0120	0.0769
VE	0.0806	0.0085	0.0625	0.0715	0.0027	0.0394	0.0855
LE	0.0232	0.0974	0.0849	0.0633	0.0223	0.0131	0.0278
HSS	0.0212	0.0096	0.0360	0.0755	0.0012	0.0575	0.0492
aj*	0.0091	0.0085	0.0242	0.0755	0.1412	0.1019	0.0278
aj**	0.1118	0.0974	0.0849	0.0422	0.0012	0.0120	0.0855

A-I.9 Ideal Solution

The "Ideal Solution" for coatings is shown in Table A-I.4.

Table A-I.4: Ideal Solution

Type of Coating	d_i^*	d_i^{**}	C_i^+	Rank
3LPE	0.0965	0.1850	0.6572	1
3p/2p CAT	0.1973	0.0755	0.2768	6
PU	0.1908	0.1720	0.4742	3
VE	0.1818	0.1047	0.3655	5
LE	0.1843	0.1099	0.3735	4
HSS	0.1494	0.1510	0.5027	2

Highest C_i^+ value represents highest performance (Rank=1)

A-I.10 Rankings of the Coatings

The "Rankings of the Coatings" are shown in Table A-I.5.

Table A-I.5: Ranking of Six Coatings

Type of coating	Rank
3LPE	1
HSS	2
PU	3
LE	4
VE	5
3p/2p CAT	6

A-I.11 Conclusion

3LPE is the best coating. The rankings of the first three coatings (3LPE, HSS and PU) evaluated by a simplified arithmetic mean system have been validated by the model for the conditions examined in the present study.

24/01/24

Raib Dey 24/1/24

Professor
Metallurgical & Material Engg. Dept.
Jadavpur University
Kolkata - 700032

Surojit Ghosal 24/01/2024

NACE CORROSION SPECIALIST
CERT NO. 14687

Appendix - II

Publication of Papers

in the International Journals

Publication of Paper

in the Web of Science Journal

Comparison of Coatings Adhesion Performances for Buried SS316L Pipelines

SURAJIT GHOSAL[1*], RAJIB DEY[2] and BUDDHADEB DUARI[3]

[1,2]Department of Metallurgical & Materials Engineering, Jadavpur University, Kolkata-700032, India.
[3]NACE Corrosion Specialist, A/172 Lake Gardens, Kolkata-700045, India.
*Corresponding author E-mail: ghosal.surajit@gmail.com

ABSTRACT

Six polymeric coatings viz. 3LPE, 3p/2p CAT, PU, VE, LE and HSS have been selected and each type of coating has been applied separately on SS316L pipe external surface. The test samples have been subjected to adhesion tests by the peel strength and pull-off methods, before and after the hot water Immersion (HWI) test for 100 days. After completing the test, the peel strength values of 3LPE, 3p/2p CAT, VE, HSS are found about 10.9, 1.8, 0.35, 6.8 N/mm respectively, whereas the pull-off adhesion values of PU, LE are found about 10.77, 22.7 N/mm^2 respectively. The experimental results are analysed, and the adhesion performances of the coatings are compared based on the dimensionless number termed as the "Coating Bond Index" in this study. The relative rankings of the adhesion performances for these coatings are evaluated in determining coatings suitability for buried SS316L pipelines in the petroleum, petrochemical and natural gas industries.

Keywords: SS316L pipes, Polymeric coatings, HWI test, Peel strength and Pull-off methods, Adhesion performances.

INTRODUCTION

The petrochemical products are transported via buried SS316L pipelines. These pipelines are installed mostly buried and marginally overground. Overground SS316L pipelines do not need corrosion protection due to 1-3 nm (nanometre) thick chromium oxide (Cr_2O_3) passive layer[1,2]. In buried condition, uncoated SS316L pipeline is excellent in high resistivity soil with a good drainage system[3], but uncoated SS316L pipeline is uncertain in low resistivity soil with chlorides ions (Cl$^-$) and a deficient in oxygen[4]. Cl$^-$ ions destroy passive layer and lead to form corrosion pits on SS316L surface[5]. Pits are covered by the porous corrosion products and remain undetectable until leaks[6]. Localized pitting corrosion penetrates rapidly to the thickness of SS316L pipeline and perforates pipeline within a few days[7]. The mechanism of pitting corrosion on buried uncoated SS316L pipeline is shown in Fig. 1 a), b). It is, therefore, imperative to apply external polymeric (organic) protective coatings on buried SS316L pipelines for safe transportation of the petrochemical products.

Publication of Paper

in the Scopus Indexed Journal

Evaluation of Coatings Suitability for Buried SS316L Pipelines

S. Ghosal[*1], R. Dey[1], B. Duari[2]

[1] Deptartment of Metallurgical and Materials Engineering, Jadavpur University, P.O. Box: 700032, Kolkata, India.
[2] Corrosion Specialist, A/172 Lake Gardens, P.O. Box: 700045, Kolkata, India.

ABSTRACT

S ix polymeric coatings viz 3LPE, 3p/2p CAT, PU, VE, LE, and HSS have been selected, and each type of coating has been applied separately on SS316L pipe external surface. The test samples were subjected to Specific Electrical Insulation Resistance (SEIR) test in 0.1 mol/liter of NaCl solution and the Electrochemical Impedance Spectroscopy (EIS) test in 3.5 % NaCl solution. After completion of the tests, SEIR values of PU, 3LPE, and LE are found to be about 2.5×10^9, 8.9×10^8, and 3.9×10^8 ohm.m^2, respectively. In contrast, the electrochemical impedance values at low frequencies (100 mHz) of 3LPE, 3p/2p CAT, and HSS are found to be about 7.9×10^{11}, 5.4×10^{11}, and 4.5×10^{11} ohm.cm^2, respectively. The experimental results are analyzed, and the ranking of coatings has been made based on each test's performance. The overall ranking of coatings is evaluated for the determination of the suitability of the coating for buried SS316L pipelines in the petroleum, petrochemical, and natural gas industries. Prog. Color Colorants Coat. 16 (2023), 361-375© Institute for Color Science and Technology.

1. Introduction

The petrochemical products are transported via buried SS316L pipelines. These pipelines are installed mostly buried and marginally overground. Overground SS316L pipelines do not need corrosion protection due to 1-3 nm (nanometre) thick chromium oxide (Cr_2O_3) passive layer [1, 2]. In buried condition, an uncoated SS316L pipeline is excellent in high-resistivity soil with a good drainage system [3]. Still, an uncoated SS316L pipeline is uncertain in low-resistivity soil with chloride ions (Cl^-) and an oxygen deficiency [4]. Cl^- ions destroy the passive layer and lead to forming of corrosion pits on the SS316L surface [5]. The porous corrosion products cover pits and remain undetectable until they leak [6]. Localized pitting corrosion penetrates rapidly to the thickness of the SS316L pipeline and perforates the SS316L pipeline within a few days [7]. The mechanism of pitting corrosion and

the subsequent failure of buried SS316L pipeline are shown in Figures 1 a and b. It is, therefore, imperative to apply external polymeric (organic) protective coatings on buried SS316L pipelines for the safe transportation of petrochemical products.

A thorough literature survey, including analysis of research papers, reveals that so far, most of the studies on polymeric coatings focused primarily on the analysis of coatings performances and suitability for buried carbon steel pipelines. Many researchers have devoted research efforts to studying metallic and organic coatings on SS316L substrates for marine environments or to studying the pitting corrosion of SS316L under thermal insulation. But, to date, less attention has been paid to the research on coatings performances and suitability for buried SS316L pipelines, and there is a research gap that remains unanswered in this field. To address this outstanding

Appendix - III
Experimental Data

Appendix-III A

Cyclic Potentiodynamic Polarization Test of SS316L

Experimental set-up for cyclic potentiodynamic polarization test (3-electrode system)

Sample 1
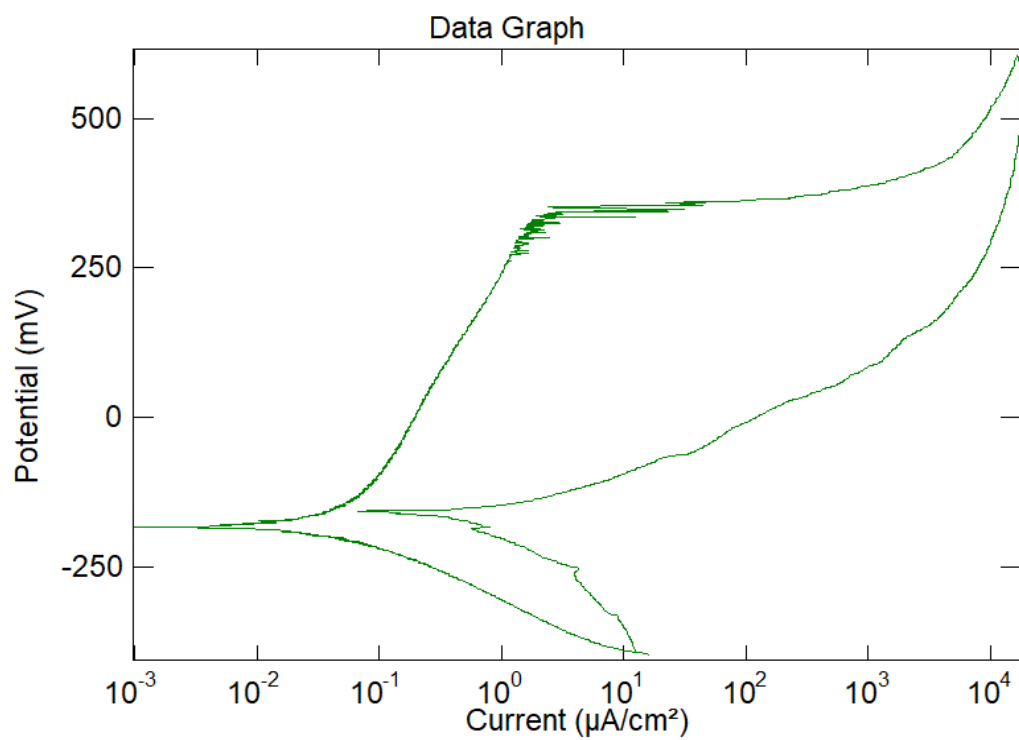
Potential (E) vs. Current Density (log i) polarization scan of SS316L (Sample 1)

Data Graph
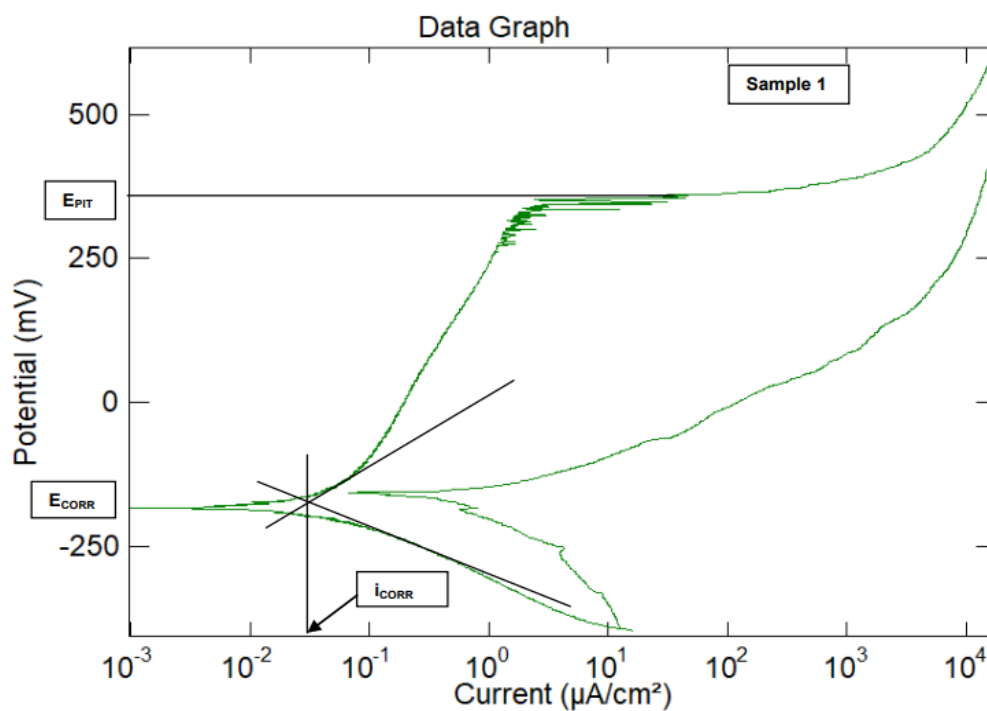
Evaluation of E_{pit}, E_{corr}, i_{corr}. E_{corr}, i_{corr} are evaluated by Tafel extrapolation method (Sample 1)

Table: E_{pit}, E_{corr}, i_{corr} values of SS316L

Sample no.	E_{pit} (mV) vs. SCE (Note-1)	E_{corr}(mV) vs. SCE (Note-1)	i_{corr} (μA/cm^2)
Sample 1	361	-195	0.05
Sample 2	363	-200	0.06
Sample 3	380	-205	0.07

Note-1: SCE - Saturated Calomel Electrode as reference electrode
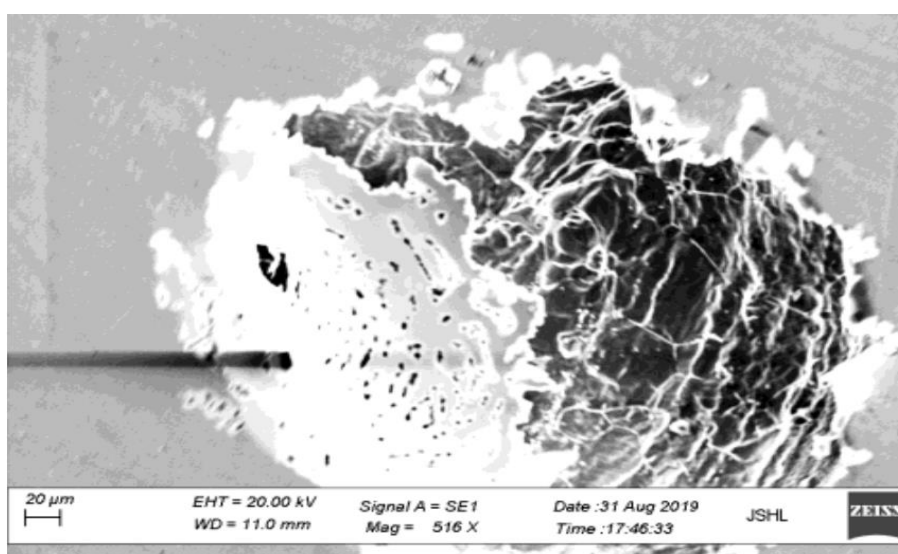
SEM photograph of pitting corrosion on SS316L surface (Sample 1)

Appendix-III B

Thickness Measurement of Coatings

Type of coating	Thickness reading (mm)								Average thickness (mm)
	1	**2**	**3**	**4**	**5**	**6**	**7**	**8**	
VE	3.03	3.09	3.07	2.95	2.91	3.03	2.89	3.1	3.0
3LPE	2.96	2.93	2.89	2.93	2.98	2.86	2.85	2.80	2.9
3p/2p CAT	2.48	2.52	2.55	2.49	2.51	2.52	2.45	2.48	2.5
HSS	2.31	2.22	2.45	2.3	2.46	2.24	2.2	2.22	2.3
PU	1.7	1.65	1.49	1.5	1.48	1.57	1.58	1.43	1.55
LE	0.96	1.06	0.92	0.97	0.92	0.9	0.92	0.95	0.95

Thickness measurement on LE coated pipe sample

Appendix-III C

Holiday Detection of Coatings

Type of coating	Average thickness (mm)	Minimum applied voltage (kV)	Maximum applied voltage (kV)	Number of holidays detected
VE	3.0	22	25	NIL
3LPE	2.9	20	22	NIL
3p/2p CAT	2.5	19	20	NIL
HSS	2.3	16	18	NIL
PU	1.55	8	12	NIL
LE	0.95	5	10	NIL

Holiday detection on 3LPE coated pipe sample

Appendix-III D

Type D Shore Durometer Hardness Measurement of Coatings

Type of coating	Shore D hardness					Average hardness
	1	**2**	**3**	**4**	**5**	
VE	31	32	32	30	34	32
3LPE	54	55	53	57	55	55
3p/2p CAT	36	37	38	36	37	37
HSS	58	57	58	58	54	57
PU	71	72	75	71	71	72
LE	90	89	89	90	88	89

Shore D hardness measurement on PU coated pipe sample

Appendix-III E

Impact Resistance Test of Coatings

Type of coating	Average thickness (mm)	Applied impact energy (J)	Applied voltage (kV) for holiday detection after impact resistance test	Number of holidays detected after impact resistance test
VE	3.0	15	22	NIL
3LPE	2.9	15	20	NIL
3p/2p CAT	2.5	15	19	NIL
HSS	2.3	15	16	NIL
PU	1.55	8	8	NIL
LE	0.95	5	5	NIL

Impact resistance test on PU coated pipe sample

Appendix-III F

Indentation Resistance Test of Coatings

Type of coating	Sample no.	Coating thickness, t (mm) (Note-1)	t_1 (mm) (Note-2)	t_2 (mm) (Note-3)	Indetentation depth, $t_3 = t_1 - t_2$ (mm)	Average indentation depth (mm)	Applied voltage (kV) and number of holidays detected after indentation test	
HSS	Sample 1	2.32	8.42	8.20	0.22	0.21	16	NIL
	Sample 2	2.38	8.48	8.24	0.24			NIL
	Sample 3	2.36	8.46	8.28	0.18			NIL

Type of coating	Sample no.	Coating thickness, t (mm) (Note-1)	t₁ (mm) (Note-2)	t₂ (mm) (Note-3)	Indententation depth, t₃ = t₁-t₂ (mm)	Average indentation depth (mm)	Applied voltage (kV) and number of holidays detected after indentation test	
LE	Sample 1	1.085	7.185	6.935	0.25	0.23	5	NIL
	Sample 2	0.99	7.09	6.84	0.25			NIL
	Sample 3	0.925	7.025	6.845	0.18			NIL
PU	Sample 1	1.38	7.48	7.28	0.20	0.20	8	NIL
	Sample 2	1.27	7.37	7.19	0.18			NIL
	Sample 3	1.19	7.29	7.07	0.22			NIL
VE	Sample 1	3.326	9.426	8.626	0.80	0.80	22	NIL
	Sample 2	3.225	9.325	8.535	0.79			NIL
	Sample 3	3.277	9.377	8.557	0.82			NIL

Note-1: Pipe thickness = 6.1 mm (SS316L 4" pipe sch.40s) , coating thickness = t_1 - pipe thickness

Note-2: t_1 = dial gauge reading (mm) with the indenter and without applying the mass positioned centrally over the coated sample

Note-3: t_2 = dial gauge reading (mm) with the indenter and with applying mass to the coated sample, giving the desired pressure on the indenter and keeping this load for 24 hours

Type of coating	Sample no.	Coating thickness, t (mm) (Note-1)	t₁ (mm) (Note-2)	t₂ (mm) (Note-3)	Indententation depth, t₃ = t₁-t₂ (mm)	Average indentation depth (mm)	Applied voltage and number of holidays detected after indentation test	
3LPE	Sample 1	2.90	9.0	8.88	0.12	0.09	20	NIL
	Sample 2	2.92	9.02	8.94	0.08			NIL
	Sample 3	2..87	8.97	8.90	0.07			NIL
3p/2p CAT	Sample 1	3.0	9.1	7.97	1.13	1.11	20	NIL
	Sample 2	2.98	9.08	7.98	1.1			NIL
	Sample 3	2.99	9.09	8.0	1.09			NIL

Indentation resistance test set-up for HSS coated pipe sample

Water Absorption Test of Coatings

Types of coating	Weight (g)	Sample 1	Sample 2	Sample 3	Average water absorption (%)
HSS	Initial Weight (g)	4.4983	4.5306	4.5496	0.071
	Final Weight (g)	4.5016	4.5338	4.5528	
	Water absorption (%)	0.0733	0.0706	0.0703	
LE	Initial Weight (g)	2.8043	2.8128	2.8638	0.72
	Final Weight (g)	2.8256	2.8336	2.8831	
	Water absorption (%)	0.76	0.74	0.674	
PU	Initial Weight (g)	0.884	0.852	0.893	0.495
	Final Weight (g)	0.889	0.856	0.897	
	Water absorption (%)	0.566	0.4694	0.4479	
VE	Initial Weight (g)	7.4914	7.0442	6.6453	0.063
	Final Weight (g)	7.4966	7.0478	6.6499	
	Water absorption (%)	0.0694	0.0511	0.0692	
3LPE	Initial Weight (g)	1.374	1.290	1.275	0.076
	Final Weight (g)	1.375	1.291	1.276	
	Water absorption (%)	0.0727	0.0775	0.0784	
3p/2p CAT	Initial Weight (g)	3.2313	3.2053	3.2355	0.58
	Final Weight (g)	3.2500	3.2235	3.2542	
	Water absorption (%)	0.58	0.5678	0.58	

Water absorption test of VE coatings

Appendix-III H

Cathodic Disbondment (CD) Test of Coatings

Type of Coating	Sample 1 CD (mm)	Sample 2 CD (mm)	Sample 3 CD (mm)	Average CD (mm)
HSS	10.35	9.885	9.99	10.07
LE	23.44	22.02	25.83	23.76
PU	16.57	17.6	15.76	16.64
VE	16.46	19.06	16.95	17.49
3LPE	7.12	6.56	6.62	6.76
3p/2p CAT	18.54	17	17.03	17.52

CD measurement of LE coated pipe sample

CD measurement of 3LPE coated pipe sample

Peel Strength Test of Tape/Layer Coatings (3LPE, HSS, VE, 3p/2p CAT)

Type of coating and testing temp.	Sample 1 (N/mm)	Sample 2 (N/mm)	Sample 3 (N/mm)	Average peel strength (N/mm)
HSS				
23^0C	5.8	4.3	6.8	5.6
55 ± 5^0C	2.3	2.2	2.5	2.3
VE				
23^0C	0.59	0.58	0.56	0.58
55 ± 5^0C	0.097	0.083	0.078	0.086
3LPE				
23^0C	24	18	24	20
55 ± 5^0C	2.7	2.9	2.5	2.7
3p/2p CAT				
23^0C	1.7	1.6	2.9	2.07
55 ± 5^0C	0.15	0.15	0.17	0.16

HSS coated pipe sample after peel strength test

Peel Strength graph legend

·············	Sample 1
·············	Sample 2
·············	Sample 3
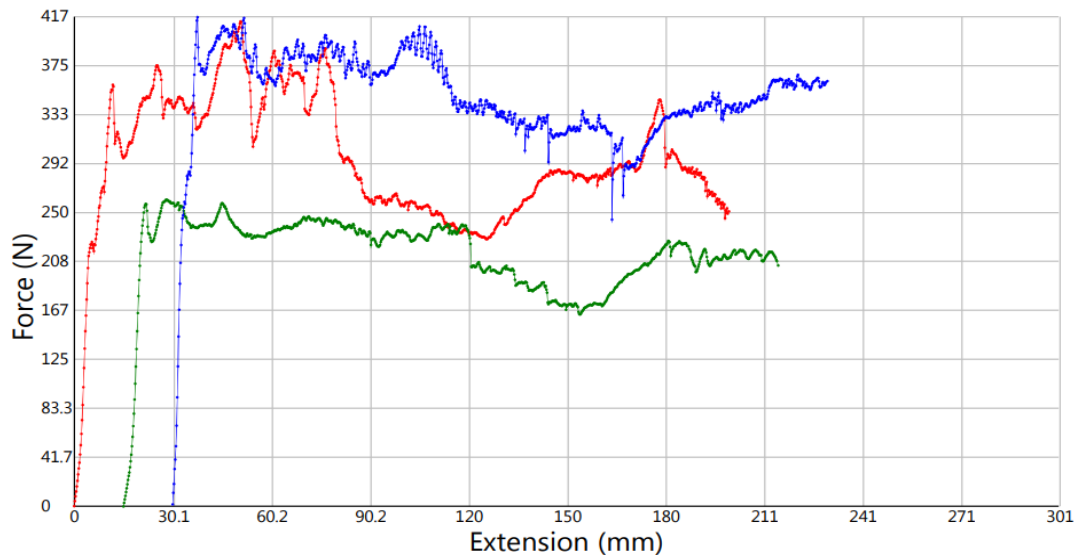
Peel strength graph of HSS coated pipe sample at 23⁰C (Sample width = 50 mm)
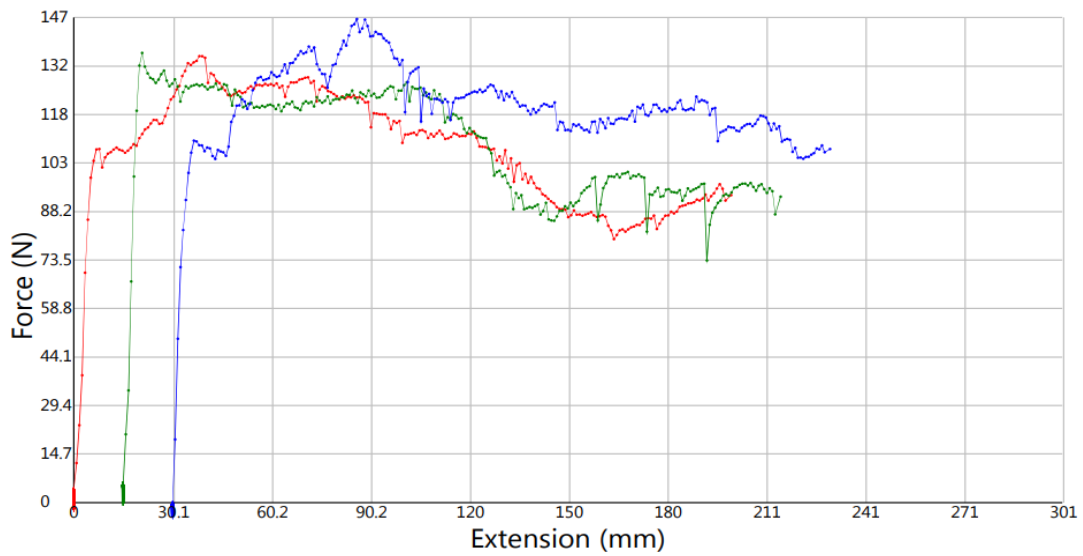
Peel strength graph of HSS coated pipe sample at 55±5⁰C (Sample width = 50 mm)

Appendix-III J

Pull-off Adhesion Test of Liquid Coatings (LE, PU)

Type of coating and testing temp.	Sample 1 (N/mm²)	Sample 2 (N/mm²)	Sample 3 (N/mm²)	Average pull-off adhesion (N/mm²)	Type of Fracture
LE					
23⁰C	29.7	27.7	28.7	28.7	Cohesive
55±5⁰C	12.1	12.4	12.5	12.3	Cohesive
PU					
23⁰C	18.6	19.9	17.3	18.6	Cohesive
55±5⁰C	11.9	12.2	12.1	12.07	Cohesive

PU coated pipe sample after pull-off adhesion test at 23^{0}C

PU coated pipe sample after pull-off adhesion test at 55±5^{0}C

Appendix-III K

Hot Water Immersion Test of Coatings

Peel Strength Test of Tape/Layer Coatings (3LPE, HSS, VE, 3p/2p CAT) before and after HWI Test

Type of coating	Sample 1 (N/mm)	Sample 2 (N/mm)	Sample 3 (N/mm)	Average peel strength (N/mm)	Ratio P_{100}/P_0
HSS					
P_0 **(Note-1)**	7.0	7.7	7.3	7.3	0.93
P_{100} **(Note-2)**	6.9	7.1	6.5	6.8	
VE					
P_0 **(Note-1)**	0.44	0.38	0.36	0.39	0.88
P_{100} **(Note-2)**	0.38	0.35	0.31	0.35	
3LPE					
P_0 **(Note-1)**	22	19	18	19.7	0.55
P_{100} **(Note-2)**	14	7.6	11	10.9	
3p/2p CAT					
P_0 **(Note-1)**	3.5	3.4	3.3	3.4	0.53
P_{100} **(Note-2)**	1.8	1.6	2.0	1.8	

Note-1: P_0 = Peel strength before hot water immersion
Note-2: P_{100} = Peel strength after hot water immersion

Peel strength graph of 3p/2p CAT coated sample before HWI (Sample width = 25 mm)
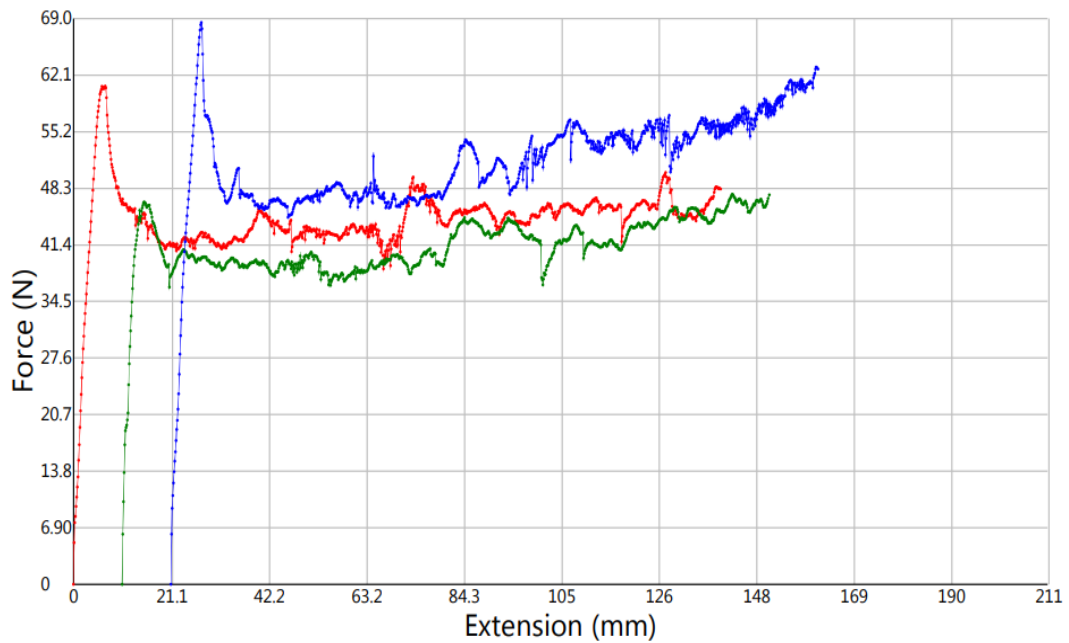
Peel strength graph of 3p/2p CAT coated sample after HWI (Sample width = 25 mm)

227

Peel strength tested 3p/2p CAT coated pipe sample before hot water immersion

Peel strength tested 3p/2p CAT coated pipe sample after hot water immersion

Pull-off Adhesion Test of Liquid Coatings (LE, PU) before and after HWI Test

Type of coating	Sample 1 (N/mm²)	Sample 2 (N/mm²)	Sample 3 (N/mm²)	Average pull-off adhesion (N/mm²)	Type of Fracture	Ratio P_{100}/P_0
LE						
P_0 **(Note-1)**	29	28.9	29	28.97	Cohesive	0.78
P_{100} **(Note-2)**	21.8	23.7	22.7	22.7	Cohesive	
PU						
P_0 **(Note-1)**	19.3	22.9	20.4	20.87	Cohesive	0.52
P_{100} **(Note-2)**	10.7	10.8	10.8	10.77	Cohesive	

Note-1: P_0 = Pull-off adhesion before hot water immersion

Note-2: P_{100} = Pull-off adhesion after hot water immersion

Pull-off adhesion tested LE coated pipe sample before hot water immersion
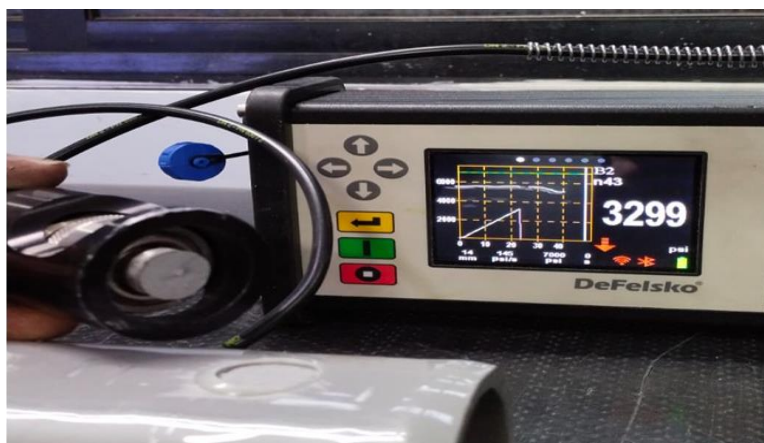
Pull-off adhesion tested LE coated pipe sample after hot water immersion

Appendix-III L

Specific Electrical Insulation Resistance (SEIR) Test of Coatings

Coatings SEIR values (ohm.m^2)						
Type of coating	**PU**			**VE**		
Day on measurement	**Sample 1**	**Sample 2**	**Sample 3**	**Sample 1**	**Sample 2**	**Sample 3**
Day 4	9.98E+09	9.26E+09	9.59E+09	2.01E+08	3.01E+07	5.01E+07
Day 18	9.46E+09	8.49E+09	9.20E+09	1.73E+08	2.94E+07	4.80E+07
Day 52	2.98E+09	1.72E+09	3.02E+09	5.38E+07	2.86E+07	1.55E+07
Day 70	2.49E+09	1.51E+09	2.61E+09	4.76E+07	2.62E+07	1.43E+07
Day 100	2.45E+09	1.40E+09	2.48E+09	4.63E+07	2.49E+07	1.30E+07

Coatings SEIR values (ohm.m²)						
Type of coating	**LE**			**3LPE**		
Day on measurement	**Sample 1**	**Sample 2**	**Sample 3**	**Sample 1**	**Sample 2**	**Sample 3**
Day 4	3.59E+09	5.98E+09	4.49E+09	2.84E+09	2.49E+09	2.19E+09
Day 18	3.03E+09	5.72E+09	4.23E+09	2.49E+09	2.23E+09	1.89E+09
Day 52	2.30E+08	4.70E+08	4.57E+08	1.03E+08	1.01E+09	1.20E+08
Day 70	2.01E+08	3.97E+08	4.92E+08	8.86E+07	9.01E+08	1.09E+08
Day 100	1.89E+08	3.86E+08	3.80E+08	8.72E+07	8.86E+08	1.02E+08

Coatings SEIR values (ohm.m²)						
Type of coating	**3p/2p CAT**			**HSS**		
Day on measurement	**Sample 1**	**Sample 2**	**Sample 3**	**Sample 1**	**Sample 2**	**Sample 3**
Day 4	6.89E+08	8.20E+08	6.35E+08	3.16E+08	2.25E+08	2.16E+08
Day 18	6.42E+08	7.95E+08	5.95E+08	2.49E+08	1.56E+08	1.49E+08
Day 52	4.21E+07	2.78E+07	2.89E+07	2.62E+07	3.84E+07	5.46E+07
Day 70	3.61E+07	2.49E+07	2.54E+07	2.30E+07	3.30E+07	4.68E+07
Day 100	3.49E+07	2.34E+07	2.43E+07	2.15E+07	3.19E+07	4.53E+07

Experimental set-up for specific electrical insulation resistance test on coated pipe samples

Appendix-III M

Electrochemical Impedance Spectroscopy (EIS) Test of Coatings

Frequency vs. Impedance for 3LPE coating

Frequency (mHz)	impedance (ohm.cm2)								
	Day1-Sample1-	Day7-Sample1-i	Day14-Sample1-	Day1-Sample2-	Day7-Sample2-	Day14-Sample2-	Day1-Sample3-	Day7-Sample3-	Day14-Sample3-i
1.996E+01	4.24E+12	3.85E+12	3.76E+12	3.30E+12	3.30E+12	3.68E+12	4.51E+12	4.17E+12	3.76E+12
2.51E+01	3.43E+12	3.08E+12	3.02E+12	2.67E+12	2.72E+12	3.08E+12	3.49E+12	3.38E+12	3.17E+12
3.16E+01	2.73E+12	2.51E+12	2.47E+12	2.15E+12	2.18E+12	2.47E+12	2.82E+12	2.61E+12	2.45E+12
3.98E+01	2.26E+12	2.06E+12	1.91E+12	1.75E+12	1.77E+12	2.03E+12	2.25E+12	2.10E+12	1.99E+12
5.01E+01	1.81E+12	1.68E+12	1.54E+12	1.40E+12	1.42E+12	1.61E+12	1.80E+12	1.66E+12	1.58E+12
6.32E+01	1.45E+12	1.36E+12	1.21E+12	1.13E+12	1.15E+12	1.31E+12	1.41E+12	1.32E+12	1.22E+12
7.95E+01	1.17E+12	1.10E+12	9.83E+11	9.22E+11	9.31E+11	1.04E+12	1.14E+12	1.06E+12	9.81E+11
1.00E+02	9.24E+11	8.72E+11	7.87E+11	7.35E+11	7.46E+11	8.34E+11	9.03E+11	8.21E+11	7.83E+11
1.26E+02	7.46E+11	7.08E+11	6.27E+11	5.91E+11	6.04E+11	6.69E+11	7.17E+11	6.61E+11	6.24E+11
1.59E+02	6.02E+11	5.70E+11	5.00E+11	4.73E+11	4.83E+11	5.35E+11	5.69E+11	5.31E+11	4.96E+11
2.00E+02	4.79E+11	4.52E+11	3.99E+11	3.78E+11	3.87E+11	4.28E+11	4.49E+11	4.20E+11	3.91E+11
2.52E+02	3.84E+11	3.66E+11	3.20E+11	3.03E+11	3.11E+11	3.43E+11	3.63E+11	3.35E+11	3.14E+11
3.17E+02	3.08E+11	2.94E+11	2.56E+11	2.44E+11	2.50E+11	2.76E+11	2.90E+11	2.67E+11	2.50E+11
4.01E+02	2.47E+11	2.35E+11	2.04E+11	1.96E+11	2.00E+11	2.21E+11	2.32E+11	2.12E+11	1.99E+11
5.04E+02	1.98E+11	1.90E+11	1.64E+11	1.57E+11	1.61E+11	1.77E+11	1.86E+11	1.71E+11	1.60E+11
6.33E+02	1.61E+11	1.54E+11	1.33E+11	1.27E+11	1.31E+11	1.44E+11	1.50E+11	1.38E+11	1.29E+11
7.92E+02	1.23E+11	1.15E+11	1.01E+11	9.77E+10	9.86E+10	1.07E+11	1.15E+11	1.06E+11	9.95E+10
9.99E+02	9.79E+10	9.15E+10	8.01E+10	7.78E+10	7.86E+10	8.49E+10	9.17E+10	8.44E+10	7.89E+10
1.27E+03	7.74E+10	7.25E+10	6.32E+10	6.16E+10	6.21E+10	6.72E+10	7.24E+10	6.66E+10	6.25E+10
1.59E+03	6.21E+10	5.82E+10	5.07E+10	4.95E+10	4.98E+10	5.37E+10	5.80E+10	5.33E+10	5.01E+10
2.00E+03	4.94E+10	4.62E+10	4.03E+10	3.94E+10	3.97E+10	4.26E+10	4.60E+10	4.24E+10	3.97E+10
2.50E+03	3.97E+10	3.70E+10	3.24E+10	3.16E+10	3.18E+10	3.44E+10	3.69E+10	3.39E+10	3.19E+10
3.16E+03	3.16E+10	2.96E+10	2.58E+10	2.52E+10	2.54E+10	2.72E+10	2.94E+10	2.70E+10	2.54E+10
3.95E+03	2.55E+10	2.37E+10	2.09E+10	2.03E+10	2.05E+10	2.19E+10	2.37E+10	2.18E+10	2.05E+10
5.01E+03	2.03E+10	1.89E+10	1.64E+10	1.62E+10	1.63E+10	1.76E+10	1.90E+10	1.73E+10	1.63E+10
6.32E+03	1.63E+10	1.52E+10	1.33E+10	1.30E+10	1.31E+10	1.41E+10	1.50E+10	1.39E+10	1.30E+10
7.95E+03	1.25E+10	1.16E+10	1.01E+10	9.93E+09	9.99E+09	1.07E+10	1.16E+10	1.06E+10	9.96E+09
9.93E+03	9.97E+09	9.29E+09	8.11E+09	7.97E+09	7.99E+09	8.57E+09	9.24E+09	8.49E+09	7.97E+09
1.24E+04	8.01E+09	7.44E+09	6.49E+09	6.38E+09	6.41E+09	6.90E+09	7.41E+09	6.82E+09	6.39E+09
1.56E+04	6.34E+09	5.92E+09	5.17E+09	5.10E+09	5.10E+09	5.45E+09	5.91E+09	5.41E+09	5.12E+09
1.99E+04	5.03E+09	4.68E+09	4.06E+09	4.00E+09	3.99E+09	4.34E+09	4.62E+09	4.24E+09	3.99E+09
2.49E+04	4.02E+09	3.74E+09	3.27E+09	3.20E+09	3.22E+09	3.46E+09	3.71E+09	3.42E+09	3.21E+09
3.13E+04	3.22E+09	3.00E+09	2.61E+09	2.57E+09	2.58E+09	2.77E+09	2.97E+09	2.73E+09	2.56E+09
3.84E+04	2.63E+09	2.45E+09	2.13E+09	2.11E+09	2.11E+09	2.26E+09	2.43E+09	2.23E+09	2.10E+09
5.02E+04	2.00E+09	1.90E+09	1.67E+09	1.64E+09	1.61E+09	1.73E+09	1.88E+09	1.72E+09	1.61E+09
6.33E+04	1.63E+09	1.52E+09	1.33E+09	1.31E+09	1.31E+09	1.41E+09	1.51E+09	1.39E+09	1.30E+09
7.90E+04	1.27E+09	1.18E+09	1.02E+09	1.01E+09	1.01E+09	1.09E+09	1.17E+09	1.07E+09	1.01E+09
1.004E+05	9.96E+08	9.25E+08	8.06E+08	7.95E+08	7.97E+08	8.55E+08	9.18E+08	8.44E+08	7.91E+08
1.3E+05	7.98E+08	7.41E+08	6.45E+08	6.37E+08	6.39E+08	6.85E+08	7.35E+08	6.77E+08	6.35E+08
1.6E+05	6.33E+08	5.88E+08	5.12E+08	5.06E+08	5.07E+08	5.43E+08	5.83E+08	5.37E+08	5.03E+08
2.0E+05	5.06E+08	4.70E+08	4.09E+08	4.04E+08	4.05E+08	4.34E+08	4.65E+08	4.29E+08	4.02E+08
2.52E+05	3.99E+08	3.71E+08	3.23E+08	3.19E+08	3.20E+08	3.43E+08	3.67E+08	3.39E+08	3.17E+08
3.16E+05	3.21E+08	2.98E+08	2.59E+08	2.56E+08	2.57E+08	2.75E+08	2.95E+08	2.72E+08	2.55E+08
4.E+05	2.56E+08	2.37E+08	2.07E+08	2.04E+08	2.05E+08	2.20E+08	2.35E+08	2.17E+08	2.03E+08
5.06E+05	2.03E+08	1.89E+08	1.65E+08	1.62E+08	1.63E+08	1.75E+08	1.87E+08	1.72E+08	1.61E+08
6.28E+05	1.65E+08	1.54E+08	1.34E+08	1.32E+08	1.33E+08	1.42E+08	1.52E+08	1.40E+08	1.31E+08
7.97E+05	1.26E+08	1.17E+08	1.02E+08	1.01E+08	1.01E+08	1.08E+08	1.16E+08	1.07E+08	1.00E+08
9.98E+05	1.00E+08	9.33E+07	8.12E+07	8.05E+07	8.08E+07	8.64E+07	9.22E+07	8.55E+07	7.98E+07
1.27E+06	7.95E+07	7.38E+07	6.41E+07	6.36E+07	6.37E+07	6.82E+07	7.29E+07	6.73E+07	6.31E+07
1.58E+06	6.38E+07	5.93E+07	5.16E+07	5.10E+07	5.12E+07	5.48E+07	5.86E+07	5.41E+07	5.07E+07
1.98E+06	5.11E+07	4.74E+07	4.12E+07	4.08E+07	4.09E+07	4.38E+07	4.69E+07	4.33E+07	4.05E+07
2.53E+06	4.00E+07	3.72E+07	3.24E+07	3.20E+07	3.21E+07	3.44E+07	3.68E+07	3.39E+07	3.18E+07
3.17E+06	3.20E+07	2.97E+07	2.59E+07	2.56E+07	2.57E+07	2.75E+07	2.94E+07	2.72E+07	2.54E+07
3.98E+06	2.56E+07	2.38E+07	2.07E+07	2.05E+07	2.06E+07	2.20E+07	2.35E+07	2.17E+07	2.04E+07
5.02E+06	2.05E+07	1.91E+07	1.66E+07	1.64E+07	1.65E+07	1.77E+07	1.89E+07	1.74E+07	1.63E+07
6.33E+06	1.65E+07	1.53E+07	1.34E+07	1.32E+07	1.32E+07	1.42E+07	1.51E+07	1.40E+07	1.31E+07
8.02E+06	1.26E+07	1.17E+07	1.02E+07	1.01E+07	1.01E+07	1.08E+07	1.16E+07	1.07E+07	1.00E+07
1.01E+07	1.00E+07	9.32E+06	8.10E+06	8.02E+06	8.03E+06	8.61E+06	9.20E+06	8.51E+06	7.98E+06
1.26E+07	8.02E+06	7.45E+06	6.48E+06	6.42E+06	6.43E+06	6.88E+06	7.36E+06	6.82E+06	6.39E+06
1.59E+07	6.37E+06	5.92E+06	5.15E+06	5.10E+06	5.11E+06	5.47E+06	5.85E+06	5.42E+06	5.09E+06
2.00E+07	5.06E+06	4.71E+06	4.09E+06	4.06E+06	4.06E+06	4.35E+06	4.65E+06	4.31E+06	4.05E+06
2.52E+07	4.04E+06	3.76E+06	3.26E+06	3.23E+06	3.24E+06	3.47E+06	3.71E+06	3.44E+06	3.23E+06
3.16E+07	3.22E+06	3.00E+06	2.61E+06	2.58E+06	2.59E+06	2.77E+06	2.96E+06	2.75E+06	2.58E+06
3.99E+07	2.57E+06	2.39E+06	2.08E+06	2.06E+06	2.06E+06	2.21E+06	2.36E+06	2.20E+06	2.06E+06
5.02E+07	2.06E+06	1.92E+06	1.67E+06	1.65E+06	1.65E+06	1.77E+06	1.89E+06	1.76E+06	1.65E+06
6.31E+07	1.65E+06	1.54E+06	1.34E+06	1.33E+06	1.33E+06	1.43E+06	1.52E+06	1.42E+06	1.33E+06
7.95E+07	1.27E+06	1.19E+06	1.03E+06	1.02E+06	1.02E+06	1.09E+06	1.17E+06	1.09E+06	1.02E+06
1.001E+08	1.01E+06	9.42E+05	8.17E+05	8.10E+05	8.10E+05	8.69E+05	9.30E+05	8.68E+05	8.13E+05

Frequency vs. Phase for 3LPE coating

Frequency (mHz)	Phase (º)								
	Day1-Sample1-	Day7-Sample1-	Day14-Sample1	Day1-Sample2-	Day7-Sample2-	Day14-Sample2	Day1-Sample3-Pha	Day7-Sample3-I	Day14-Sample3-
1.996E+01	-81.73	-79.85	-84.94	-81.59	-81.09	-83.43	-84.98	-85.41	-85.26
2.512E+01	-81.68	-79.14	-83.38	-82.35	-81.48	-85.07	-85.06	-86.38	-86.13
3.163E+01	-80.98	-80.98	-86.2	-81.79	-81.07	-84.43	-85.31	-86.84	-88.44
3.983E+01	-80.74	-80.57	-85.24	-82.14	-80.73	-84.75	-87.77	-87.15	-86.94
5.013E+01	-82.15	-81.71	-85.4	-83.03	-80.97	-85.05	-87.32	-87.51	-87.76
6.317E+01	-82.46	-81.73	-85.43	-83.15	-81.73	-84.39	-87.05	-86.7	-87.45
7.945E+01	-83.53	-81.96	-86	-83.14	-82.55	-84.57	-87.37	-87.08	-87.2
1.002E+02	-84.37	-83.07	-86.14	-83.7	-83.05	-84.62	-87.34	-88.04	-87.43
1.260E+02	-84.51	-83.08	-86.28	-84.36	-83.27	-84.75	-87.13	-87.62	-87.63
1.589E+02	-84.47	-83.88	-86.03	-84.24	-83.63	-85.17	-86.78	-87.86	-88.17
2.003E+02	-84.82	-83.8	-85.8	-84.19	-83.67	-84.73	-86.5	-87.27	-87.52
2.520E+02	-84.66	-84.08	-85.37	-84.05	-83.79	-84.79	-86.31	-86.72	-86.4
3.167E+02	-84.51	-83.99	-85.03	-83.64	-83.56	-84.39	-85.46	-85.99	-86.08
4.006E+02	-83.35	-83.46	-84.35	-83	-83.07	-83.89	-84.78	-85.12	-85.23
5.040E+02	-82.96	-83	-83.49	-82.48	-82.46	-83.31	-84.03	-83.83	-84.41
6.334E+02	-82.38	-82.49	-82.69	-81.72	-81.89	-82.63	-83.4	-83.24	-83.34
7.923E+02	-87.5	-87.57	-88.21	-87.52	-87.38	-88.1	-88.77	-88.57	-88.55
9.990E+02	-87.54	-87.47	-88.06	-87.39	-87.29	-87.85	-88.36	-88.69	-88.49
1.267E+03	-87.37	-87.44	-87.76	-87.22	-87.18	-87.67	-88.13	-88.21	-88.16
1.585E+03	-87.16	-87.17	-87.4	-86.96	-86.95	-87.46	-87.95	-87.88	-87.99
1.998E+03	-86.86	-86.85	-87.03	-86.61	-86.61	-86.87	-87.46	-87.44	-87.36
2.504E+03	-86.36	-86.34	-86.52	-86.17	-86.1	-86.49	-86.9	-86.86	-86.96
3.159E+03	-85.7	-85.66	-85.75	-85.43	-85.47	-85.65	-86.15	-86.14	-86.26
3.946E+03	-85.01	-85.1	-84.97	-84.87	-84.62	-84.86	-85.37	-85.4	-85.38
5.008E+03	-84.18	-84.38	-84.06	-83.82	-83.73	-83.9	-84.63	-84.41	-84.34
6.317E+03	-83.16	-83.33	-82.76	-82.6	-82.6	-82.84	-82.81	-83.24	-83.11
7.945E+03	-88.57	-88.76	-88.69	-88.53	-88.57	-88.52	-88.68	-88.91	-88.9
9.931E+03	-88.4	-88.41	-88.5	-88.28	-88.31	-88.43	-88.56	-88.7	-88.62
1.240E+04	-88.07	-88.2	-88.1	-88.02	-88	-88.21	-88.38	-88.6	-88.49
1.563E+04	-87.89	-88.04	-87.8	-87.57	-87.75	-87.62	-88.44	-88.02	-88.21
1.986E+04	-87.44	-87.42	-87.06	-87.15	-87.25	-87.13	-87.74	-87.46	-87.57
2.493E+04	-86.88	-86.93	-86.85	-86.65	-86.73	-86.66	-86.86	-86.95	-87.02
3.125E+04	-86.23	-86.29	-85.92	-86.06	-86	-86.03	-86.42	-86.13	-86.11
3.842E+04	-85.45	-85.53	-85.3	-85.35	-85.18	-85.21	-85.72	-85.38	-85.51
5.022E+04	-84.09	-83.71	-83.76	-83.77	-83.75	-84.27	-84.87	-84.78	-83.9
6.334E+04	-83.43	-83.54	-82.85	-83.13	-83.06	-82.91	-83.41	-83.21	-83.32
7.900E+04	-88.86	-88.94	-88.86	-88.78	-88.77	-88.8	-89.01	-88.9	-88.95
1.004E+05	-88.61	-88.65	-88.66	-88.53	-88.57	-88.54	-88.73	-88.64	-88.75
1.256E+05	-88.38	-88.43	-88.28	-88.25	-88.28	-88.27	-88.5	-88.37	-88.47
1.584E+05	-88.05	-88.08	-87.92	-87.91	-87.93	-87.89	-88.11	-87.98	-88.06
1.986E+05	-87.64	-87.67	-87.46	-87.47	-87.48	-87.43	-87.68	-87.53	-87.63
2.524E+05	-87.09	-87.12	-86.85	-86.9	-86.91	-86.81	-87.1	-86.95	-87.03
3.155E+05	-86.47	-86.51	-86.14	-86.24	-86.23	-86.12	-86.43	-86.27	-86.36
3.980E+05	-85.67	-85.71	-85.24	-85.41	-85.39	-85.24	-85.59	-85.41	-85.5
5.055E+05	-84.69	-84.73	-84.17	-84.4	-84.37	-84.18	-84.57	-84.37	-84.47
6.278E+05	-83.69	-83.74	-83.05	-83.37	-83.32	-83.09	-83.52	-83.29	-83.39
7.969E+05	-88.97	-89	-88.91	-88.86	-88.93	-88.83	-89.03	-88.87	-88.9
9.983E+05	-88.78	-88.77	-88.66	-88.68	-88.69	-88.6	-88.73	-88.72	-88.69
1.266E+06	-88.45	-88.43	-88.34	-88.33	-88.35	-88.31	-88.48	-88.4	-88.33
1.578E+06	-88.13	-88.11	-87.95	-88.04	-88.03	-87.94	-88.13	-88.02	-87.99
1.976E+06	-87.75	-87.73	-87.49	-87.59	-87.6	-87.5	-87.68	-87.55	-87.53
2.528E+06	-87.18	-87.14	-86.86	-86.98	-86.99	-86.85	-87.08	-86.9	-86.93
3.171E+06	-86.54	-86.52	-86.16	-86.31	-86.31	-86.17	-86.4	-86.19	-86.21
3.984E+06	-85.75	-85.73	-85.27	-85.51	-85.5	-85.31	-85.58	-85.33	-85.35
5.016E+06	-84.82	-84.8	-84.26	-84.54	-84.53	-84.3	-84.61	-84.3	-84.35
6.328E+06	-83.75	-83.73	-83.07	-83.42	-83.4	-83.12	-83.46	-83.1	-83.17
8.016E+06	-89.02	-88.92	-88.9	-88.87	-88.95	-88.9	-88.95	-88.74	-88.68
1.008E+07	-88.86	-88.73	-88.68	-88.73	-88.73	-88.67	-88.74	-88.46	-88.5
1.261E+07	-88.62	-88.49	-88.43	-88.47	-88.49	-88.43	-88.49	-88.2	-88.22
1.589E+07	-88.32	-88.16	-88.05	-88.14	-88.16	-88.07	-88.14	-87.82	-87.85
2.002E+07	-87.93	-87.78	-87.6	-87.72	-87.73	-87.62	-87.72	-87.39	-87.43
2.517E+07	-87.44	-87.3	-87.04	-87.21	-87.2	-87.08	-87.2	-86.82	-86.91
3.164E+07	-86.86	-86.71	-86.36	-86.59	-86.57	-86.43	-86.57	-86.15	-86.27
3.989E+07	-86.14	-85.97	-85.52	-85.81	-85.79	-85.61	-85.79	-85.35	-85.49
5.020E+07	-85.28	-85.11	-84.54	-84.91	-84.87	-84.64	-84.88	-84.41	-84.57
6.314E+07	-84.32	-84.12	-83.4	-83.86	-83.81	-83.53	-83.82	-83.32	-83.52
7.945E+07	-89.72	-89.42	-89.31	-89.46	-89.46	-89.43	-89.46	-89.1	-89.22
1.001E+08	-89.67	-89.31	-89.18	-89.37	-89.33	-89.31	-89.33	-89.01	-89.14

Frequency vs. Impedance for HSS coating

Frequency (mHz)	impedance (ohm.cm2)								
	Day1-Sample1-	Day7-Sample1-	Day14-Sample1	Day1-Sample2-	Day7-Sample2	Day14-Sample2-	Day1-Sample3-	Day7-Sample3-i	Day14-Sample3-i
1.996E+01	3.70E+11	6.61E+11	1.54E+12	1.87E+12	2.09E+12	2.04E+12	2.61E+12	2.63E+12	3.244E+12
2.51E+01	3.15E+11	5.91E+11	1.30E+12	1.55E+12	1.70E+12	1.63E+12	2.08E+12	2.09E+12	2.60E+12
3.16E+01	2.74E+11	5.57E+11	1.08E+12	1.27E+12	1.38E+12	1.31E+12	1.68E+12	1.70E+12	2.10E+12
3.98E+01	2.49E+11	5.12E+11	8.99E+11	1.03E+12	1.12E+12	1.06E+12	1.36E+12	1.35E+12	1.68E+12
5.01E+01	2.34E+11	4.63E+11	7.43E+11	8.40E+11	9.02E+11	8.52E+11	1.09E+12	1.09E+12	1.35E+12
6.32E+01	2.20E+11	4.12E+11	6.07E+11	6.80E+11	7.26E+11	6.85E+11	8.76E+11	8.76E+11	1.08E+12
7.95E+01	2.09E+11	3.64E+11	4.97E+11	5.51E+11	5.83E+11	5.52E+11	7.04E+11	6.92E+11	8.54E+11
1.00E+02	1.98E+11	3.16E+11	4.04E+11	4.45E+11	4.68E+11	4.44E+11	5.60E+11	5.57E+11	6.80E+11
1.26E+02	1.84E+11	2.70E+11	3.27E+11	3.59E+11	3.76E+11	3.58E+11	4.50E+11	4.45E+11	5.41E+11
1.59E+02	1.66E+11	2.29E+11	2.65E+11	2.90E+11	3.02E+11	2.88E+11	3.62E+11	3.56E+11	4.31E+11
2.00E+02	1.48E+11	1.91E+11	2.13E+11	2.33E+11	2.42E+11	2.31E+11	2.88E+11	2.84E+11	3.42E+11
2.52E+02	1.29E+11	1.59E+11	1.72E+11	1.89E+11	1.94E+11	1.87E+11	2.30E+11	2.27E+11	2.73E+11
3.17E+02	1.11E+11	1.33E+11	1.39E+11	1.53E+11	1.56E+11	1.51E+11	1.86E+11	1.83E+11	2.19E+11
4.01E+02	9.40E+10	1.09E+11	1.12E+11	1.23E+11	1.25E+11	1.21E+11	1.49E+11	1.45E+11	1.74E+11
5.04E+02	7.95E+10	9.04E+10	9.05E+10	9.99E+10	1.01E+11	9.82E+10	1.21E+11	1.18E+11	1.40E+11
6.33E+02	6.69E+10	7.48E+10	7.35E+10	8.15E+10	8.19E+10	7.97E+10	9.80E+10	9.47E+10	1.13E+11
7.92E+02	5.36E+10	5.87E+10	5.73E+10	6.38E+10	6.37E+10	6.22E+10	7.69E+10	7.37E+10	8.82E+10
9.99E+02	4.40E+10	4.76E+10	4.58E+10	5.14E+10	5.09E+10	4.98E+10	6.18E+10	5.89E+10	7.04E+10
1.27E+03	3.57E+10	3.83E+10	3.64E+10	4.11E+10	4.04E+10	3.96E+10	4.92E+10	4.66E+10	5.58E+10
1.59E+03	2.92E+10	3.11E+10	2.93E+10	3.34E+10	3.25E+10	3.19E+10	3.97E+10	3.74E+10	4.49E+10
2.00E+03	2.37E+10	2.50E+10	2.34E+10	2.69E+10	2.60E+10	2.55E+10	3.18E+10	2.99E+10	3.59E+10
2.50E+03	1.93E+10	2.02E+10	1.88E+10	2.18E+10	2.09E+10	2.05E+10	2.55E+10	2.40E+10	2.88E+10
3.16E+03	1.56E+10	1.63E+10	1.51E+10	1.75E+10	1.67E+10	1.64E+10	2.05E+10	1.91E+10	2.30E+10
3.95E+03	1.27E+10	1.32E+10	1.22E+10	1.42E+10	1.35E+10	1.33E+10	1.65E+10	1.54E+10	1.86E+10
5.01E+03	1.01E+10	1.06E+10	9.72E+09	1.14E+10	1.08E+10	1.06E+10	1.32E+10	1.23E+10	1.48E+10
6.32E+03	8.20E+09	8.51E+09	7.83E+09	9.20E+09	8.69E+09	8.55E+09	1.06E+10	9.88E+09	1.19E+10
7.95E+03	6.35E+09	6.60E+09	6.04E+09	7.11E+09	6.70E+09	6.62E+09	8.16E+09	7.65E+09	9.20E+09
9.93E+03	5.11E+09	5.31E+09	4.87E+09	5.74E+09	5.40E+09	5.34E+09	6.55E+09	6.13E+09	7.39E+09
1.24E+04	4.12E+09	4.28E+09	3.92E+09	4.62E+09	4.35E+09	4.30E+09	5.26E+09	4.93E+09	5.94E+09
1.56E+04	3.28E+09	3.43E+09	3.14E+09	3.69E+09	3.48E+09	3.44E+09	4.19E+09	3.92E+09	4.74E+09
1.99E+04	2.59E+09	2.73E+09	2.48E+09	2.94E+09	2.77E+09	2.72E+09	3.31E+09	3.13E+09	3.76E+09
2.49E+04	2.09E+09	2.18E+09	1.99E+09	2.35E+09	2.22E+09	2.19E+09	2.65E+09	2.49E+09	3.01E+09
3.13E+04	1.68E+09	1.76E+09	1.60E+09	1.89E+09	1.79E+09	1.77E+09	2.13E+09	2.00E+09	2.42E+09
3.84E+04	1.38E+09	1.44E+09	1.31E+09	1.55E+09	1.47E+09	1.45E+09	1.74E+09	1.64E+09	1.98E+09
5.02E+04	1.07E+09	1.11E+09	1.01E+09	1.20E+09	1.15E+09	1.13E+09	1.35E+09	1.27E+09	1.54E+09
6.33E+04	8.62E+08	9.03E+08	8.18E+08	9.66E+08	9.23E+08	9.09E+08	1.08E+09	1.02E+09	1.24E+09
7.90E+04	6.74E+08	7.09E+08	6.39E+08	7.56E+08	7.22E+08	7.13E+08	8.41E+08	8.00E+08	9.66E+08
1.004E+05	5.34E+08	5.62E+08	5.05E+08	5.97E+08	5.72E+08	5.64E+08	6.63E+08	6.32E+08	7.634E+08
1.3E+05	4.30E+08	4.53E+08	4.05E+08	4.81E+08	4.61E+08	4.54E+08	5.32E+08	5.08E+08	6.1E+08
1.6E+05	3.44E+08	3.62E+08	3.23E+08	3.83E+08	3.68E+08	3.62E+08	4.23E+08	4.05E+08	4.9E+08
2.0E+05	2.76E+08	2.90E+08	2.59E+08	3.08E+08	2.96E+08	2.90E+08	3.38E+08	3.24E+08	3.9E+08
2.52E+05	2.19E+08	2.31E+08	2.05E+08	2.44E+08	2.35E+08	2.30E+08	2.67E+08	2.57E+08	3.09E+08
3.16E+05	1.77E+08	1.86E+08	1.65E+08	1.97E+08	1.89E+08	1.85E+08	2.15E+08	2.07E+08	2.49E+08
4.E+05	1.42E+08	1.49E+08	1.31E+08	1.58E+08	1.51E+08	1.48E+08	1.71E+08	1.65E+08	2.E+08
5.06E+05	1.13E+08	1.19E+08	1.05E+08	1.26E+08	1.21E+08	1.18E+08	1.36E+08	1.31E+08	1.58E+08
6.28E+05	9.27E+07	9.67E+07	8.52E+07	1.04E+08	9.84E+07	9.58E+07	1.11E+08	1.07E+08	1.29E+08
7.97E+05	7.18E+07	7.48E+07	6.56E+07	8.04E+07	7.55E+07	7.37E+07	8.52E+07	8.27E+07	9.91E+07
9.98E+05	5.75E+07	5.99E+07	5.24E+07	6.46E+07	6.04E+07	5.91E+07	6.80E+07	6.60E+07	7.92E+07
1.27E+06	4.57E+07	4.74E+07	4.14E+07	5.17E+07	4.80E+07	4.66E+07	5.37E+07	5.24E+07	5.35E+07
1.58E+06	3.68E+07	3.82E+07	3.33E+07	4.21E+07	3.87E+07	3.75E+07	4.33E+07	4.23E+07	4.31E+07
1.98E+06	2.96E+07	3.06E+07	2.67E+07	3.40E+07	3.10E+07	3.01E+07	3.47E+07	3.40E+07	3.45E+07
2.53E+06	2.34E+07	2.41E+07	2.10E+07	2.70E+07	2.44E+07	2.36E+07	2.73E+07	2.68E+07	2.71E+07
3.17E+06	1.88E+07	1.94E+07	1.68E+07	2.19E+07	1.96E+07	1.89E+07	2.19E+07	2.15E+07	2.17E+07
3.98E+06	1.51E+07	1.55E+07	1.35E+07	1.77E+07	1.57E+07	1.52E+07	1.75E+07	1.73E+07	1.74E+07
5.02E+06	1.21E+07	1.25E+07	1.08E+07	1.43E+07	1.26E+07	1.22E+07	1.41E+07	1.39E+07	1.39E+07
6.33E+06	9.75E+06	1.00E+07	8.66E+06	1.16E+07	1.02E+07	9.75E+06	1.13E+07	1.12E+07	1.12E+07
8.02E+06	7.53E+06	7.74E+06	6.67E+06	9.01E+06	7.84E+06	7.52E+06	8.73E+06	8.63E+06	8.61E+06
1.01E+07	6.02E+06	6.19E+06	5.32E+06	7.24E+06	6.27E+06	6.00E+06	6.98E+06	6.90E+06	6.87E+06
1.26E+07	4.83E+06	4.97E+06	4.26E+06	5.84E+06	5.05E+06	4.82E+06	5.60E+06	5.53E+06	5.50E+06
1.59E+07	3.85E+06	3.96E+06	3.39E+06	4.68E+06	4.04E+06	3.84E+06	4.46E+06	4.41E+06	4.38E+06
2.00E+07	3.07E+06	3.16E+06	2.70E+06	3.74E+06	3.23E+06	3.06E+06	3.56E+06	3.51E+06	3.49E+06
2.52E+07	2.46E+06	2.53E+06	2.16E+06	3.00E+06	2.59E+06	2.45E+06	2.84E+06	2.81E+06	2.78E+06
3.16E+07	1.97E+06	2.03E+06	1.72E+06	2.41E+06	2.08E+06	1.96E+06	2.27E+06	2.25E+06	2.22E+06
3.99E+07	1.57E+06	1.62E+06	1.38E+06	1.93E+06	1.67E+06	1.57E+06	1.82E+06	1.79E+06	1.77E+06
5.02E+07	1.26E+06	1.30E+06	1.10E+06	1.55E+06	1.34E+06	1.26E+06	1.45E+06	1.44E+06	1.42E+06
6.31E+07	1.01E+06	1.05E+06	8.86E+05	1.25E+06	1.08E+06	1.01E+06	1.17E+06	1.16E+06	1.14E+06
7.95E+07	7.85E+05	8.14E+05	6.87E+05	9.67E+05	8.40E+05	7.85E+05	9.08E+05	8.98E+05	8.86E+05
1.001E+08	6.25E+05	6.49E+05	5.47E+05	7.70E+05	6.70E+05	6.25E+05	7.23E+05	7.14E+05	7.04E+05

Frequency vs. Phase for HSS coating

Frequency (mHz)	Phase (°)								
	Day1-Sample1	Day7-Sample1	Day14-Sample1	Day1-Sample2	Day7-Sample2	Day14-Sample2	Day1-Sample3	Day7-Sample3	Day14-Sample3
1.996E+01	-56.26	-43.57	-64.78	-70.63	-78.75	-79.69	-83.33	-83.26	-84.55
2.51E+01	-54.31	-42.94	-66.99	-73.14	-80.29	-80.42	-84.74	-84.89	-86.33
3.16E+01	-51.67	-43.85	-69.48	-74.9	-80.76	-81.06	-85.08	-83.55	-84.61
3.98E+01	-48.16	-45.83	-71.61	-76.61	-81.58	-81.59	-85.15	-84.37	-85.03
5.01E+01	-45.4	-48.16	-73.08	-77.79	-82.28	-81.93	-84.37	-85.22	-85.55
6.32E+01	-43.77	-50.99	-74.85	-78.9	-82.86	-82.24	-85.89	-85.8	-86.83
7.95E+01	-43.57	-54.01	-76.44	-79.7	-83.26	-82.5	-85.61	-85.58	-86.41
1.00E+02	-44.64	-57.37	-78.09	-80.32	-83.7	-82.65	-84.66	-85.3	-85.4
1.26E+02	-47.06	-60.37	-78.8	-80.81	-83.89	-82.69	-85.41	-85.34	-86.56
1.59E+02	-49.87	-63.2	-79.51	-80.98	-83.95	-82.74	-84.95	-85.58	-86.39
2.00E+02	-52.94	-65.58	-80.32	-81.08	-83.87	-82.7	-84.8	-85.39	-85.93
2.52E+02	-56.01	-67.53	-80.59	-80.97	-83.6	-82.54	-84.08	-84.98	-85.69
3.17E+02	-58.81	-69.2	-80.95	-80.8	-83.27	-82.28	-83.44	-84.88	-84.75
4.01E+02	-61.2	-70.42	-80.74	-80.29	-82.67	-81.87	-82.85	-84.29	-84.45
5.04E+02	-63.31	-71.56	-80.56	-79.76	-82.11	-81.4	-81.96	-83.51	-83.96
6.33E+02	-65.08	-72.39	-80.22	-79.11	-81.38	-80.83	-81.18	-82.91	-83.28
7.92E+02	-71.97	-77.99	-85.18	-83.72	-86.4	-85.46	-85.7	-87.38	-87.46
9.99E+02	-73.9	-79.18	-85.35	-83.64	-86.23	-85.51	-85.69	-87.24	-87.34
1.27E+03	-75.63	-80.14	-85.37	-83.55	-86.09	-85.44	-85.66	-87.11	-87.18
1.59E+03	-76.98	-80.84	-85.3	-83.44	-85.89	-85.3	-85.57	-86.85	-86.95
2.00E+03	-78.09	-81.4	-85.1	-83.31	-85.55	-85.07	-85.43	-86.46	-86.61
2.50E+03	-78.89	-81.7	-84.81	-83.15	-85.08	-84.76	-85.21	-86.12	-86.2
3.16E+03	-79.47	-81.83	-84.38	-82.89	-84.52	-84.31	-84.96	-85.58	-85.67
3.95E+03	-79.8	-81.68	-83.83	-82.53	-83.85	-83.72	-84.54	-85	-85.09
5.01E+03	-79.59	-81.38	-83.1	-82.08	-83.02	-82.96	-83.94	-83.94	-84.31
6.32E+03	-79.47	-80.89	-82.28	-81.42	-81.96	-82.08	-83.25	-83.16	-83.4
7.95E+03	-84.9	-85.55	-86.99	-86.27	-86.87	-86.67	-87.78	-87.74	-87.69
9.93E+03	-85.16	-85.63	-86.82	-86.22	-86.66	-86.5	-87.72	-87.51	-87.47
1.24E+04	-85.32	-85.55	-86.69	-86.16	-86.37	-86.28	-87.58	-87.3	-87.31
1.56E+04	-85.31	-85.43	-86.42	-85.94	-85.98	-85.97	-87.5	-86.79	-87.02
1.99E+04	-85.25	-85.18	-86.12	-85.75	-85.5	-85.62	-87.07	-86.51	-86.87
2.49E+04	-84.85	-84.84	-85.73	-85.34	-84.93	-85.13	-86.75	-86.1	-86.18
3.13E+04	-84.38	-84.41	-85.25	-84.86	-84.32	-84.59	-86.3	-85.6	-85.71
3.84E+04	-83.81	-83.82	-84.67	-84.28	-83.68	-84.01	-85.77	-84.87	-85.17
5.02E+04	-82.52	-83.11	-84.02	-83.23	-82.4	-83.09	-84.79	-83.78	-83.96
6.33E+04	-82.07	-82.17	-82.96	-82.47	-81.64	-82.3	-84.03	-83.18	-83.38
7.90E+04	-86.72	-86.63	-87.67	-87.01	-86.64	-87	-88.45	-87.67	-87.74
1.004E+05	-86.48	-86.53	-87.54	-86.76	-86.5	-86.92	-88.29	-87.48	-87.61
1.3E+05	-86.26	-86.33	-87.37	-86.47	-86.35	-86.82	-88.07	-87.26	-87.43
1.6E+05	-85.94	-86.12	-87.12	-86.08	-86.12	-86.65	-87.8	-86.98	-87.2
2.0E+05	-85.57	-85.84	-86.8	-85.58	-85.82	-86.41	-87.46	-86.64	-86.9
2.52E+05	-85.07	-85.5	-86.36	-84.95	-85.41	-86.06	-87	-86.18	-86.52
3.16E+05	-84.54	-85.07	-85.87	-84.23	-84.91	-85.62	-86.48	-85.65	-86.05
4.E+05	-83.86	-84.51	-85.21	-83.34	-84.27	-85.03	-85.81	-84.97	-85.46
5.06E+05	-83.04	-83.79	-84.4	-82.27	-83.44	-84.27	-84.99	-84.13	-84.71
6.28E+05	-82.2	-83.04	-83.55	-81.2	-82.56	-83.47	-84.14	-83.25	-83.94
7.97E+05	-86.73	-87.39	-88.11	-85.44	-87.51	-87.99	-88.34	-87.61	-88.22
9.98E+05	-86.67	-87.27	-88.02	-85.05	-87.34	-87.89	-88.19	-87.37	-88.1
1.27E+06	-86.47	-87.12	-87.76	-84.66	-87.07	-87.71	-87.91	-87.08	-87.91
1.58E+06	-86.24	-86.87	-87.53	-84.28	-86.78	-87.45	-87.55	-86.74	-87.66
1.98E+06	-85.95	-86.55	-87.19	-83.86	-86.37	-87.11	-87.14	-86.35	-87.36
2.53E+06	-85.54	-86.11	-86.72	-83.4	-85.83	-86.62	-86.65	-85.89	-86.94
3.17E+06	-85.09	-85.6	-86.19	-82.91	-85.2	-86.07	-86.06	-85.4	-86.45
3.98E+06	-84.49	-84.98	-85.56	-82.35	-84.42	-85.39	-85.38	-84.81	-85.83
5.02E+06	-83.79	-84.22	-84.76	-81.69	-83.49	-84.56	-84.6	-84.11	-85.09
6.33E+06	-82.95	-83.33	-83.84	-80.97	-82.39	-83.61	-83.7	-83.28	-84.23
8.02E+06	-87.51	-87.59	-88.39	-85.63	-87.16	-88.08	-87.98	-87.75	-88.48
1.01E+07	-87.47	-87.43	-88.21	-85.69	-86.91	-87.88	-87.84	-87.65	-88.35
1.26E+07	-87.32	-87.27	-88.04	-85.73	-86.63	-87.65	-87.67	-87.53	-88.17
1.59E+07	-87.15	-87.04	-87.76	-85.71	-86.3	-87.36	-87.45	-87.34	-87.92
2.00E+07	-86.9	-86.75	-87.41	-85.64	-85.91	-87.01	-87.2	-87.07	-87.66
2.52E+07	-86.56	-86.39	-86.97	-85.48	-85.48	-86.58	-86.85	-86.71	-87.3
3.16E+07	-86.13	-85.94	-86.47	-85.23	-84.98	-86.07	-86.41	-86.26	-86.85
3.99E+07	-85.57	-85.4	-85.83	-84.86	-84.36	-85.44	-85.87	-85.7	-86.31
5.02E+07	-84.9	-84.74	-85.07	-84.36	-83.64	-84.7	-85.24	-85.02	-85.66
6.31E+07	-84.1	-83.98	-84.18	-83.72	-82.82	-83.82	-84.49	-84.23	-84.87
7.95E+07	-88.73	-88.38	-88.8	-88.47	-87.9	-88.55	-88.88	-88.78	-89.33
1.001E+08	-88.72	-88.37	-88.72	-88.59	-87.94	-88.53	-88.88	-88.75	-89.34

Frequency vs. Impedance for LE coating

Frequency (mHz)	impedance (ohm.cm2)								
	Day1-Sample1-	Day7-Sample1-	Day14-Sample1	Day1-Sample2-i	Day7-Sample2-i	Day14-Sample2-	Day1-Sample3-i	Day7-Sample3-in	Day14-Sample3-
1.996E+01	6.79E+11	5.68E+11	5.67E+11	4.70E+11	1.04E+11	4.65E+11	7.18E+11	4.97E+11	4.30E+11
2.51E+01	5.48E+11	4.57E+11	4.57E+11	3.81E+11	1.03E+11	3.75E+11	5.83E+11	4.02E+11	3.50E+11
3.16E+01	4.42E+11	3.68E+11	3.68E+11	3.11E+11	8.64E+10	3.02E+11	4.68E+11	3.24E+11	2.85E+11
3.98E+01	3.59E+11	2.96E+11	2.96E+11	2.53E+11	7.28E+10	2.43E+11	3.83E+11	2.61E+11	2.32E+11
5.01E+01	2.91E+11	2.38E+11	2.38E+11	2.06E+11	6.21E+10	1.95E+11	3.10E+11	2.11E+11	1.88E+11
6.32E+01	2.35E+11	1.91E+11	1.91E+11	1.67E+11	5.28E+10	1.57E+11	2.51E+11	1.71E+11	1.53E+11
7.95E+01	1.90E+11	1.54E+11	1.54E+11	1.36E+11	4.48E+10	1.26E+11	2.04E+11	1.38E+11	1.24E+11
1.00E+02	1.54E+11	1.24E+11	1.23E+11	1.10E+11	3.78E+10	1.01E+11	1.65E+11	1.11E+11	1.01E+11
1.26E+02	1.25E+11	9.93E+10	9.91E+10	8.96E+10	3.19E+10	8.16E+10	1.34E+11	8.98E+10	8.19E+10
1.59E+02	1.01E+11	7.97E+10	7.96E+10	7.28E+10	2.67E+10	6.55E+10	1.08E+11	7.23E+10	6.62E+10
2.00E+02	8.17E+10	6.40E+10	6.39E+10	5.93E+10	2.24E+10	5.27E+10	8.77E+10	5.82E+10	5.36E+10
2.52E+02	6.64E+10	5.16E+10	5.15E+10	4.84E+10	1.91E+10	4.24E+10	7.12E+10	4.70E+10	4.35E+10
3.17E+02	5.41E+10	4.16E+10	4.16E+10	3.97E+10	1.59E+10	3.43E+10	5.79E+10	3.81E+10	3.53E+10
4.01E+02	4.39E+10	3.35E+10	3.34E+10	3.24E+10	1.32E+10	2.72E+10	4.69E+10	3.07E+10	2.80E+10
5.04E+02	3.59E+10	2.63E+10	2.61E+10	2.59E+10	1.10E+10	2.18E+10	3.84E+10	2.43E+10	2.26E+10
6.33E+02	2.77E+10	2.12E+10	2.10E+10	2.11E+10	9.15E+09	1.76E+10	3.15E+10	1.96E+10	1.82E+10
7.92E+02	2.26E+10	1.71E+10	1.69E+10	1.73E+10	7.63E+09	1.42E+10	2.45E+10	1.58E+10	1.48E+10
9.99E+02	1.83E+10	1.37E+10	1.36E+10	1.40E+10	6.31E+09	1.14E+10	1.97E+10	1.27E+10	1.19E+10
1.27E+03	1.47E+10	1.09E+10	1.08E+10	1.13E+10	5.19E+09	9.08E+09	1.58E+10	1.01E+10	9.51E+09
1.59E+03	1.20E+10	8.81E+09	8.73E+09	9.27E+09	4.31E+09	7.34E+09	1.29E+10	8.19E+09	7.71E+09
2.00E+03	9.68E+09	7.07E+09	7.00E+09	7.52E+09	3.56E+09	5.90E+09	1.04E+10	6.57E+09	6.21E+09
2.50E+03	7.89E+09	5.71E+09	5.65E+09	6.14E+09	2.94E+09	4.77E+09	8.42E+09	5.31E+09	5.03E+09
3.16E+03	6.39E+09	4.59E+09	4.54E+09	4.99E+09	2.39E+09	3.84E+09	6.80E+09	4.27E+09	4.05E+09
3.95E+03	5.24E+09	3.73E+09	3.69E+09	4.09E+09	1.97E+09	3.13E+09	5.58E+09	3.47E+09	3.30E+09
5.01E+03	4.24E+09	3.00E+09	2.96E+09	3.32E+09	1.60E+09	2.44E+09	4.46E+09	2.71E+09	2.58E+09
6.32E+03	3.47E+09	2.33E+09	2.30E+09	2.60E+09	1.31E+09	1.96E+09	3.66E+09	2.17E+09	2.07E+09
7.95E+03	2.67E+09	1.87E+09	1.85E+09	2.11E+09	1.07E+09	1.58E+09	2.81E+09	1.74E+09	1.66E+09
9.93E+03	2.18E+09	1.51E+09	1.49E+09	1.71E+09	8.75E+08	1.28E+09	2.28E+09	1.41E+09	1.35E+09
1.24E+04	1.77E+09	1.22E+09	1.21E+09	1.40E+09	7.19E+08	1.04E+09	1.85E+09	1.14E+09	1.09E+09
1.56E+04	1.43E+09	9.84E+08	9.70E+08	1.13E+09	5.86E+08	8.34E+08	1.49E+09	9.12E+08	8.75E+08
1.99E+04	1.14E+09	7.82E+08	7.73E+08	9.08E+08	4.74E+08	6.65E+08	1.18E+09	7.26E+08	6.96E+08
2.49E+04	9.25E+08	6.33E+08	6.23E+08	7.41E+08	3.88E+08	5.39E+08	9.55E+08	5.85E+08	5.63E+08
3.13E+04	7.51E+08	5.12E+08	5.04E+08	6.05E+08	3.18E+08	4.37E+08	7.72E+08	4.73E+08	4.55E+08
3.84E+04	6.21E+08	4.23E+08	4.15E+08	5.04E+08	2.62E+08	3.61E+08	6.37E+08	3.89E+08	3.75E+08
5.02E+04	4.86E+08	3.31E+08	3.24E+08	4.00E+08	2.06E+08	2.83E+08	4.99E+08	3.04E+08	2.93E+08
6.33E+04	3.97E+08	2.59E+08	2.54E+08	3.30E+08	1.67E+08	2.22E+08	4.04E+08	2.37E+08	2.29E+08
7.90E+04	3.09E+08	2.11E+08	2.06E+08	2.61E+08	1.37E+08	1.80E+08	3.13E+08	1.92E+08	1.85E+08
1.004E+05	2.46E+08	1.68E+08	1.64E+08	2.11E+08	1.11E+08	1.44E+08	2.48E+08	1.52E+08	1.47E+08
1.3E+05	1.99E+08	1.36E+08	1.33E+08	1.74E+08	9.06E+07	1.17E+08	2.00E+08	1.23E+08	1.19E+08
1.6E+05	1.60E+08	1.09E+08	1.07E+08	1.43E+08	7.36E+07	9.40E+07	1.60E+08	9.83E+07	9.51E+07
2.0E+05	1.29E+08	8.85E+07	8.62E+07	1.17E+08	6.02E+07	7.61E+07	1.28E+08	7.92E+07	7.66E+07
2.52E+05	1.03E+08	7.08E+07	6.89E+07	9.56E+07	4.86E+07	6.10E+07	1.02E+08	6.30E+07	6.10E+07
3.16E+05	8.35E+07	5.76E+07	5.60E+07	7.89E+07	3.99E+07	4.97E+07	8.24E+07	5.11E+07	4.94E+07
4.E+05	6.73E+07	4.66E+07	4.52E+07	6.46E+07	3.26E+07	4.03E+07	6.61E+07	4.11E+07	3.98E+07
5.06E+05	5.40E+07	3.76E+07	3.64E+07	5.26E+07	2.58E+07	3.25E+07	5.28E+07	3.30E+07	3.19E+07
6.28E+05	4.44E+07	3.10E+07	3.00E+07	4.37E+07	2.13E+07	2.60E+07	4.33E+07	2.62E+07	2.53E+07
7.97E+05	3.40E+07	2.39E+07	2.31E+07	3.38E+07	1.71E+07	2.09E+07	3.29E+07	2.08E+07	2.02E+07
9.98E+05	2.74E+07	1.94E+07	1.87E+07	2.74E+07	1.40E+07	1.69E+07	2.64E+07	1.68E+07	1.63E+07
1.27E+06	2.19E+07	1.55E+07	1.50E+07	2.20E+07	1.13E+07	1.36E+07	2.10E+07	1.34E+07	1.30E+07
1.58E+06	1.77E+07	1.26E+07	1.22E+07	1.79E+07	9.28E+06	1.11E+07	1.69E+07	1.09E+07	1.05E+07
1.98E+06	1.43E+07	1.03E+07	9.89E+06	1.45E+07	7.58E+06	9.05E+06	1.35E+07	8.80E+06	8.52E+06
2.53E+06	1.13E+07	8.18E+06	7.87E+06	1.15E+07	6.09E+06	7.23E+06	1.07E+07	6.99E+06	6.77E+06
3.17E+06	9.08E+06	6.65E+06	6.39E+06	9.26E+06	4.98E+06	6.00E+06	8.56E+06	5.66E+06	5.48E+06
3.98E+06	7.32E+06	5.41E+06	5.20E+06	7.48E+06	4.08E+06	4.91E+06	6.88E+06	4.59E+06	4.45E+06
5.02E+06	5.90E+06	4.41E+06	4.23E+06	6.04E+06	3.34E+06	3.93E+06	5.54E+06	3.73E+06	3.62E+06
6.33E+06	4.77E+06	3.60E+06	3.45E+06	4.89E+06	2.65E+06	3.24E+06	4.46E+06	3.04E+06	2.95E+06
8.02E+06	3.65E+06	2.79E+06	2.68E+06	3.75E+06	2.14E+06	2.52E+06	3.40E+06	2.36E+06	2.28E+06
1.01E+07	2.93E+06	2.26E+06	2.17E+06	3.00E+06	1.74E+06	2.05E+06	2.72E+06	1.90E+06	1.85E+06
1.26E+07	2.35E+06	1.84E+06	1.77E+06	2.41E+06	1.42E+06	1.67E+06	2.18E+06	1.55E+06	1.50E+06
1.59E+07	1.88E+06	1.48E+06	1.43E+06	1.93E+06	1.15E+06	1.35E+06	1.73E+06	1.25E+06	1.22E+06
2.00E+07	1.50E+06	1.20E+06	1.16E+06	1.54E+06	9.35E+05	1.10E+06	1.38E+06	1.01E+06	9.85E+05
2.52E+07	1.20E+06	9.72E+05	9.39E+05	1.24E+06	7.60E+05	8.92E+05	1.11E+06	8.20E+05	8.00E+05
3.16E+07	9.63E+05	7.88E+05	7.63E+05	9.91E+05	6.19E+05	7.26E+05	8.85E+05	6.66E+05	6.51E+05
3.99E+07	7.71E+05	6.38E+05	6.19E+05	7.94E+05	5.04E+05	5.90E+05	7.09E+05	5.41E+05	5.30E+05
5.02E+07	6.20E+05	5.18E+05	5.04E+05	6.39E+05	4.12E+05	4.82E+05	5.70E+05	4.41E+05	4.32E+05
6.31E+07	5.01E+05	4.23E+05	4.12E+05	5.17E+05	3.39E+05	3.95E+05	4.60E+05	3.61E+05	3.55E+05
7.95E+07	3.86E+05	3.29E+05	3.21E+05	3.97E+05	2.65E+05	3.08E+05	3.53E+05	2.81E+05	2.77E+05
1.001E+08	3.07E+05	2.64E+05	2.59E+05	3.17E+05	2.15E+05	2.49E+05	2.81E+05	2.26E+05	2.24E+05

Frequency vs. Phase for LE coating

Frequency (mHz)	Phase (º)								
	Day1-Sample1	Day7-Sample1	Day14-Sample1P	Day1-Sample2	Day7-Sample2-	Day14-Sample2-	Day1-Sample3-	Day7-Sample3-	Day14-Sample3-I
1.996E+01	-82.97	-84.02	-84.72	-79.16	-51.49	-83.71	-81.7	-82.42	-78.58
2.51E+01	-83.23	-84.23	-84.62	-79.39	-57.51	-83.86	-81.57	-82.38	-79.18
3.16E+01	-82.5	-84.08	-84.7	-79.6	-56.94	-83.97	-81.81	-82.61	-79.42
3.98E+01	-82.49	-84.32	-84.6	-79.77	-58.31	-84.02	-81.54	-82.67	-79.86
5.01E+01	-82.46	-84.46	-84.6	-79.69	-59.47	-84.11	-81.68	-82.65	-80.01
6.32E+01	-82.13	-84.39	-84.47	-79.52	-60.78	-84.13	-81.6	-82.79	-80.33
7.95E+01	-81.9	-84.35	-84.25	-79.38	-62	-83.96	-81.64	-82.82	-80.46
1.00E+02	-81.66	-84.21	-84.26	-79.1	-62.9	-83.89	-81.29	-82.8	-80.58
1.26E+02	-81.29	-84.05	-84.11	-78.82	-63.81	-83.64	-81.1	-82.62	-80.6
1.59E+02	-80.83	-83.7	-83.84	-78.38	-66.5	-83.32	-80.8	-82.47	-80.63
2.00E+02	-80.43	-83.35	-83.49	-77.9	-67.78	-82.9	-80.46	-82.17	-80.42
2.52E+02	-79.87	-82.84	-83.02	-77.25	-69.95	-82.35	-79.91	-81.78	-80.12
3.17E+02	-79.17	-82.2	-82.42	-76.54	-70.36	-81.67	-79.25	-81.17	-79.69
4.01E+02	-78.36	-81.36	-81.69	-75.7	-70.84	-85.09	-78.53	-80.48	-83.22
5.04E+02	-77.45	-85.44	-85.51	-79.97	-71.27	-84.99	-77.53	-84.6	-83.3
6.33E+02	-82.23	-85.32	-85.4	-80	-71.75	-84.86	-76.58	-84.5	-83.33
7.92E+02	-82.04	-85.16	-85.26	-79.96	-72.15	-84.68	-82.69	-84.48	-83.33
9.99E+02	-81.8	-84.92	-85.05	-79.88	-72.55	-84.41	-82.51	-84.34	-83.25
1.27E+03	-81.47	-84.6	-84.75	-79.74	-72.87	-84.07	-82.32	-84.11	-83.08
1.59E+03	-81.12	-84.23	-84.41	-79.54	-73.1	-83.64	-82.02	-83.83	-82.84
2.00E+03	-80.71	-83.75	-83.93	-79.2	-73.24	-83.11	-81.62	-83.42	-82.49
2.50E+03	-80.18	-83.17	-83.41	-78.74	-73.25	-82.49	-81.19	-82.92	-82.04
3.16E+03	-79.55	-82.42	-82.7	-78.13	-76.54	-81.69	-80.52	-82.28	-81.49
3.95E+03	-78.83	-81.58	-81.91	-77.39	-76.95	-80.8	-79.95	-81.52	-80.77
5.01E+03	-77.89	-80.56	-80.95	-76.41	-77.34	-84.81	-78.92	-85.53	-84.82
6.32E+03	-76.87	-85.27	-85.5	-81.5	-77.62	-84.58	-77.95	-85.42	-84.74
7.95E+03	-82.85	-85.05	-85.28	-81.29	-77.81	-84.31	-84.28	-85.28	-84.65
9.93E+03	-82.74	-84.74	-85.03	-81.04	-77.92	-84	-84.09	-85.09	-84.49
1.24E+04	-82.6	-84.38	-84.72	-80.71	-77.9	-83.64	-83.9	-84.84	-84.3
1.56E+04	-82.37	-83.93	-84.28	-80.19	-77.77	-83.19	-83.79	-84.5	-83.99
1.99E+04	-82.08	-83.4	-83.77	-79.49	-77.52	-82.64	-83.39	-84.06	-83.59
2.49E+04	-81.56	-82.67	-83.14	-78.66	-77.07	-81.97	-82.92	-83.49	-83.05
3.13E+04	-81	-81.89	-82.4	-77.69	-76.52	-81.2	-82.32	-82.81	-82.41
3.84E+04	-80.38	-81.05	-81.6	-76.64	-79.83	-80.38	-81.69	-82.06	-81.68
5.02E+04	-79.55	-79.88	-80.48	-75.19	-79.9	-79.17	-80.61	-80.92	-80.49
6.33E+04	-78.33	-84.45	-84.9	-73.45	-79.76	-83.91	-79.5	-85.76	-85.41
7.90E+04	-84.35	-84.18	-84.64	-79.18	-79.65	-83.64	-85.87	-85.56	-85.26
1.004E+05	-84.26	-83.83	-84.32	-78.68	-79.47	-83.29	-85.77	-85.3	-85.03
1.3E+05	-84.08	-83.47	-83.95	-78.24	-79.24	-82.9	-85.59	-84.96	-84.74
1.6E+05	-83.82	-83.02	-83.5	-77.86	-78.92	-82.4	-85.33	-84.54	-84.35
2.0E+05	-83.47	-82.49	-82.98	-77.54	-78.53	-81.81	-84.96	-84.02	-83.87
2.52E+05	-82.97	-81.82	-82.31	-77.22	-77.99	-81.06	-84.44	-83.34	-83.23
3.16E+05	-82.36	-81.07	-81.57	-76.93	-77.36	-80.21	-83.81	-82.56	-82.5
4.E+05	-81.58	-80.14	-80.65	-76.57	-76.56	-79.18	-82.98	-81.59	-81.56
5.06E+05	-80.61	-79.01	-79.54	-76.09	-80.48	-77.95	-81.95	-80.41	-80.42
6.28E+05	-79.61	-77.86	-78.4	-75.55	-80.37	-82.62	-80.87	-85.18	-85.16
7.97E+05	-85.49	-83.39	-83.79	-82.03	-80.22	-82.27	-87.15	-84.86	-84.81
9.98E+05	-85.32	-83.1	-83.45	-82.36	-80	-81.87	-86.94	-84.48	-84.45
1.27E+06	-85.15	-82.69	-83.05	-82.55	-79.73	-81.42	-86.7	-84	-83.97
1.58E+06	-84.9	-82.26	-82.58	-82.67	-79.39	-80.93	-86.37	-83.5	-83.46
1.98E+06	-84.58	-81.72	-82.04	-82.68	-78.97	-80.37	-85.96	-82.87	-82.83
2.53E+06	-84.12	-81.01	-81.32	-82.5	-78.39	-79.77	-85.36	-82.06	-81.99
3.17E+06	-83.55	-80.26	-80.51	-82.17	-77.75	-78	-84.67	-81.18	-81.11
3.98E+06	-82.82	-79.36	-79.57	-81.65	-76.97	-76.82	-83.8	-80.14	-80.04
5.02E+06	-81.93	-78.32	-78.48	-80.93	-76.04	-77.07	-82.77	-78.93	-78.81
6.33E+06	-80.88	-77.14	-77.25	-80.02	-80.72	-75.64	-81.55	-77.56	-77.42
8.02E+06	-86.73	-82.77	-82.64	-86.06	-80.63	-81.4	-87.75	-83.16	-82.87
1.01E+07	-86.61	-82.58	-82.35	-86.05	-80.49	-81.19	-87.54	-82.82	-82.45
1.26E+07	-86.47	-82.38	-82.07	-85.94	-80.3	-80.96	-87.26	-82.43	-81.99
1.59E+07	-86.2	-82.13	-81.74	-85.76	-80.05	-80.7	-86.92	-81.99	-81.5
2.00E+07	-85.85	-81.82	-81.35	-85.5	-79.69	-80.35	-86.48	-81.5	-80.96
2.52E+07	-85.4	-81.43	-80.91	-85.08	-79.22	-79.93	-85.91	-80.95	-80.36
3.16E+07	-84.82	-80.95	-80.37	-84.55	-78.63	-79.39	-85.22	-80.3	-79.67
3.99E+07	-84.08	-80.33	-79.72	-83.85	-77.87	-78.72	-84.36	-79.54	-78.88
5.02E+07	-83.19	-79.58	-78.94	-82.99	-76.93	-77.91	-83.32	-78.63	-77.94
6.31E+07	-82.1	-78.66	-78	-81.94	-75.85	-76.94	-82.1	-77.59	-76.88
7.95E+07	-88.04	-84.67	-83.84	-87.96	-81.62	-83.06	-88.45	-83.73	-82.89
1.001E+08	-87.97	-84.78	-83.92	-87.94	-81.59	-83.16	-88.32	-83.77	-82.92

Frequency vs. Impedance for PU coating

Frequency (mHz)	impedance (ohm.cm2)								
	Day1-Sample1	Day7-Sample1	Day14-Sample1	Day1-Sample2	Day7-Sample2	Day14-Sample2	Day1-Sample3	Day7-Sample3	Day14-Sample3
1.996E+01	2.11E+11	1.15E+11	6.80E+10	4.44E+11	3.27E+11	2.57E+11	2.93E+11	1.05E+11	7.65E+10
2.51E+01	1.87E+11	1.05E+11	6.46E+10	3.83E+11	2.82E+11	2.25E+11	2.46E+11	9.48E+10	7.07E+10
3.16E+01	1.64E+11	9.52E+10	6.13E+10	3.29E+11	2.44E+11	1.97E+11	2.06E+11	8.49E+10	6.47E+10
3.98E+01	1.42E+11	8.53E+10	5.79E+10	2.82E+11	2.09E+11	1.71E+11	1.72E+11	7.54E+10	5.88E+10
5.01E+01	1.23E+11	7.58E+10	5.38E+10	2.40E+11	1.78E+11	1.48E+11	1.43E+11	6.66E+10	5.30E+10
6.32E+01	1.06E+11	6.67E+10	4.94E+10	2.03E+11	1.51E+11	1.27E+11	1.19E+11	5.84E+10	4.75E+10
7.95E+01	9.18E+10	5.85E+10	4.48E+10	1.72E+11	1.28E+11	1.09E+11	9.90E+10	5.11E+10	4.23E+10
1.00E+02	7.87E+10	5.08E+10	4.01E+10	1.45E+11	1.08E+11	9.30E+10	8.17E+10	4.43E+10	3.72E+10
1.26E+02	6.73E+10	4.39E+10	3.55E+10	1.22E+11	9.06E+10	7.89E+10	6.76E+10	3.83E+10	3.26E+10
1.59E+02	5.72E+10	3.77E+10	3.10E+10	1.02E+11	7.59E+10	6.66E+10	5.56E+10	3.29E+10	2.83E+10
2.00E+02	4.85E+10	3.23E+10	2.65E+10	8.48E+10	6.34E+10	5.61E+10	4.57E+10	2.83E+10	2.44E+10
2.52E+02	4.11E+10	2.68E+10	2.28E+10	7.07E+10	5.30E+10	4.72E+10	3.76E+10	2.40E+10	2.10E+10
3.17E+02	3.47E+10	2.27E+10	1.95E+10	5.88E+10	4.43E+10	3.96E+10	3.10E+10	2.04E+10	1.79E+10
4.01E+02	2.76E+10	1.91E+10	1.66E+10	4.86E+10	3.69E+10	3.32E+10	2.50E+10	1.72E+10	1.51E+10
5.04E+02	2.30E+10	1.61E+10	1.40E+10	4.04E+10	3.08E+10	2.67E+10	2.04E+10	1.46E+10	1.28E+10
6.33E+02	1.91E+10	1.36E+10	1.18E+10	3.13E+10	2.45E+10	2.22E+10	1.66E+10	1.23E+10	1.08E+10
7.92E+02	1.59E+10	1.14E+10	1.00E+10	2.57E+10	2.03E+10	1.84E+10	1.36E+10	1.03E+10	9.08E+09
9.99E+02	1.32E+10	9.55E+09	8.36E+09	2.09E+10	1.66E+10	1.51E+10	1.10E+10	8.63E+09	7.57E+09
1.27E+03	1.08E+10	7.94E+09	6.94E+09	1.69E+10	1.35E+10	1.24E+10	8.84E+09	7.15E+09	6.28E+09
1.59E+03	8.97E+09	6.66E+09	5.81E+09	1.38E+10	1.11E+10	1.02E+10	7.20E+09	5.98E+09	5.25E+09
2.00E+03	7.38E+09	5.55E+09	4.83E+09	1.12E+10	9.06E+09	8.33E+09	5.82E+09	4.95E+09	4.35E+09
2.50E+03	6.09E+09	4.64E+09	4.02E+09	9.12E+09	7.42E+09	6.84E+09	4.73E+09	4.11E+09	3.62E+09
3.16E+03	5.00E+09	3.86E+09	3.33E+09	7.38E+09	6.03E+09	5.59E+09	3.82E+09	3.39E+09	2.99E+09
3.95E+03	4.14E+09	3.24E+09	2.72E+09	6.03E+09	4.96E+09	4.60E+09	3.12E+09	2.82E+09	2.45E+09
5.01E+03	3.39E+09	2.59E+09	2.22E+09	4.86E+09	4.02E+09	3.74E+09	2.45E+09	2.25E+09	2.00E+09
6.32E+03	2.66E+09	2.14E+09	1.82E+09	3.95E+09	3.28E+09	3.07E+09	1.97E+09	1.84E+09	1.64E+09
7.95E+03	2.17E+09	1.76E+09	1.50E+09	3.04E+09	2.54E+09	2.38E+09	1.59E+09	1.50E+09	1.34E+09
9.93E+03	1.77E+09	1.45E+09	1.24E+09	2.45E+09	2.06E+09	1.94E+09	1.29E+09	1.23E+09	1.11E+09
1.24E+04	1.45E+09	1.20E+09	1.02E+09	1.98E+09	1.67E+09	1.58E+09	1.05E+09	1.01E+09	9.12E+08
1.56E+04	1.18E+09	9.79E+08	8.32E+08	1.59E+09	1.35E+09	1.27E+09	8.49E+08	8.19E+08	7.45E+08
1.99E+04	9.52E+08	7.92E+08	6.75E+08	1.26E+09	1.08E+09	1.02E+09	6.83E+08	6.58E+08	6.03E+08
2.49E+04	7.77E+08	6.49E+08	5.52E+08	1.02E+09	8.67E+08	8.26E+08	5.57E+08	5.36E+08	4.93E+08
3.13E+04	6.35E+08	5.32E+08	4.53E+08	8.21E+08	7.02E+08	6.70E+08	4.57E+08	4.36E+08	4.04E+08
3.84E+04	5.28E+08	4.43E+08	3.77E+08	6.75E+08	5.78E+08	5.54E+08	3.82E+08	3.62E+08	3.37E+08
5.02E+04	4.17E+08	3.51E+08	3.00E+08	5.26E+08	4.50E+08	4.32E+08	3.05E+08	2.85E+08	2.60E+08
6.33E+04	3.41E+08	2.75E+08	2.35E+08	4.25E+08	3.66E+08	3.52E+08	2.42E+08	2.23E+08	2.10E+08
7.90E+04	2.67E+08	2.25E+08	1.92E+08	3.29E+08	2.84E+08	2.74E+08	1.99E+08	1.81E+08	1.71E+08
1.004E+05	2.13E+08	1.80E+08	1.54E+08	2.60E+08	2.25E+08	2.18E+08	1.61E+08	1.45E+08	1.37E+08
1.3E+05	1.73E+08	1.47E+08	1.25E+08	2.10E+08	1.82E+08	1.75E+08	1.31E+08	1.17E+08	1.12E+08
1.6E+05	1.39E+08	1.18E+08	1.01E+08	1.67E+08	1.45E+08	1.40E+08	1.06E+08	9.40E+07	8.99E+07
2.0E+05	1.12E+08	9.58E+07	8.18E+07	1.34E+08	1.17E+08	1.13E+08	8.62E+07	7.58E+07	7.28E+07
2.52E+05	8.98E+07	7.68E+07	6.55E+07	1.06E+08	9.26E+07	8.98E+07	6.90E+07	6.05E+07	5.82E+07
3.16E+05	7.28E+07	6.25E+07	5.32E+07	8.57E+07	7.47E+07	7.26E+07	5.60E+07	4.90E+07	4.73E+07
4.E+05	5.87E+07	5.05E+07	4.30E+07	6.86E+07	5.99E+07	5.83E+07	4.51E+07	3.94E+07	3.81E+07
5.06E+05	4.71E+07	4.07E+07	3.46E+07	5.47E+07	4.79E+07	4.66E+07	3.61E+07	3.16E+07	3.06E+07
6.28E+05	3.87E+07	3.35E+07	2.75E+07	4.48E+07	3.92E+07	3.82E+07	2.96E+07	2.51E+07	2.43E+07
7.97E+05	2.96E+07	2.57E+07	2.19E+07	3.40E+07	2.99E+07	2.91E+07	2.27E+07	1.99E+07	1.93E+07
9.98E+05	2.39E+07	2.07E+07	1.77E+07	2.74E+07	2.40E+07	2.34E+07	1.82E+07	1.60E+07	1.56E+07
1.27E+06	1.89E+07	1.65E+07	1.41E+07	2.17E+07	1.90E+07	1.86E+07	1.44E+07	1.27E+07	1.24E+07
1.58E+06	1.53E+07	1.34E+07	1.14E+07	1.75E+07	1.54E+07	1.50E+07	1.16E+07	1.03E+07	1.00E+07
1.98E+06	1.24E+07	1.08E+07	9.20E+06	1.40E+07	1.23E+07	1.20E+07	9.34E+06	8.26E+06	8.08E+06
2.53E+06	9.75E+06	8.57E+06	7.28E+06	1.10E+07	9.70E+06	9.49E+06	7.35E+06	6.52E+06	6.39E+06
3.17E+06	7.85E+06	6.92E+06	5.88E+06	8.85E+06	7.79E+06	7.63E+06	5.90E+06	5.25E+06	5.15E+06
3.98E+06	6.32E+06	5.59E+06	4.74E+06	7.11E+06	6.26E+06	6.13E+06	4.74E+06	4.22E+06	4.15E+06
5.02E+06	5.10E+06	4.52E+06	3.83E+06	5.71E+06	5.04E+06	4.94E+06	3.81E+06	3.40E+06	3.35E+06
6.33E+06	4.12E+06	3.66E+06	3.10E+06	4.60E+06	4.06E+06	3.98E+06	3.07E+06	2.65E+06	2.62E+06
8.02E+06	3.15E+06	2.81E+06	2.39E+06	3.52E+06	3.11E+06	3.05E+06	2.36E+06	2.11E+06	2.08E+06
1.01E+07	2.52E+06	2.26E+06	1.92E+06	2.81E+06	2.49E+06	2.44E+06	1.88E+06	1.69E+06	1.67E+06
1.26E+07	2.03E+06	1.82E+06	1.54E+06	2.26E+06	2.00E+06	1.96E+06	1.51E+06	1.36E+06	1.35E+06
1.59E+07	1.62E+06	1.46E+06	1.24E+06	1.80E+06	1.59E+06	1.56E+06	1.21E+06	1.09E+06	1.08E+06
2.00E+07	1.30E+06	1.17E+06	9.90E+05	1.44E+06	1.27E+06	1.25E+06	9.63E+05	8.70E+05	8.63E+05
2.52E+07	1.04E+06	9.43E+05	7.96E+05	1.15E+06	1.02E+06	9.99E+05	7.71E+05	6.98E+05	6.93E+05
3.16E+07	8.35E+05	7.60E+05	6.41E+05	9.22E+05	8.17E+05	8.01E+05	6.19E+05	5.61E+05	5.58E+05
3.99E+07	6.70E+05	6.12E+05	5.15E+05	7.39E+05	6.55E+05	6.42E+05	4.96E+05	4.50E+05	4.49E+05
5.02E+07	5.40E+05	4.95E+05	4.16E+05	5.94E+05	5.27E+05	5.17E+05	3.99E+05	3.63E+05	3.62E+05
6.31E+07	4.37E+05	4.02E+05	3.38E+05	4.80E+05	4.26E+05	4.19E+05	3.23E+05	2.94E+05	2.94E+05
7.95E+07	3.37E+05	3.11E+05	2.62E+05	3.70E+05	3.29E+05	3.22E+05	2.49E+05	2.27E+05	2.27E+05
1.001E+08	2.69E+05	2.49E+05	2.10E+05	2.95E+05	2.62E+05	2.57E+05	1.98E+05	1.81E+05	1.81E+05

Frequency vs. Phase for PU coating

Frequency (mHz)	Phase (°)								
	Day1-Sample1-P	Day7-Sample1-P	Day14-Sample1P	Day1-Sample2	Day7-Sample2-	Day14-Sample2-P	Day1-Sample3-P	Day7-Sample3-P	Day14-Sample3-P
1.996E+01	-46.45	-36.25	-34	-54.42	-52.94	-45.72	-67.49	-36.7	-29.62
2.51E+01	-48.85	-38.97	-34.78	-56.36	-55.09	-48.14	-68.52	-39.52	-32.27
3.16E+01	-51.05	-41.6	-35.98	-58.28	-57.15	-50.62	-69.45	-42.2	-34.99
3.98E+01	-52.99	-44.24	-37.65	-60.16	-59.03	-52.9	-70.31	-44.71	-37.7
5.01E+01	-54.82	-46.7	-39.62	-61.97	-60.74	-55.05	-71.04	-47.09	-40.4
6.32E+01	-56.39	-48.98	-41.94	-63.31	-62.28	-57.02	-71.83	-49.3	-43.06
7.95E+01	-57.96	-51.21	-44.35	-64.68	-63.7	-58.84	-72.6	-51.36	-45.63
1.00E+02	-59.55	-53.14	-46.81	-66.04	-64.89	-60.56	-73.15	-53.18	-48.09
1.26E+02	-60.78	-54.87	-49.1	-67.13	-65.92	-62.04	-73.76	-54.78	-50.32
1.59E+02	-61.98	-56.39	-51.28	-68.15	-66.84	-63.24	-74.18	-56.23	-52.43
2.00E+02	-63.05	-57.66	-55.61	-69.17	-67.58	-64.32	-74.55	-57.53	-56.44
2.52E+02	-63.92	-61.79	-57.81	-69.94	-68.16	-65.28	-74.77	-61.17	-58.58
3.17E+02	-64.61	-63.13	-59.79	-70.54	-68.56	-65.94	-74.76	-62.65	-60.58
4.01E+02	-69.57	-64.37	-61.66	-70.95	-68.78	-66.42	-78.57	-64.11	-62.44
5.04E+02	-70.56	-65.47	-63.33	-71.24	-68.87	-71.66	-79.12	-65.44	-64.1
6.33E+02	-71.4	-66.41	-64.81	-76.99	-74.68	-72.67	-79.59	-66.67	-65.57
7.92E+02	-72.13	-67.21	-66.1	-77.74	-75.39	-73.5	-79.95	-67.78	-66.84
9.99E+02	-72.78	-67.91	-67.26	-78.41	-76.06	-74.3	-80.25	-68.83	-67.98
1.27E+03	-73.32	-68.49	-68.26	-78.94	-76.63	-74.99	-80.45	-69.77	-68.94
1.59E+03	-73.71	-68.9	-69.03	-79.33	-77.06	-75.47	-80.5	-70.55	-69.66
2.00E+03	-73.98	-69.2	-69.64	-79.57	-77.36	-75.84	-80.38	-71.22	-70.23
2.50E+03	-74.12	-69.36	-70.05	-79.64	-77.48	-76.02	-80.09	-71.69	-70.58
3.16E+03	-74.08	-69.41	-70.31	-79.54	-77.47	-76.05	-79.6	-72.07	-70.77
3.95E+03	-73.87	-69.33	-74.34	-79.27	-77.28	-75.97	-78.99	-72.19	-74.81
5.01E+03	-73.39	-74.27	-75.02	-78.82	-76.88	-75.59	-82.84	-76.95	-75.48
6.32E+03	-78.78	-74.92	-75.61	-78.15	-76.31	-74.95	-82.69	-77.65	-76.02
7.95E+03	-79.06	-75.56	-76.13	-84.25	-82.52	-81.27	-82.36	-78.25	-76.52
9.93E+03	-79.24	-76.11	-76.55	-84.36	-82.74	-81.52	-81.87	-78.74	-76.89
1.24E+04	-79.29	-76.58	-76.9	-84.38	-82.89	-81.71	-81.4	-79.14	-77.21
1.56E+04	-79.29	-76.99	-77.17	-84.39	-82.9	-81.79	-80.81	-79.4	-77.4
1.99E+04	-79.14	-77.18	-77.27	-84.1	-82.77	-81.52	-79.91	-79.53	-77.5
2.49E+04	-78.89	-77.19	-77.3	-83.79	-82.55	-81.5	-79.01	-79.48	-77.43
3.13E+04	-78.54	-77.03	-77.18	-83.32	-82.17	-81.15	-78.07	-79.27	-77.24
3.84E+04	-78.09	-76.72	-76.95	-82.79	-81.66	-80.66	-77.2	-78.95	-76.92
5.02E+04	-77.41	-75.96	-76.43	-82.05	-80.78	-79.72	-76.05	-78.28	-81.4
6.33E+04	-76.56	-81.43	-81.45	-80.82	-79.9	-78.95	-80.84	-83.38	-81.63
7.90E+04	-82.79	-81.59	-81.67	-86.67	-85.81	-85.02	-80.97	-83.54	-81.88
1.004E+05	-82.92	-81.71	-81.84	-86.54	-85.75	-85.04	-81.19	-83.64	-82.06
1.3E+05	-82.98	-81.73	-81.92	-86.37	-85.64	-84.94	-81.43	-83.65	-82.16
1.6E+05	-82.93	-81.67	-81.92	-86.11	-85.43	-84.77	-81.67	-83.57	-82.16
2.0E+05	-82.77	-81.51	-81.82	-85.74	-85.12	-84.49	-81.85	-83.37	-82.05
2.52E+05	-82.46	-81.21	-81.58	-85.24	-84.66	-84.06	-81.92	-83.03	-81.79
3.16E+05	-82.01	-80.78	-81.2	-84.63	-84.1	-83.51	-81.82	-82.56	-81.39
4.E+05	-81.38	-80.18	-80.65	-83.84	-83.35	-82.78	-81.5	-81.92	-80.79
5.06E+05	-80.54	-79.37	-79.9	-82.85	-82.4	-81.85	-80.94	-81.07	-79.98
6.28E+05	-79.65	-78.48	-84.65	-81.84	-81.42	-80.86	-80.25	-85.95	-85.01
7.97E+05	-85.57	-84.49	-84.7	-87.51	-87.06	-86.69	-86.04	-85.87	-85.11
9.98E+05	-85.5	-84.42	-84.58	-87.3	-86.88	-86.54	-86.15	-85.78	-85.02
1.27E+06	-85.35	-84.27	-84.44	-87	-86.63	-86.33	-86.08	-85.61	-84.89
1.58E+06	-85.15	-84.03	-84.26	-86.68	-86.34	-86.05	-85.92	-85.36	-84.65
1.98E+06	-84.81	-83.72	-83.95	-86.25	-85.95	-85.65	-85.63	-85.02	-84.3
2.53E+06	-84.33	-83.21	-83.48	-85.66	-85.36	-85.08	-85.15	-84.5	-83.78
3.17E+06	-83.74	-82.59	-82.92	-84.99	-84.72	-84.42	-84.55	-83.89	-83.14
3.98E+06	-82.98	-81.81	-82.22	-84.16	-83.9	-83.6	-83.81	-83.1	-82.33
5.02E+06	-82.05	-80.85	-81.34	-83.16	-82.93	-82.61	-82.86	-82.13	-81.35
6.33E+06	-80.96	-79.71	-80.31	-82.01	-81.79	-81.45	-81.75	-86.72	-86.16
8.02E+06	-86.66	-85.46	-85.72	-87.59	-87.35	-87.18	-87.3	-86.57	-86.02
1.01E+07	-86.46	-85.24	-85.54	-87.34	-87.14	-86.96	-87.1	-86.36	-85.82
1.26E+07	-86.26	-84.98	-85.3	-87.08	-86.83	-86.71	-86.84	-86.08	-85.55
1.59E+07	-85.94	-84.65	-85	-86.72	-86.51	-86.34	-86.52	-85.75	-85.22
2.00E+07	-85.52	-84.24	-84.57	-86.27	-86.08	-85.9	-86.1	-85.33	-84.8
2.52E+07	-85	-83.74	-84.06	-85.72	-85.54	-85.35	-85.58	-84.82	-84.31
3.16E+07	-84.38	-83.14	-83.4	-85.06	-84.9	-84.68	-84.97	-84.2	-83.67
3.99E+07	-83.61	-82.4	-82.6	-84.27	-84.13	-83.87	-84.2	-83.43	-82.9
5.02E+07	-82.67	-81.52	-81.64	-83.31	-83.19	-82.89	-83.27	-82.48	-81.95
6.31E+07	-81.57	-80.48	-80.51	-82.18	-82.09	-81.73	-82.19	-81.39	-80.88
7.95E+07	-87.44	-86.47	-85.98	-87.94	-87.84	-87.65	-87.97	-87.2	-86.93
1.001E+08	-87.35	-86.47	-85.82	-87.82	-87.76	-87.53	-87.89	-87.1	-86.9

Frequency vs. Impedance for 3p/2p CAT coating

| Frequency (mHz)	impedance (ohm.cm2)								
	Day1-Sample1	Day7-Sample1-	Day14-Sample1	Day1-Sample2	Day7-Sample2-	Day14-Sample2-	Day1-Sample3-	Day7-Sample3-i	Day14-Sample3-
1.996E+01	2.83E+12	2.47E+12	2.25E+12	2.37E+12	2.45E+12	2.12E+12	2.16E+12	2.04E+12	2.42E+12
2.51E+01	2.23E+12	2.00E+12	1.85E+12	1.93E+12	1.98E+12	1.71E+12	1.73E+12	1.62E+12	1.61E+12
3.16E+01	1.82E+12	1.63E+12	1.51E+12	1.55E+12	1.61E+12	1.37E+12	1.39E+12	1.30E+12	1.41E+12
3.98E+01	1.49E+12	1.32E+12	1.24E+12	1.27E+12	1.30E+12	1.11E+12	1.12E+12	1.05E+12	1.30E+12
5.01E+01	1.21E+12	1.08E+12	1.00E+12	1.03E+12	1.05E+12	9.04E+11	9.00E+11	8.32E+11	9.35E+11
6.32E+01	9.80E+11	8.73E+11	8.19E+11	8.34E+11	8.40E+11	7.30E+11	7.17E+11	6.66E+11	6.55E+11
7.95E+01	7.92E+11	7.00E+11	6.71E+11	6.74E+11	6.76E+11	5.91E+11	5.74E+11	5.32E+11	5.47E+11
1.00E+02	6.36E+11	5.61E+11	5.41E+11	5.43E+11	5.41E+11	4.74E+11	4.61E+11	4.24E+11	4.16E+11
1.26E+02	5.15E+11	4.51E+11	4.41E+11	4.40E+11	4.34E+11	3.82E+11	3.69E+11	3.40E+11	3.04E+11
1.59E+02	4.11E+11	3.62E+11	3.57E+11	3.53E+11	3.47E+11	3.09E+11	2.96E+11	2.69E+11	2.32E+11
2.00E+02	3.29E+11	2.90E+11	2.89E+11	2.85E+11	2.77E+11	2.45E+11	2.37E+11	2.15E+11	2.18E+11
2.52E+02	2.65E+11	2.33E+11	2.35E+11	2.30E+11	2.23E+11	1.96E+11	1.89E+11	1.73E+11	1.31E+11
3.17E+02	2.13E+11	1.87E+11	1.91E+11	1.85E+11	1.79E+11	1.58E+11	1.53E+11	1.38E+11	1.14E+11
4.01E+02	1.70E+11	1.50E+11	1.54E+11	1.49E+11	1.43E+11	1.26E+11	1.22E+11	1.10E+11	1.05E+11
5.04E+02	1.38E+11	1.21E+11	1.26E+11	1.20E+11	1.15E+11	1.02E+11	9.82E+10	8.87E+10	9.02E+10
6.33E+02	1.11E+11	9.85E+10	1.03E+11	9.76E+10	9.32E+10	8.23E+10	7.97E+10	7.16E+10	8.02E+10
7.92E+02	8.50E+10	7.50E+10	7.36E+10	7.38E+10	7.23E+10	6.27E+10	6.18E+10	5.58E+10	6.90E+10
9.99E+02	6.76E+10	5.98E+10	5.86E+10	5.89E+10	5.75E+10	5.00E+10	4.93E+10	4.45E+10	4.28E+10
1.27E+03	5.36E+10	4.74E+10	4.65E+10	4.67E+10	4.56E+10	3.95E+10	3.91E+10	3.52E+10	3.32E+10
1.59E+03	4.31E+10	3.81E+10	3.75E+10	3.76E+10	3.67E+10	3.18E+10	3.14E+10	2.83E+10	3.49E+10
2.00E+03	3.43E+10	3.04E+10	2.99E+10	3.00E+10	2.93E+10	2.53E+10	2.51E+10	2.26E+10	2.49E+10
2.50E+03	2.75E+10	2.44E+10	2.40E+10	2.42E+10	2.35E+10	2.03E+10	2.01E+10	1.81E+10	2.00E+10
3.16E+03	2.20E+10	1.95E+10	1.92E+10	1.93E+10	1.88E+10	1.62E+10	1.61E+10	1.45E+10	1.83E+10
3.95E+03	1.77E+10	1.57E+10	1.55E+10	1.56E+10	1.51E+10	1.31E+10	1.30E+10	1.17E+10	1.40E+10
5.01E+03	1.41E+10	1.25E+10	1.23E+10	1.25E+10	1.21E+10	1.04E+10	1.04E+10	9.31E+09	9.29E+09
6.32E+03	1.14E+10	1.01E+10	9.93E+09	1.01E+10	9.70E+09	8.38E+09	8.35E+09	7.49E+09	8.34E+09
7.95E+03	8.68E+09	7.72E+09	7.51E+09	7.71E+09	7.48E+09	6.44E+09	6.45E+09	5.80E+09	6.03E+09
9.93E+03	6.96E+09	6.20E+09	6.04E+09	6.19E+09	6.01E+09	5.17E+09	5.18E+09	4.66E+09	4.97E+09
1.24E+04	5.58E+09	4.98E+09	4.84E+09	4.98E+09	4.83E+09	4.13E+09	4.16E+09	3.75E+09	4.34E+09
1.56E+04	4.46E+09	3.97E+09	3.85E+09	3.96E+09	3.86E+09	3.32E+09	3.32E+09	2.99E+09	3.35E+09
1.99E+04	3.51E+09	3.13E+09	3.06E+09	3.17E+09	3.07E+09	2.60E+09	2.64E+09	2.37E+09	2.19E+09
2.49E+04	2.81E+09	2.51E+09	2.44E+09	2.53E+09	2.44E+09	2.09E+09	2.11E+09	1.91E+09	1.76E+09
3.13E+04	2.25E+09	2.02E+09	1.96E+09	2.03E+09	1.96E+09	1.68E+09	1.70E+09	1.54E+09	1.46E+09
3.84E+04	1.84E+09	1.65E+09	1.61E+09	1.67E+09	1.60E+09	1.37E+09	1.39E+09	1.26E+09	1.39E+09
5.02E+04	1.42E+09	1.28E+09	1.25E+09	1.29E+09	1.24E+09	1.06E+09	1.08E+09	9.78E+08	1.00E+09
6.33E+04	1.15E+09	1.03E+09	9.99E+08	1.04E+09	9.98E+08	8.53E+08	8.70E+08	7.91E+08	8.55E+08
7.90E+04	8.91E+08	7.99E+08	7.73E+08	8.08E+08	7.79E+08	6.64E+08	6.80E+08	6.21E+08	6.51E+08
1.004E+05	7.00E+08	6.29E+08	6.10E+08	6.39E+08	6.14E+08	5.24E+08	5.39E+08	4.92E+08	5.33E+08
1.3E+05	5.61E+08	5.05E+08	4.89E+08	5.13E+08	4.93E+08	4.20E+08	4.34E+08	3.97E+08	4.06E+08
1.6E+05	4.46E+08	4.02E+08	3.89E+08	4.08E+08	3.93E+08	3.34E+08	3.47E+08	3.18E+08	3.55E+08
2.0E+05	3.56E+08	3.22E+08	3.12E+08	3.27E+08	3.14E+08	2.67E+08	2.79E+08	2.56E+08	2.26E+08
2.52E+05	2.82E+08	2.55E+08	2.46E+08	2.58E+08	2.48E+08	2.11E+08	2.22E+08	2.04E+08	2.16E+08
3.16E+05	2.26E+08	2.05E+08	1.98E+08	2.08E+08	2.00E+08	1.70E+08	1.80E+08	1.65E+08	1.36E+08
4.E+05	1.80E+08	1.64E+08	1.58E+08	1.66E+08	1.59E+08	1.35E+08	1.45E+08	1.33E+08	1.28E+08
5.06E+05	1.43E+08	1.30E+08	1.26E+08	1.32E+08	1.27E+08	1.08E+08	1.16E+08	1.07E+08	1.23E+08
6.28E+05	1.17E+08	1.06E+08	1.03E+08	1.08E+08	1.03E+08	8.77E+07	9.55E+07	8.76E+07	8.82E+07
7.97E+05	8.90E+07	8.10E+07	7.88E+07	8.22E+07	7.93E+07	6.74E+07	7.42E+07	6.80E+07	6.66E+07
9.98E+05	7.13E+07	6.51E+07	6.29E+07	6.57E+07	6.32E+07	5.38E+07	6.01E+07	5.51E+07	5.28E+07
1.27E+06	5.65E+07	5.15E+07	4.98E+07	5.21E+07	5.00E+07	4.25E+07	4.80E+07	4.42E+07	4.14E+07
1.58E+06	4.54E+07	4.15E+07	4.02E+07	4.19E+07	4.03E+07	3.42E+07	3.89E+07	3.59E+07	3.38E+07
1.98E+06	3.64E+07	3.32E+07	3.22E+07	3.35E+07	3.23E+07	2.74E+07	3.14E+07	2.91E+07	2.82E+07
2.53E+06	2.85E+07	2.61E+07	2.53E+07	2.63E+07	2.53E+07	2.15E+07	2.49E+07	2.31E+07	2.34E+07
3.17E+06	2.29E+07	2.09E+07	2.03E+07	2.11E+07	2.03E+07	1.72E+07	2.01E+07	1.87E+07	1.29E+07
3.98E+06	1.83E+07	1.68E+07	1.63E+07	1.69E+07	1.63E+07	1.38E+07	1.62E+07	1.52E+07	1.15E+07
5.02E+06	1.47E+07	1.35E+07	1.31E+07	1.36E+07	1.30E+07	1.11E+07	1.31E+07	1.23E+07	1.36E+07
6.33E+06	1.18E+07	1.08E+07	1.05E+07	1.09E+07	1.05E+07	8.90E+06	1.06E+07	9.95E+06	8.19E+06
8.02E+06	9.05E+06	8.31E+06	8.06E+06	8.38E+06	8.06E+06	6.85E+06	8.21E+06	7.75E+06	6.17E+06
1.01E+07	7.21E+06	6.64E+06	6.44E+06	6.69E+06	6.44E+06	5.47E+06	6.60E+06	6.25E+06	5.27E+06
1.26E+07	5.78E+06	5.32E+06	5.16E+06	5.37E+06	5.17E+06	4.39E+06	5.33E+06	5.06E+06	3.93E+06
1.59E+07	4.60E+06	4.24E+06	4.11E+06	4.28E+06	4.12E+06	3.50E+06	4.28E+06	4.07E+06	3.93E+06
2.00E+07	3.66E+06	3.37E+06	3.28E+06	3.41E+06	3.29E+06	2.79E+06	3.45E+06	3.28E+06	3.15E+06
2.52E+07	2.92E+06	2.70E+06	2.62E+06	2.73E+06	2.63E+06	2.23E+06	2.78E+06	2.65E+06	2.10E+06
3.16E+07	2.34E+06	2.16E+06	2.10E+06	2.18E+06	2.10E+06	1.79E+06	2.25E+06	2.14E+06	2.03E+06
3.99E+07	1.87E+06	1.72E+06	1.68E+06	1.75E+06	1.68E+06	1.43E+06	1.81E+06	1.73E+06	2.01E+06
5.02E+07	1.49E+06	1.38E+06	1.34E+06	1.40E+06	1.35E+06	1.15E+06	1.47E+06	1.40E+06	1.73E+06
6.31E+07	1.20E+06	1.11E+06	1.08E+06	1.13E+06	1.09E+06	9.22E+05	1.19E+06	1.14E+06	1.36E+06
7.95E+07	9.28E+05	8.57E+05	8.37E+05	8.73E+05	8.44E+05	7.15E+05	9.32E+05	8.90E+05	7.24E+05
1.001E+08	7.38E+05	6.82E+05	6.66E+05	6.95E+05	6.73E+05	5.69E+05	7.48E+05	7.15E+05	6.41E+05

Frequency vs. Phase for 3p/2p CAT coating

Frequency (mHz)	Phase (°)								
	Day1-Sample1	Day7-Sample1	Day14-Sample1	Day1-Sample2	Day7-Sample2-	Day14-Sample2-	Day1-Sample3-	Day7-Sample3-	Day14-Sample3-
1.996E+01	-80.72	-76.39	-73.27	-80.42	-83.19	-78.87	-83.17	-85.46	-66.78
2.51E+01	-80.14	-78.36	-74.47	-79.43	-82.94	-79.11	-84.32	-86.08	-73.98
3.16E+01	-80.87	-78.67	-75.91	-79.8	-83.39	-79.38	-84.76	-86.13	-69.75
3.98E+01	-81.09	-79.24	-76.94	-80.74	-83.65	-80.91	-85.33	-86.58	-77.53
5.01E+01	-81.93	-80.35	-77.57	-80.76	-83.59	-81.89	-85.69	-86.77	-78.74
6.32E+01	-82.38	-81.62	-78.66	-81.22	-84.34	-82.51	-85.83	-86.67	-80.72
7.95E+01	-82.6	-82.02	-79.05	-82.02	-84.58	-83.31	-85.72	-86.75	-81.17
1.00E+02	-83.12	-82.51	-79.63	-82.41	-84.73	-83.63	-85.87	-86.81	-83.11
1.26E+02	-83.19	-83.27	-80.26	-82.31	-84.79	-84.14	-85.8	-86.57	-83.84
1.59E+02	-83.81	-83.36	-79.66	-82.77	-84.82	-84.91	-85.65	-86.36	-85.04
2.00E+02	-83.78	-83.47	-80.02	-82.87	-84.87	-84.35	-85.34	-86.11	-85.56
2.52E+02	-83.9	-83.36	-80.35	-82.8	-84.58	-84.27	-85.03	-85.77	-86.49
3.17E+02	-83.35	-83.11	-80.47	-82.57	-84.27	-84.07	-84.47	-85.22	-86.78
4.01E+02	-83.14	-82.77	-80.65	-82.17	-83.63	-83.51	-83.78	-84.55	-86.33
5.04E+02	-82.47	-82.04	-80.47	-81.61	-83	-83.03	-83.11	-83.85	-86.79
6.33E+02	-81.63	-81.43	-80.39	-81.05	-82.3	-82.49	-82.39	-83.07	-87.55
7.92E+02	-87.2	-86.79	-86.28	-86.27	-87.21	-87.34	-87.04	-87.49	-87.4
9.99E+02	-87.11	-86.79	-86.31	-86.26	-87.05	-87.15	-86.9	-87.35	-87.06
1.27E+03	-86.99	-86.58	-86.28	-86.1	-86.89	-87	-86.7	-87.08	-86.63
1.59E+03	-86.72	-86.39	-86.13	-85.83	-86.62	-86.82	-86.44	-86.79	-86.03
2.00E+03	-86.33	-86.1	-85.88	-85.53	-86.33	-86.44	-86.12	-86.37	-84.29
2.50E+03	-85.99	-85.65	-85.53	-85.04	-85.87	-86.02	-85.62	-85.91	-80.24
3.16E+03	-85.41	-85.05	-84.98	-84.48	-85.29	-85.45	-85.1	-85.29	-88.77
3.95E+03	-84.77	-84.38	-84.43	-83.78	-84.68	-84.93	-84.44	-84.62	-88.87
5.01E+03	-83.87	-83.51	-83.55	-82.9	-83.82	-83.98	-83.59	-83.74	-88.9
6.32E+03	-82.94	-82.51	-82.67	-81.94	-82.86	-82.99	-82.64	-82.77	-88.96
7.95E+03	-88.22	-87.82	-87.87	-87.24	-87.77	-88.01	-87.36	-87.23	-89.1
9.93E+03	-88.09	-87.63	-87.79	-87.15	-87.57	-87.96	-87.16	-86.94	-89.21
1.24E+04	-87.93	-87.4	-87.5	-86.78	-87.4	-87.78	-86.94	-86.61	-89.04
1.56E+04	-87.54	-87.05	-87.51	-86.56	-87.01	-86.75	-86.51	-86.19	-89.26
1.99E+04	-87.01	-86.66	-86.74	-86.09	-86.73	-86.33	-86.03	-85.76	-89.5
2.49E+04	-86.64	-86.15	-86.42	-85.63	-86.28	-86.29	-85.58	-85.17	-89.27
3.13E+04	-86.02	-85.55	-85.6	-85.04	-85.73	-85.96	-84.95	-84.52	-89.7
3.84E+04	-85.39	-84.84	-84.93	-84.32	-85.2	-85.29	-84.23	-83.82	-88.4
5.02E+04	-84.47	-83.62	-83.37	-82.79	-84.8	-84.73	-82.87	-82.9	-89.67
6.33E+04	-83.3	-82.79	-82.8	-82.41	-83.26	-83.4	-82.02	-81.68	-88.95
7.90E+04	-88.59	-88.1	-88.19	-87.76	-88.05	-88.33	-86.68	-86.14	-89.49
1.004E+05	-88.23	-87.92	-87.98	-87.65	-87.86	-88.07	-86.29	-85.82	-89.25
1.3E+05	-88.08	-87.65	-87.66	-87.42	-87.67	-87.9	-85.89	-85.44	-89.21
1.6E+05	-87.73	-87.32	-87.29	-87.15	-87.4	-87.59	-85.38	-85.01	-89.32
2.0E+05	-87.33	-86.9	-86.86	-86.79	-87.07	-87.2	-84.82	-84.49	-89.29
2.52E+05	-86.79	-86.34	-86.29	-86.3	-86.61	-86.7	-84.09	-83.83	-89.29
3.16E+05	-86.18	-85.7	-85.64	-85.72	-86.08	-86.13	-83.3	-83.07	-89.25
4.E+05	-85.4	-84.9	-84.83	-84.97	-85.4	-85.4	-82.34	-82.18	-89.2
5.06E+05	-84.44	-83.92	-83.84	-84.04	-84.55	-84.5	-81.27	-81.11	-89.17
6.28E+05	-83.48	-82.92	-82.84	-83.08	-83.67	-83.59	-80.23	-80.05	-89.1
7.97E+05	-88.57	-88.07	-87.98	-88.19	-88.33	-88.35	-84.83	-84.45	-89.39
9.98E+05	-88.32	-87.8	-87.79	-87.98	-88.12	-88.15	-84.64	-84.12	-89.14
1.27E+06	-88.04	-87.56	-87.5	-87.74	-87.91	-87.87	-84.44	-83.79	-89.45
1.58E+06	-87.69	-87.24	-87.2	-87.38	-87.58	-87.55	-84.28	-83.49	-89.07
1.98E+06	-87.31	-86.83	-86.79	-86.99	-87.2	-87.15	-84.01	-83.13	-89.1
2.53E+06	-86.75	-86.3	-86.24	-86.41	-86.67	-86.6	-83.57	-82.65	-89.02
3.17E+06	-86.13	-85.68	-85.62	-85.76	-86.07	-86	-83.04	-82.12	-89.04
3.98E+06	-85.37	-84.94	-84.85	-84.98	-85.35	-85.27	-82.37	-81.47	-88.88
5.02E+06	-84.48	-84.06	-83.94	-84.05	-84.49	-84.39	-81.52	-80.68	-88.93
6.33E+06	-83.44	-83.02	-82.89	-82.97	-83.48	-83.37	-80.5	-79.74	-88.9
8.02E+06	-88.47	-88.18	-88.03	-88.04	-88.05	-88.04	-85.1	-84.26	-88.7
1.01E+07	-88.28	-88.01	-87.82	-87.84	-87.83	-87.87	-84.86	-84.09	-89.01
1.26E+07	-88.05	-87.81	-87.6	-87.56	-87.59	-87.62	-84.58	-83.91	-89.04
1.59E+07	-87.77	-87.52	-87.28	-87.23	-87.27	-87.3	-84.23	-83.66	-89.19
2.00E+07	-87.41	-87.17	-86.9	-86.83	-86.89	-86.92	-83.83	-83.39	-89.2
2.52E+07	-86.97	-86.72	-86.44	-86.34	-86.44	-86.48	-83.37	-83.03	-89.31
3.16E+07	-86.41	-86.17	-85.88	-85.75	-85.91	-85.93	-82.85	-82.63	-89.32
3.99E+07	-85.73	-85.49	-85.18	-85.05	-85.29	-85.29	-82.28	-82.13	-89.45
5.02E+07	-84.94	-84.69	-84.34	-84.23	-84.55	-84.54	-81.62	-81.55	-89.52
6.31E+07	-84.01	-83.75	-83.38	-83.29	-83.71	-83.65	-80.9	-80.9	-89.6
7.95E+07	-89.15	-89.01	-88.59	-88.53	-88.49	-88.53	-85.83	-85.75	-89.76
1.001E+08	-89.11	-88.95	-88.5	-88.49	-88.48	-88.48	-86	-85.98	-89.95

240

Frequency vs. Impedance for VE coating

Frequency (mHz)	impedance (ohm.cm2)								
	Day1-Sample1-i	Day7-Sample1-	Day14-Sample1-	Day1-Sample2	Day7-Sample2	Day14-Sample2	Day1-Sample3-i	Day7-Sample3-	Day14-Sample3-i
1.996E+01	1.35E+11	1.55E+11	1.13E+12	1.09E+12	1.27E+11	9.87E+11	2.02E+12	1.53E+12	1.16E+12
2.51E+01	1.13E+11	1.37E+11	1.98E+11	9.44E+11	1.08E+11	8.38E+11	1.67E+12	1.26E+12	9.41E+11
3.16E+01	9.19E+10	1.20E+11	1.27E+11	7.98E+11	9.40E+10	7.06E+11	1.36E+12	1.03E+12	7.46E+11
3.98E+01	7.62E+10	1.05E+11	1.09E+11	6.76E+11	8.38E+10	5.92E+11	1.10E+12	8.46E+11	5.70E+11
5.01E+01	6.43E+10	9.29E+10	9.33E+10	5.66E+11	7.50E+10	4.95E+11	8.93E+11	6.85E+11	4.41E+11
6.32E+01	5.49E+10	8.30E+10	7.98E+10	4.76E+11	6.78E+10	4.11E+11	7.22E+11	5.53E+11	3.91E+11
7.95E+01	4.76E+10	7.54E+10	6.87E+10	3.97E+11	6.04E+10	3.43E+11	5.80E+11	4.50E+11	3.75E+11
1.00E+02	4.16E+10	6.96E+10	5.96E+10	3.29E+11	5.38E+10	2.84E+11	4.69E+11	3.64E+11	3.04E+11
1.26E+02	3.68E+10	6.44E+10	5.27E+10	2.72E+11	4.79E+10	2.35E+11	3.77E+11	2.95E+11	2.46E+11
1.59E+02	3.28E+10	5.96E+10	4.67E+10	2.23E+11	4.29E+10	1.93E+11	3.02E+11	2.39E+11	1.99E+11
2.00E+02	2.95E+10	5.51E+10	4.22E+10	1.82E+11	3.84E+10	1.58E+11	2.43E+11	1.93E+11	1.61E+11
2.52E+02	2.57E+10	5.05E+10	3.82E+10	1.49E+11	3.46E+10	1.30E+11	1.95E+11	1.56E+11	1.30E+11
3.17E+02	2.35E+10	4.57E+10	3.43E+10	1.23E+11	2.80E+10	1.07E+11	1.57E+11	1.27E+11	1.05E+11
4.01E+02	2.16E+10	4.08E+10	3.08E+10	9.99E+10	2.49E+10	8.72E+10	1.26E+11	1.02E+11	8.47E+10
5.04E+02	1.97E+10	3.61E+10	2.65E+10	8.21E+10	2.21E+10	7.14E+10	1.02E+11	8.29E+10	6.89E+10
6.33E+02	1.80E+10	3.17E+10	2.31E+10	6.77E+10	1.97E+10	5.87E+10	8.26E+10	6.75E+10	5.61E+10
7.92E+02	1.63E+10	2.59E+10	2.01E+10	5.09E+10	1.75E+10	4.43E+10	6.40E+10	5.30E+10	4.40E+10
9.99E+02	1.46E+10	2.19E+10	1.72E+10	4.11E+10	1.54E+10	3.58E+10	5.11E+10	4.25E+10	3.54E+10
1.27E+03	1.28E+10	1.83E+10	1.46E+10	3.29E+10	1.34E+10	2.87E+10	4.06E+10	3.39E+10	2.83E+10
1.59E+03	1.13E+10	1.54E+10	1.24E+10	2.67E+10	1.17E+10	2.33E+10	3.27E+10	2.74E+10	2.30E+10
2.00E+03	9.77E+09	1.28E+10	1.04E+10	2.15E+10	1.01E+10	1.87E+10	2.61E+10	2.20E+10	1.85E+10
2.50E+03	8.42E+09	1.07E+10	8.81E+09	1.74E+10	8.74E+09	1.52E+10	2.10E+10	1.77E+10	1.50E+10
3.16E+03	7.17E+09	8.83E+09	7.40E+09	1.41E+10	7.45E+09	1.22E+10	1.68E+10	1.42E+10	1.21E+10
3.95E+03	6.12E+09	7.37E+09	6.26E+09	1.15E+10	6.36E+09	9.96E+09	1.36E+10	1.16E+10	9.84E+09
5.01E+03	5.16E+09	6.08E+09	5.23E+09	9.22E+09	5.35E+09	8.00E+09	1.08E+10	9.25E+09	7.92E+09
6.32E+03	4.36E+09	5.05E+09	4.40E+09	7.50E+09	4.51E+09	6.49E+09	8.72E+09	7.47E+09	6.43E+09
7.95E+03	3.47E+09	3.99E+09	3.53E+09	5.72E+09	3.48E+09	4.99E+09	6.73E+09	5.80E+09	5.01E+09
9.93E+03	2.90E+09	3.30E+09	2.95E+09	4.61E+09	2.90E+09	4.04E+09	5.42E+09	4.68E+09	4.06E+09
1.24E+04	2.42E+09	2.73E+09	2.46E+09	3.73E+09	2.40E+09	3.28E+09	4.36E+09	3.79E+09	3.29E+09
1.56E+04	2.01E+09	2.24E+09	2.05E+09	3.00E+09	1.97E+09	2.63E+09	3.48E+09	3.04E+09	2.65E+09
1.99E+04	1.66E+09	1.82E+09	1.68E+09	2.38E+09	1.61E+09	2.09E+09	2.76E+09	2.42E+09	2.11E+09
2.49E+04	1.38E+09	1.51E+09	1.39E+09	1.92E+09	1.32E+09	1.69E+09	2.22E+09	1.94E+09	1.70E+09
3.13E+04	1.15E+09	1.24E+09	1.16E+09	1.55E+09	1.09E+09	1.36E+09	1.78E+09	1.57E+09	1.37E+09
3.84E+04	9.73E+08	1.04E+09	9.82E+08	1.28E+09	9.09E+08	1.12E+09	1.46E+09	1.29E+09	1.13E+09
5.02E+04	7.87E+08	8.33E+08	7.93E+08	1.00E+09	7.24E+08	8.74E+08	1.14E+09	1.00E+09	8.82E+08
6.33E+04	6.54E+08	6.86E+08	6.56E+08	8.12E+08	5.95E+08	7.09E+08	9.10E+08	8.10E+08	7.10E+08
7.90E+04	5.25E+08	5.46E+08	5.26E+08	6.29E+08	4.71E+08	5.56E+08	7.13E+08	6.37E+08	5.57E+08
1.004E+05	4.28E+08	4.40E+08	4.27E+08	4.99E+08	3.81E+08	4.42E+08	5.64E+08	5.06E+08	4.42E+08
1.3E+05	3.54E+08	3.61E+08	3.51E+08	4.03E+08	3.13E+08	3.57E+08	4.53E+08	4.08E+08	3.56E+08
1.6E+05	2.89E+08	2.93E+08	2.86E+08	3.23E+08	2.56E+08	2.86E+08	3.62E+08	3.26E+08	2.85E+08
2.0E+05	2.37E+08	2.38E+08	2.33E+08	2.60E+08	2.10E+08	2.31E+08	2.90E+08	2.62E+08	2.29E+08
2.52E+05	1.92E+08	1.92E+08	1.87E+08	2.07E+08	1.71E+08	1.84E+08	2.30E+08	2.08E+08	1.82E+08
3.16E+05	1.57E+08	1.57E+08	1.53E+08	1.67E+08	1.42E+08	1.49E+08	1.85E+08	1.68E+08	1.47E+08
4.E+05	1.28E+08	1.27E+08	1.24E+08	1.35E+08	1.16E+08	1.20E+08	1.48E+08	1.35E+08	1.18E+08
5.06E+05	1.04E+08	1.03E+08	9.94E+07	1.08E+08	9.50E+07	9.57E+07	1.18E+08	1.08E+08	9.39E+07
6.28E+05	8.55E+07	8.47E+07	8.17E+07	8.88E+07	7.93E+07	7.85E+07	9.64E+07	8.81E+07	7.68E+07
7.97E+05	6.64E+07	6.57E+07	6.32E+07	6.78E+07	6.19E+07	6.06E+07	7.41E+07	6.83E+07	5.93E+07
9.98E+05	5.39E+07	5.30E+07	5.10E+07	5.47E+07	5.06E+07	4.87E+07	5.95E+07	5.49E+07	4.76E+07
1.27E+06	4.31E+07	4.25E+07	4.07E+07	4.35E+07	4.07E+07	3.89E+07	4.74E+07	4.35E+07	3.78E+07
1.58E+06	3.51E+07	3.45E+07	3.30E+07	3.53E+07	3.32E+07	3.15E+07	3.82E+07	3.51E+07	3.06E+07
1.98E+06	2.83E+07	2.79E+07	2.66E+07	2.85E+07	2.69E+07	2.54E+07	3.07E+07	2.83E+07	2.46E+07
2.53E+06	2.25E+07	2.21E+07	2.11E+07	2.25E+07	2.14E+07	2.01E+07	2.42E+07	2.23E+07	1.94E+07
3.17E+06	1.82E+07	1.78E+07	1.70E+07	1.82E+07	1.73E+07	1.62E+07	1.95E+07	1.79E+07	1.56E+07
3.98E+06	1.47E+07	1.44E+07	1.37E+07	1.47E+07	1.40E+07	1.31E+07	1.56E+07	1.44E+07	1.26E+07
5.02E+06	1.19E+07	1.16E+07	1.10E+07	1.19E+07	1.13E+07	1.05E+07	1.26E+07	1.16E+07	1.01E+07
6.33E+06	9.65E+06	9.37E+06	8.87E+06	9.63E+06	9.13E+06	8.49E+06	1.01E+07	9.34E+06	8.13E+06
8.02E+06	7.50E+06	7.25E+06	6.88E+06	7.39E+06	7.06E+06	6.58E+06	7.86E+06	7.23E+06	6.29E+06
1.01E+07	6.04E+06	5.82E+06	5.51E+06	5.93E+06	5.66E+06	5.28E+06	6.30E+06	5.79E+06	5.03E+06
1.26E+07	4.89E+06	4.69E+06	4.44E+06	4.78E+06	4.56E+06	4.25E+06	5.07E+06	4.66E+06	4.05E+06
1.59E+07	3.93E+06	3.75E+06	3.55E+06	3.82E+06	3.65E+06	3.40E+06	4.06E+06	3.72E+06	3.23E+06
2.00E+07	3.16E+06	3.01E+06	2.84E+06	3.06E+06	2.92E+06	2.72E+06	3.25E+06	2.98E+06	2.58E+06
2.52E+07	2.55E+06	2.41E+06	2.28E+06	2.45E+06	2.34E+06	2.18E+06	2.61E+06	2.38E+06	2.07E+06
3.16E+07	2.06E+06	1.94E+06	1.83E+06	1.97E+06	1.88E+06	1.75E+06	2.10E+06	1.91E+06	1.66E+06
3.99E+07	1.66E+06	1.55E+06	1.46E+06	1.58E+06	1.51E+06	1.40E+06	1.69E+06	1.53E+06	1.33E+06
5.02E+07	1.34E+06	1.25E+06	1.18E+06	1.27E+06	1.21E+06	1.13E+06	1.36E+06	1.23E+06	1.07E+06
6.31E+07	1.09E+06	1.01E+06	9.49E+05	1.03E+06	9.77E+05	9.11E+05	1.10E+06	9.92E+05	8.61E+05
7.95E+07	8.50E+05	7.87E+05	7.40E+05	7.92E+05	7.59E+05	7.09E+05	8.55E+05	7.73E+05	6.69E+05
1.001E+08	6.81E+05	6.30E+05	5.91E+05	6.32E+05	6.07E+05	5.66E+05	6.83E+05	6.17E+05	5.34E+05

Frequency vs. Phase for VE coating

Frequency (mHz)	Phase (º)								
	Day1-Sample1	Day7-Sample1-	Day14-Sample1	Day1-Sample2-	Day7-Sample2-	Day14-Sample2	Day1-Sample3	Day7-Sample3-F	Day14-Sample3-
1.996E+01	-52.45	-52.47	-55.65	-54.63	-33.47	-64.04	-76.65	-73.66	-69.76
2.51E+01	-52.38	-53.67	-54.46	-57.35	-34.69	-65.51	-77.56	-75.15	-71.45
3.16E+01	-52.78	-53.8	-52.66	-59.97	-35.87	-66.59	-78.89	-76.26	-72.84
3.98E+01	-53.09	-52.89	-51.79	-61.82	-38.23	-68.09	-79.86	-77.21	-73.83
5.01E+01	-52.87	-51.28	-50.84	-64.28	-39.7	-69.19	-80.37	-78.32	-77.37
6.32E+01	-52.27	-49.09	-49.77	-66.42	-41.31	-70.31	-81.11	-79.42	-78.43
7.95E+01	-51.36	-46.93	-48.68	-67.94	-41.37	-71.68	-82.17	-79.89	-78.41
1.00E+02	-49.85	-44.98	-47.41	-69.74	-42.71	-72.59	-82.47	-80.36	-79.46
1.26E+02	-48.08	-43.83	-46.2	-71.54	-43.14	-73.51	-82.93	-80.51	-79.86
1.59E+02	-45.84	-43.58	-45.3	-72.67	-43.23	-74.32	-83.05	-80.79	-80.42
2.00E+02	-43.77	-44.15	-44.72	-73.72	-42.9	-75.13	-83.25	-80.86	-80.55
2.52E+02	-45.26	-45.44	-44.87	-74.3	-42.17	-75.68	-83.05	-80.88	-80.53
3.17E+02	-44.25	-47.15	-45.41	-74.6	-48.34	-76.07	-83.01	-80.85	-80.34
4.01E+02	-43.93	-49.22	-46.56	-74.82	-48.73	-76.42	-82.7	-80.55	-79.93
5.04E+02	-44.42	-51.28	-52.25	-74.82	-49.47	-76.46	-82.12	-80.08	-79.39
6.33E+02	-45.55	-53.34	-54.26	-74.57	-50.4	-76.52	-81.69	-79.63	-78.72
7.92E+02	-47.13	-60.84	-56.44	-81.2	-51.52	-81.67	-86.05	-84.29	-83.51
9.99E+02	-49.16	-63.09	-58.53	-81.49	-52.85	-81.96	-86.18	-84.34	-83.43
1.27E+03	-51.38	-65	-60.36	-81.67	-54.39	-82.1	-85.99	-84.32	-83.19
1.59E+03	-53.55	-66.51	-61.77	-81.7	-55.97	-82.2	-85.91	-84.17	-83.02
2.00E+03	-55.67	-67.76	-62.92	-81.59	-57.63	-82.11	-85.54	-84.01	-82.7
2.50E+03	-57.55	-68.62	-63.73	-81.31	-59.24	-81.92	-85.24	-83.72	-82.27
3.16E+03	-59.24	-69.22	-64.35	-80.88	-60.85	-81.57	-84.78	-83.27	-81.75
3.95E+03	-60.49	-69.48	-64.72	-80.27	-62.2	-81.12	-84.23	-82.74	-81.16
5.01E+03	-61.46	-69.48	-64.89	-79.46	-63.41	-80.47	-83.5	-82.04	-80.41
6.32E+03	-62.06	-69.22	-64.9	-78.49	-64.33	-79.75	-82.68	-81.2	-79.58
7.95E+03	-68.31	-74.77	-70.46	-84.76	-70.82	-84.71	-87.13	-85.7	-84.39
9.93E+03	-69.18	-75.08	-70.96	-84.69	-71.94	-84.57	-87.02	-85.52	-84.37
1.24E+04	-69.87	-75.28	-71.46	-84.49	-72.87	-84.48	-86.77	-85.32	-84.32
1.56E+04	-70.42	-75.39	-71.75	-84.07	-73.58	-84.18	-86.56	-85.08	-84.22
1.99E+04	-70.63	-75.43	-71.95	-83.69	-74.12	-84.03	-86.11	-84.69	-84.1
2.49E+04	-70.78	-75.21	-72.03	-83.08	-74.34	-83.48	-85.79	-84.34	-83.7
3.13E+04	-70.8	-75.04	-72.07	-82.53	-74.34	-83.01	-85.27	-83.83	-83.34
3.84E+04	-70.7	-74.83	-72.06	-81.82	-74.14	-82.44	-84.71	-83.32	-82.87
5.02E+04	-70.4	-74.58	-71.6	-80.79	-73.44	-81.86	-83.87	-82.6	-82.1
6.33E+04	-70.15	-73.89	-71.76	-79.48	-72.87	-80.54	-82.87	-81.6	-81.2
7.90E+04	-75.63	-79.27	-77.2	-85.56	-77.96	-85.37	-87.35	-86.1	-86.03
1.004E+05	-76.21	-79.54	-77.89	-85.35	-77.85	-85.19	-87.14	-85.96	-85.92
1.3E+05	-76.73	-79.75	-78.49	-85.03	-77.62	-84.98	-86.91	-85.8	-85.79
1.6E+05	-77.19	-79.89	-79.04	-84.67	-77.34	-84.7	-86.62	-85.55	-85.57
2.0E+05	-77.56	-79.94	-79.47	-84.21	-77.02	-84.37	-86.26	-85.25	-85.26
2.52E+05	-77.84	-79.88	-79.77	-83.6	-76.66	-83.9	-85.77	-84.83	-84.85
3.16E+05	-77.94	-79.71	-79.9	-82.9	-76.32	-83.36	-85.23	-84.35	-84.34
4.E+05	-77.88	-79.41	-79.85	-82	-75.95	-82.68	-84.54	-83.72	-83.68
5.06E+05	-77.62	-78.93	-79.59	-80.91	-75.57	-81.83	-83.69	-82.95	-82.85
6.28E+05	-77.22	-78.39	-79.21	-79.79	-75.21	-80.95	-82.81	-82.16	-81.98
7.97E+05	-82.36	-83.44	-84.13	-85.67	-80.7	-85.6	-87.12	-86.53	-86.72
9.98E+05	-82.59	-83.62	-84.29	-85.38	-81.1	-85.52	-86.92	-86.43	-86.45
1.27E+06	-82.72	-83.7	-84.42	-85.03	-81.49	-85.3	-86.68	-86.24	-86.22
1.58E+06	-82.71	-83.67	-84.36	-84.67	-81.83	-85.03	-86.34	-86	-85.95
1.98E+06	-82.6	-83.59	-84.28	-84.21	-81.99	-84.74	-85.96	-85.68	-85.59
2.53E+06	-82.32	-83.33	-84.03	-83.6	-82.05	-84.29	-85.42	-85.27	-85.13
3.17E+06	-81.92	-82.97	-83.68	-82.92	-81.96	-83.8	-84.82	-84.77	-84.59
3.98E+06	-81.36	-82.46	-83.21	-82.11	-81.68	-83.19	-84.12	-84.16	-83.96
5.02E+06	-80.65	-81.8	-82.57	-81.17	-81.23	-82.43	-83.28	-83.42	-83.19
6.33E+06	-79.77	-80.99	-81.8	-80.07	-80.59	-81.54	-82.3	-82.55	-82.28
8.02E+06	-84.43	-85.78	-86.27	-86.01	-85.53	-86.24	-86.57	-86.89	-86.93
1.01E+07	-84.34	-85.71	-86.2	-85.91	-85.59	-86.15	-86.36	-86.77	-86.81
1.26E+07	-84.17	-85.63	-86.09	-85.74	-85.57	-85.97	-86.13	-86.6	-86.64
1.59E+07	-83.96	-85.45	-85.92	-85.54	-85.49	-85.8	-85.83	-86.37	-86.43
2.00E+07	-83.67	-85.21	-85.67	-85.21	-85.29	-85.51	-85.49	-86.07	-86.13
2.52E+07	-83.33	-84.85	-85.33	-84.79	-85.01	-85.19	-85.11	-85.72	-85.74
3.16E+07	-82.92	-84.39	-84.9	-84.24	-84.62	-84.74	-84.66	-85.27	-85.28
3.99E+07	-82.42	-83.79	-84.37	-83.54	-84.08	-84.18	-84.12	-84.72	-84.68
5.02E+07	-81.83	-83.06	-83.71	-82.68	-83.4	-83.5	-83.48	-84.05	-83.97
6.31E+07	-81.13	-82.2	-82.94	-81.67	-82.61	-82.68	-82.73	-83.29	-83.14
7.95E+07	-86.02	-86.92	-87.42	-87.66	-87.4	-87.45	-87.27	-87.76	-87.9
1.001E+08	-86.16	-86.87	-87.42	-87.63	-87.4	-87.43	-87.32	-87.74	-87.87
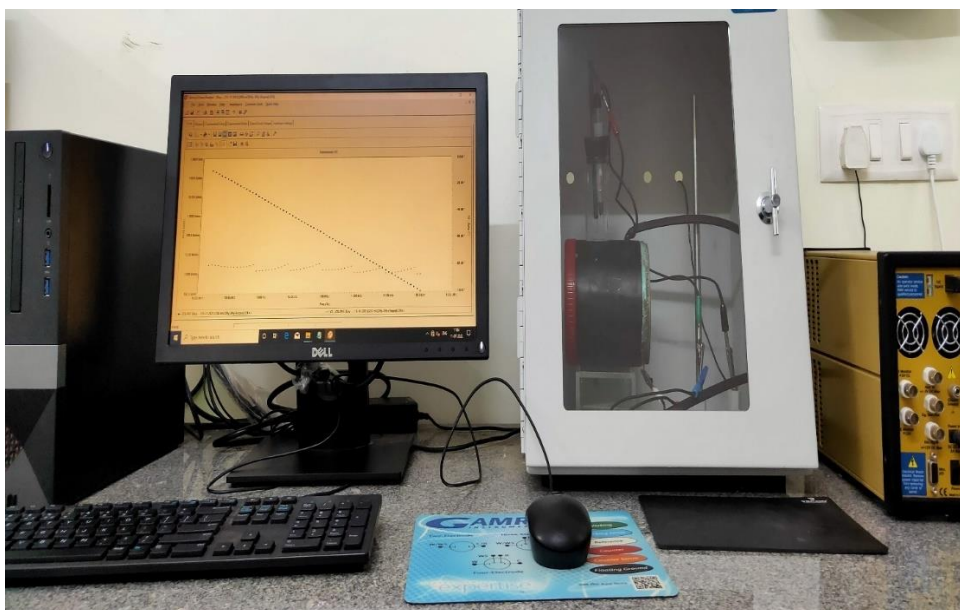
Experimental set-up for EIS test on coated pipe sample inside Faraday Cage

Appendix-III N

Type D Shore Durometer Hardness Measurement of Coatings before and after Salt Spray Test

Type of coating	Type D Shore Durometer Hardness Measurement											
	Virgin coating before salt spray						Coating after salt spray					
	1	2	3	4	5	Average Hardness	1	2	3	4	5	Average Hardness
3LPE	54	57	55	53	56	55	46.5	43	42.5	45	43	44
3p/2p CAT	36	38	37	36	38	37	28.5	32	26	25.5	33	29
PU	71	71	75	71	72	72	47	44.5	45	47	46.5	46
VE	33	34	30	31	32	32	19	18.5	20.5	19	18	19
LE	89	90	88	88	90	89	78.5	76.5	77	78	75	77
HSS	57	58	54	58	58	57	46	45.5	44	43	42	44

| a) | b) |

Shore D hardness measurement on LE coated pipe sample a) before salt spray test, b) after salt spray test